29th May- 2nd June 2017, GdR EGRIN Cargèse 2017

Complex rheology in geophysical granular flows: from field to laboratory scale

Anne Mangeney[1,1’]

[1]Institut de Physique du Globe de Paris, Université Paris Diderot, SPC
[1’] Equipe ANGE INRIA-Lab. Jacques Louis Lions-CEREMA

Outline

I – Geophysical reality:
- Complexity of flows and physical processes
- Field data to validate rheological models of real flows
- From field observation to laboratory experiments

II – Modelling of natural landslides
- Shallow model and rheology
- Unexplained high mobility of natural landslides
- Investigating landslide dynamics: seismic data and models

III – Back to the rheology of granular materials
- Laboratory experiments
- 2D visco-plastic models
- Insight into the static/flowing interface
- Multi-layer models

Outline

I – Geophysical reality:
- Complexity of flows and physical processes
- Field data to validate rheological models of real flows
- From field observation to laboratory experiments

II – Modelling of natural landslides
- Shallow model and rheology
- Unexplained high mobility of natural landslides
- Investigating landslide dynamics: seismic data and models

III – Back to the rheology of granular materials
- Laboratory experiments
- 2D visco-plastic models
- Insight into the static/flowing interface
- Multi-layer models

Large variety of natural flows

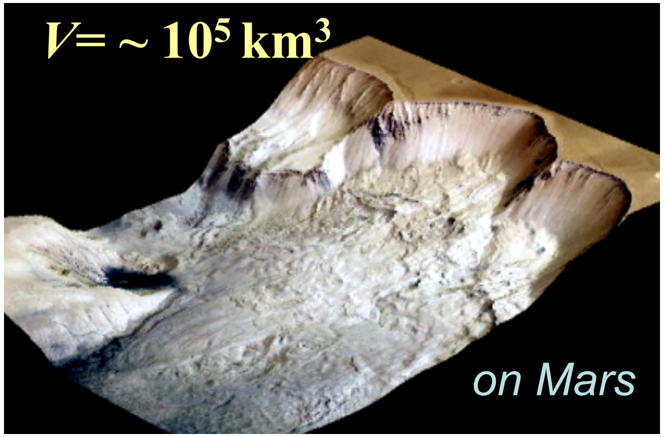

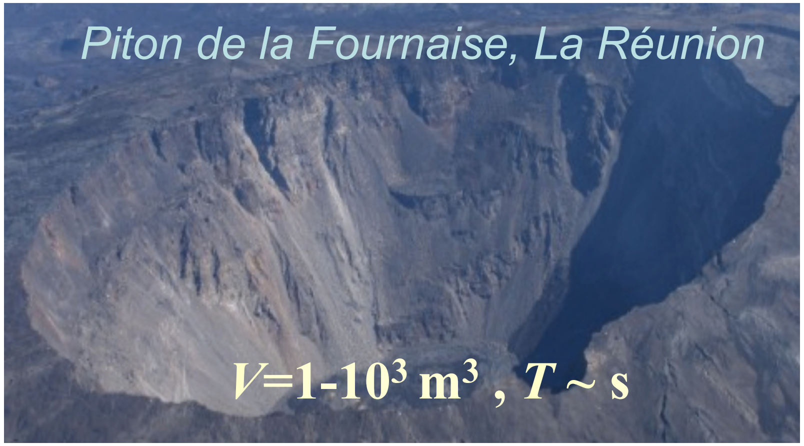

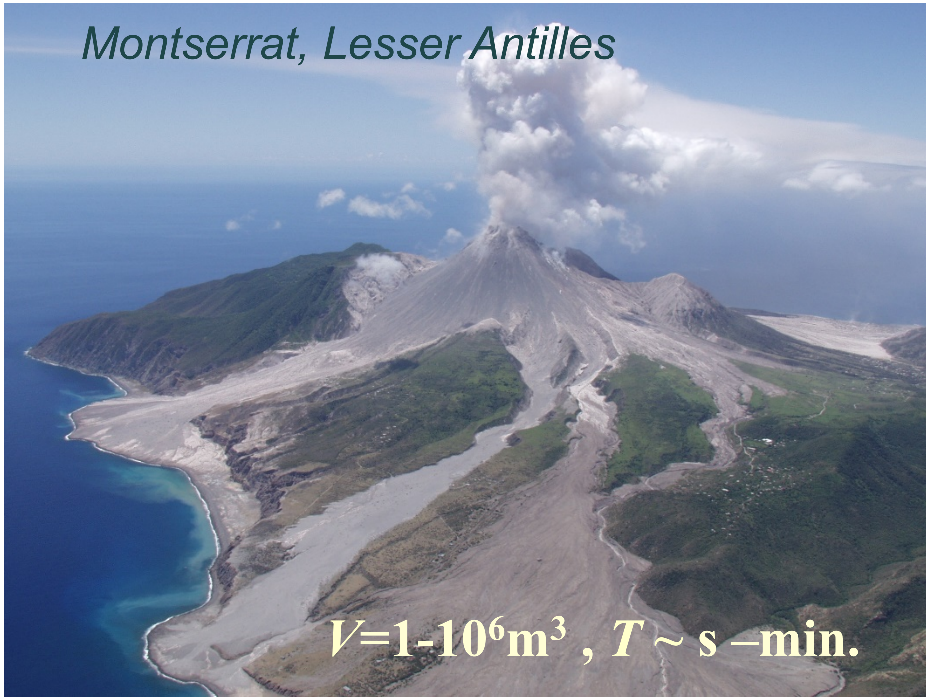

Volume scale : m^3 $\longrightarrow$ 10^5 km^3
Time scale : second $\longrightarrow$ year
$\neq$ Sources, $\neq$ Topographies

Very different rheological behavior !

Huge polydispersity

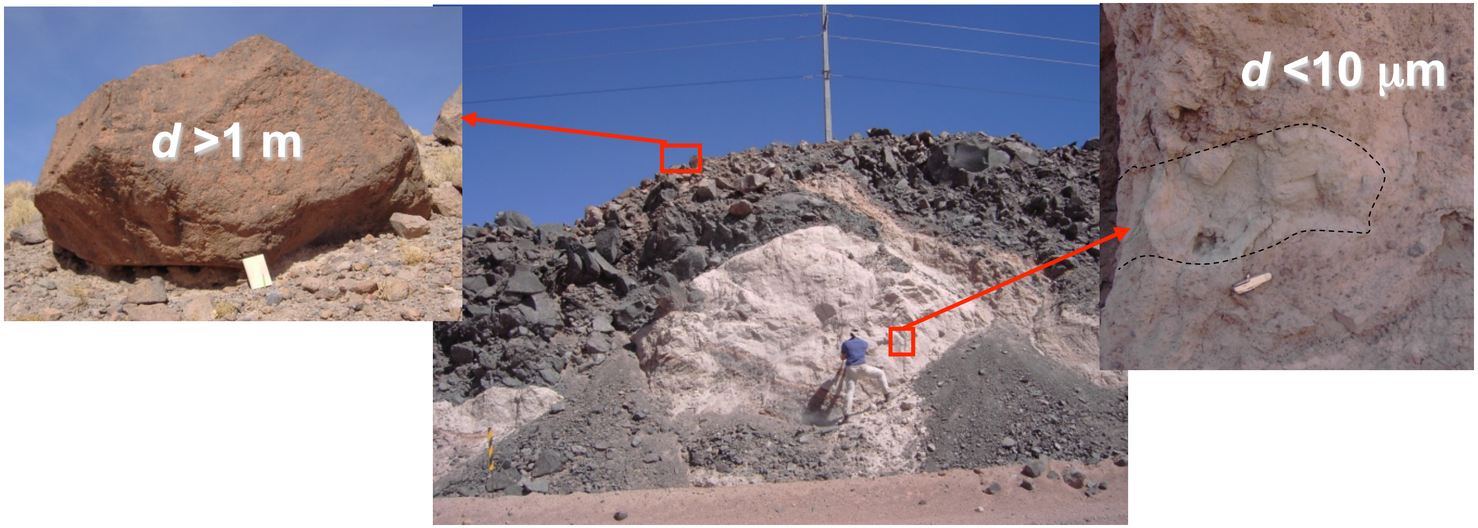

Debris avalanche deposit, Socompa, Chile

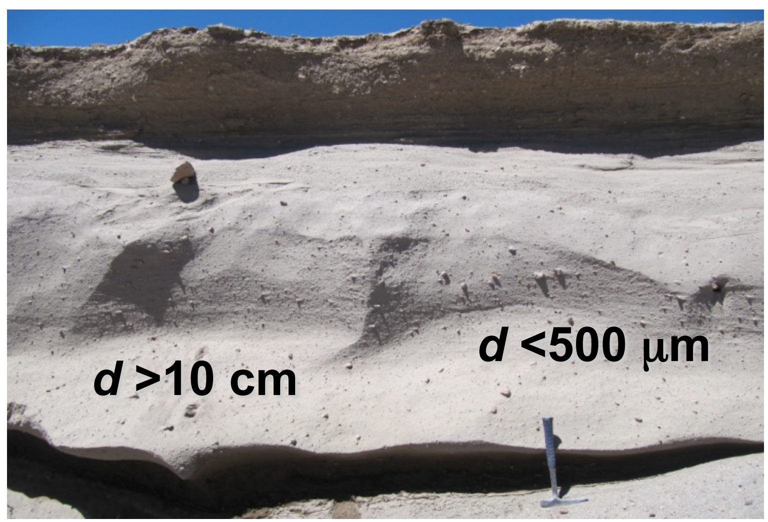

Pyroclastic flow deposit,Tutupaca volcano, Peru

Pyroclastic flows

Strong role of gaz

Significant erosion

Snow avalanches

Dense granular flow

Strong role of air

Significant erosion

Very different types of snow avalanche behavior: phase transitions, etc.

Debris flows

Debris flows, Alps

Debris flows, Iceland

Strong role of water
Significant erosion

Debris flows

Avalanches may turn into debris flows

Mud flows

(Photo H. Hubl, Vienna)

QUINDICI, Italy

Strong role of water

Fine particles

Mine collapse

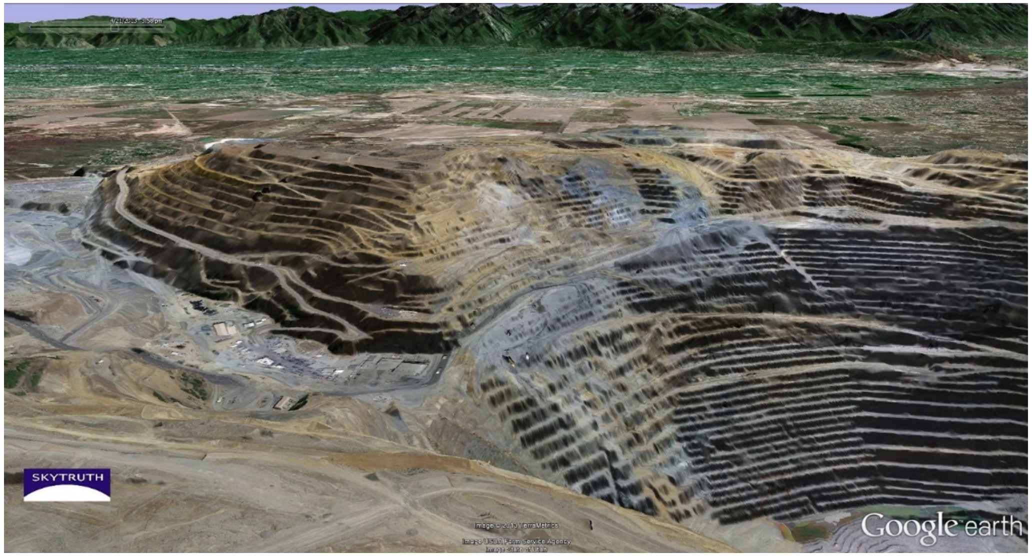

Bingham Canyon, Utah,
Avril 2013, 65 Mm^3

Two landslides

On other planets

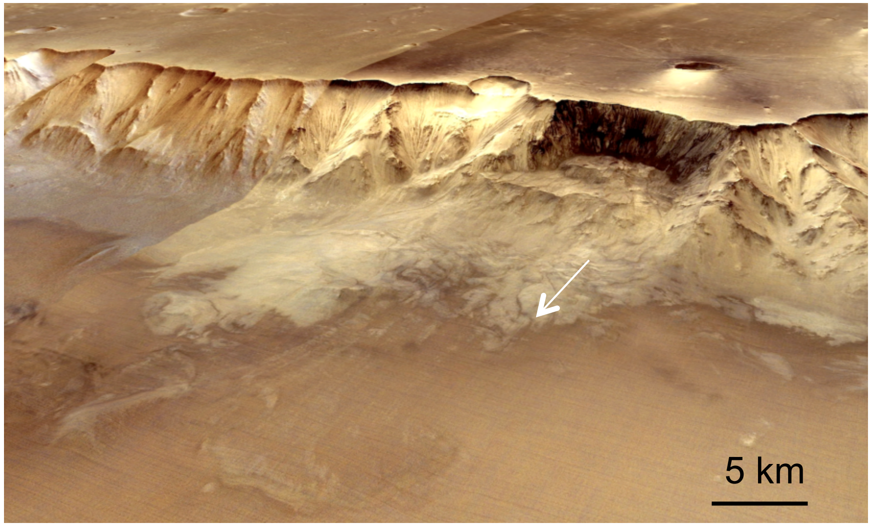

Ganges Chasma landslide,Valles Marineris, Mars

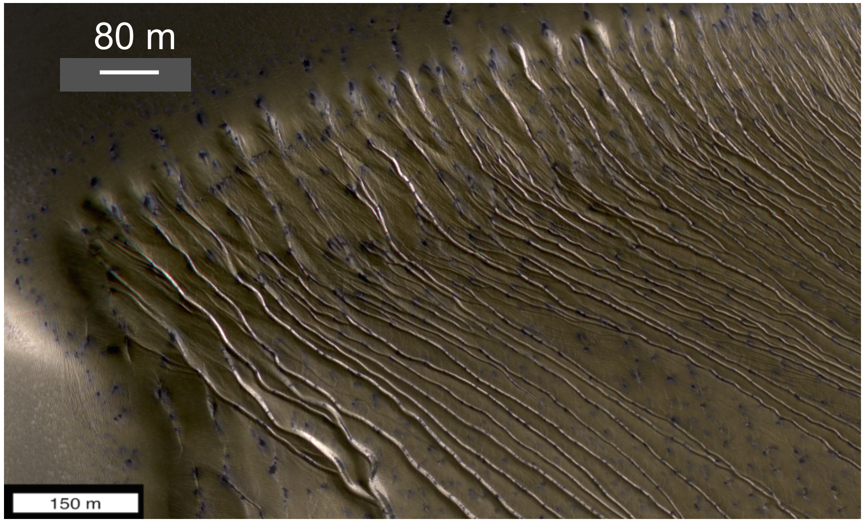

Gullies, mega-dune of Russell crater, Mars

Flow type and range of main parameters

Flow type	Setting, ambient fluid	Interstitial fluid	Particle size (m)	Particle density (kg m^{-3})	Particle volume fraction
Subaerial landslides, rockfalls, rock or debris avalanches	Subaerial, extraterrestrial[a]	Air, none, small water content	10^{-3}–10^{1}	~2000–3000	~0.4–0.7
Submarine landslides	Subaqueous	Water	—	—	—
Turbidity currents	Subaqueous	Water	10^{-4}–10^{-1}	~1500–2500	~0.001–0.1
Snow avalanches (dense, powder[c])	Subaerial	Air (water)	10^{-4}–10^{-1}	~100–1000	~0.1–0.4[b] ~0.001–0.01[c]
Pyroclastic density currents (dense[d], dilute[e])	Subaerial, subaqueous, extraterrestrial	Volcanic gases, air	10^{-6}–10^{0}	~500–3000	~0.1–0.5[d] ~0.001–0.01[e]
Debris flows, lahars	Subaerial, extraterrestrial	Water	10^{-4}–10^{0}	~2000–3000	~0.2–0.8

Flow type	Volume (m^{3})	Velocity (m s^{-1})	Thickness (m)	Runout distance (km)
Subaerial landslides, rockfalls, rock or debris avalanches	10^{0}–10^{10} 10^{9}–10^{13}[a]	10^{-1}–10^{2}	10^{-1}–10^{2}	10^{0}–10^{1} 10^{1}–10^{2}
Submarine landslides	10^{0}–10^{13}	—	10^{-1}–10^{2}	10^{1}–10^{2}
Turbidity currents	10^{6}–10^{10}	10^{0}–10^{1}	10^{1}–10^{2}	10^{1}– 10^{3}
Snow avalanches (dense, powder[c])	10^{4}–10^{6}	10^{1}–10^{2}	10^{0}–10^{1}	10^{-1}–10^{0}
Pyroclastic density currents (dense[d], dilute[e])	10^{4}–10^{8}	10^{0}–10^{1}[d] 10^{1}–10^{2}[e]	10^{0}–10^{2}	10^{0}–10^{2}
Debris flows, lahars	10^{4}–10^{9}	10^{0}–10^{1}	10^{0}–10^{1}	10^{0}–10^{2}

Delannay et al., 2017

Different physical processes

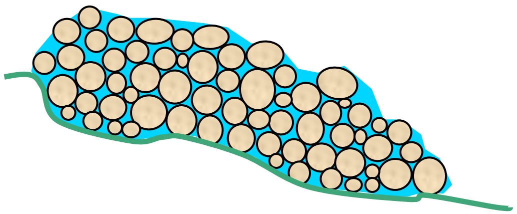

Fluid phase (water, mud)

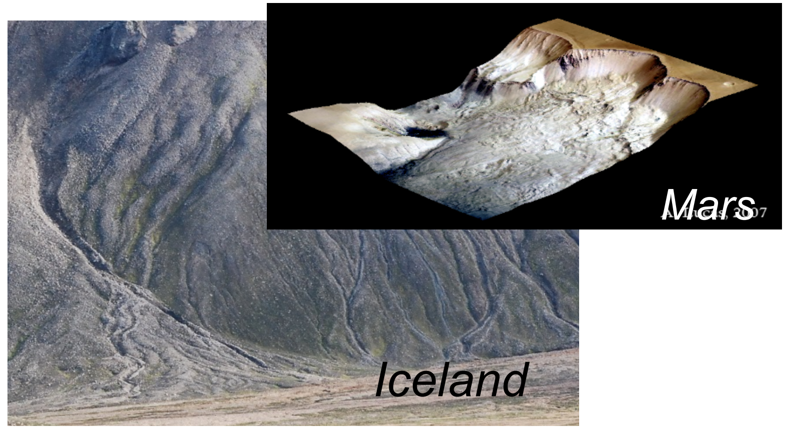

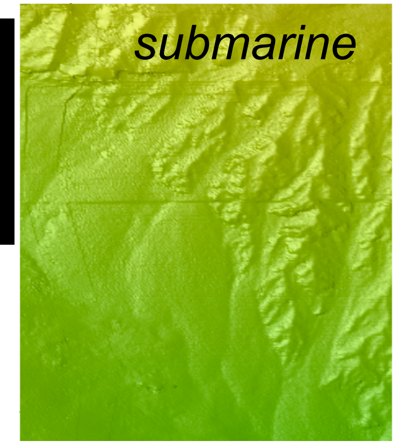

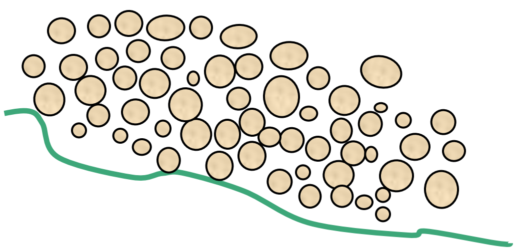

Fluidization (gaz, air)

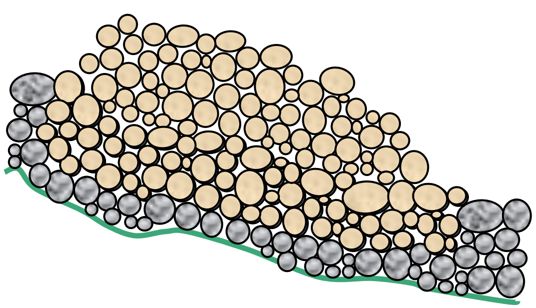

Erosion: static/flowing transition

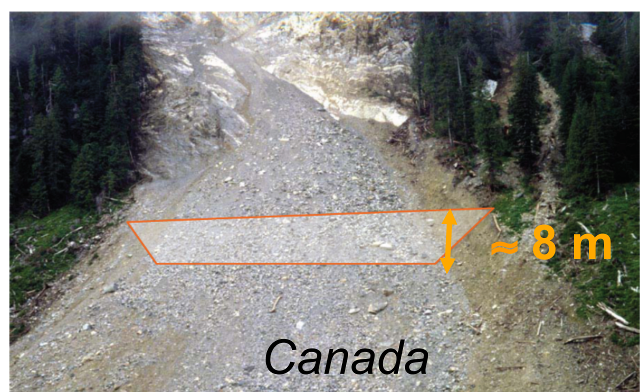

Main questions in geophysics

- How to detect geophysical flows and to assess their related hazards and indirect impact (tsunamis, etc)?
- What is the contribution of gravitational flows in erosion processes and relief evolution at the surface of the Earth and other planets?
- How are gravitational flows related to external forcing? Could they provide indicators or precursors of these forcing processes?
- What physical processes may be at the origin of the high mobility of large landslides?
- How to quantify and model erosion/deposition processes, solid/fluid interaction, polydispersity and fragmentation at the natural scale?
- How to retrieve the mechanisms of propagation and the characteristics of the flows from their deposit and/or from the generated seismic or geophysical signal?

Review paper: *Delannay, Valance, Mangeney, Roche, Richard, 2017*

Outline

I – Geophysical reality:
- Complexity of flows and physical processes
- Field data to validate rheological models of real flows
- From field observation to laboratory experiments

II – Modelling of natural landslides
- Shallow model and rheology
- Unexplained high mobility of natural landslides
- Investigating landslide dynamics: seismic data and models

III – Back to the rheology of granular materials
- Laboratory experiments
- 2D visco-plastic models
- Insight into the static/flowing interface
- Multi-layer models

What does a model need to provide results QUANTITAVELY comparable to observations ?

- Initial and boundary conditions (volume identification by geologists)
- Underlying topography (space physics, imagery)
- Detailed shape and thickness of the deposit (geology, volcanology, marine geoscientists)
- Data on the dynamics (seismologist)

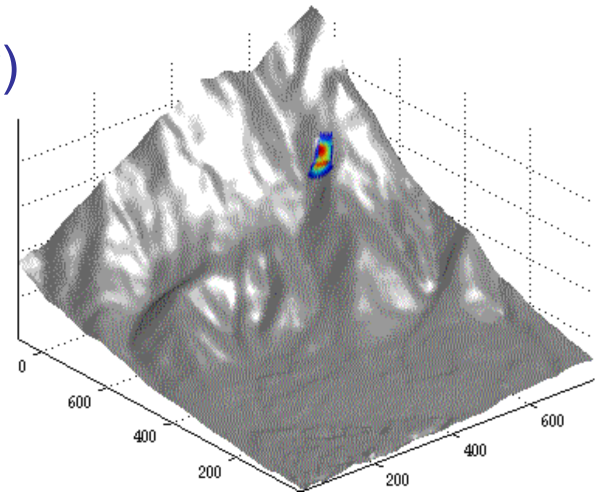

+

- Accurate description of physical processes in the models, rheological behavior (physics, mechanics)
- Develop and solve accurately the equations of flows over real topography (mathematicians)

Field data

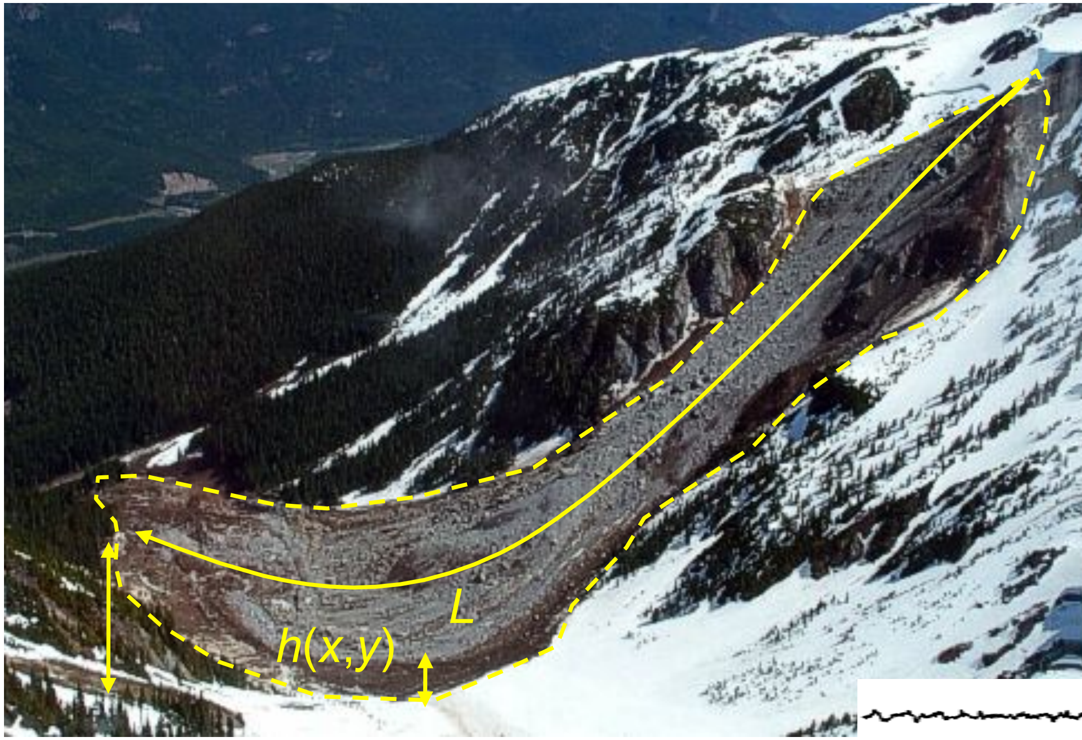

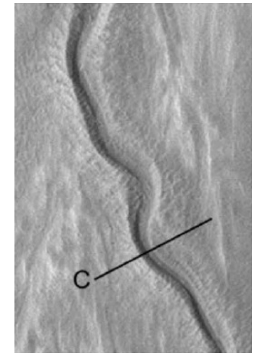

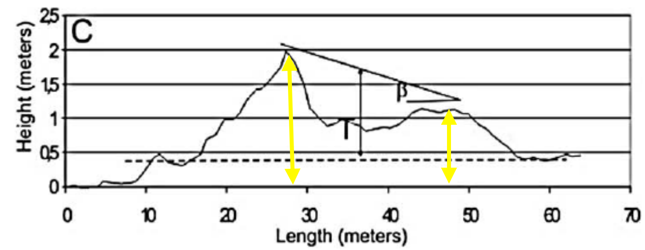

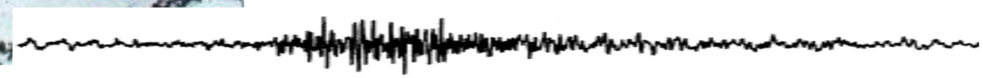

Initial conditions :

- Scar, topography pre-event

Deposit :

- Runout, area of deposit, local thickness
- Spatial distribution of thickness deposit: Fine morphology (levées, front shape…)

Dynamics:

- Witness
- Camera
- Generated seismic waves

Interaction flow/topography

Specific structures of the deposit

Hummocks, debris avalanches, Socompa, Chile

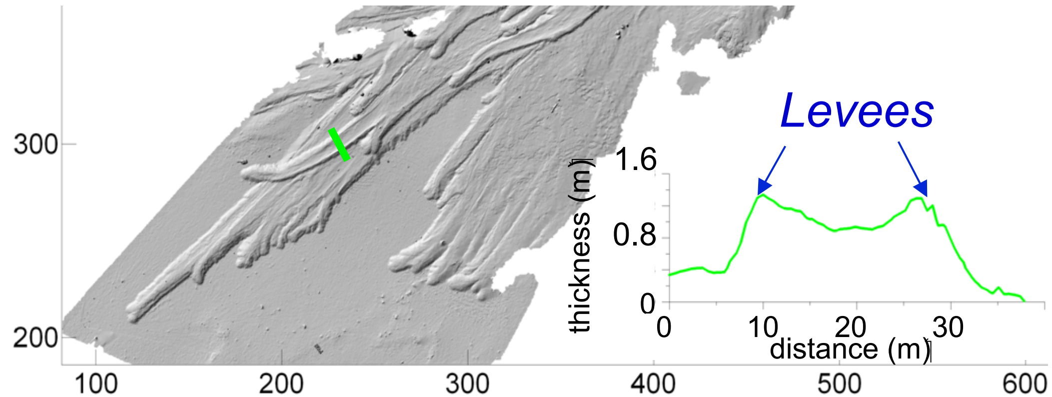

Pyroclastic flows, Lascar, Chile

Jessop et al., 2012

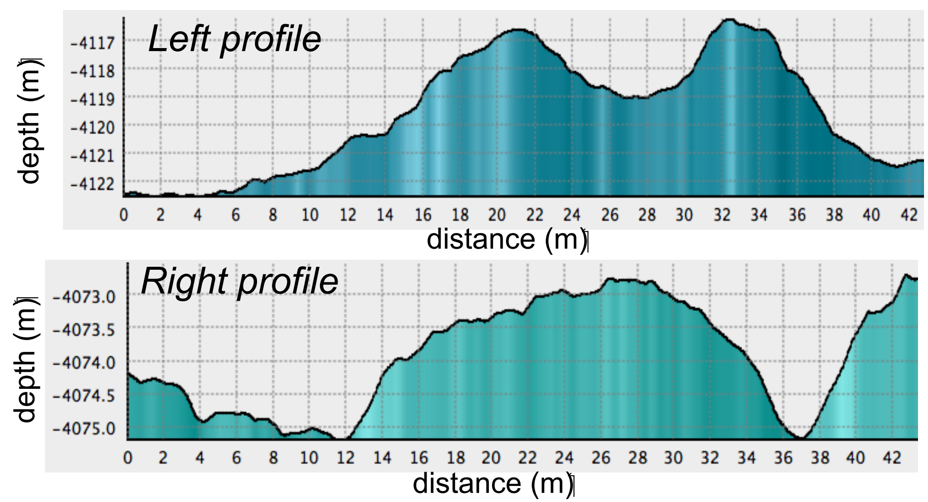

Submarine deposits, *Cannat et al., 2013*

Landslide generated seismic waves

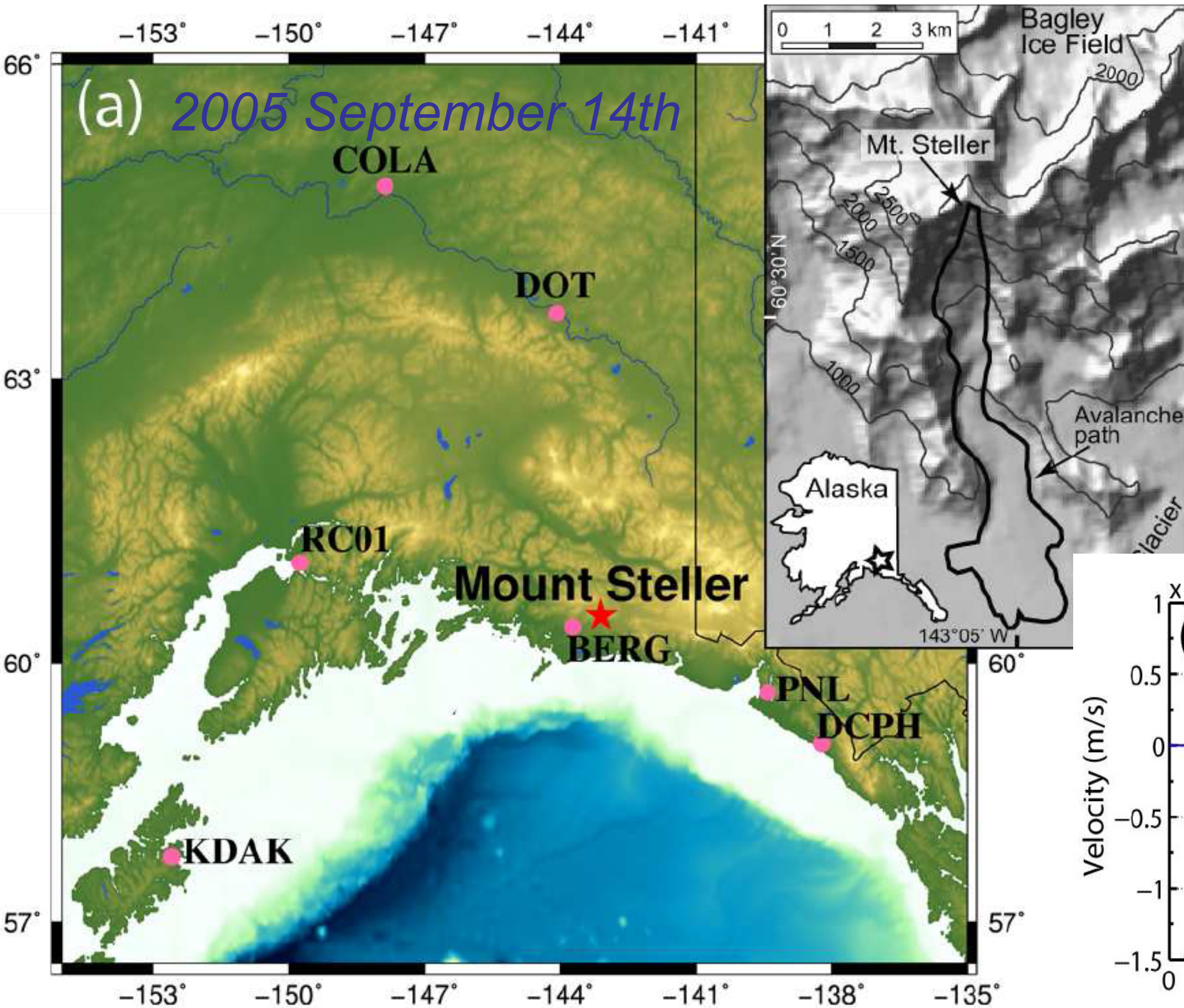

Traveled distance ~9 km

Volume : 40-60 Mm^3

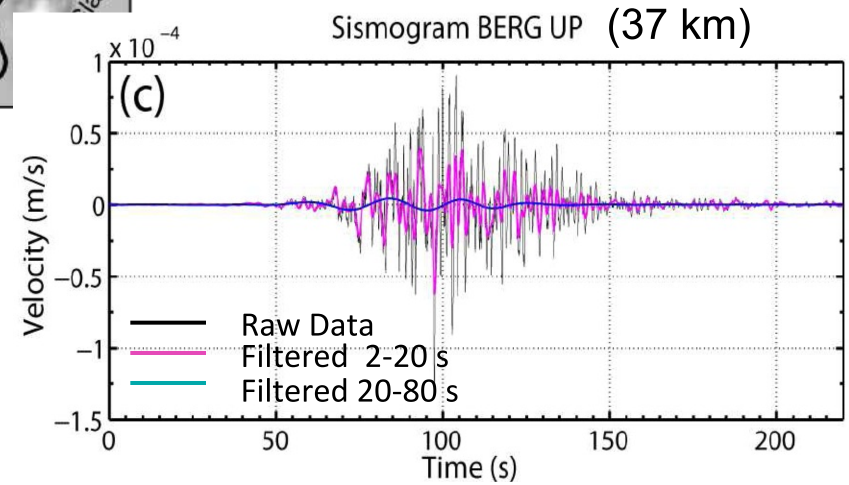

Favreau, 2010, Moretti et al., 2012, 2015

Outline

I – Geophysical reality:

- Complexity of flows and physical processes
- Field data to validate rheological models of real flows
- From field observation to laboratory experiments

II – Modelling of natural landslides

- Shallow model and rheology
- Unexplained high mobility of natural landslides
- Investigating landslide dynamics: seismic data and models

III – Back to the rheology of granular materials

- Laboratory experiments
- 2D visco-plastic models
- Insight into the static/flowing interface
- Multi-layer models

From field to laboratory scale

Natural flows
km^3

Same physical processes ?

Laboratory granular flows
cm^3

Heterogeneous materials
Few **field data**

Velocity and thickness
measurements

Numerical simulation

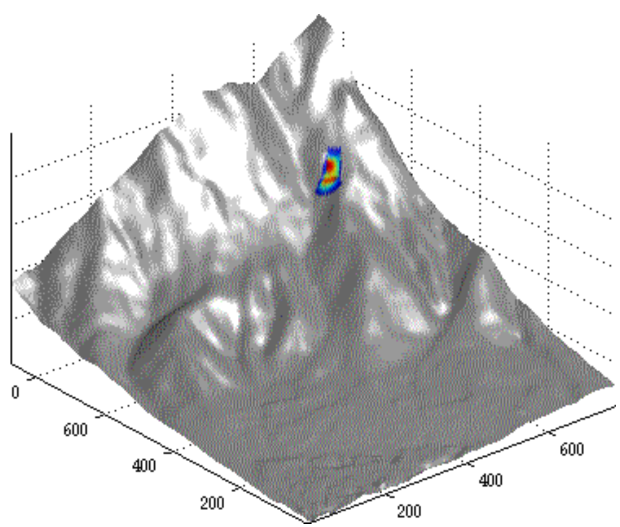

A lot of laboratory experiments !

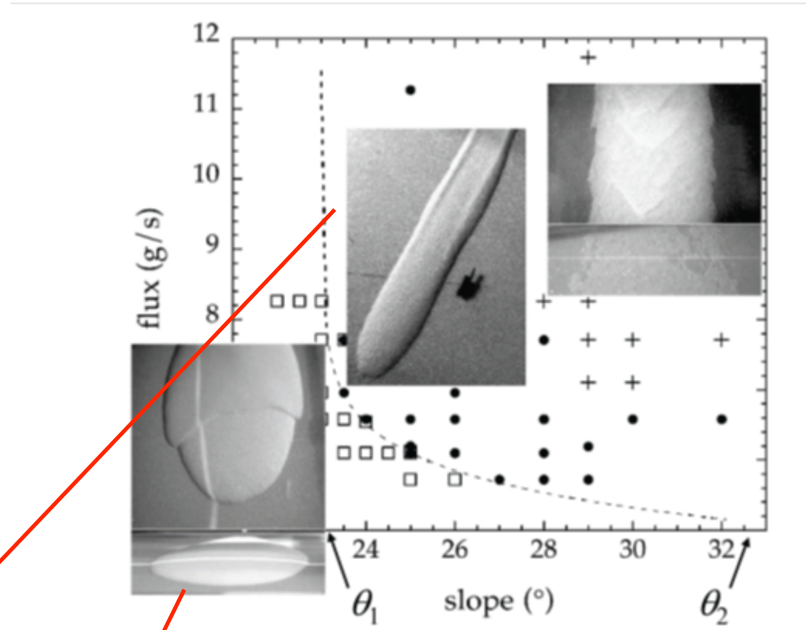

Laboratory experiments

Félix and Thomas, 2007

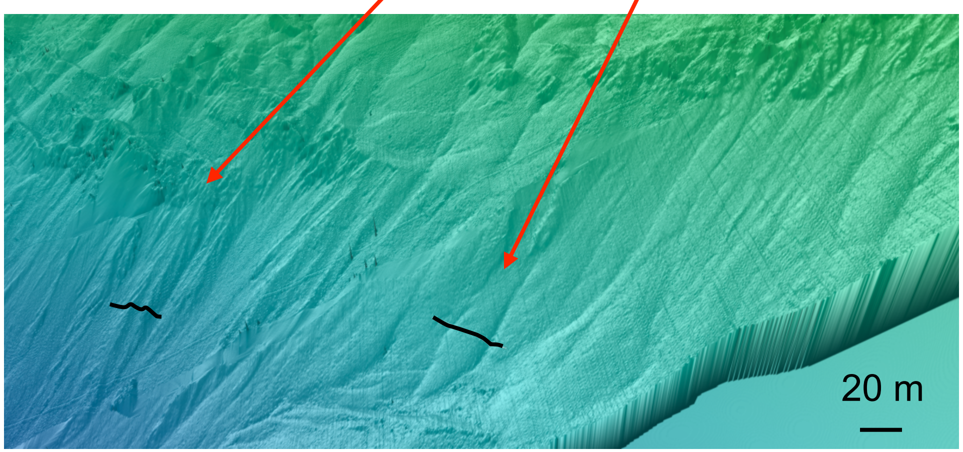

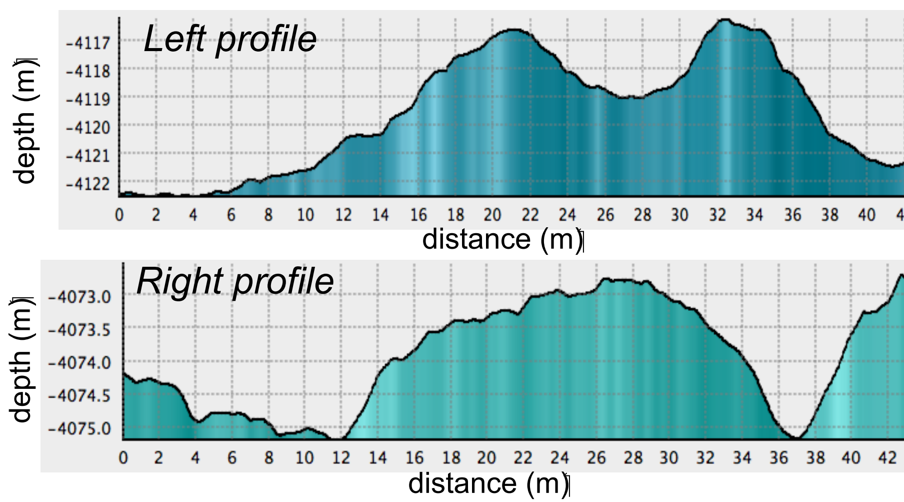

Submarine deposits, *Cannat et al., 2013*

A lot of laboratory experiments !

Role of particle size in erosion processes

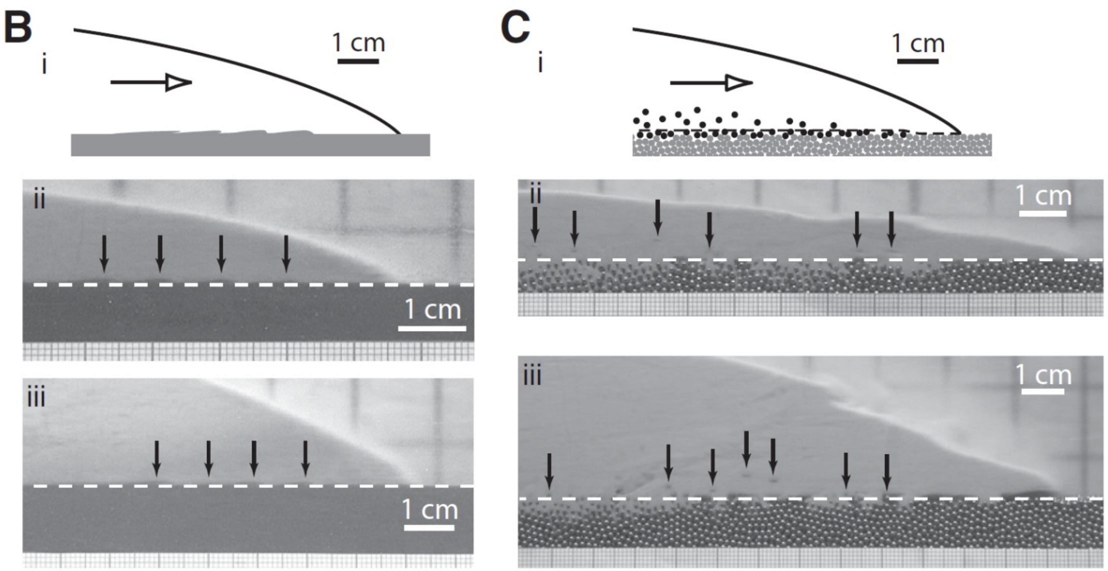

Roche et al., 2013

Segregation in self-channeling flows

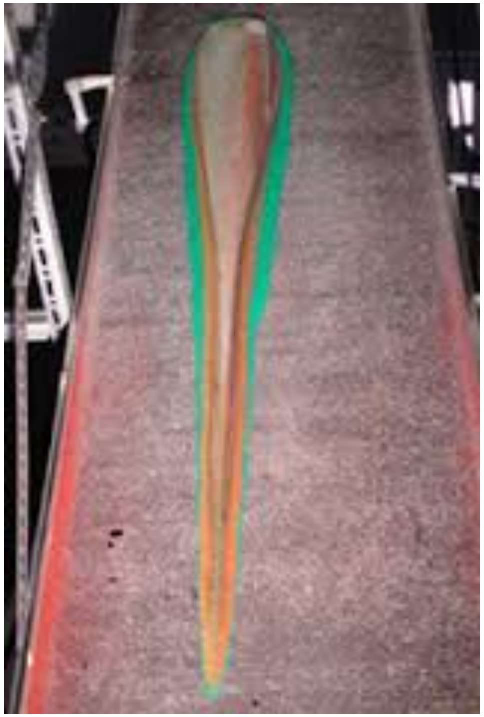

Félix and Thomas, 2004

Johnson et al., 2012

...

Main questions in physics

• How to describe the grains/fluid coupling, taking into account in particular dilatation/compression effects?

• Can we obtain constitutive relations giving a complete description of the granular flows and of their transitions (jammed, dense, dilute)?

• How can be captured the boundary conditions and how do they affect the flow? This includes mobile interfaces related to erosion/deposition

• How to quantify and describe theoretically the evolution of granular size distribution in space and time (segregation, fragmentation processes) and its coupling with the flow?

Physics and Geophysics

• How to measure granular and fluid stresses, particle volume fraction, etc. in both experimental and natural flows?

Review paper: *Delannay, Valance, Mangeney, Roche, Richard, 2017*

Outline

I – Geophysical reality:
- Complexity of flows and physical processes
- Field data to validate rheological models of real flows
- From field observation to laboratory experiments

II – Modelling of natural landslides
- Shallow model and rheology
- Unexplained high mobility of natural landslides
- Investigating landslide dynamics: seismic data and models

III – Back to the rheology of granular materials
- Laboratory experiments
- 2D visco-plastic models
- Insight into the static/flowing interface
- Multi-layer models

Equations

Mass and momentum conservation equations:

Compressibility ?

$$\frac{\partial \rho}{\partial t} + \nabla.(\rho \mathbf{u}) = 0$$

rheology

$$\frac{\partial (\rho \mathbf{u})}{\partial t} = -\mathbf{u}\nabla.(\rho \mathbf{u}) - \rho \mathbf{u}.\nabla \mathbf{u} + \mathrm{div}\,\sigma + \rho \mathbf{g}$$

Issues:

- Rheology of natural granular materials
- Applicability to natural flows : computational time requires approximations

Hard to discriminate model approximation and rheological behaviour!

Numerical modelling of landslides

- Modeling

2D thin layer model

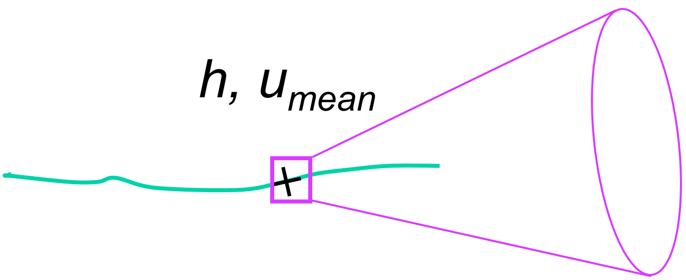

Mean scale

Reasonable computational cost

Empirical flow law …

$\mu = \tan\delta$

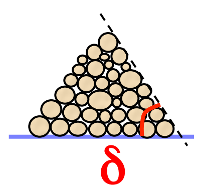

3D continuum model

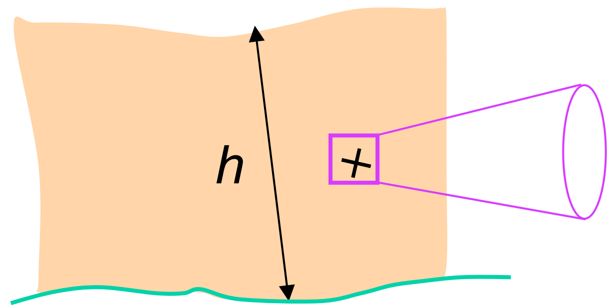

Local scale

High computational cost

Local flow law $\mu(I)$

Discrete element model

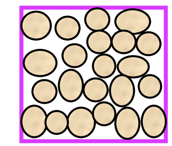

Grain scale

High computational cost

Particle size distribution ???

Yet far from the precise description of the rheology of natural materials !!!!

Semi-empirical modelling

Thin layer approximation on 2D topography

- Flow on complex natural topography

$\Downarrow$

high computational cost $\Rightarrow$ $\boxed{a = \dfrac{H}{L} << 1}$ small aspect ratio

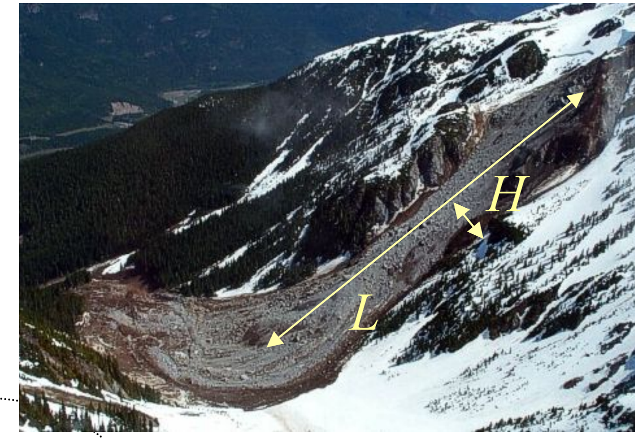

Savage and Hutter, 1989

- Depth-averaged thin layer model model

$$h = \mathcal{O}(\epsilon) \quad \nabla b = \mathcal{O}(\epsilon) \quad u^{\mathbf{x}} = \overline{u^{\mathbf{x}}}(t, \mathbf{x}) + \mathcal{O}(\epsilon^2)$$

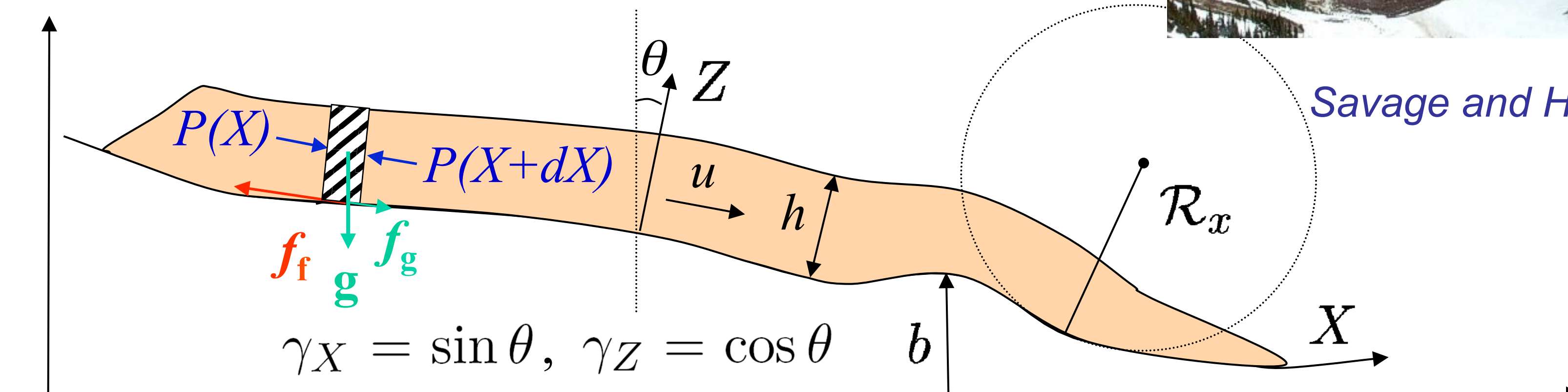

$$\underbrace{\frac{\partial u}{\partial t} + u\frac{\partial u}{\partial X}}_{\text{inertia}} = \underbrace{\gamma_X g}_{\text{gravity}} \underbrace{- K\frac{\partial}{\partial X}(g\gamma_Z h)}_{\text{pressure gradient}} \underbrace{- \mu\left(g\gamma_Z + \frac{u^2}{\mathcal{R}_x}\right)\frac{u}{|u|}}_{\text{Coulomb friction}}$$

$\mu = \tan\delta$

Coulomb friction law:

$$\| \mathbf{T}_t \| \geq \sigma_c \Rightarrow T_i = -\sigma_c \frac{u_i}{\| \mathbf{u} \|} \quad \text{with} \quad \sigma_c = \mu\rho g \gamma_z h = \mu \| \mathbf{T}_n \|$$

$$\| \mathbf{T}_t \| < \sigma_c \Rightarrow \mathbf{u} = 0$$

Thin layer approximation on 3D topography

- Until very recently and still used :

  arbitrary extension of 1D equations …

- **Full curvature tensor**

SHALTOP

$$\mathcal{H} = c^3 \begin{pmatrix} \frac{\partial^2 b}{\partial x^2} & \frac{\partial^2 b}{\partial x \partial y} \\ \frac{\partial^2 b}{\partial x \partial y} & \frac{\partial^2 b}{\partial y^2} \end{pmatrix}$$

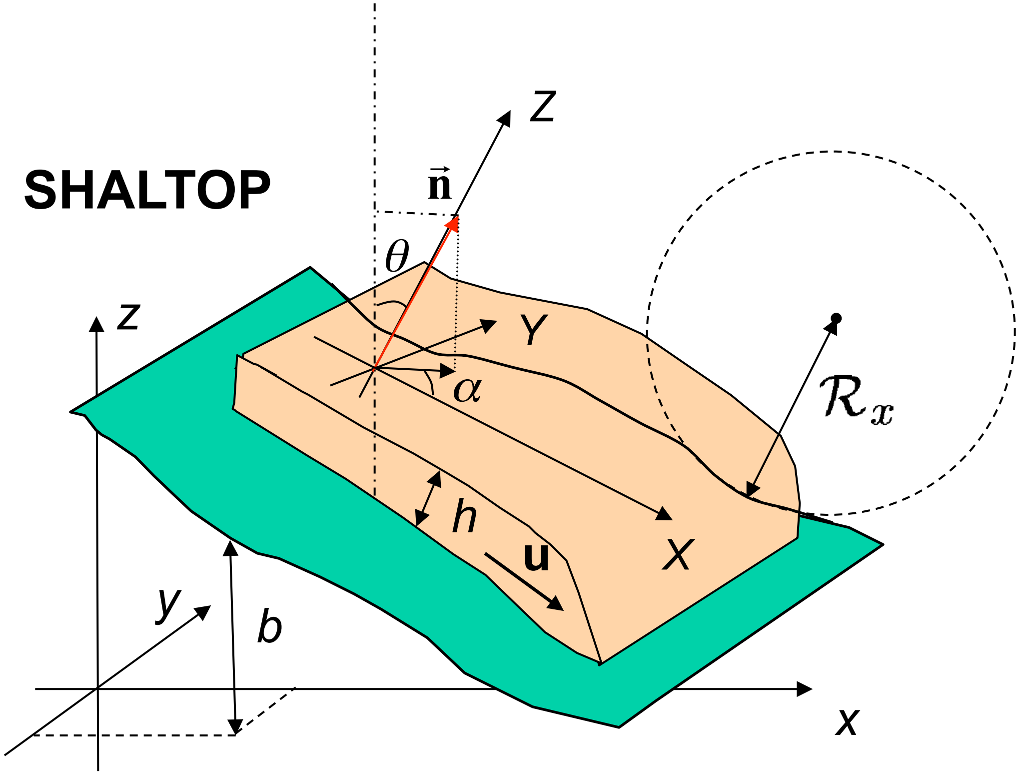

First equations including these « centrifugal » forces

Bouchut, Mangeney, Perthame, Vilotte, 2003;
Bouchut and Westdickenberg, 2004;
Mangeney, Bouchut, Thomas, Vilotte, Bristeau, 2007

Empirical law deduced from experiments

Steady uniform flows on planes with different inclinations

Pouliquen 1999, Forterre and Pouliquen 2003

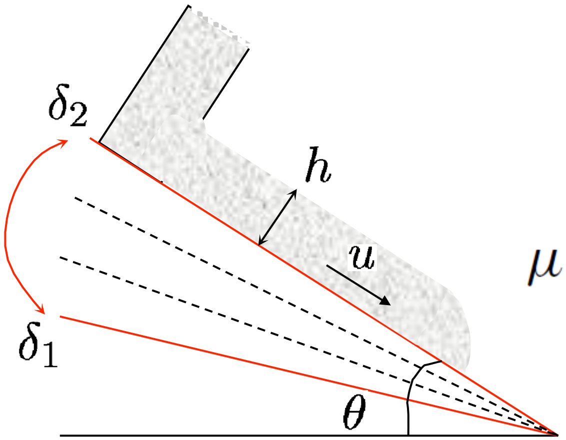

Steady uniform flows: tan $\theta = \mu$, with μ = tan δ

$$\mu(Fr, h) = \mu_s + \frac{\mu_2 - \mu_s}{\frac{\beta h}{\mathscr{L} Fr} + 1} \qquad Fr = \frac{\bar{u}}{\sqrt{gh\cos\theta}}$$

Origin of the $\mu(I)$ rheology

$$\delta_s = 20.9° \quad \delta_2 = 32.76° \quad \beta = 0.136 \quad \mathscr{L} = 0.825 \times 10^{-3} \text{ m}$$

Friction ↗ when thickness ↘

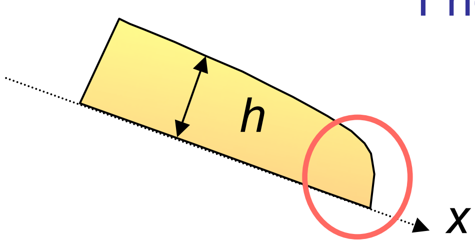

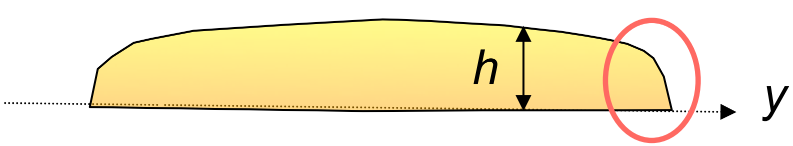

Additional viscous terms *Gray and Edwards, 2014*

Granular flows over complex topography

$$\partial_t(h/c) + \nabla_x \cdot (h\boldsymbol{u}') = 0$$

$$\partial_t \boldsymbol{u}' + c\boldsymbol{u}' \cdot \nabla_x \boldsymbol{u}' + \frac{1}{c}(Id - \boldsymbol{s}\boldsymbol{s}^t)\nabla_x(g(hc+b)) =$$
$$\frac{-1}{c}(\boldsymbol{u}'^t H \boldsymbol{u}')\boldsymbol{s} + \frac{1}{c}(\boldsymbol{s}^t H \boldsymbol{u}')\boldsymbol{u}' - \frac{g\mu c \boldsymbol{u}'}{\sqrt{c^2\|\boldsymbol{u}'\|^2 + (\boldsymbol{s}\cdot\boldsymbol{u}')^2}}\left(1 + \frac{\boldsymbol{u}'^t H \boldsymbol{u}'}{gc}\right)_+$$

$$\overrightarrow{n} = \left(-\frac{\nabla_{\mathbf{x}} b}{\sqrt{1+||\nabla_{\mathbf{x}} b||^2}}, \frac{1}{\sqrt{1+||\nabla_{\mathbf{x}} b||^2}}\right) \equiv (-\mathbf{s}, c) \in \mathbb{R}^2 \times \mathbb{R}$$

$$\mu = \mu_s$$

or

$$\mu(Fr, h) = \mu_s + \frac{\mu_2 - \mu_s}{\dfrac{\beta h}{\mathscr{L} Fr} + 1}$$

Other empirical terms can be added …. with more unconstrained parameters…

Limits of the Thin Layer Approximation

Initial aspect ratio: $a = H_i / R_i$

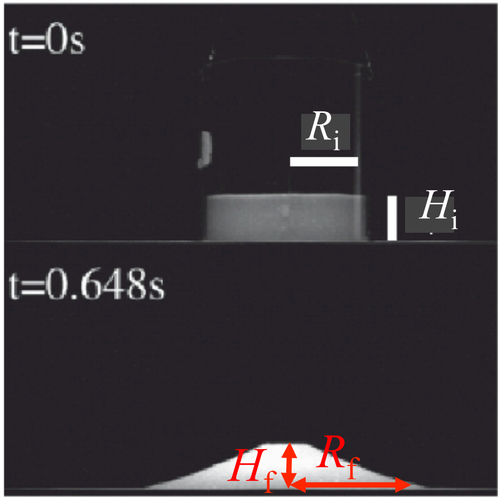

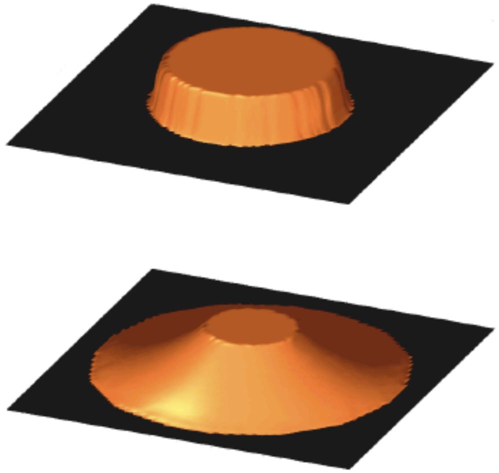

a=0.8

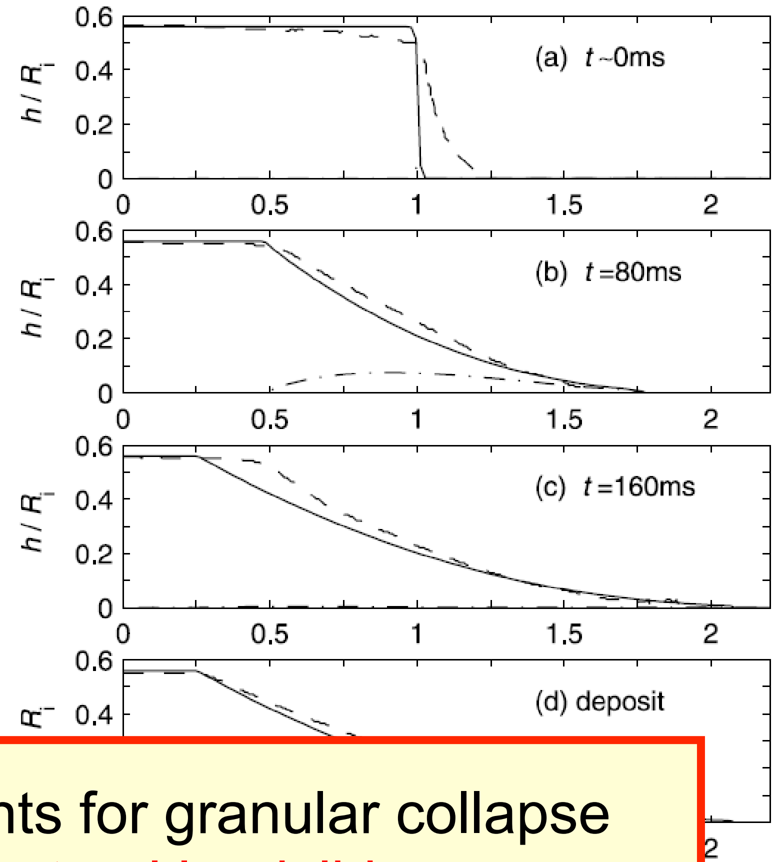

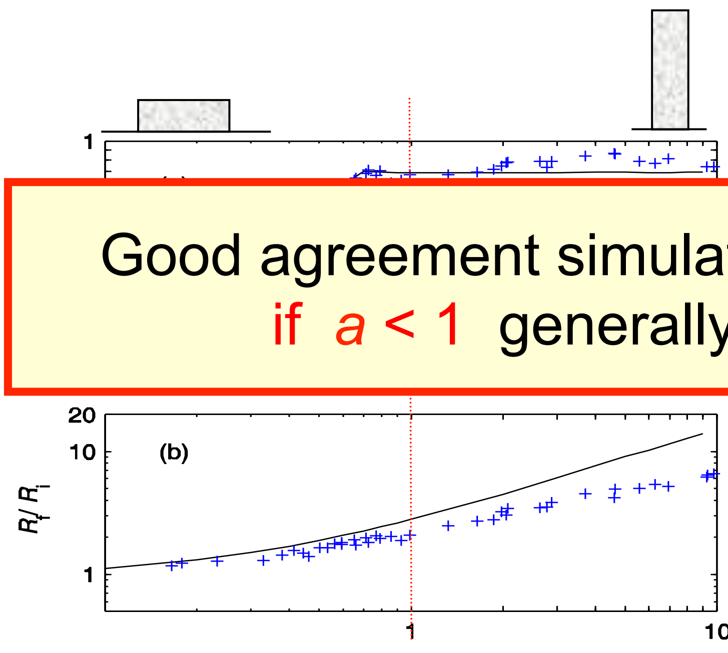

Good agreement simulation/experiments for granular collapse
if $a < 1$ generally the case for natural landslides

$$\mu = \tan \delta$$

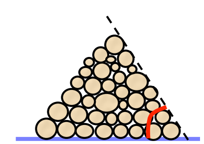

$\delta \approx 30° > \delta_r = 21°,\ \delta_a = 29°$

Granular flow experiments

Granular column collapse over an inclined channel

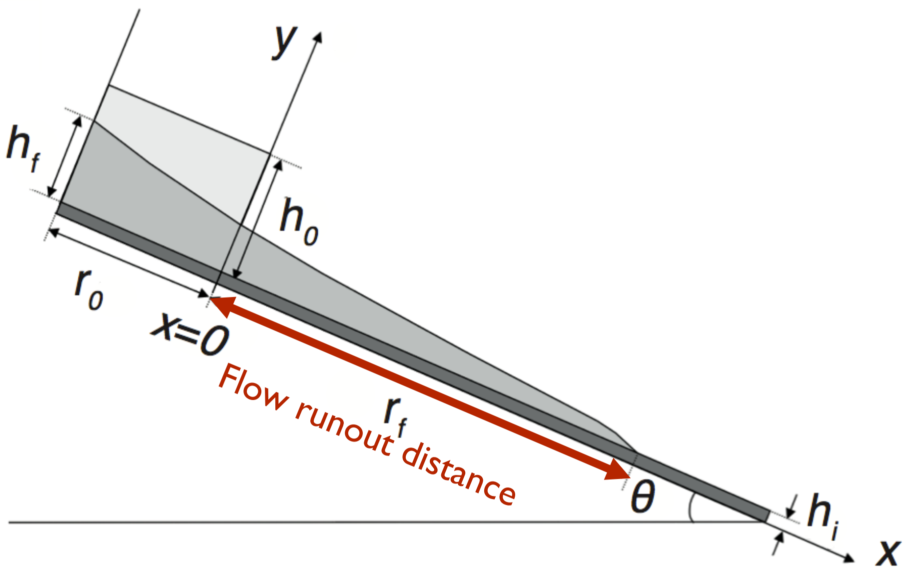

Friction angles:
repose $\delta_r \approx 23° \pm 0.5°$, avalanche $\delta_a \approx 25° \pm 0.5°$

Control parameters:
- slope angle: $0° < \theta < \delta$
- volume $V = h_0\, r_0\, W$
- aspect ratio $a = h_0 / r_0$
- column shape
- channel width

Mangeney, Roche, Hungr, Mangold, Faccanoni, Lucas, 2010
Farin, Mangeney, Roche, 2014

Granular collapse over a rigid bed

Laboratory experiments

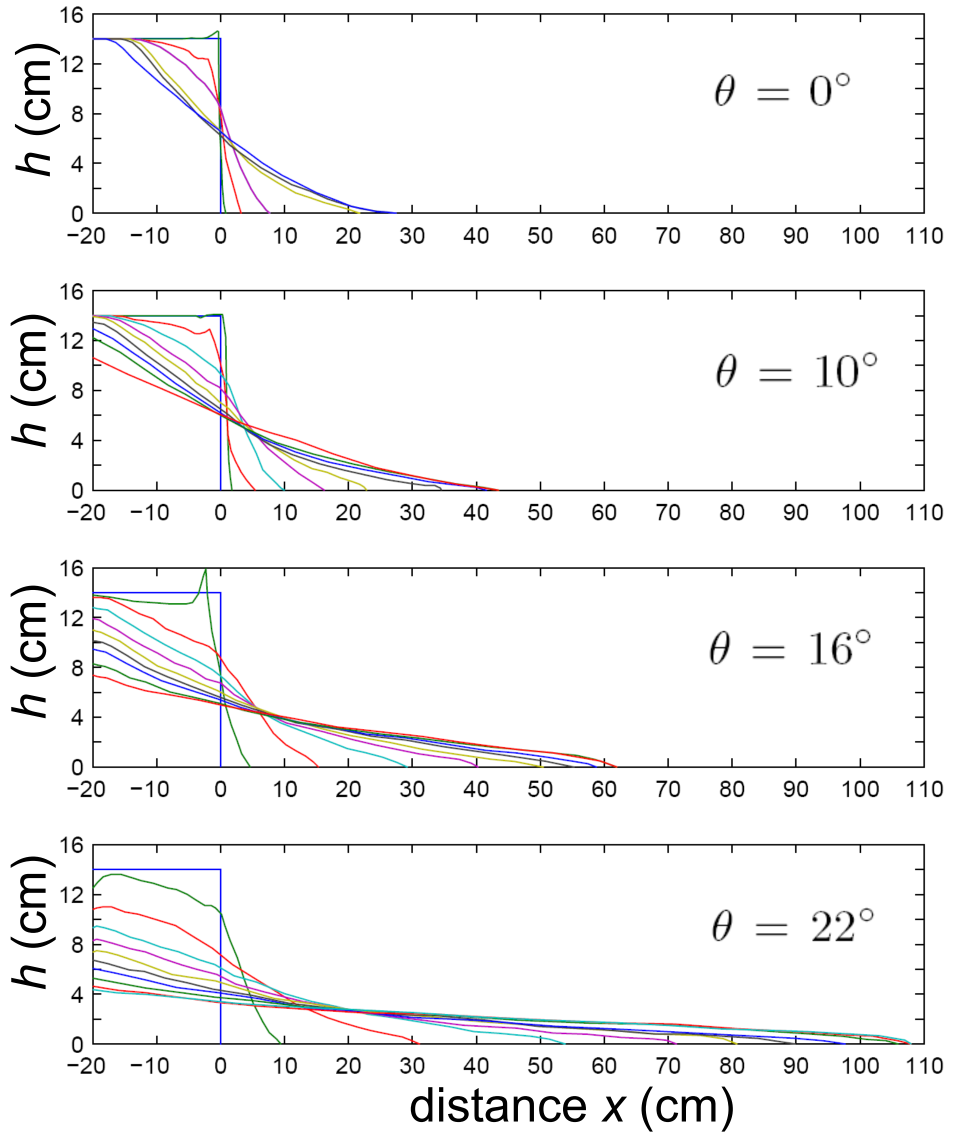

Monolayer (Saint-Venant) versus Multilayer models

$\mu_s = \tan(25.5°) \approx 0.48$ $\theta = 22^\circ$ $\mu(I)$

t=0.16 s

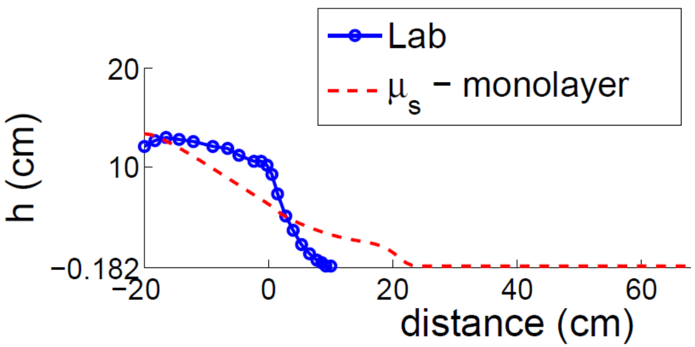

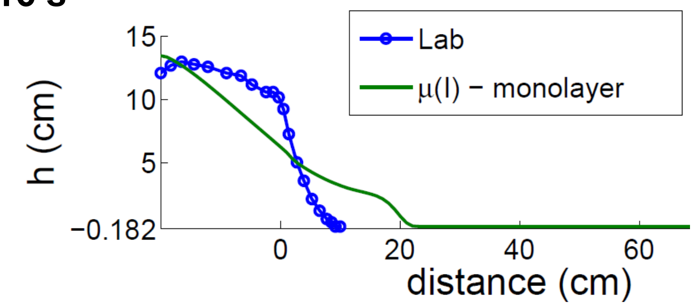

t=0.8 s

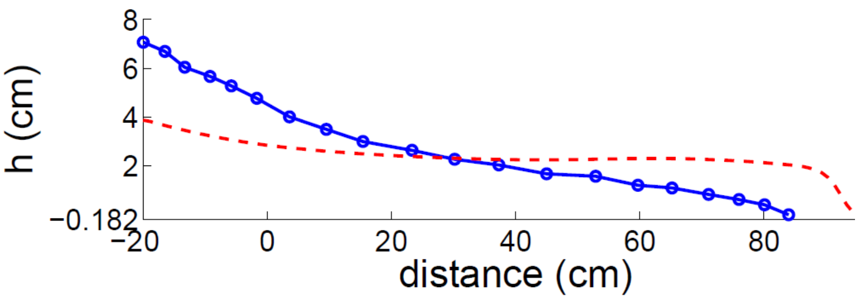

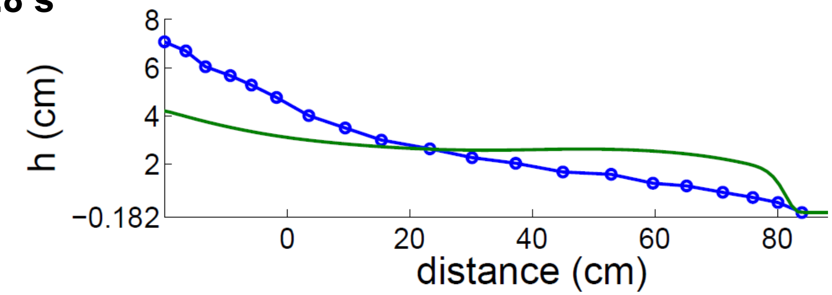

t=2.56 s

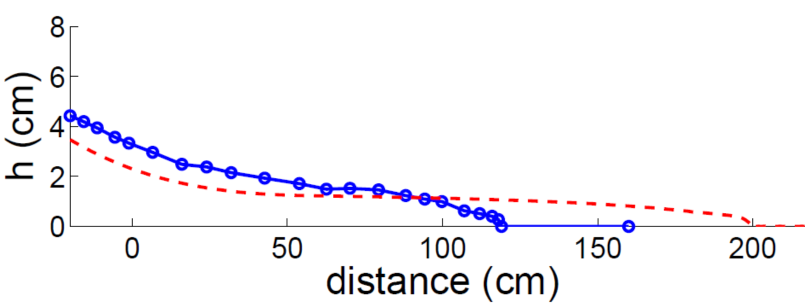

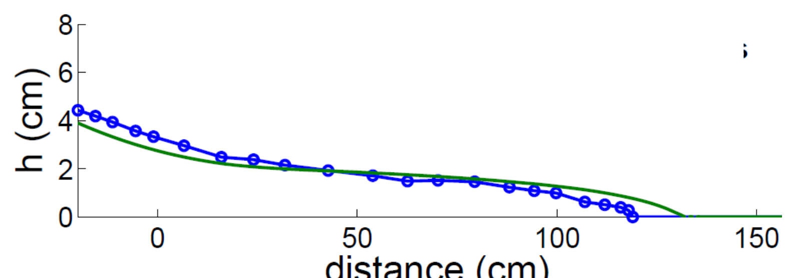

Fernandez-Nieto, Garres, Mangeney, Narbona-Reina, 2016

Calibration of the constant friction angle

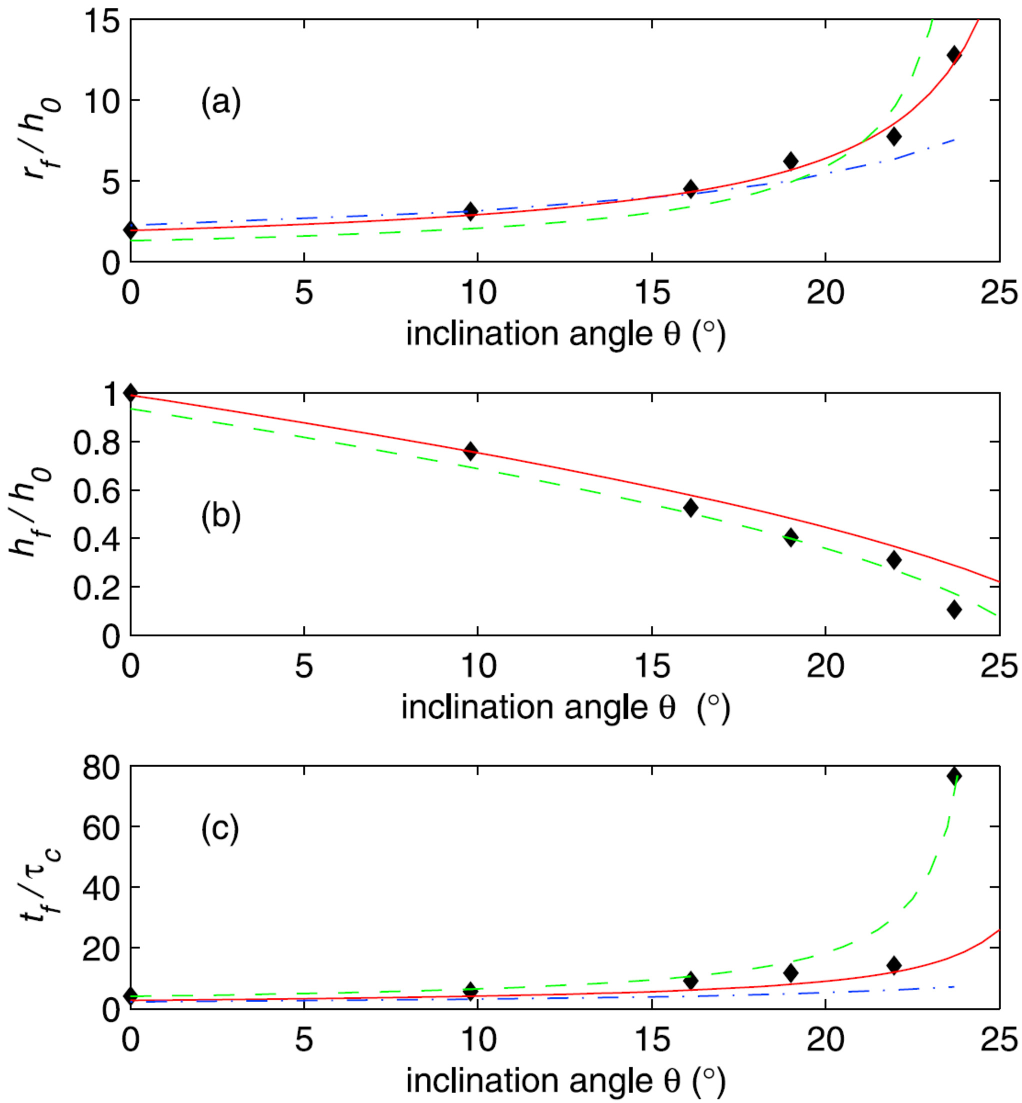

δ_s = 27.5°, μ_s=0.52

Simulation of self-channeling flows

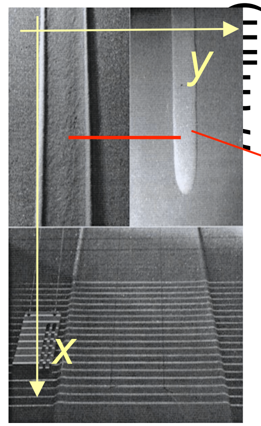

Numerical simulation

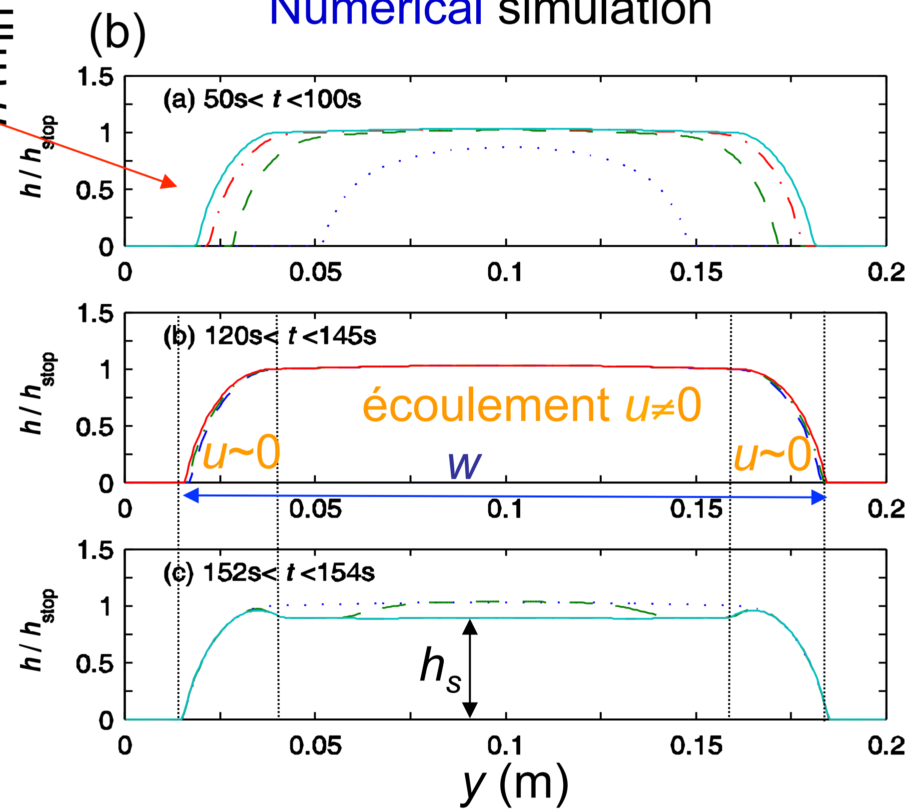

Experimental results

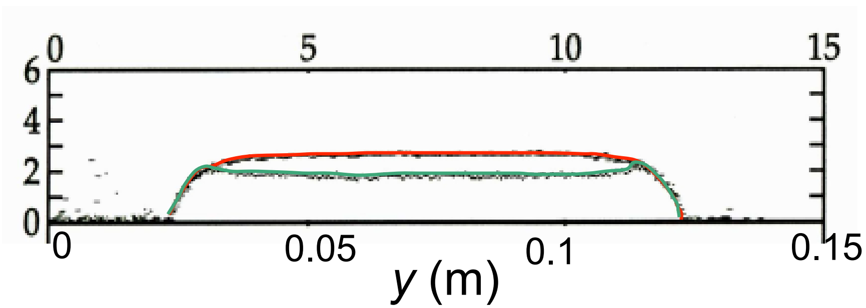

Very good qualitative agreement between experimental and numerical results

only with
$$\mu(Fr, h) = \mu_s + \frac{\mu_2 - \mu_s}{\dfrac{\beta h}{\mathscr{L} Fr} + 1}$$

Mangeney et al. 2007, Johnson and Gray, 2011

Outline

I – Geophysical reality:
- Complexity of flows and physical processes
- Field data to validate rheological models of real flows
- From field observation to laboratory experiments

II – Modelling of natural landslides
- Shallow model and rheology
- Unexplained high mobility of natural landslides
- Investigating landslide dynamics: seismic data and models

III – Back to the rheology of granular materials
- Laboratory experiments
- 2D visco-plastic models
- Insight into the static/flowing interface
- Multi-layer models

Simulation of natural flows

Simulation of observed deposits (Switzerland)

$\mu = \tan\delta$: empirical description of the mean dissipation

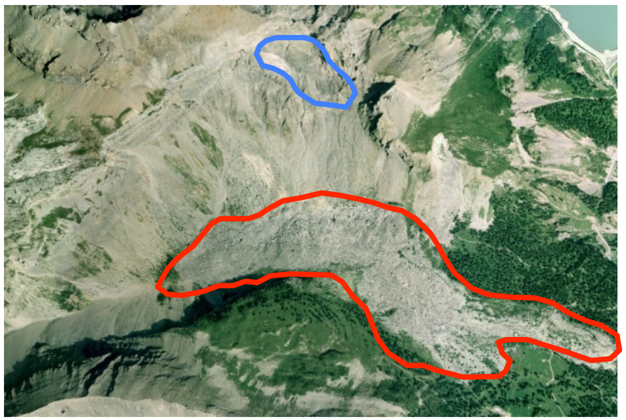

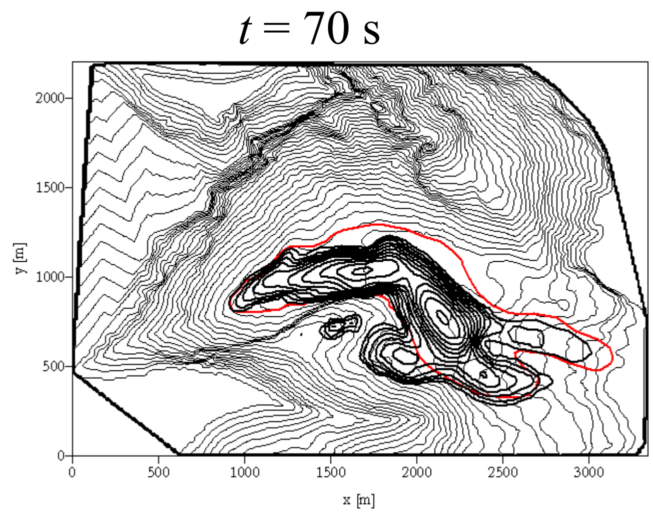

Calibrated friction angle : $\delta = 17°$

Small compared to friction angles of natural materials ! $\delta_r \approx 35°$

Origin of the high mobility of natural flows ?

Pirulli and Mangeney, 2008

Simulation of a large variety of natural flows

Simulation with empirical friction coefficient

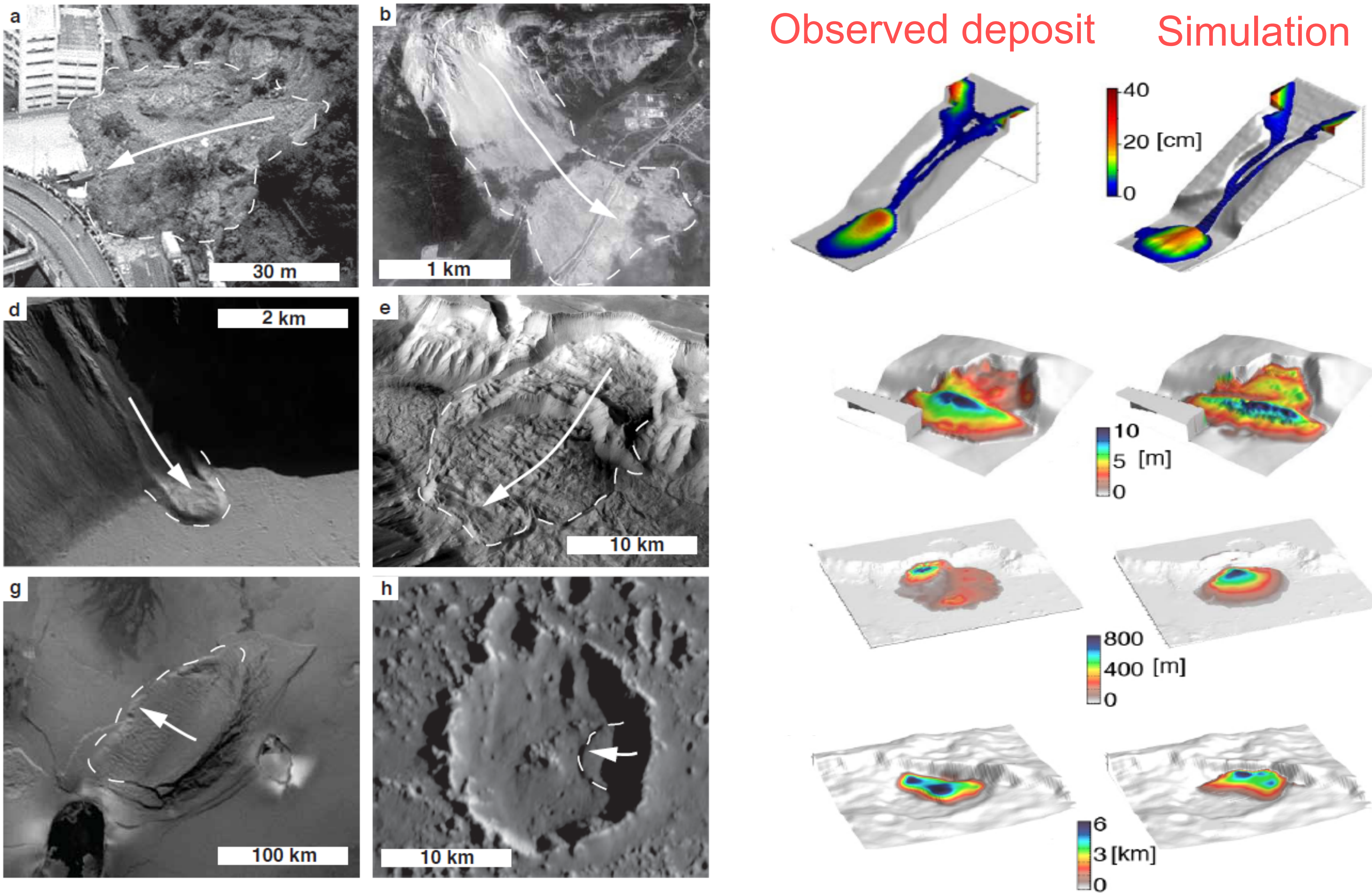

Lucas, Mangeney, Ampuero, Nature Communications, 2014

Empirical friction laws based on deposit data

Friction coefficient $\mu = \tan \delta$

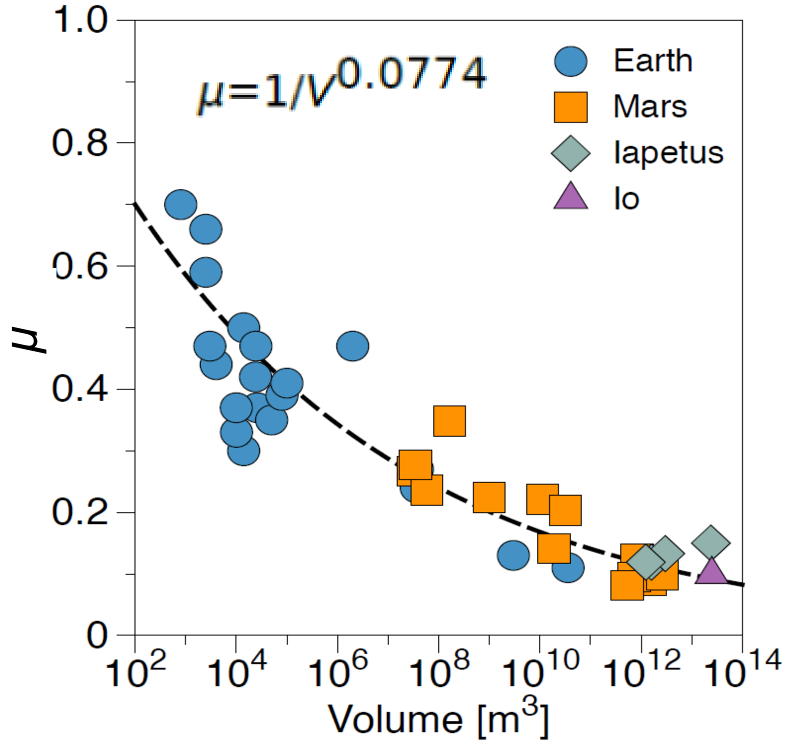

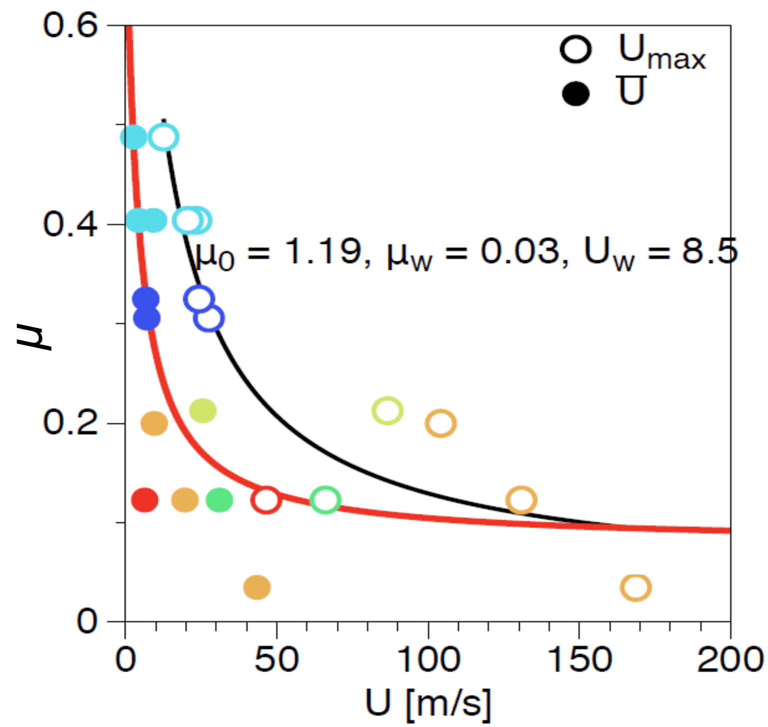

$$\mu(U) = \frac{\mu_o - \mu_w}{(1 + \|U\|/U_w)} + \mu_w$$

Physical origin ?

$$\mu_o = 0.84,\ \mu_w = 0.11,\ U_w = 4\ \mathrm{m.s}^{-1}$$

Laboratory experiments at high velocity :

Roche, Van Den Wildenberg, Delannay, Valance, Mangeney, 2017

Reproduce small to large landslides

Well reproduce observed deposits of 40 landslides

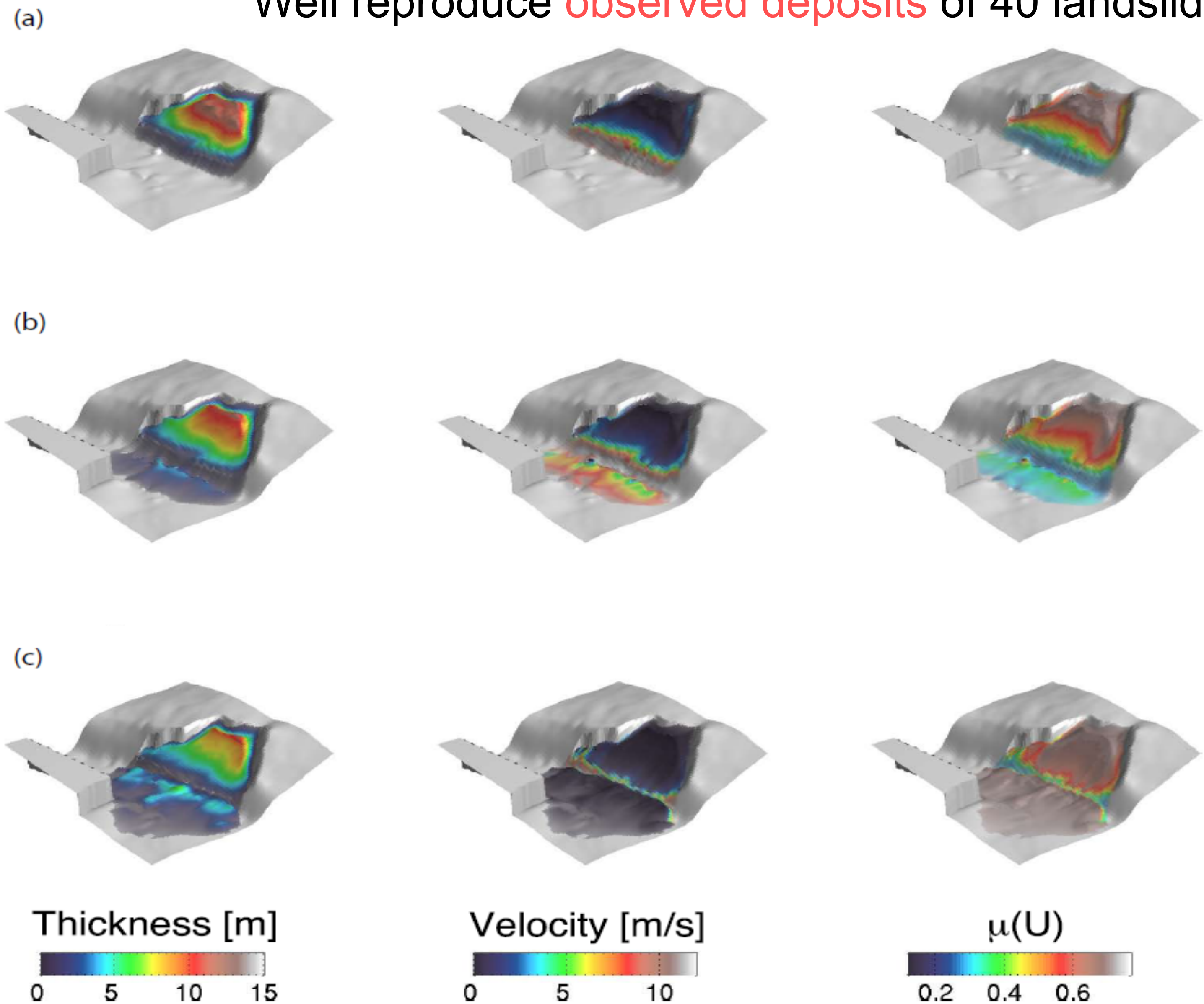

With the same parameters

Improve deposit morphology

Friction coefficient $0.1 < \mu < 0.8$

Simulation of the Mt-Steller landslide

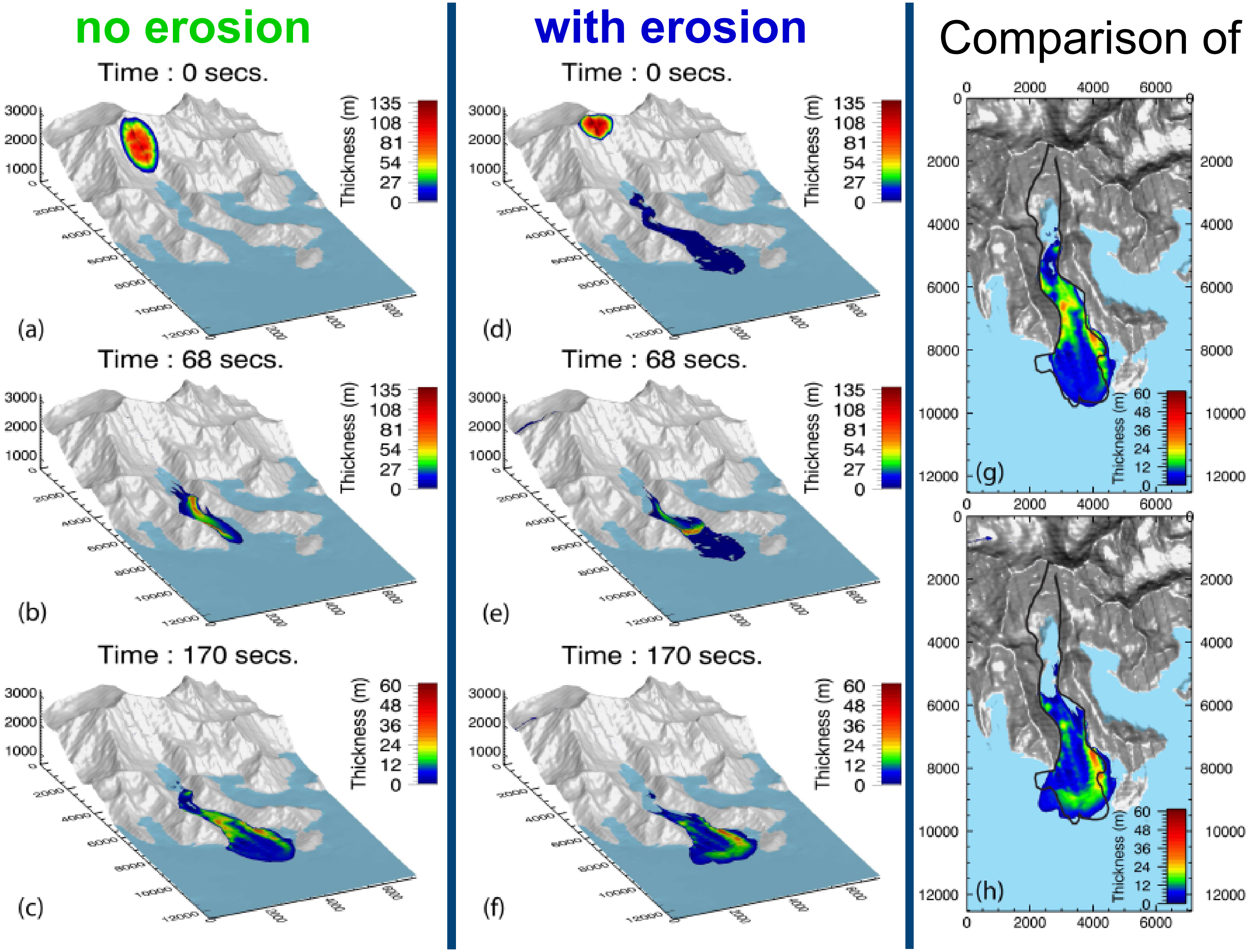

Moretti et al. 2012, 2015

The deposit area is not enough to constrain landslide models !!

Outline

I – Geophysical reality:
- Complexity of flows and physical processes
- Field data to validate rheological models of real flows
- From field observation to laboratory experiments

II – Modelling of natural landslides
- Shallow model and rheology
- Unexplained high mobility of natural landslides
- Investigating landslide dynamics: seismic data and models

III – Back to the rheology of granular materials
- Laboratory experiments
- 2D visco-plastic models
- Insight into the static/flowing interface
- Multi-layer models

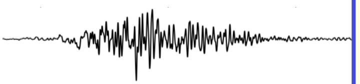

Data on the landslide dynamics

- Measurements of flow dynamics: seismic waves

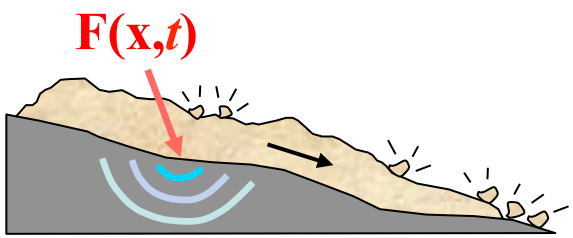

Information on landslides

- Basic picture

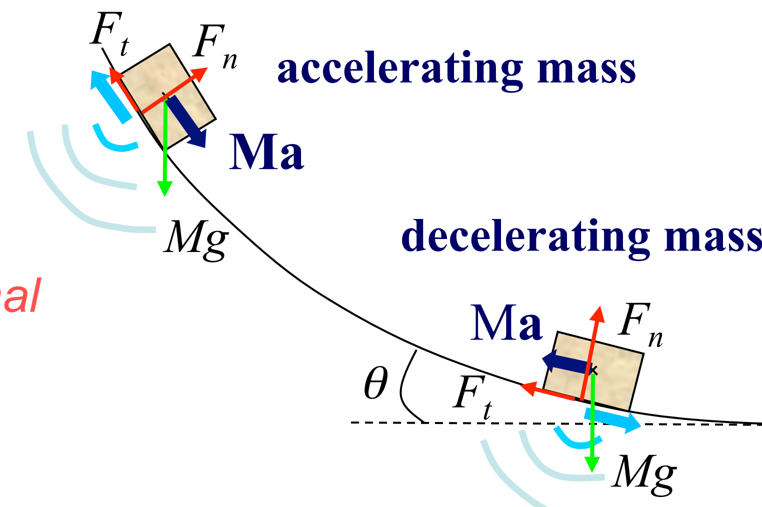

Long period signal

Seismic data interpreted with oversimplified landslide source models

Brodsky et al. 2003, Yamada et al. 2013, Allstadt 2013, Zhao et al. 2014, …

Numerical simulation and inversion of landquakes

Low frequency direct or inverse approach

Landslide simulation **Earth Green functions** **Seismic data**

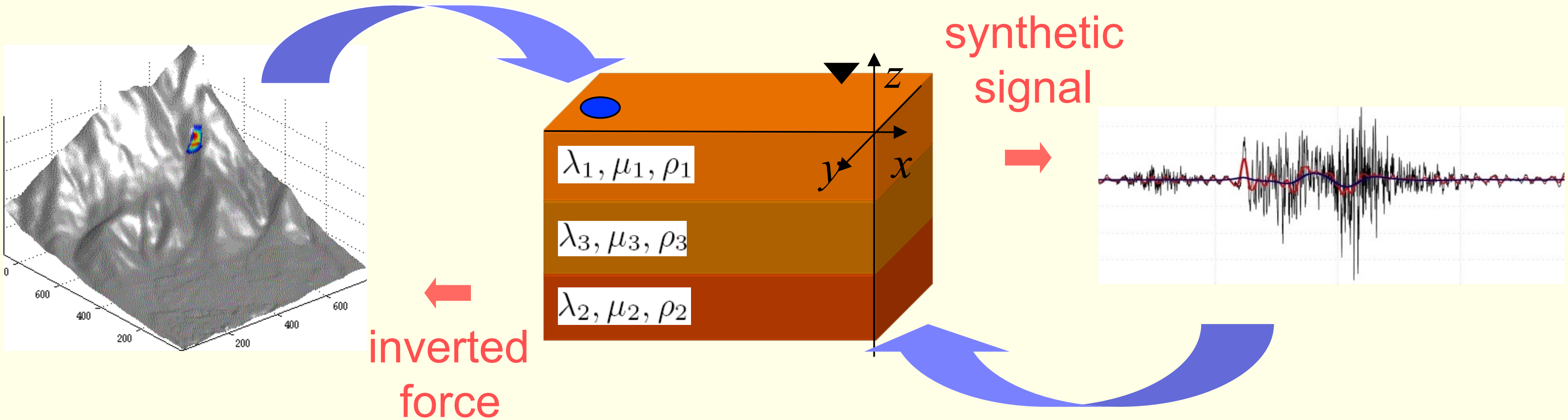

Mangeney et al., 2005, 2007

Favreau et al., 2010
Moretti et al., 2012, 2015

Time-dependent basal stress field applied on top of the terrain

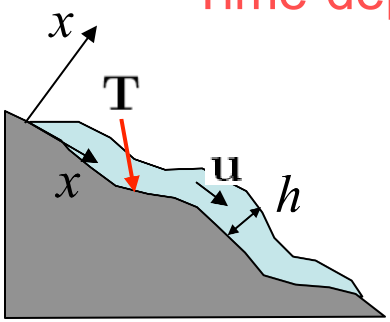

$$\mathbf{T} = \rho g h \left(\cos\theta + \boxed{\frac{\mathbf{u}_h^t \mathcal{H} \mathbf{u}_h}{g \cos^2\theta}} \right) \left(\mu \frac{u_X}{\|\mathbf{u}\|}, \mu \frac{u_Y}{\|\mathbf{u}\|}, -1 \right)$$

Curvature effects

Thurweiser landslide

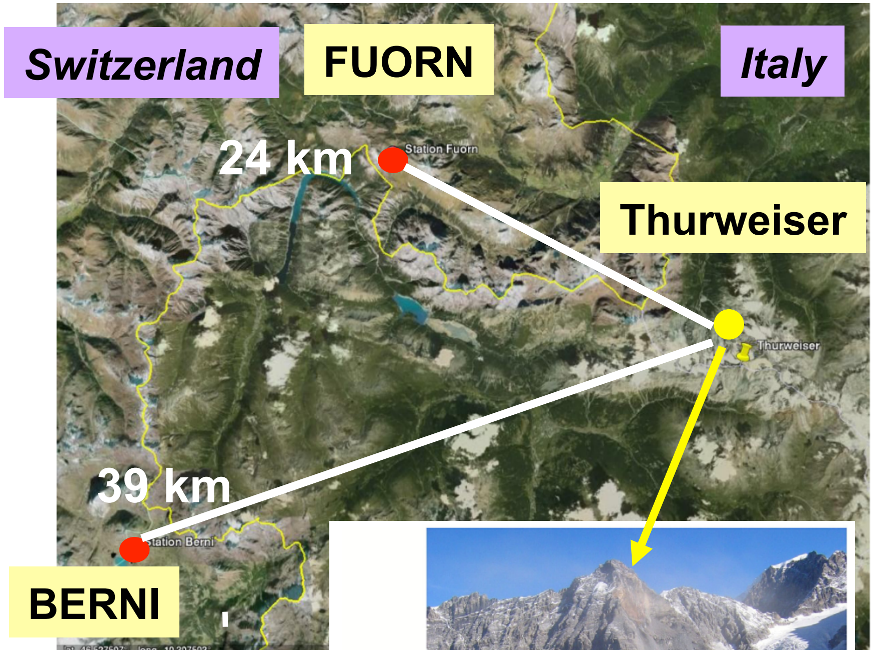

September 2004

V=2.5×10^6 m^3

R_f=2.9 km

$T_\mathrm{f} \approx$ 90 s

Sosio et al., 2008

Numerical simulation

without glacier

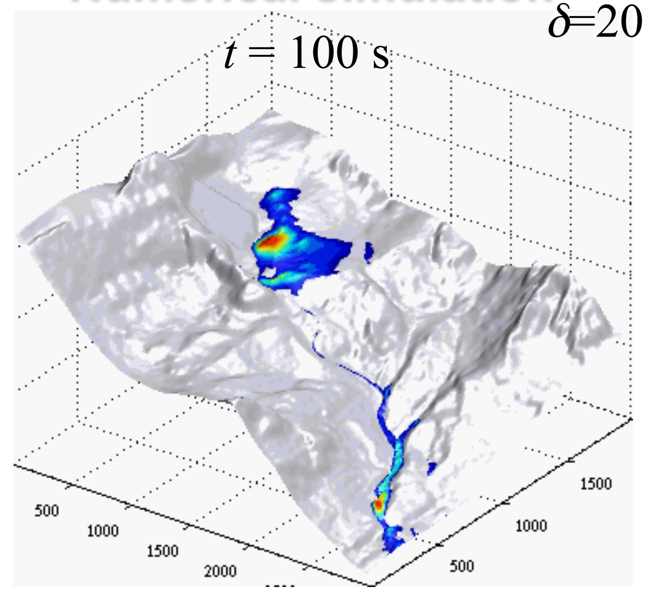

with glacier

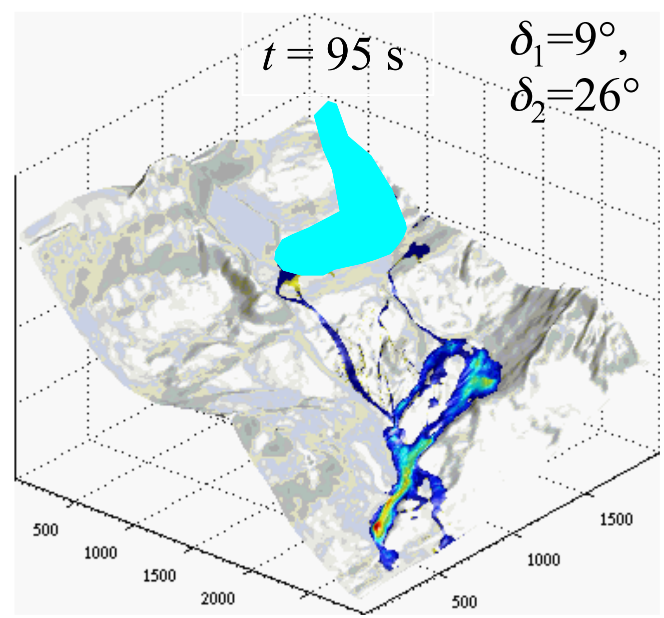

Thurweiser landslide seismic waves

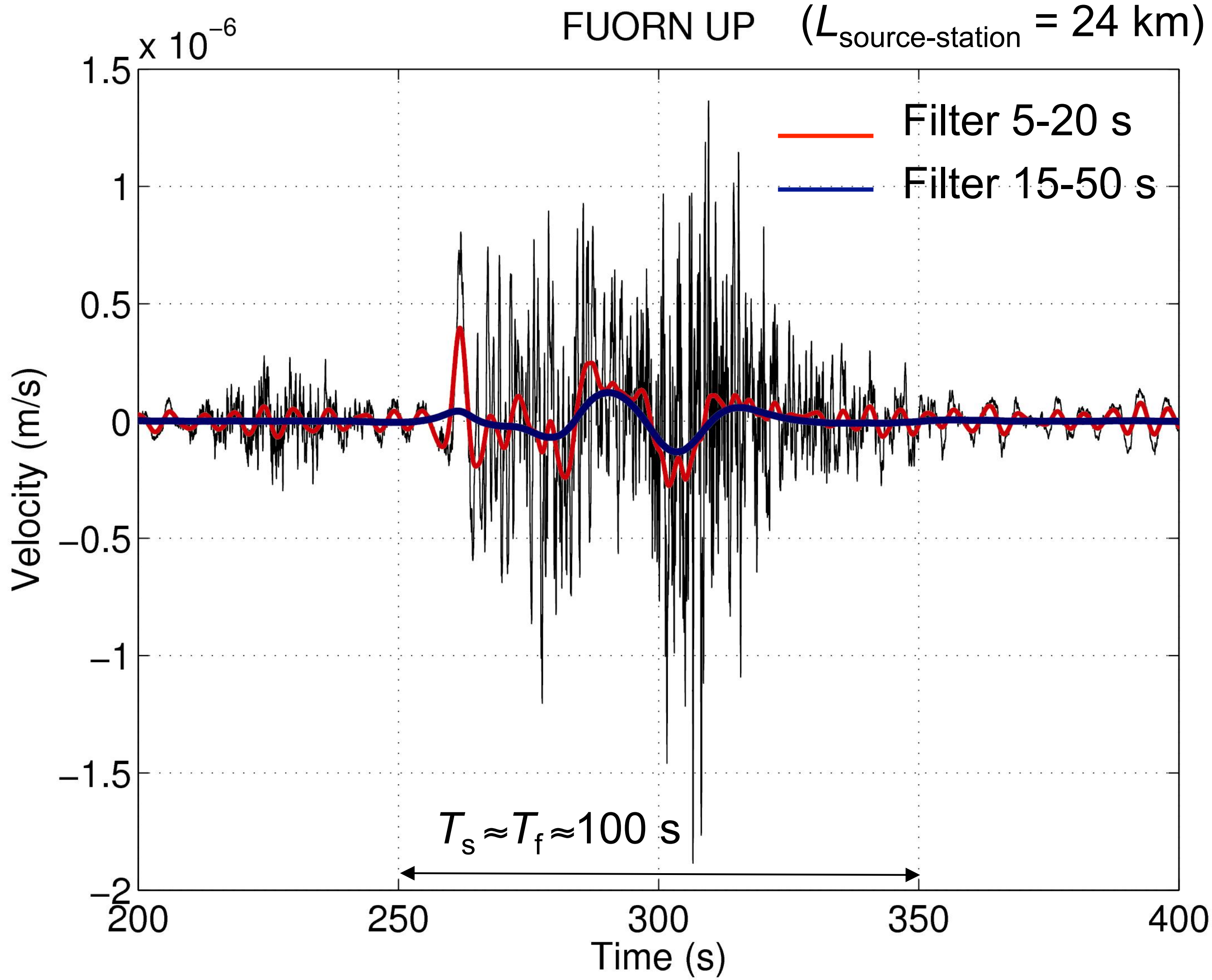

For $T > 15$ s, $\lambda = cT \approx 45$ km

small topographic and complex media effects are expected

Thurweiser landslide seismic waves

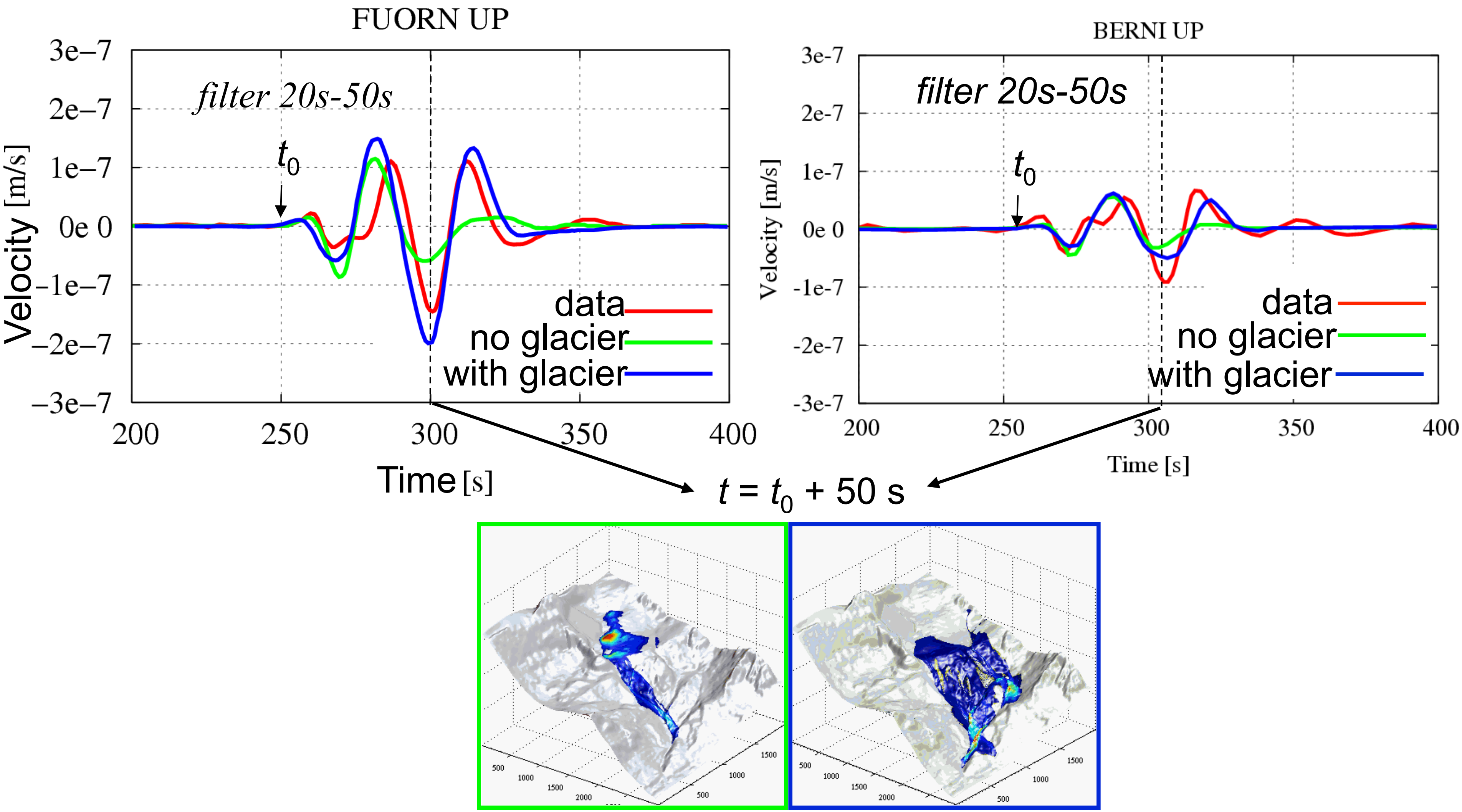

- The scenario **with glacier** better reproduces the vertical waveform

Thurweiser landslide seismic waves

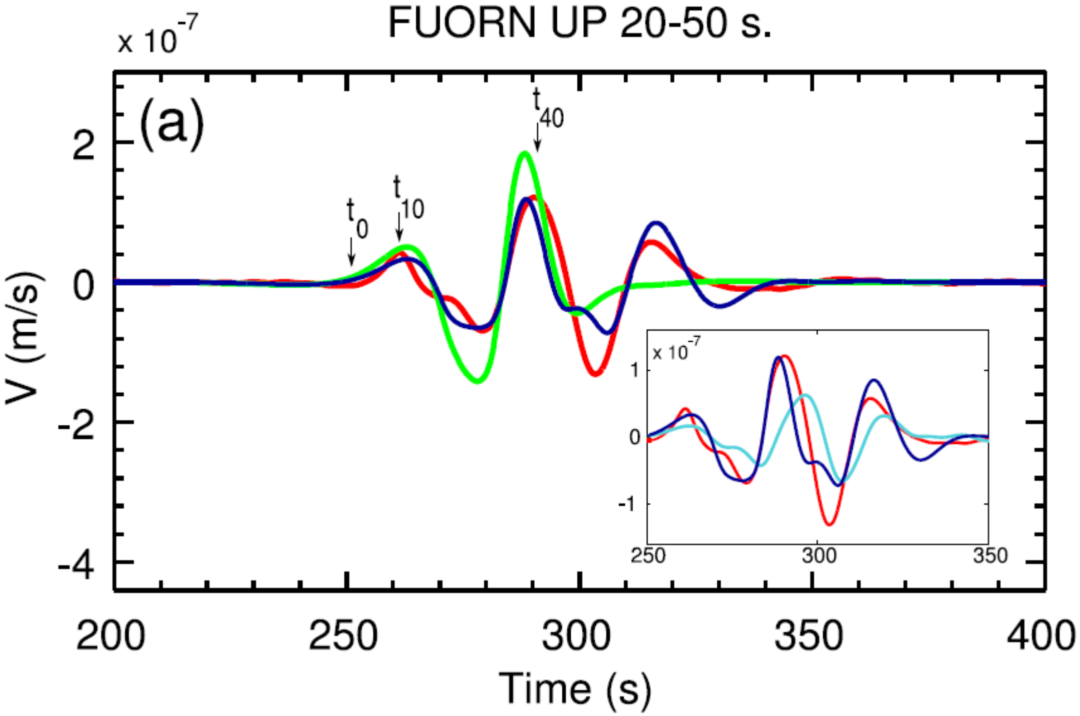

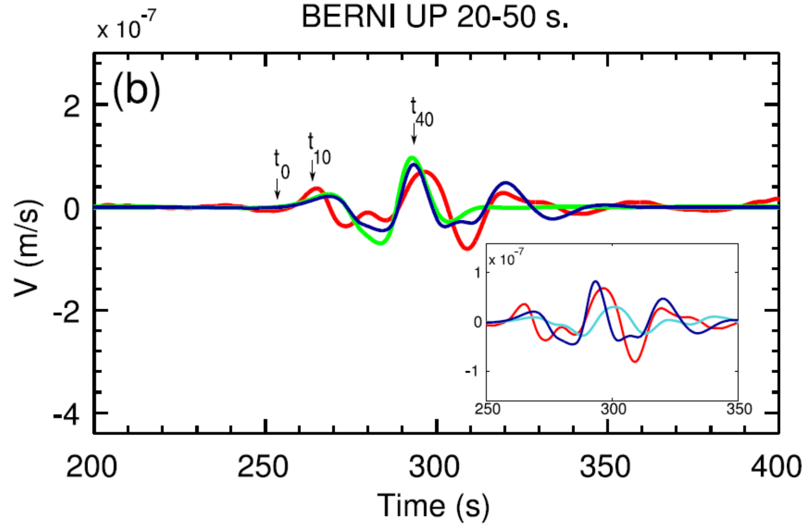

49 km from the landslide

$$\mathbf{T} = \rho g h \left(\cos\theta + \boxed{\frac{\mathbf{u}_h^t \mathcal{H} \mathbf{u}_h}{g \cos^2\theta}} \right) \left(\mu \frac{u_X}{\|\mathbf{u}\|}, \mu \frac{u_Y}{\|\mathbf{u}\|}, -1 \right)$$

Curvature effects

- Strong effect of centrigulal acceleration on landslide dynamics

Mt-Steller rock-ice avalanche

Role of erosion in landslide dynamics ?

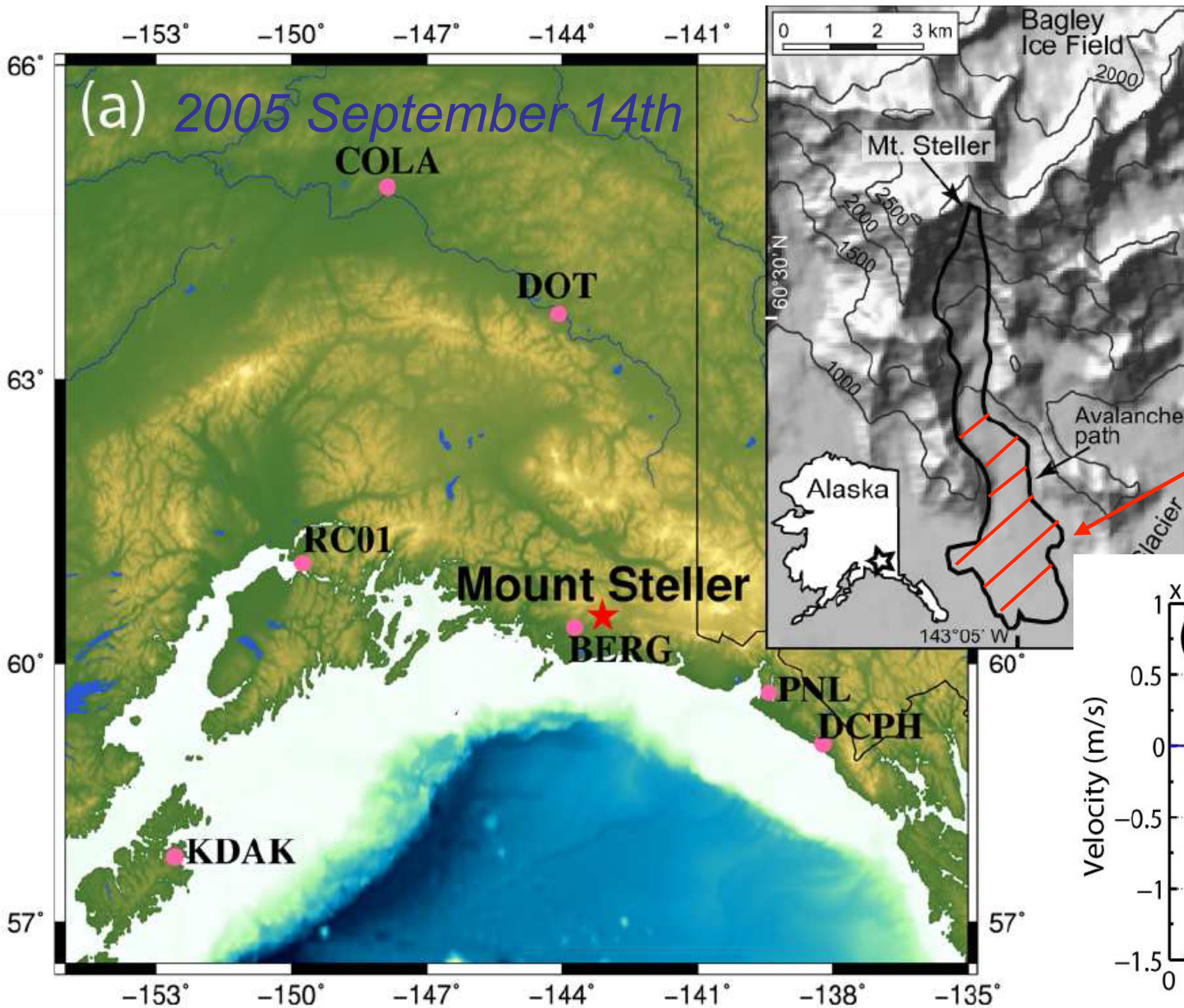

Traveled distance ~9 km

Volume : 40-60 Mm^3

Ice eroded on the avalanche path : ~20 Mm^3

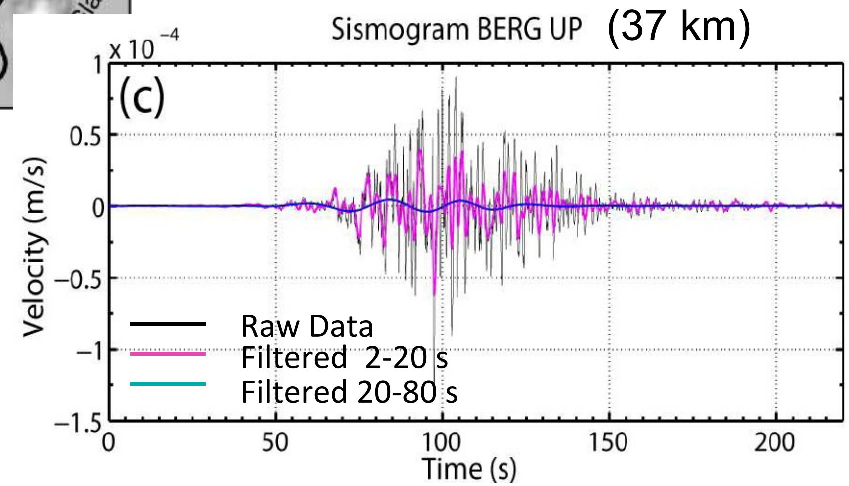

Moretti et al., 2012, 2015

Simulation of the Mt-Steller landslide

no erosion | **with erosion** | Comparison of deposits

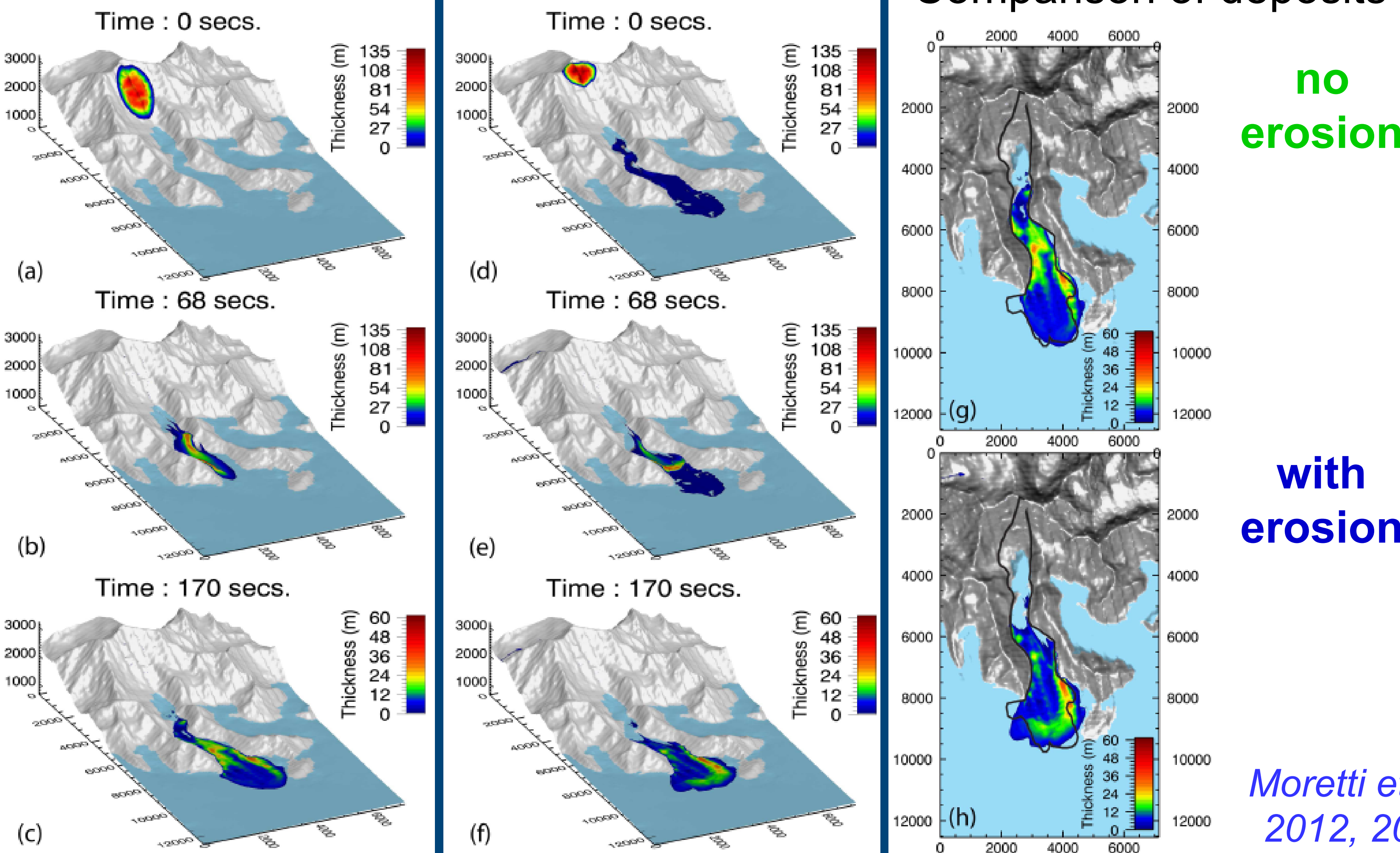

Moretti et al. 2012, 2015

The deposit area is not enough to constrain landslide models !!

Long period : inverted and simulated force

Force filtered between 20-80s

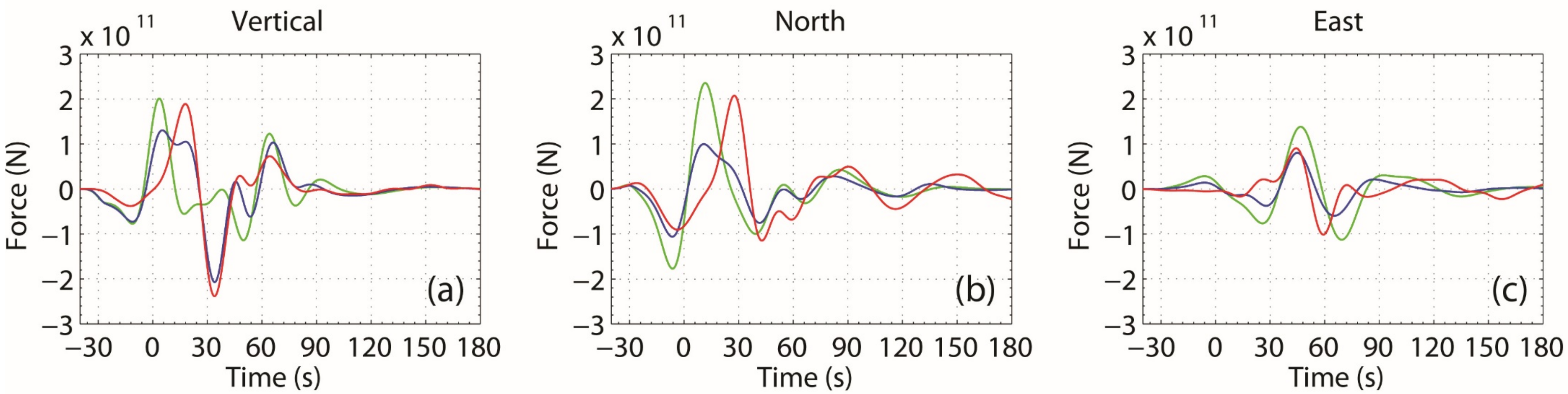

Data
Scenario without erosion
Scenario with erosion

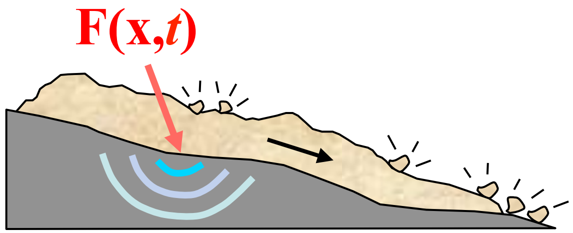

Taking into account erosion is necessary to reproduce the dynamics !

Sensitivity to friction coefficient

Simulation of Mount Meager landslide

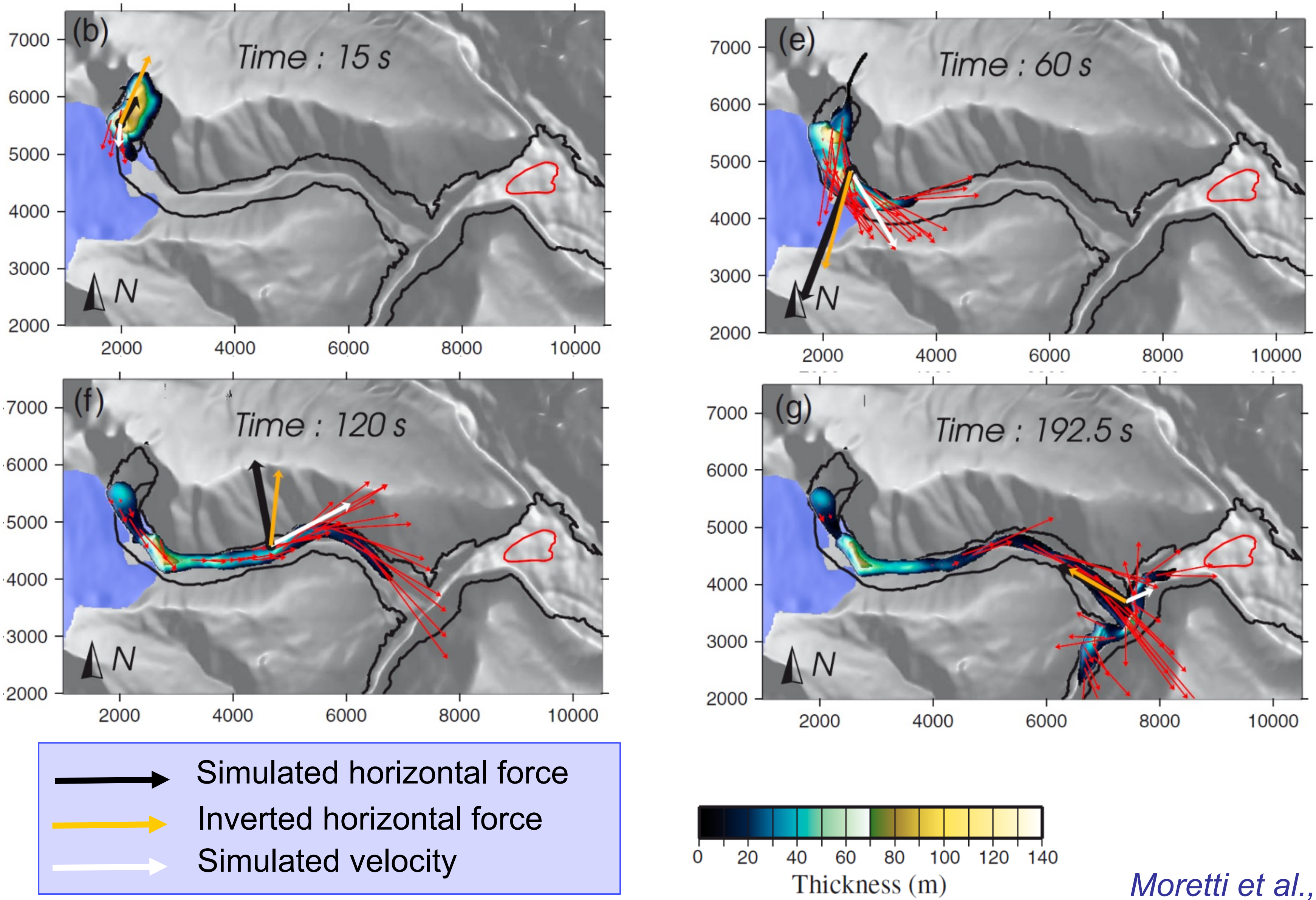

Moretti et al., 2015

Sensitivity to friction coefficient

Best scenario $\mu = 0.33$ (δ =18°)

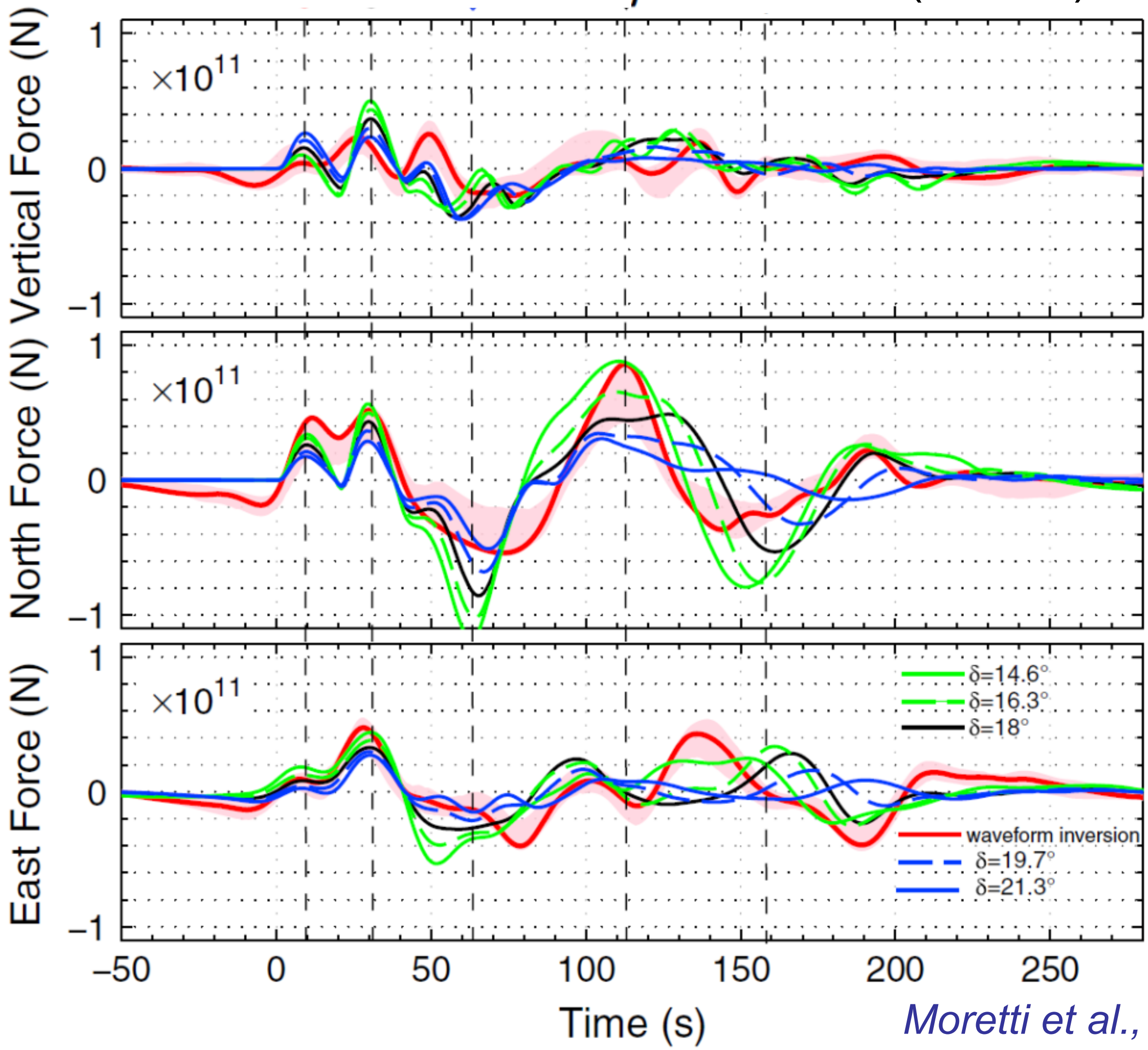

Moretti et al., 2015

Physical origin of these low friction coefficients?

Outline

I – Geophysical reality:
- Complexity of flows and physical processes
- Field data to validate rheological models of real flows
- From field observation to laboratory experiments

II – Modelling of natural landslides
- Shallow model and rheology
- Unexplained high mobility of natural landslides
- Investigating landslide dynamics: seismic data and models

III – Back to the rheology of granular materials
- Laboratory experiments
- 2D visco-plastic models
- Insight into the static/flowing interface
- Multi-layer models

Experiments of granular flows

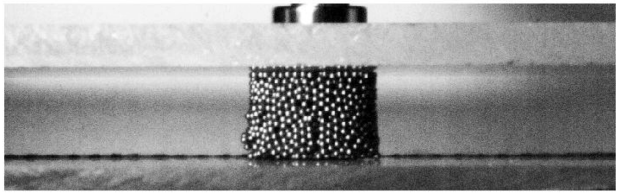

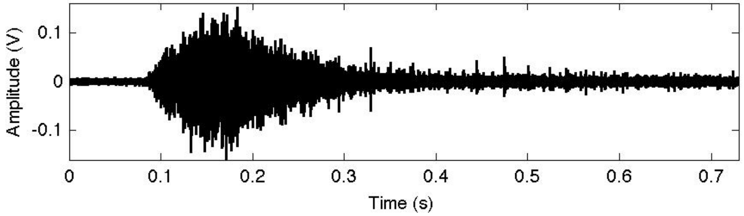

Scale effects ?

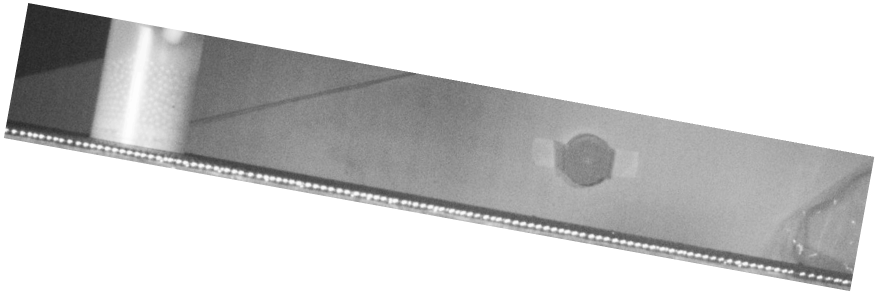

Farin, Mangeney, Toussaint, De Rosny, Shapiro, et al. 2015

Farin, Mangeney, Toussaint, De Rosny, Trinh, et al. 2017

Iverson, Logan, LaHusen, Berti, 2010, USGS

Granular materials

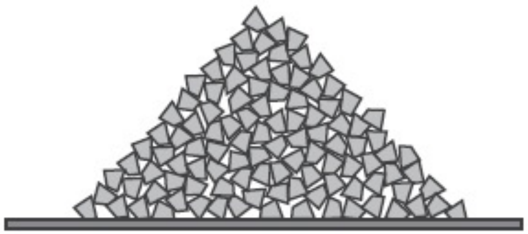

“solide”

“liquide”

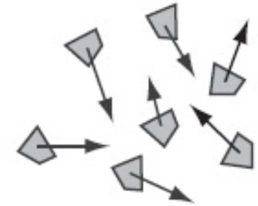

“gaz”

Static-flowing interface

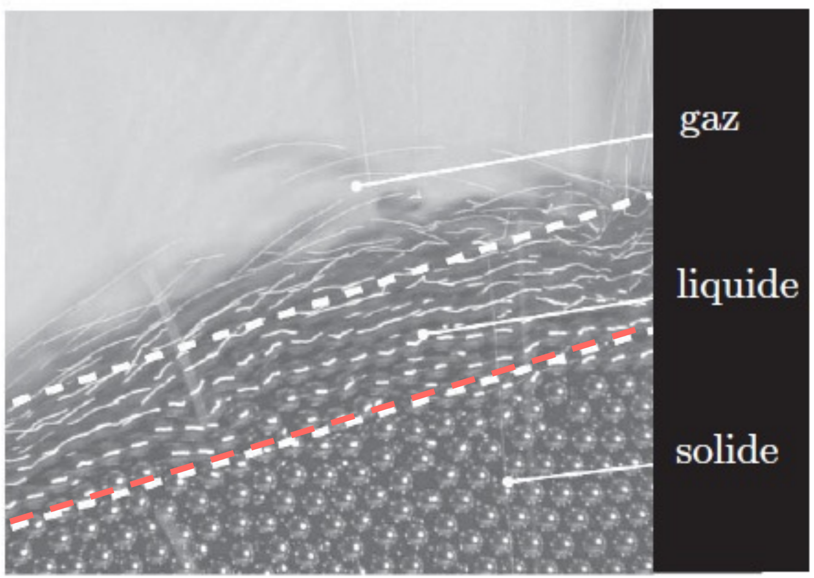

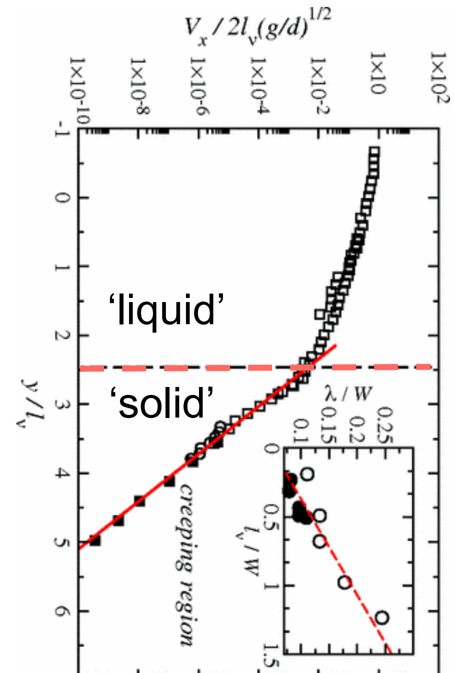

Richard et al., 2008

Dense granular flows

Three subcategories depending on the nature of particle/particle interactions

For simple shear flows:

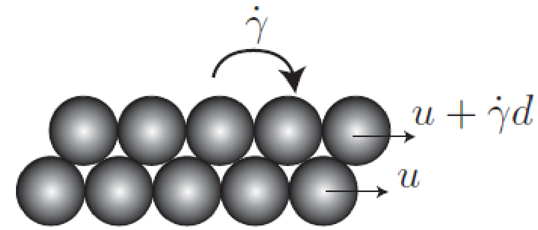

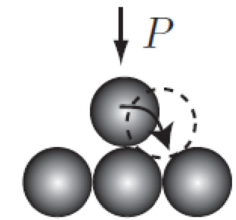

(i) particle inertia-dominated regime (dry)

$$I = I_{\mathrm{pi}} = \sqrt{\rho_{\mathrm{p}} \dot{\gamma}^2 d^2 / P_{\mathrm{p}}}$$

t macroscopic strain rate

$1/\dot{\gamma}$

t particle rearangment under confining pressure

$d / \sqrt{P_{\mathrm{p}} / \rho_{\mathrm{p}}}$

(ii) viscous resistance-dominated regime (grain+fluid)

$$I = I_{\mathrm{v}} = \frac{\eta_{\mathrm{f}} \dot{\gamma}}{P_{\mathrm{p}}}$$

$t_{\mathrm{micro}}^{\mathrm{visq}} = \eta / P^p$

(iii) fluid inertial resistance-dominated regime (grain + fluid)

$$I = I_{\mathrm{fi}} = \sqrt{\rho_{\mathrm{f}} \dot{\gamma}^2 d^2 / P_{\mathrm{p}}}$$

$\Rightarrow$ $\mu(I)$ rheology

Classification based on analysis of time scales of the particle displacement

e. g. *Savage, 1984, Ancey et al.1999, Courrech du Pont et al 2003, Cassar et al 2005*

Inertial number

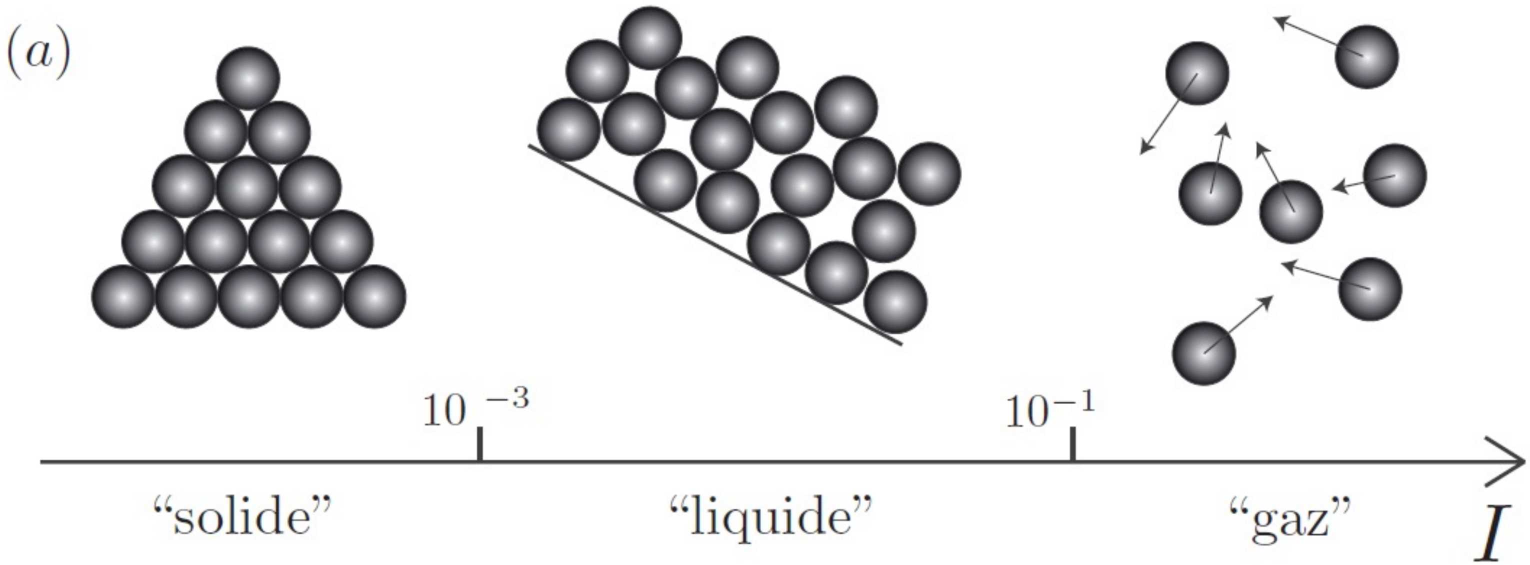

Evolution of contact network (2D discrete element simulations)

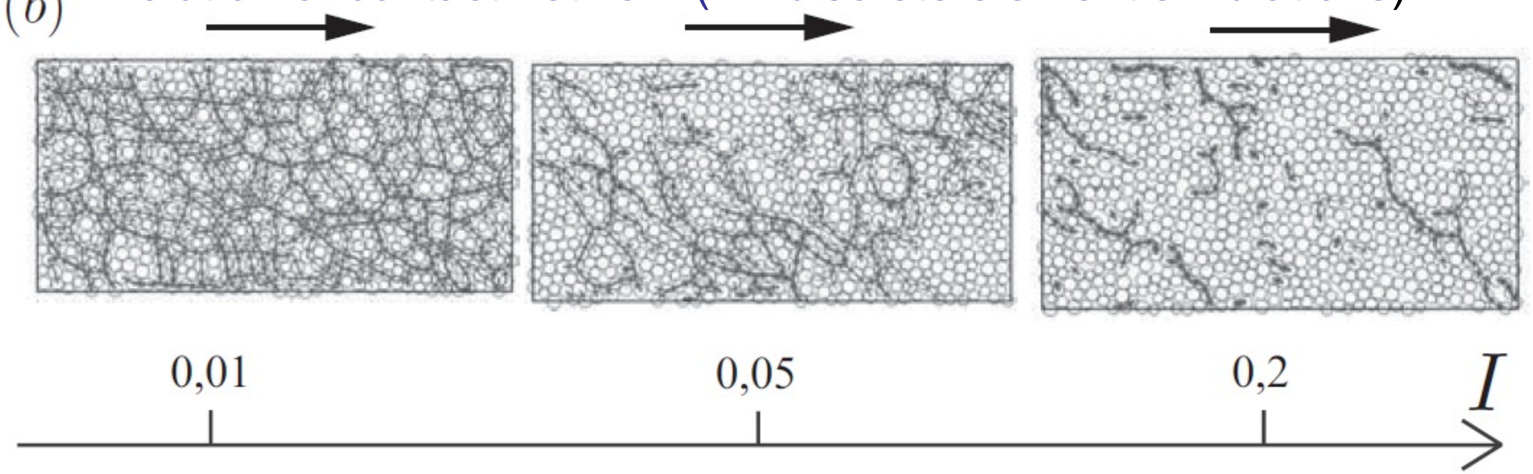

Rognon, 2006

Unsteady flows on inclined planes

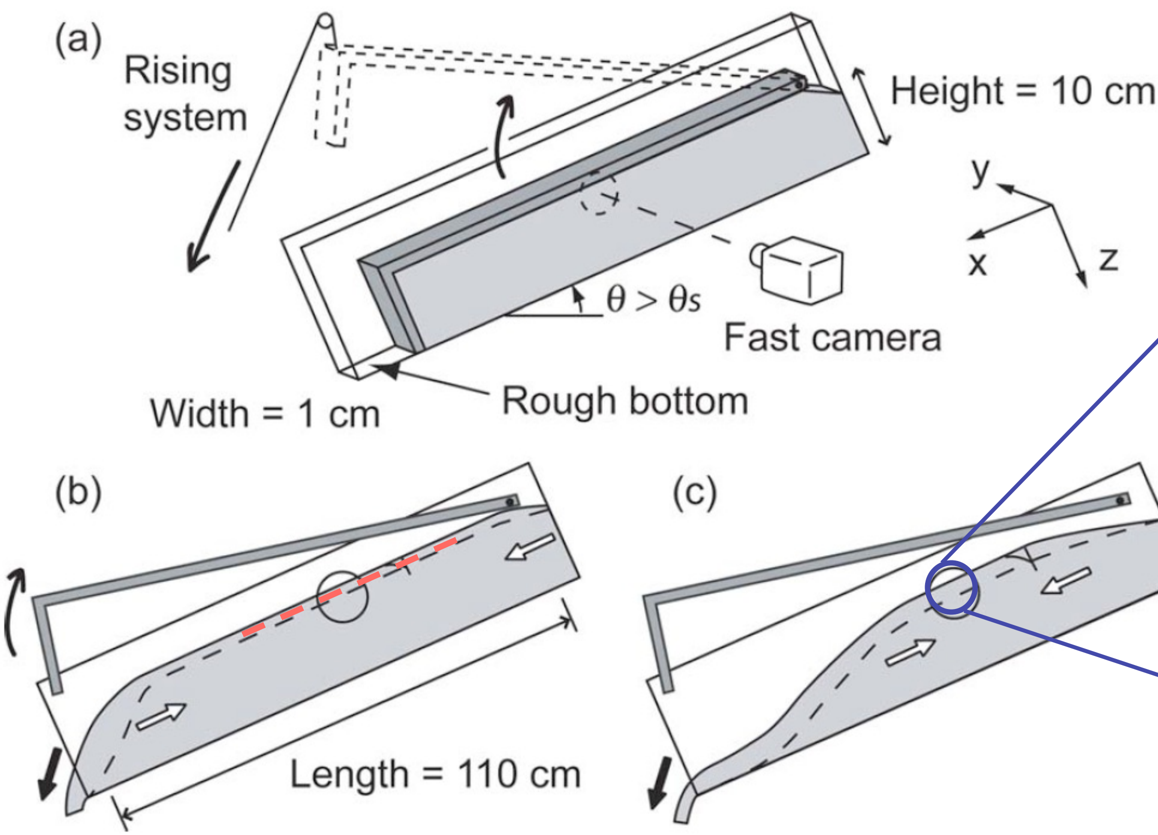

Measurement of velocity profiles

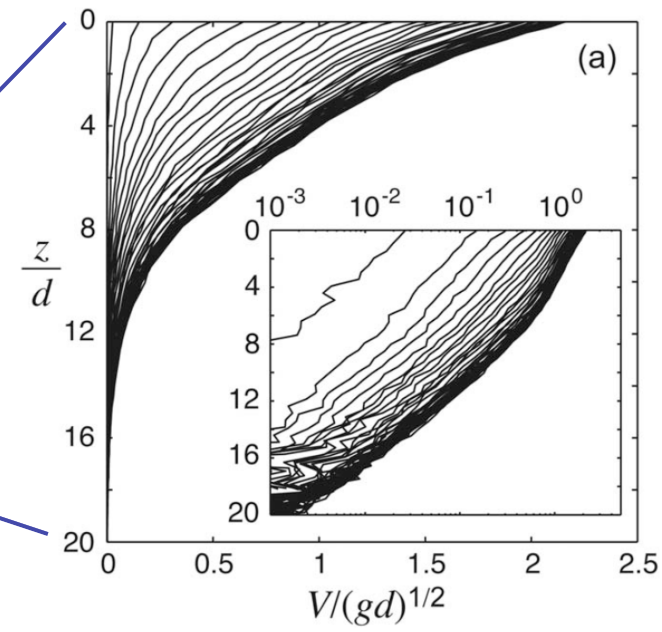

Jop, Forterre, Pouliquen, 2007

Granular flow experiments

Granular column collapse over an inclined channel

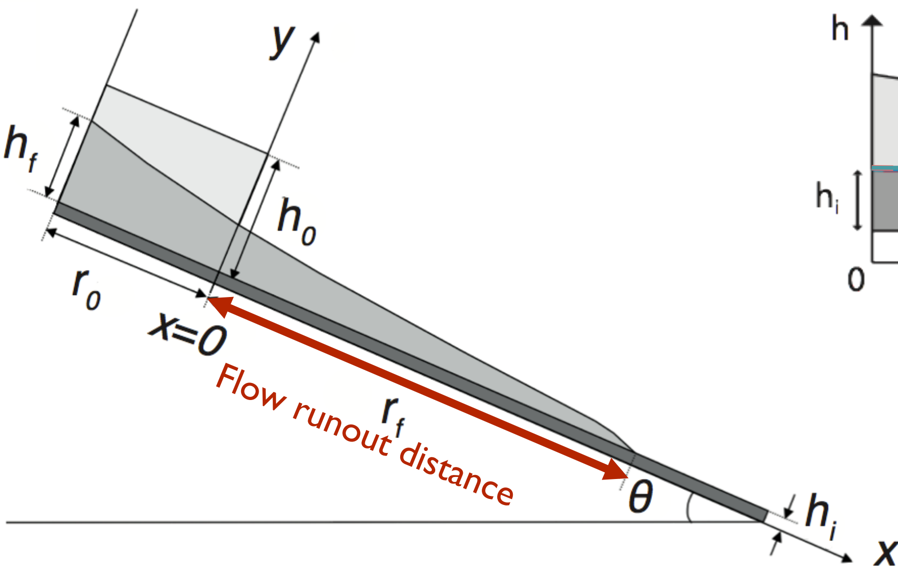

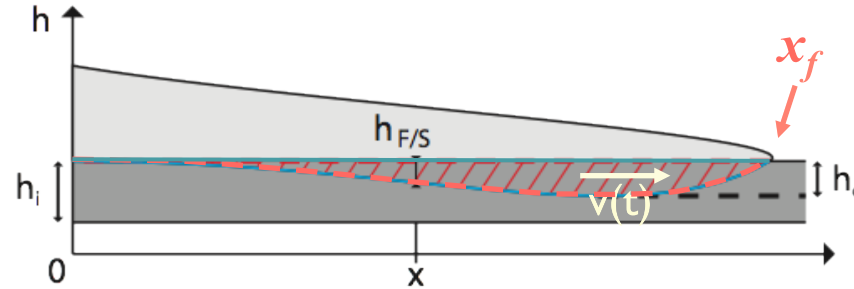

Friction angles:
repose δ≈23°±0.5°, avalanche δ≈25°±0.5°

Control parameters:
- slope angle: 0° < θ < δ
- volume $V = h_0\, r_0\, W$
- aspect ratio $a = h_0 / r_0$
- erodible bed thickness h_i
- column shape
- degree of bed compaction
- channel width

Granular collapse over a rigid bed

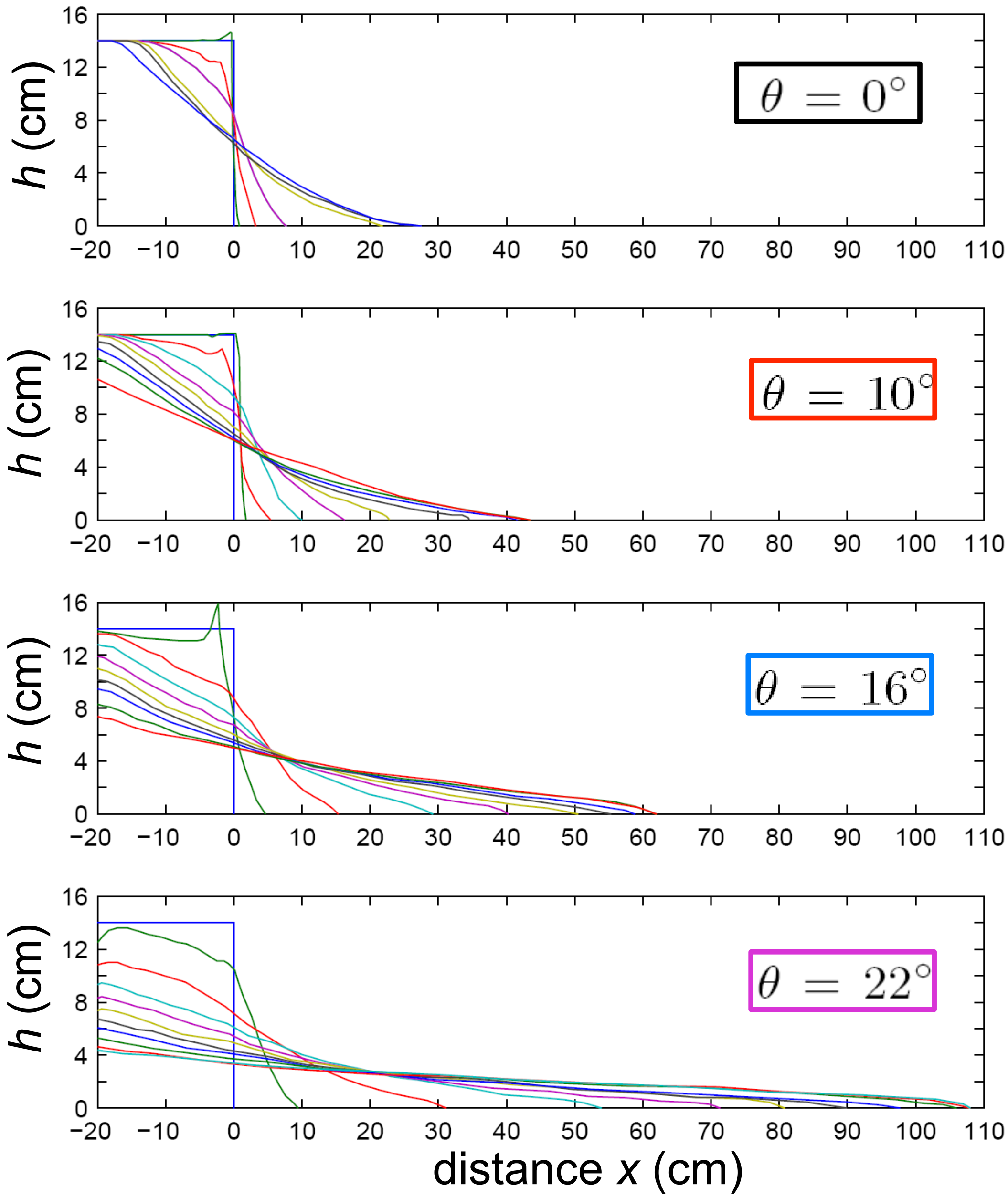

Measurement of front velocity

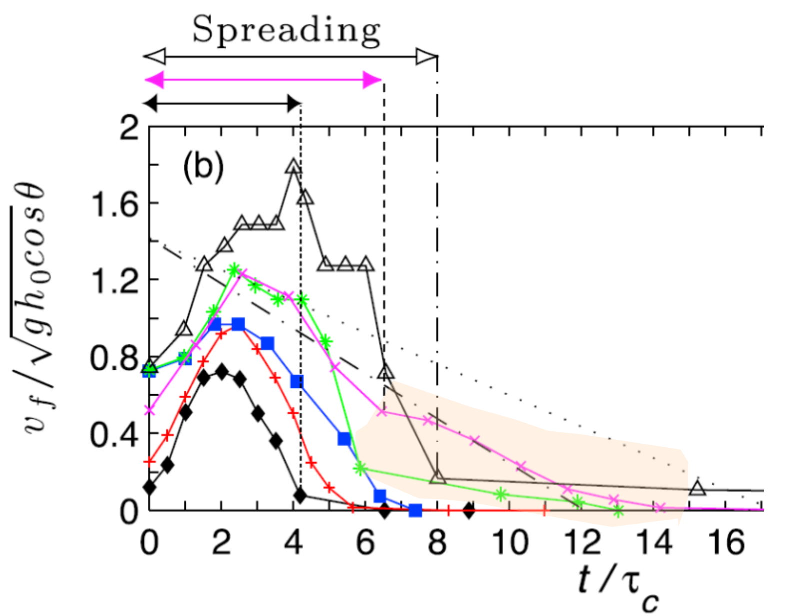

Granular collapse over an erodible bed

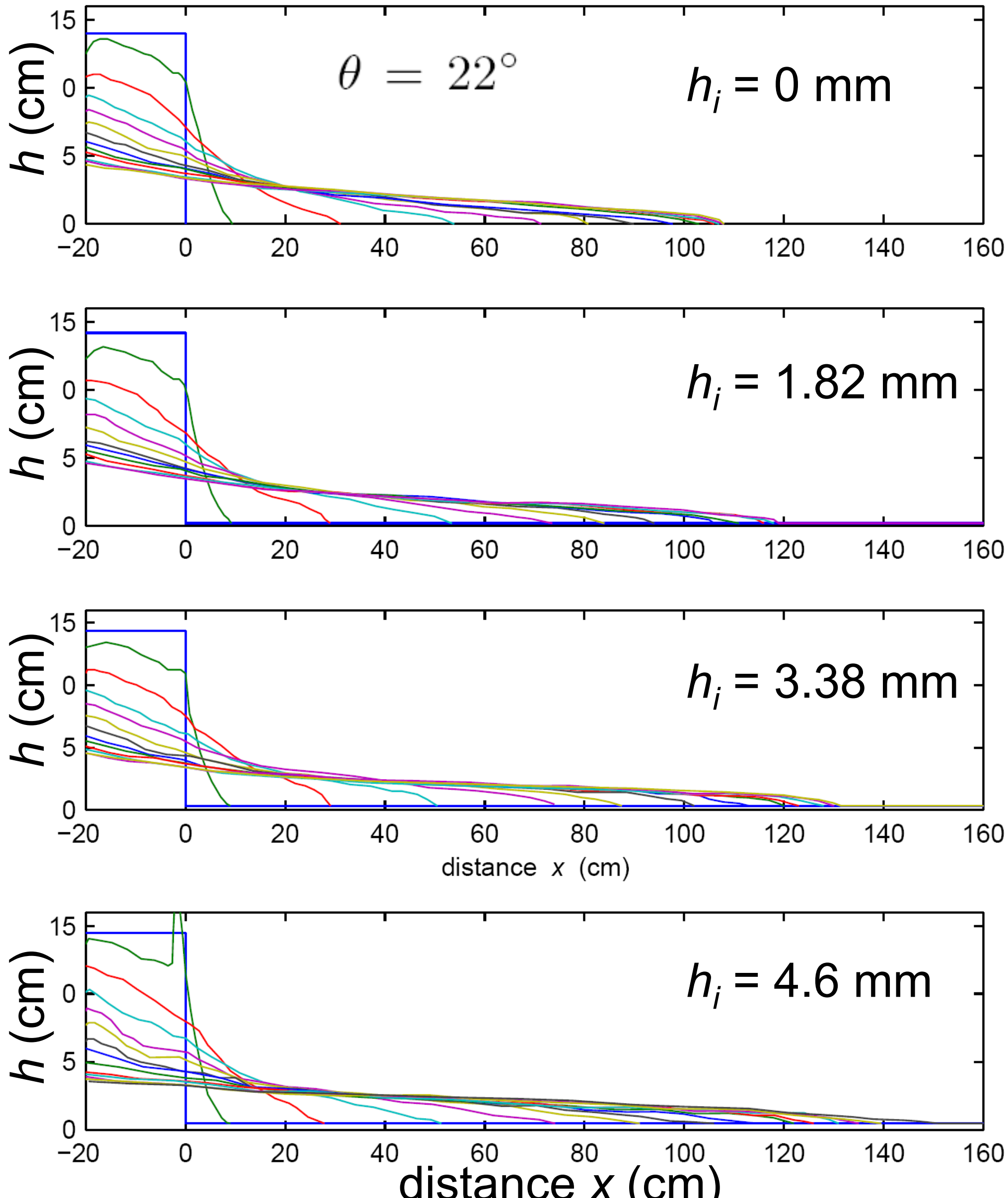

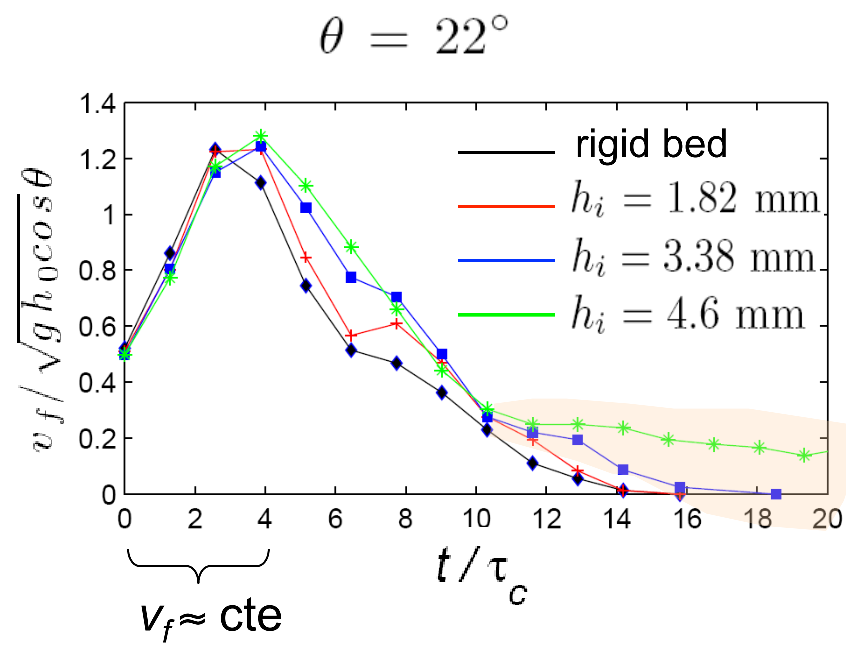

$t \geq 4 - 5\tau_c$, $v_f \nearrow$ if $h_i \nearrow$

For $t \geq 10\tau_c$ and $h_i = 4.6$ mm

Slow flow

Outline

I – Geophysical reality:
- Complexity of flows and physical processes
- Field data to validate rheological models of real flows
- From field observation to laboratory experiments

II – Modelling of natural landslides
- Shallow model and rheology
- Unexplained high mobility of natural landslides
- Investigating landslide dynamics: seismic data and models

III – Back to the rheology of granular materials
- Laboratory experiments
- 2D visco-plastic models
- Insight into the static/flowing interface
- Multi-layer models

2D granular flow modelling

- Momentum equation: $$\rho \left(\frac{\partial \boldsymbol{u}}{\partial t} + \nabla \cdot (\boldsymbol{u} \otimes \boldsymbol{u}) \right) = \nabla \cdot \boldsymbol{\sigma} + \rho \boldsymbol{g}$$
- Incompressibility: $$\nabla \cdot \boldsymbol{u} = 0$$

$$\boldsymbol{\sigma} = -p\mathrm{Id} + \boldsymbol{\sigma}'$$, pressure: $p = -\mathrm{trace}(\boldsymbol{\sigma})/3$

Strain rate tensor: $$\boldsymbol{D}(\boldsymbol{u}) = \frac{1}{2}(\boldsymbol{\nabla} \boldsymbol{u} + \boldsymbol{\nabla}^T \boldsymbol{u})$$

Constitutive relation

$$\boldsymbol{\sigma}' = \mu(I)p\frac{\boldsymbol{D}}{\|\boldsymbol{D}\|}$$

can be called viscosity

$$\|\boldsymbol{D}\| = \sqrt{\tfrac{1}{2}\mathrm{tr}\,\boldsymbol{D}^2}$$

Jop et al. 2005, 2006

$$\mu(I) = \mu_s + \frac{\mu_2 - \mu_s}{1 + I_0/I} \quad \text{with} \quad I = \frac{2\|\boldsymbol{D}\|d}{\sqrt{p/\rho_s}}$$

$$\boldsymbol{\sigma}' = \mu_s p\frac{\boldsymbol{D}}{\|\boldsymbol{D}\|} + 2\frac{(\mu_2 - \mu_s)p}{2\|\boldsymbol{D}\| + I_0\sqrt{p}/k}\boldsymbol{D} \qquad k = d\sqrt{\rho_s}$$

can be called viscosity η

Drücker-Prager yield stress

Constitutive relation

$$\begin{cases} \boldsymbol{\sigma}' = 2\eta(|\boldsymbol{D}|, p)\boldsymbol{D} + \mu_s p \dfrac{\boldsymbol{D}}{|\boldsymbol{D}|} & \text{if } |\boldsymbol{D}| \neq 0, \\ |\boldsymbol{\sigma}'| \leq \mu_s p & \text{if } |\boldsymbol{D}| = 0. \end{cases}$$

Plasticity (flow/no flow) criterion

Constant viscosity: $\eta(|\boldsymbol{D}|, p) =$ Cte

$\mu(I)$ rheology : $2\eta(|\boldsymbol{D}|, p) = \dfrac{k(\mu_2 - \mu_s)p}{k|\boldsymbol{D}| + I_0\sqrt{p}}$

Ionescu, Mangeney, Bouchut, Roche 2015

Boundary conditions

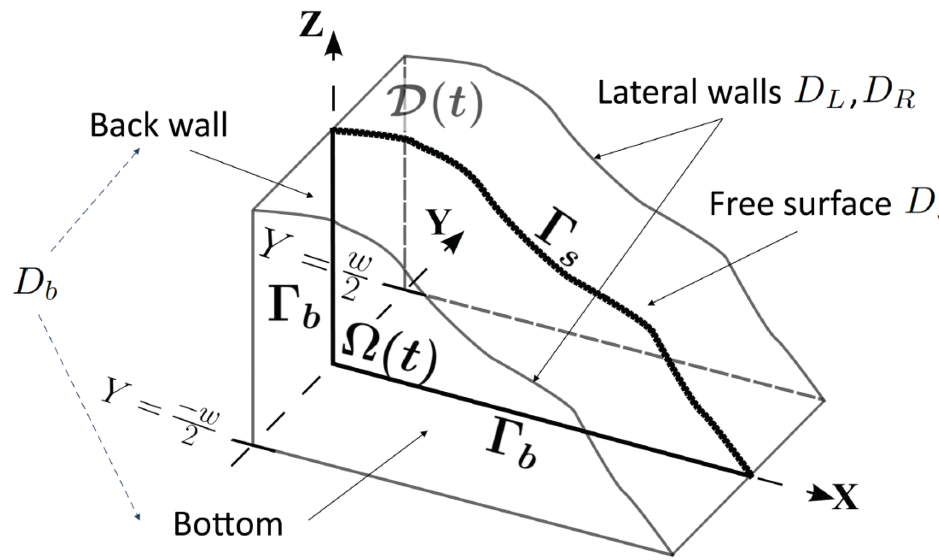

- At the free surface : $\mathcal{D}(t)$

characteristic function of the domain

$$\boldsymbol{\sigma n} = 0 \qquad \text{on} \quad \Gamma_s(t),$$

$$\mathrm{St}\frac{\partial 1_{\mathcal{D}(t)}}{\partial t} + \boldsymbol{u}\cdot\nabla 1_{\mathcal{D}(t)} = 0,$$

- At the base and walls: Coulomb friction

$$\boldsymbol{u}\cdot\boldsymbol{n} = 0, \quad \boldsymbol{\sigma}_T = \boldsymbol{F}^f$$

$$\begin{cases} \boldsymbol{F}^f = -\mu^f[-\sigma_n]_+ \dfrac{\boldsymbol{u}_T}{|\boldsymbol{u}_T|} \text{ if } \boldsymbol{u}_T \neq 0, \\ |\boldsymbol{F}^f| \leq \mu^f[-\sigma_n]_+ \text{ if } \boldsymbol{u}_T = 0. \end{cases}$$

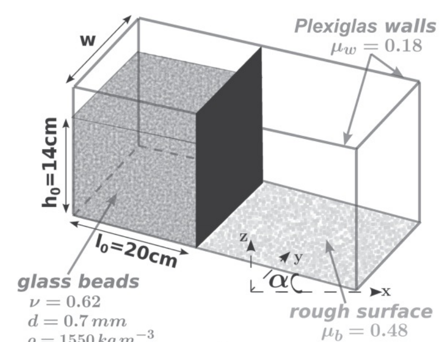

$$\mu^f = \begin{cases} \mu_w^f \text{ on the back wall and on the lateral walls,} \\ \mu_b^f \text{ on the rough bottom.} \end{cases}$$

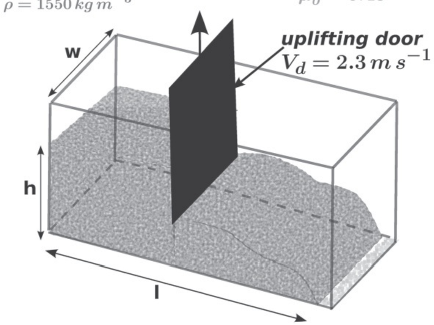

Side wall effects

$$\rho\,(\partial_t \boldsymbol{u} + (\boldsymbol{u}\cdot\nabla)\boldsymbol{u}) + \nabla p - \operatorname{div}(\boldsymbol{\sigma}') = \frac{2}{w}\boldsymbol{F}_w^f + \rho\boldsymbol{g}$$

$$\begin{cases} \boldsymbol{F}_w^f = -\mu_w^f[p]_+ \dfrac{\boldsymbol{u}}{|\boldsymbol{u}|} \text{ if } \boldsymbol{u} \neq 0, \\ |\boldsymbol{F}_w^f| \leq \mu_w^f\,[p]_+ \text{if } \boldsymbol{u} = 0, \end{cases}$$

For a laminar shear flow with hydrostatic pressure, equivalent to:

Taberlet et al., 2003; Jop et al., 2005

$$\mu(I) = \mu_s + \frac{\mu_2 - \mu_s}{I_0 + I} I + \mu_w \frac{H - z}{W}$$

Martin, Ionescu, Mangeney, Bouchut, Farin, 2017

Unsteady flows on inclined planes

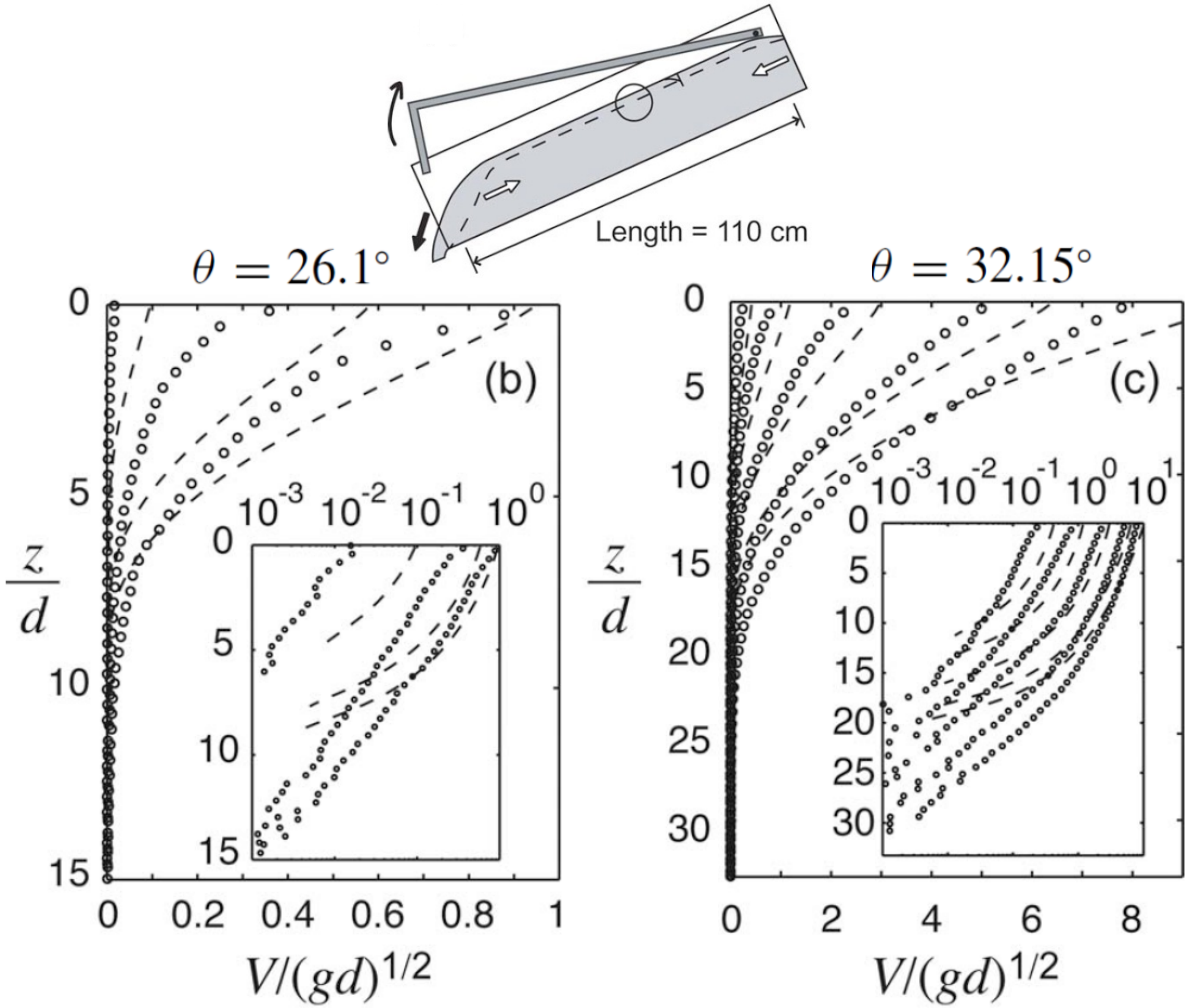

Jop, Forterre, Pouliquen, 2007

Granular collapses

ALE (Arbitrary Lagrangian-Eulerian) description to compute the evolution of the fluid domain
- iterative decomposition-coordination formulation, coupled with the augmented Lagrangian method: *Ionescu, Mangeney, Bouchut, Roche, 2014*

or

-regularization method: *Lusso, Ern, Bouchut, Mangeney, Farin, Roche, 2017*

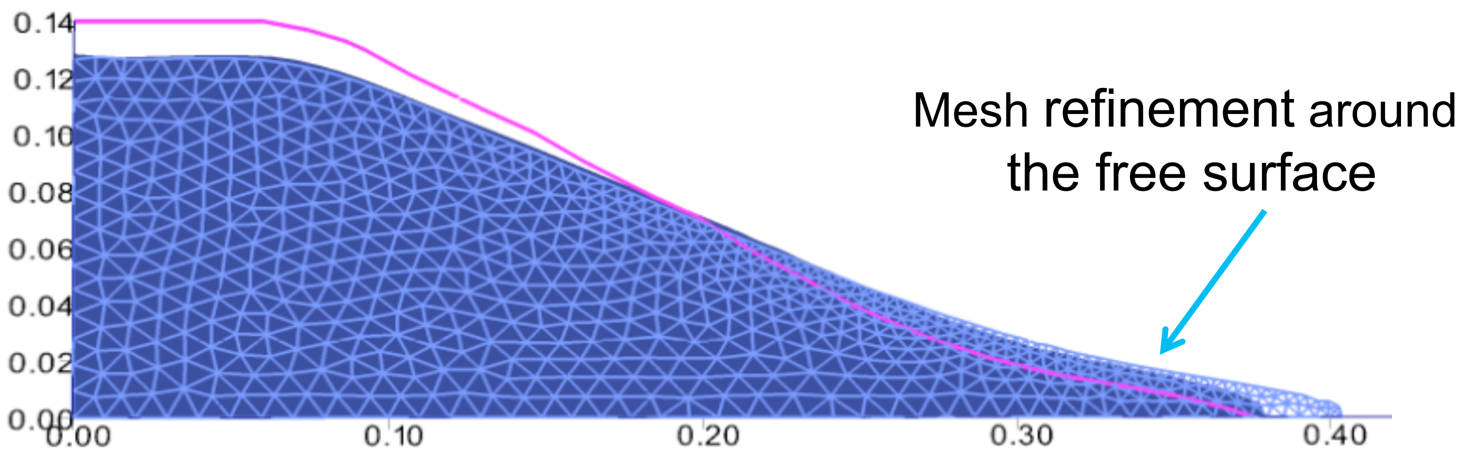

Crosta et al. 2009, Lagrée et al. 2011

Parameters deduced from the experiments

Grain diameter: $d = 0.7 \pm 0.1\mathrm{mm}$

Density: $\rho_s = 2500 \ \mathrm{kg\ m}^{-3}$, $\nu = 0.62$ ➡ $\rho = 1550 \ \mathrm{kg\ m}^{-3}$

Repose angle: $\theta_r = 23.5^o \pm 0.5^o \ (\mu_r = 0.43 \pm 0.01)$

Avalanche angle: $\theta_a = 25.5^o \pm 0.5^o \ (\mu_a = 0.48 \pm 0.01)$

Wall friction: $\mu_w = \tan(10.5^o) = 0.18$ *Pouliquen and Forterre 2002*

Additional friction due to the wall: + $\mu_w h/W$ *Jop et al. 2005*

⬇

Constant viscosity: $\mu = \mu_s = \tan(25.5^\circ)$,

$\mu(I)$ rheology : $\mu_s = \tan(25.5^o)$, $\mu_2 = \tan(36^o)$, $I_0 = 0.279$

Friction at the base: $\mu_b = \mu = \tan(25.5^\circ)$

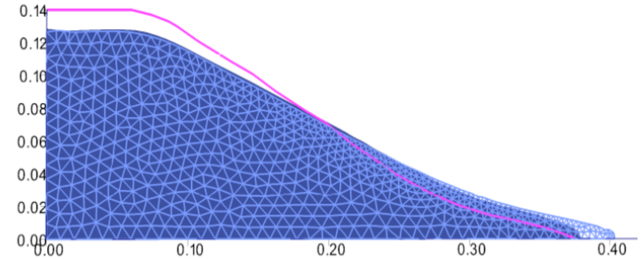

Simulation with the variable viscosity (μ (I))

Granular collapse over an horizontal plane: $\theta = 0°$

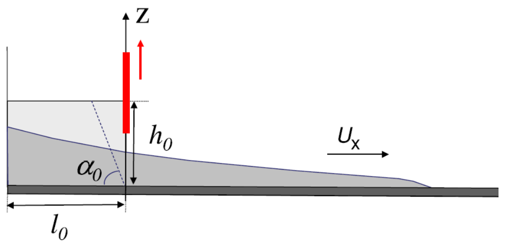

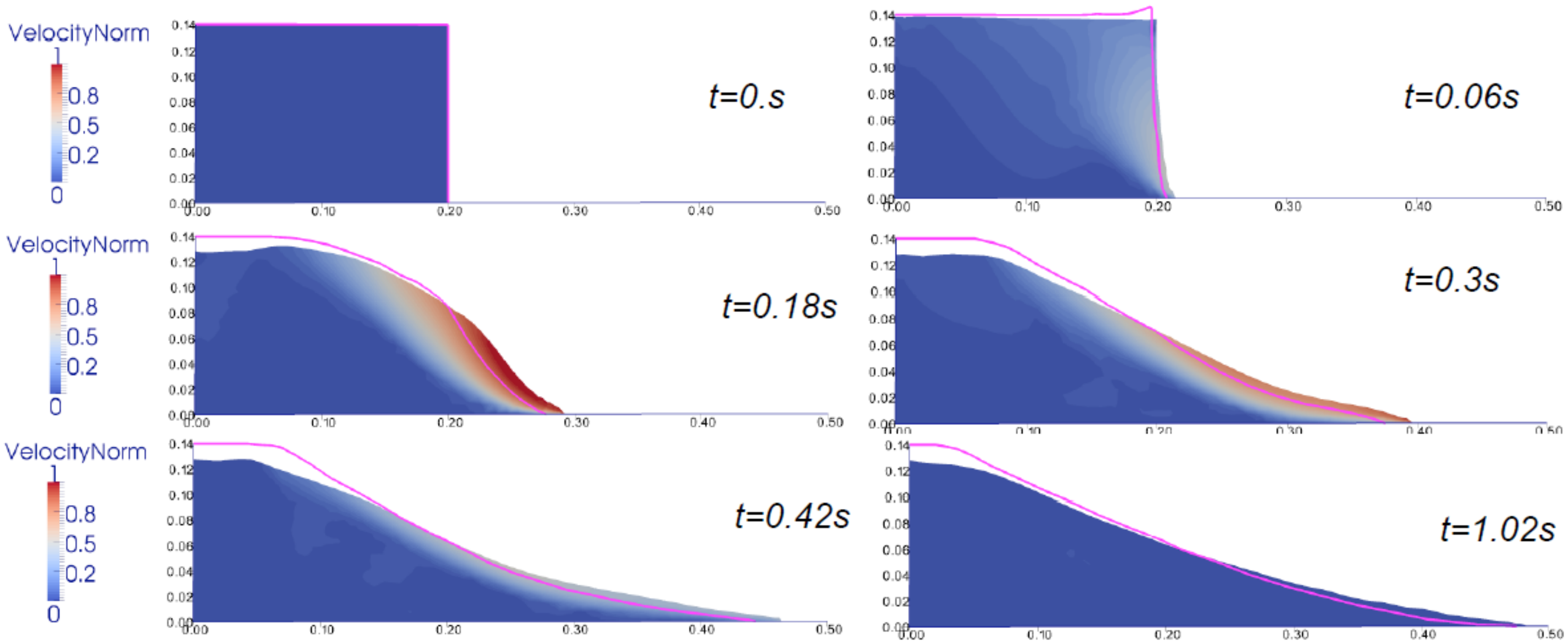

Well reproduces the dynamics

The gate has to be taken into account !

Effect of the gate

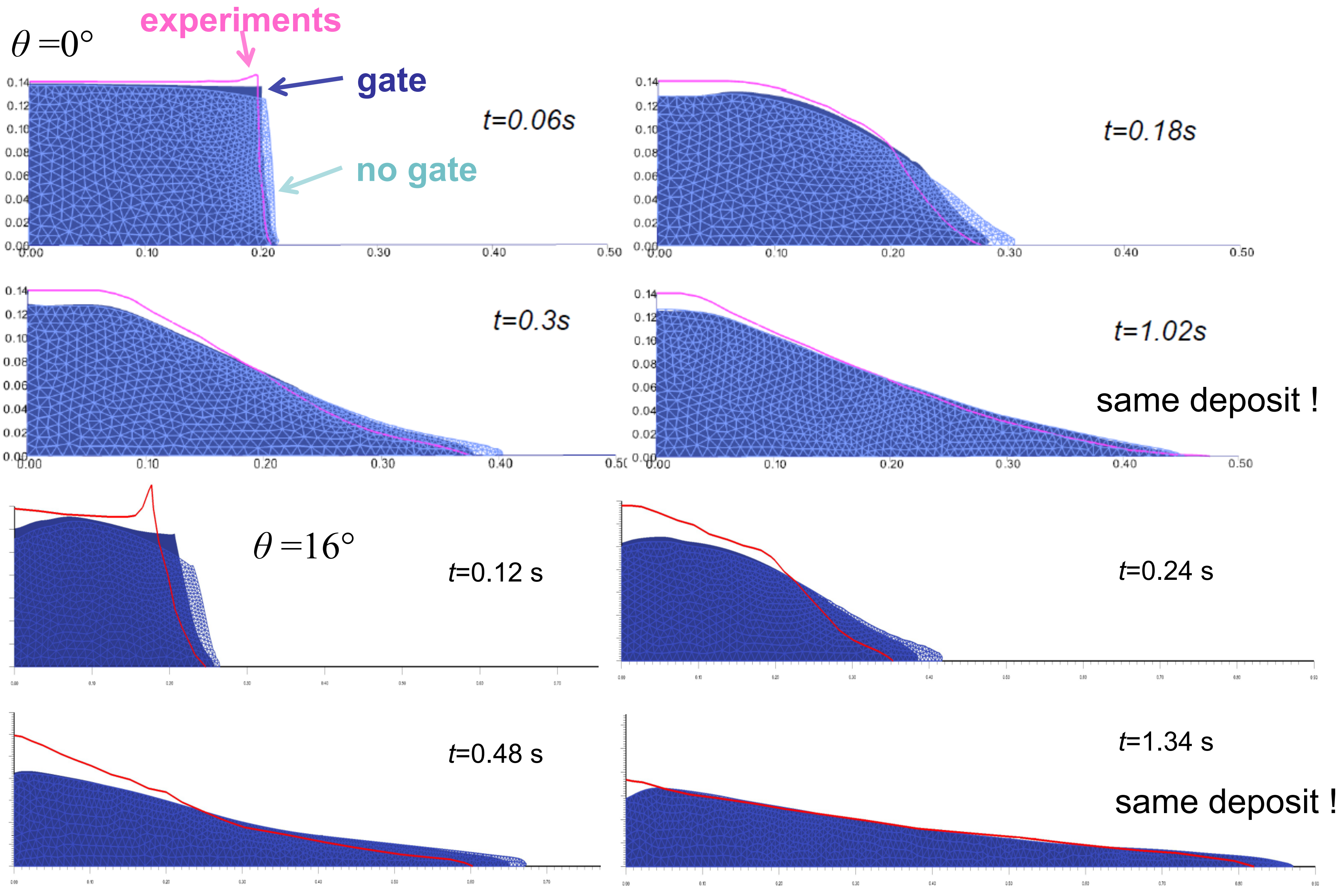

Effect of the side walls

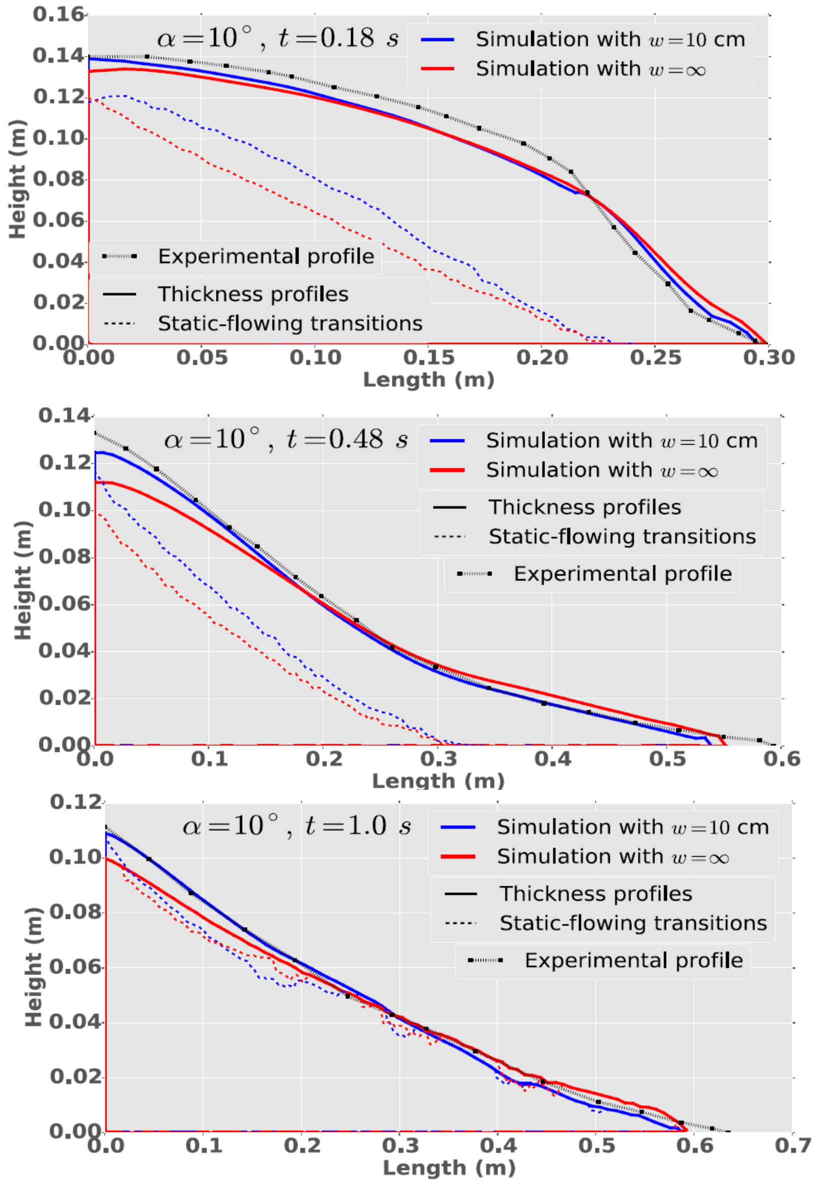

Side wall friction: the static-flowing interface closer to the free surface

Effect of the side walls

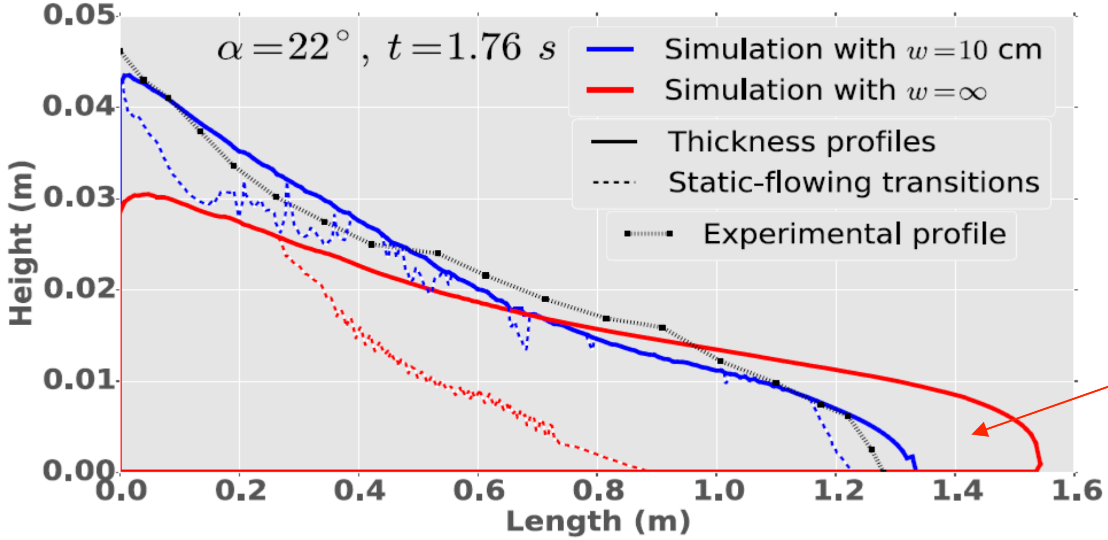

The material still flows

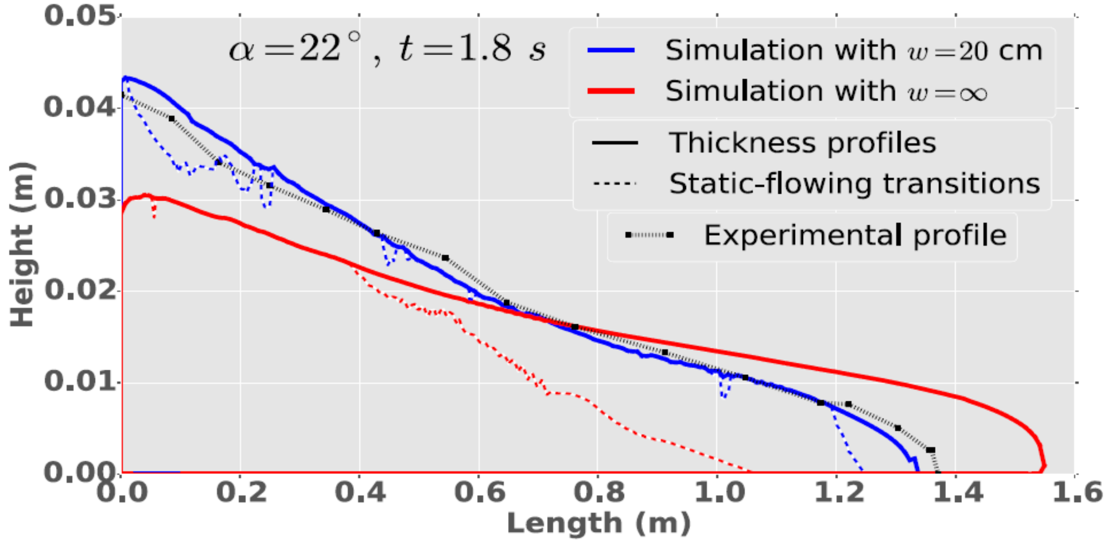

Martin, Ionescu, Mangeney, Bouchut, Farin, 2017

Horizontal velocity field and profiles

$\theta = 0°$

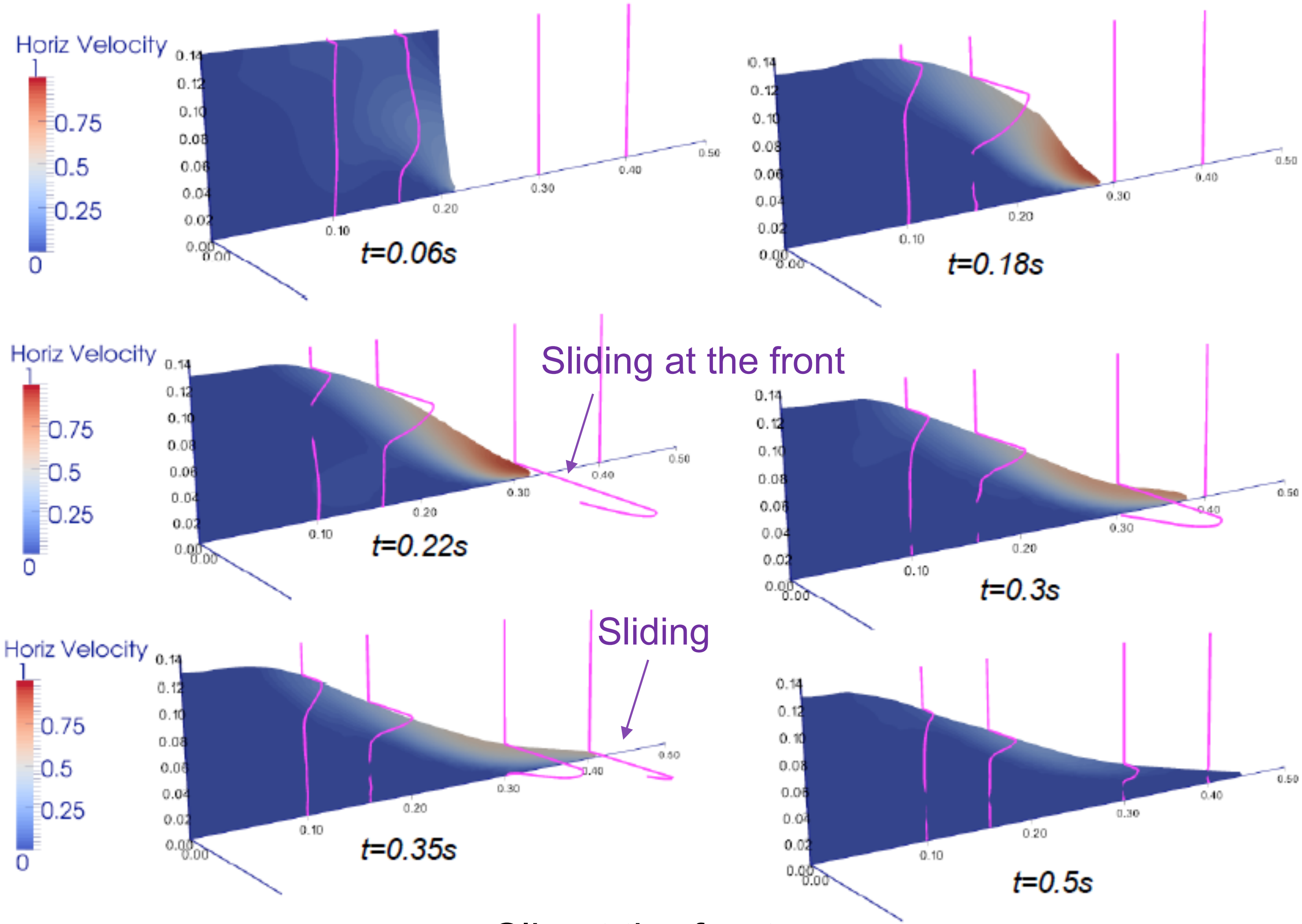

Slip at the front

Insight into the flow dynamics

Strain rate (s^{-1})

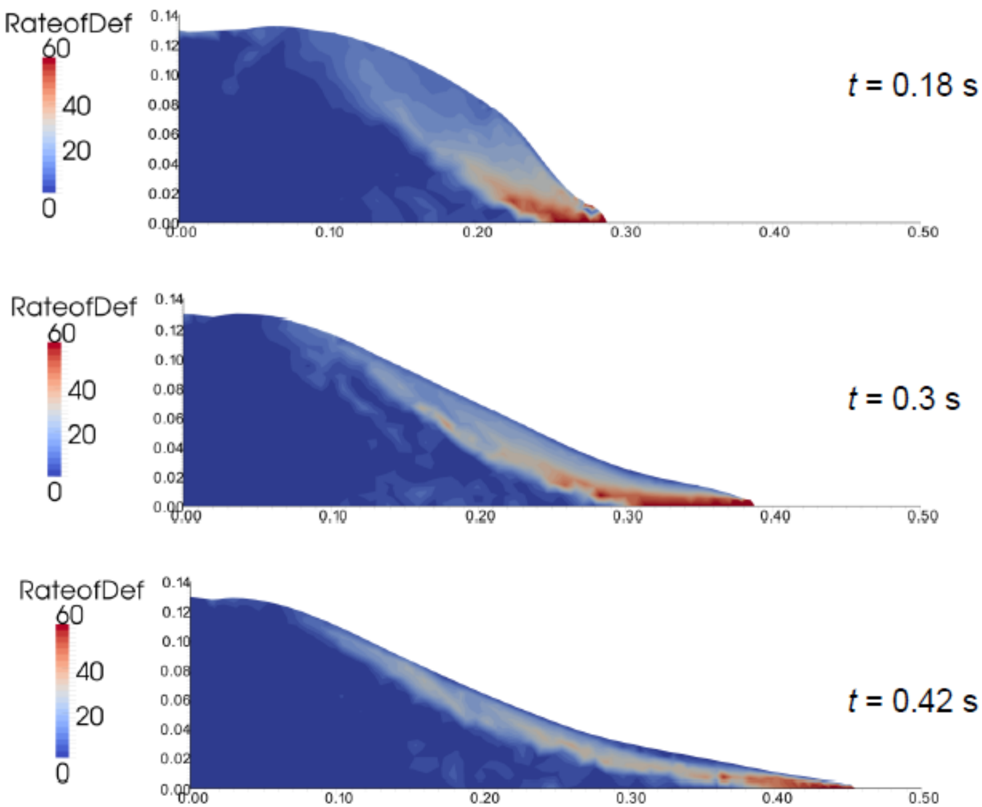

Pressure (Pa)

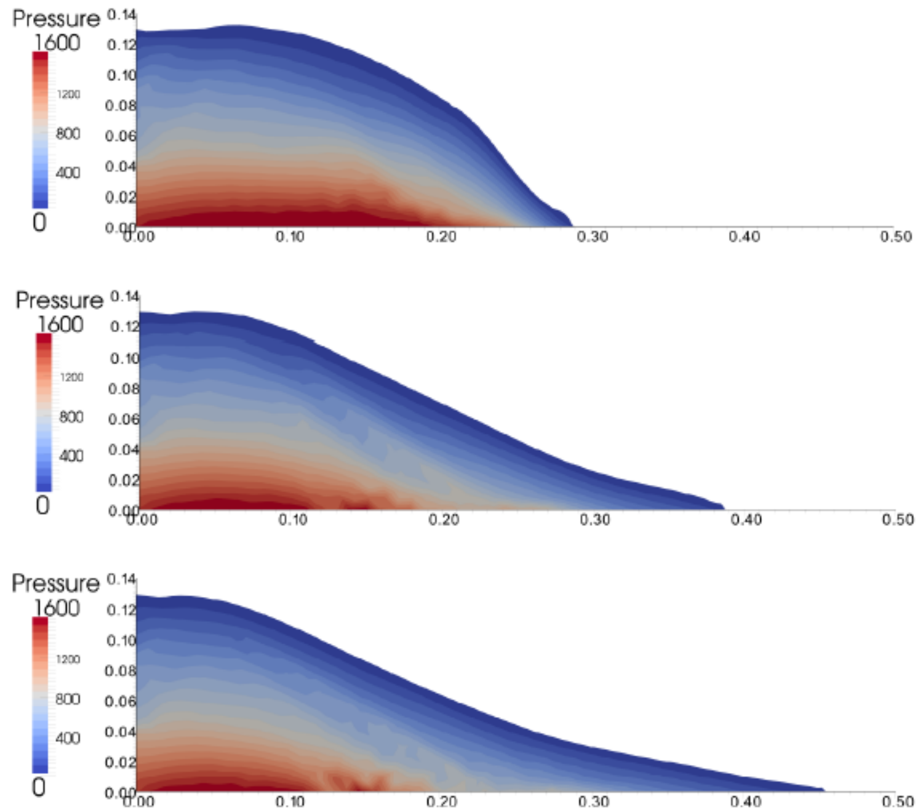

Strain rate localization

$$2\eta(|\boldsymbol{D}|, p) = \frac{k(\mu_2 - \mu_s)p}{k|\boldsymbol{D}| + I_0\sqrt{p}},$$

Viscosity η in the $\mu(I)$ rheology

$$2\eta_I(|\boldsymbol{D}|, p) = \frac{k(\mu_2 - \mu_s)p}{k|\boldsymbol{D}| + I_0\sqrt{p}},$$

Pa.s

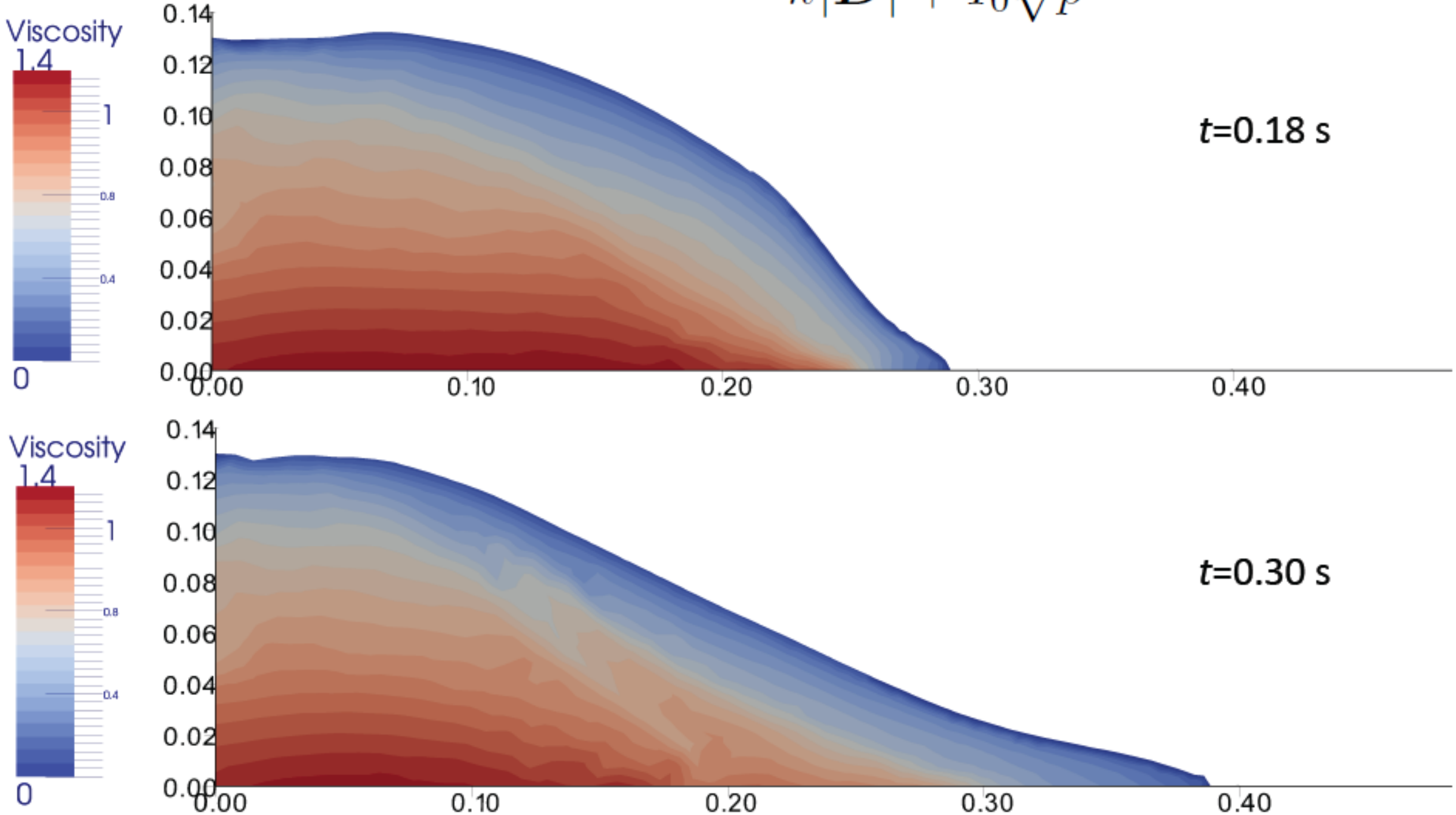

η ~ 1 Pa.s

Very similar results with η = 1 Pa.s

Effect of viscosity

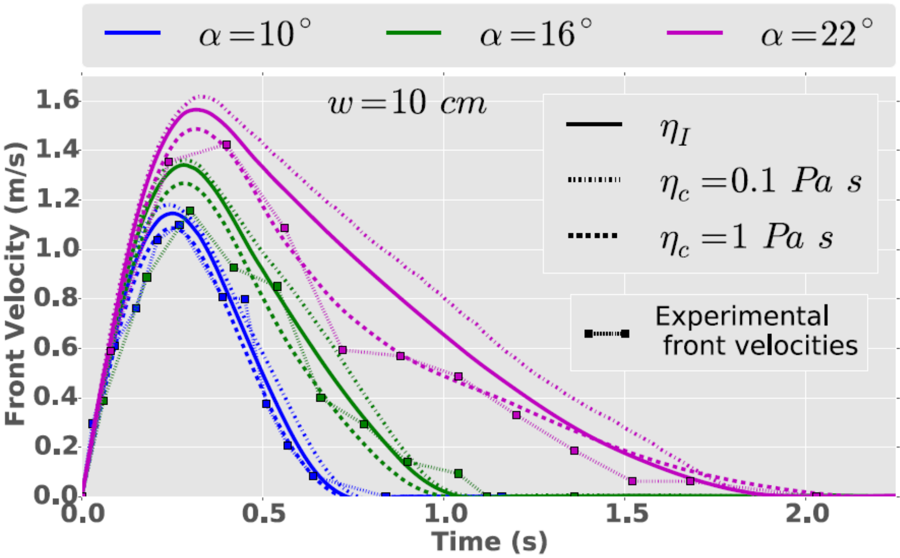

$$2\eta_I(|\boldsymbol{D}|, p) = \frac{k(\mu_2 - \mu_s)p}{k|\boldsymbol{D}| + I_0\sqrt{p}},$$

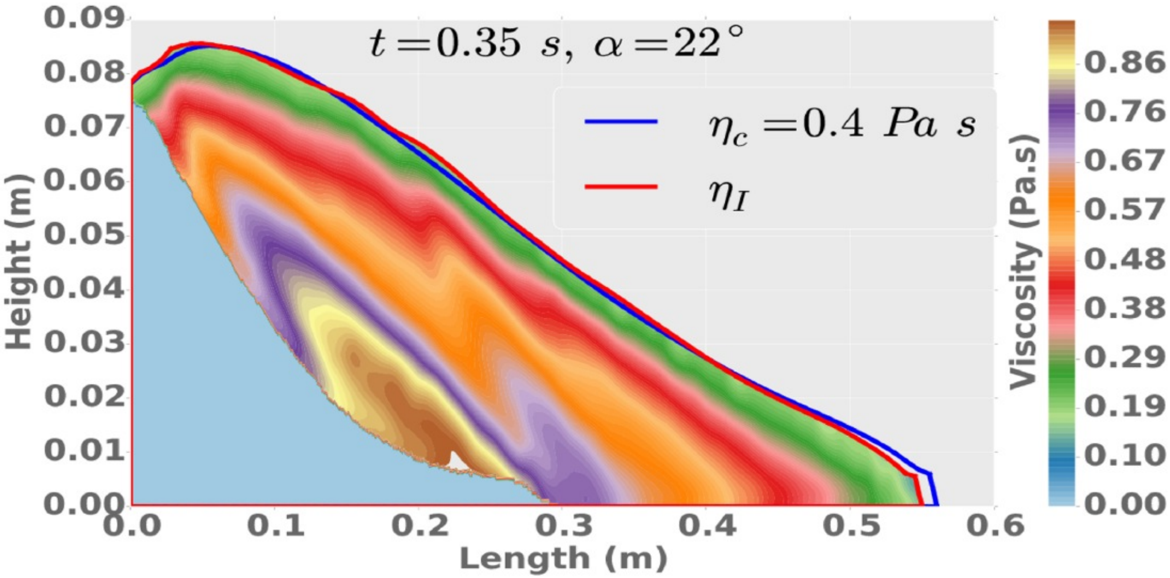

(d)$\alpha = 22^\circ$

Static/flowing interface

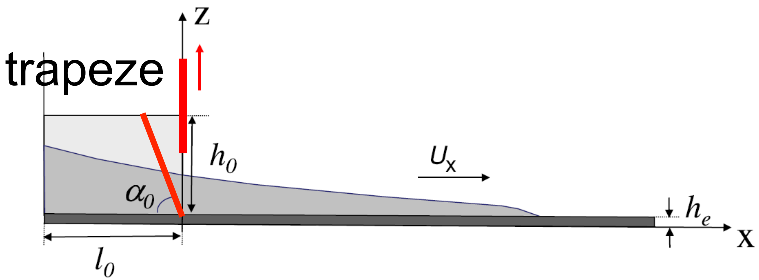

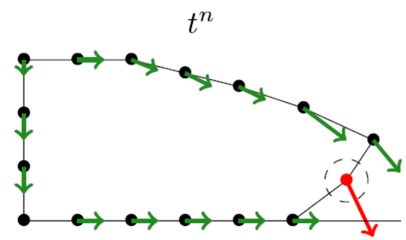

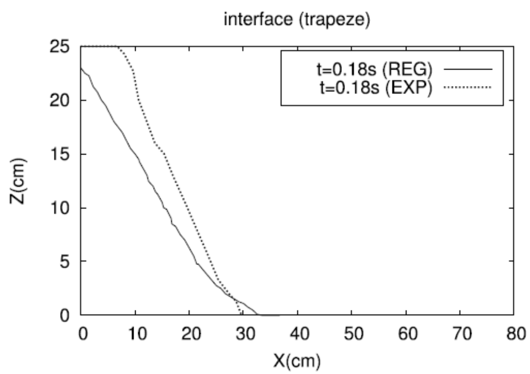

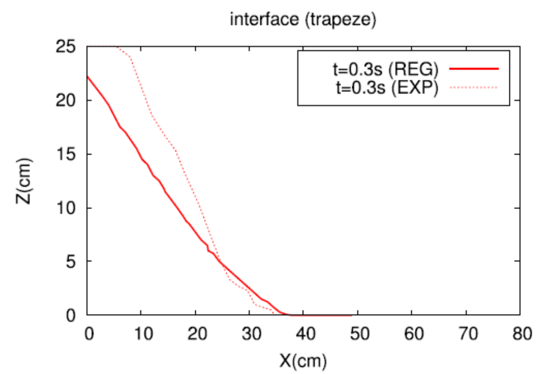

Good quantitative results

High computational time

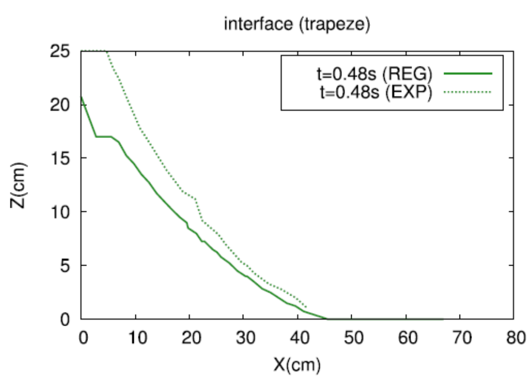

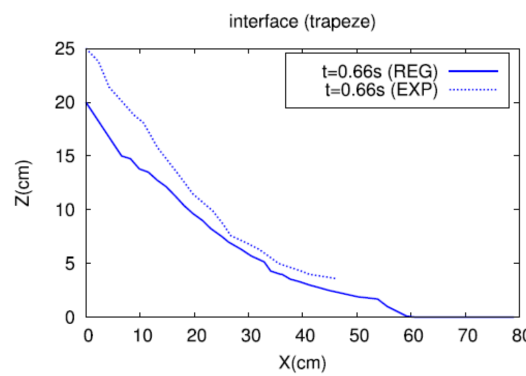

Difficult to deal with erosion at the front

Lusso, Ern, Bouchut, Mangeney, Farin, Roche, 2017

Outline

I – Geophysical reality:
- Complexity of flows and physical processes
- Field data to validate rheological models of real flows
- From field observation to laboratory experiments

II – Modelling of natural landslides
- Shallow model and rheology
- Unexplained high mobility of natural landslides
- Investigating landslide dynamics: seismic data and models

III – Back to the rheology of granular materials
- Laboratory experiments
- 2D visco-plastic models
- Insight into the static/flowing interface
- Multi-layer models

Insight into the static/flowing interface dynamics

A thin flowing layer above a static layer:

Equation for the static/flowing transition $\dot{b}(t)$?

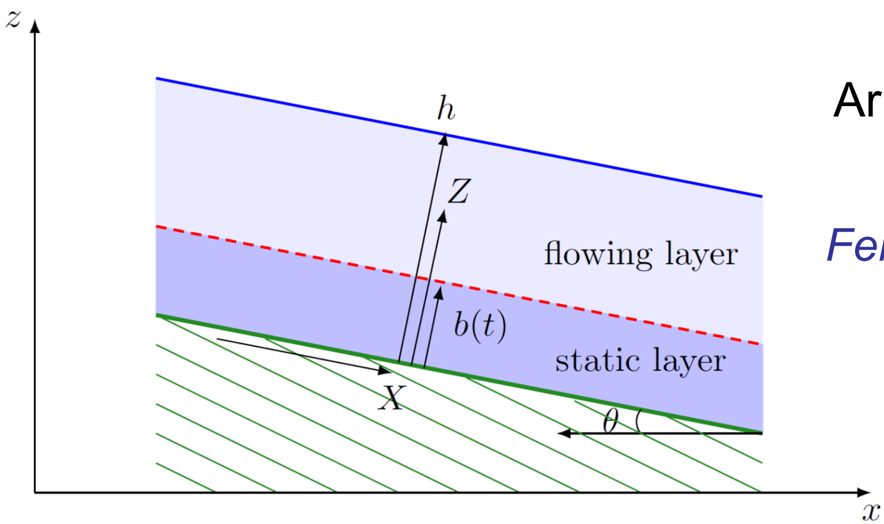

UP TO NOW
Arbitrary closure relations and non-consistent energy in depth-averaged models

Fernandez-Nieto, 2008, Iverson and Ouyang, 2015

Go back to non-depth-averaged models

Viscoplastic models CONTAIN the static/flowing transition

without having to prescribe arbitrary exchange rates,

velocity profiles (*Capart et al. 2015, Gray et al. 2015*,…), etc…

Bouchut, Ionescu, Mangeney, 2015

Simplified 1D shallow viscoplastic model

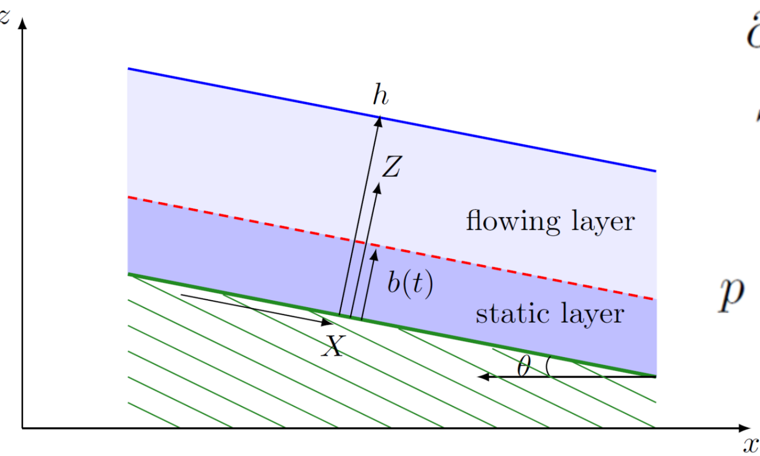

$$\partial_t U(t,Z) + S(t,Z) - \partial_Z\big(\nu \partial_Z U(t,Z)\big) = 0$$
$$S = g(-\sin\theta + \partial_X(h\cos\theta)) - \mu_s \partial_Z p$$

Thin-layer approximation

$$p = g\cos\theta(h - Z) \Rightarrow S = g\cos\theta\,(\tan\delta - \tan\theta + \partial_X h)$$

Boundary conditions

$$\begin{cases} U = 0 & \text{at } Z = b(t), \\ \nu\partial_Z U = 0 & \text{at } Z = b(t), \\ \nu\partial_Z U = 0 & \text{at } Z = h. \end{cases}$$

Initial condition $U(0,Z) = U^0(Z)$

Static/flowing interface

- If $\nu = 0$ and $\partial_Z U(t,b(t)) \neq 0$, then

$$\boxed{\dot b(t) = \frac{S(t,b(t))}{\partial_Z U(t,b(t))}}$$

$$U(t,Z) = \max\Big(U^0(Z) - St, 0\Big)$$

- If $\nu > 0$ and $S(t,b(t)) \neq 0$, then

$$\boxed{\dot b(t,X) = \frac{-\partial^2_{ZZ}(\nu\partial_Z U)(t,X,b(t))}{S(t,X)}\nu.}$$

Lusso, Bouchut, Ern, Mangeney, 2017

Measurements of the static/flowing interface

Laboratory experiments

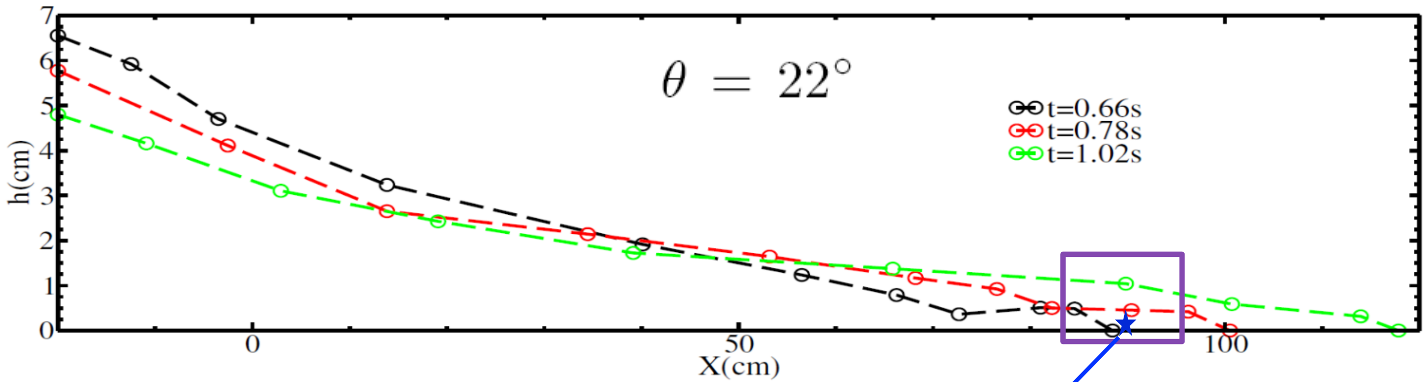

Static/flowing interface at *x*=90 cm

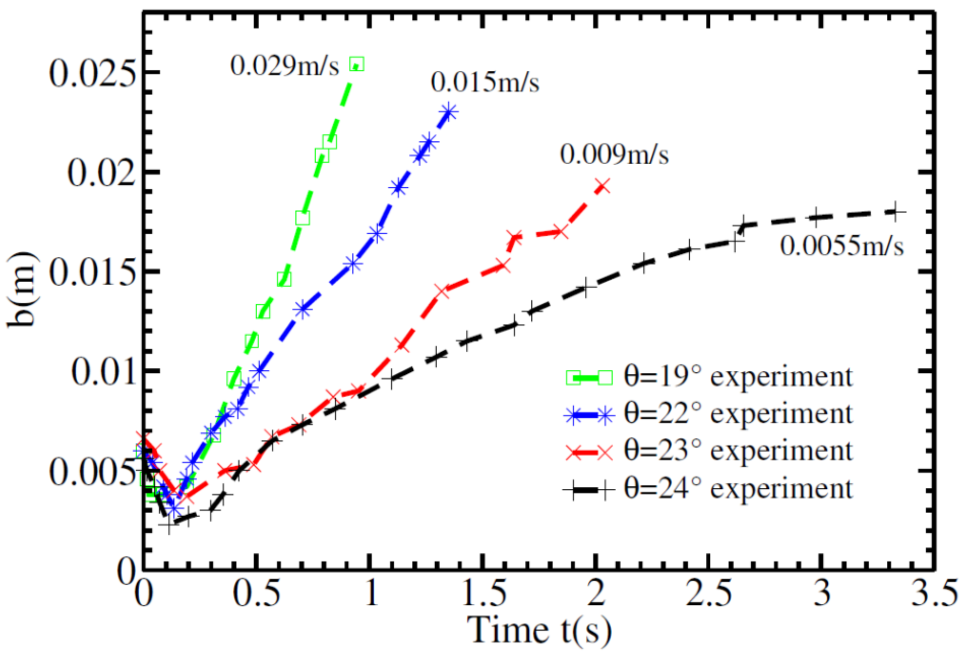

Simplified 1D shallow viscoplastic model

no viscosity (i. e. $\mu(I) = \mu_s$)

Initial linear velocity profile

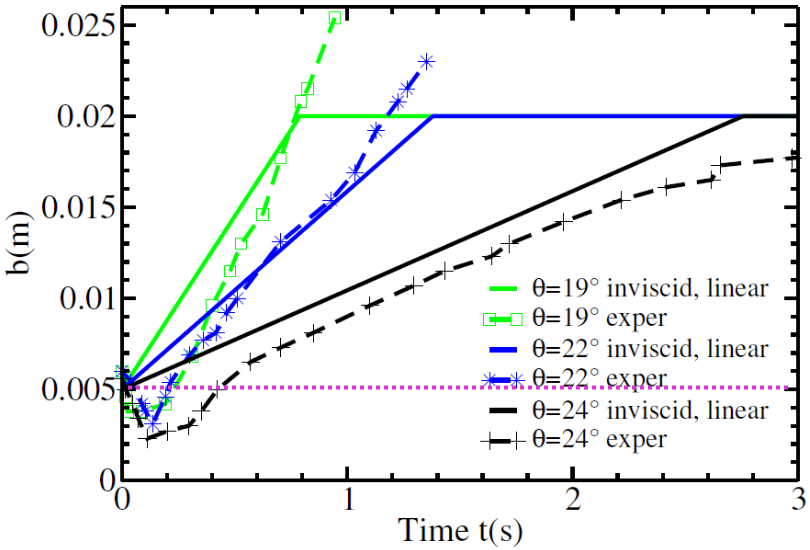

Initial Bagnold velocity profile

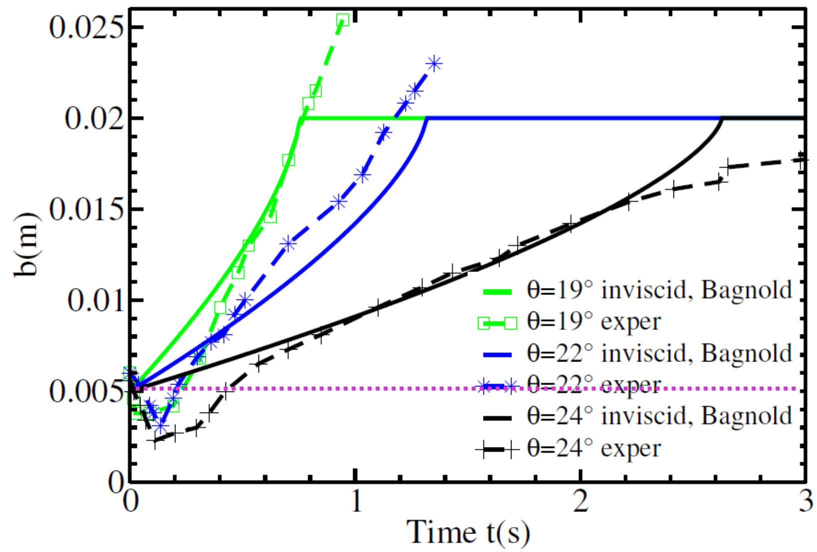

$$U(t, Z) = \max\Big(U^0(Z) - St, 0\Big)$$

$$\dot{b}(t) = \frac{g\cos\theta(\tan\delta - \tan\theta)}{\partial_Z U(t, b(t))} \geq 0$$

$\Rightarrow$ the initially static bed is not put into motion

Simplified 1D shallow viscoplastic model

(b) $\nu = 5 \times 10^{-5} \mathrm{m}^2/\mathrm{s}$ η = 0.075 Pa.s

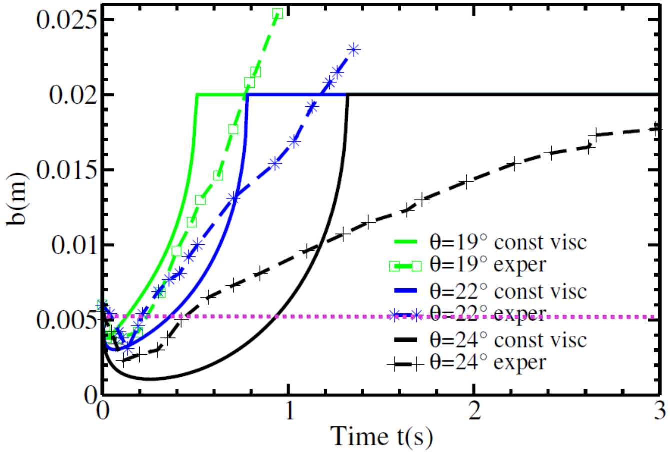

(c) $\nu = 10^{-4} \mathrm{m}^2/\mathrm{s}$ η = 0.15 Pa.s

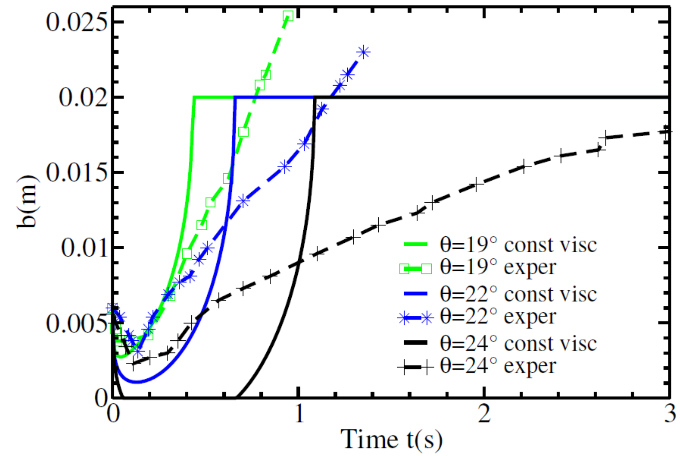

$\mu(I)$ law

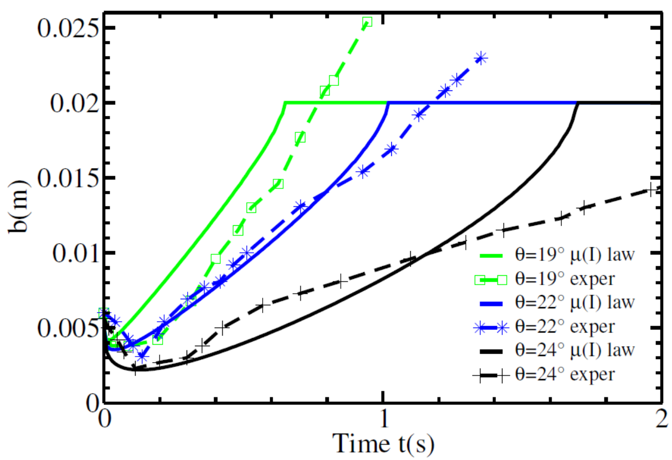

$\theta = 22^o$

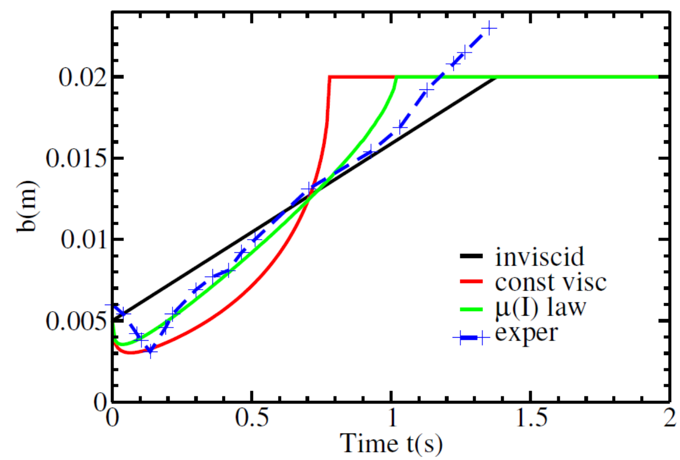

$\mu(I)$ rheology : $2\eta(|\boldsymbol{D}|, p) = \dfrac{k(\mu_2 - \mu_s)p}{k|\boldsymbol{D}| + I_0\sqrt{p}}$

$$\dot{b}(t, X) = \frac{-\partial^2_{ZZ}(\nu \partial_Z U)(t, X, b(t))}{g \cos\theta(\tan\delta - \tan\theta)} \nu.$$

Simplified 1D shallow viscoplastic model

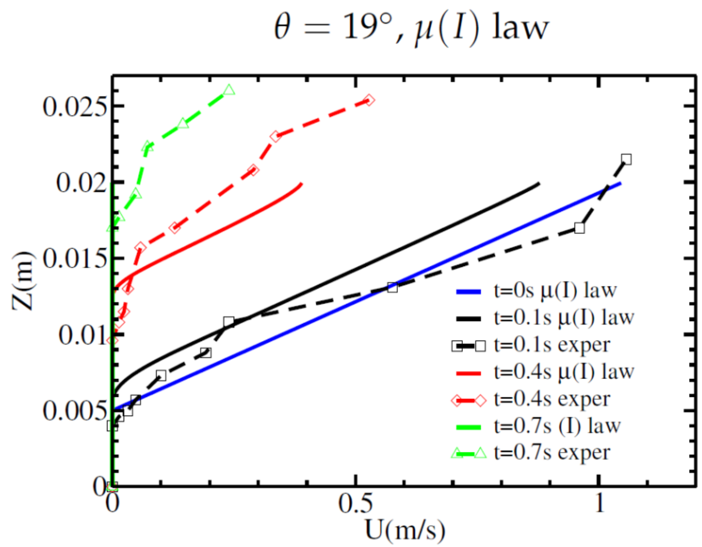

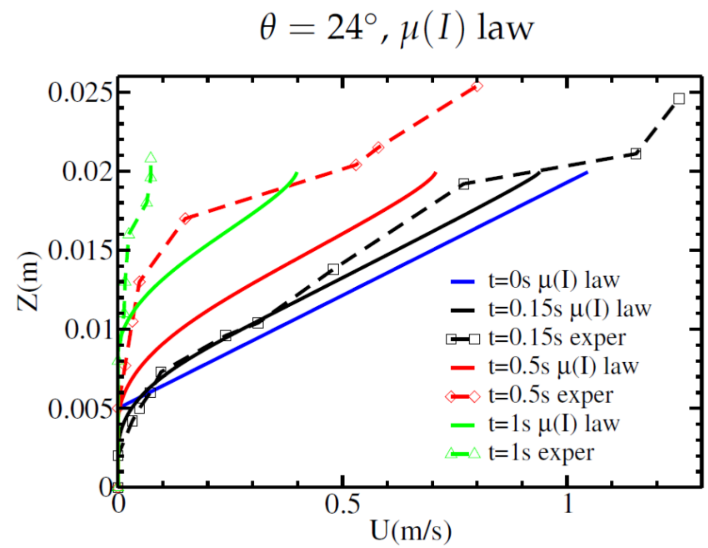

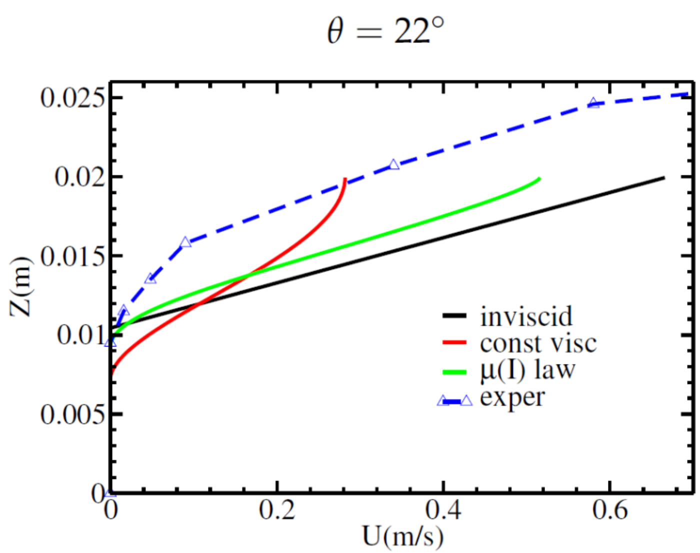

The velocity decreases more rapidly in the model

No wall friction !

Simplified 1D shallow viscoplastic model

Role of downslope gradients

- If $\nu = 0$ and $\partial_Z U(t, X, b(t)) \neq 0$, then

$$\dot{b}(t) = \frac{g\cos\theta\,(\tan\delta - \tan\theta + \partial_X h)}{\partial_Z U(t, b(t))}$$

- If $\nu > 0$ and $S(t, X) \neq 0$, then

$$\dot{b}(t) = \frac{-\partial^2_{ZZ}(\nu\partial_Z U)(t, X, b(t))}{g\cos\theta\,(\tan\delta - \tan\theta + \partial_X h)}\,\nu$$

In the case of granular collapse:

$\tan\delta - \tan\theta = 0.0837$ $\quad\quad$ $\partial_X h(t = 0.66\,\mathrm{s}, X = 90\,\mathrm{cm}) \simeq -0.125$

S<0, erosion occurs even in the inviscid case : instantaneous erosion of the full layer

Then S is posivite : deposion occurs progressively

Modelling of the static/flowing transition

Two thin-layer depth-averaged model

➡ Equation for the static/flowing transition $\dot{b}(t)$?

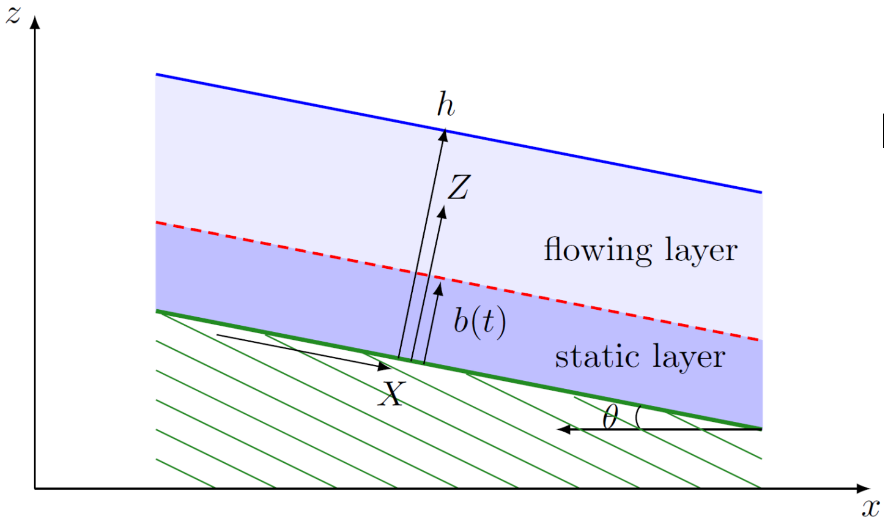

Not possible without assumptions on the velocity profiles !!!

Capart et al. 2015 : S-shaped profile
Gray et al. 2015 : Bagnold profile

The shape of the velocity profile changes with time (*GDR MiDi, 2004*, etc.) !

Bouchut, Ionescu, Mangeney, 2015

Outline

I – Geophysical reality:
- Complexity of flows and physical processes
- Field data to validate rheological models of real flows
- From field observation to laboratory experiments

II – Modelling of natural landslides
- Shallow model and rheology
- Unexplained high mobility of natural landslides
- Investigating landslide dynamics: seismic data and models

III – Back to the rheology of granular materials
- Laboratory experiments
- 2D visco-plastic models
- Insight into the static/flowing interface
- Multi-layer models

Multilayer Shallow Model

For application to natural flows, equations have to be simplified to lower the computational cost !

➡ Thin-layer (i. e. shallow) approximation $a=h/L<<1$

➡ $p = g\cos\theta(h - Z)$ pression hydrostatique

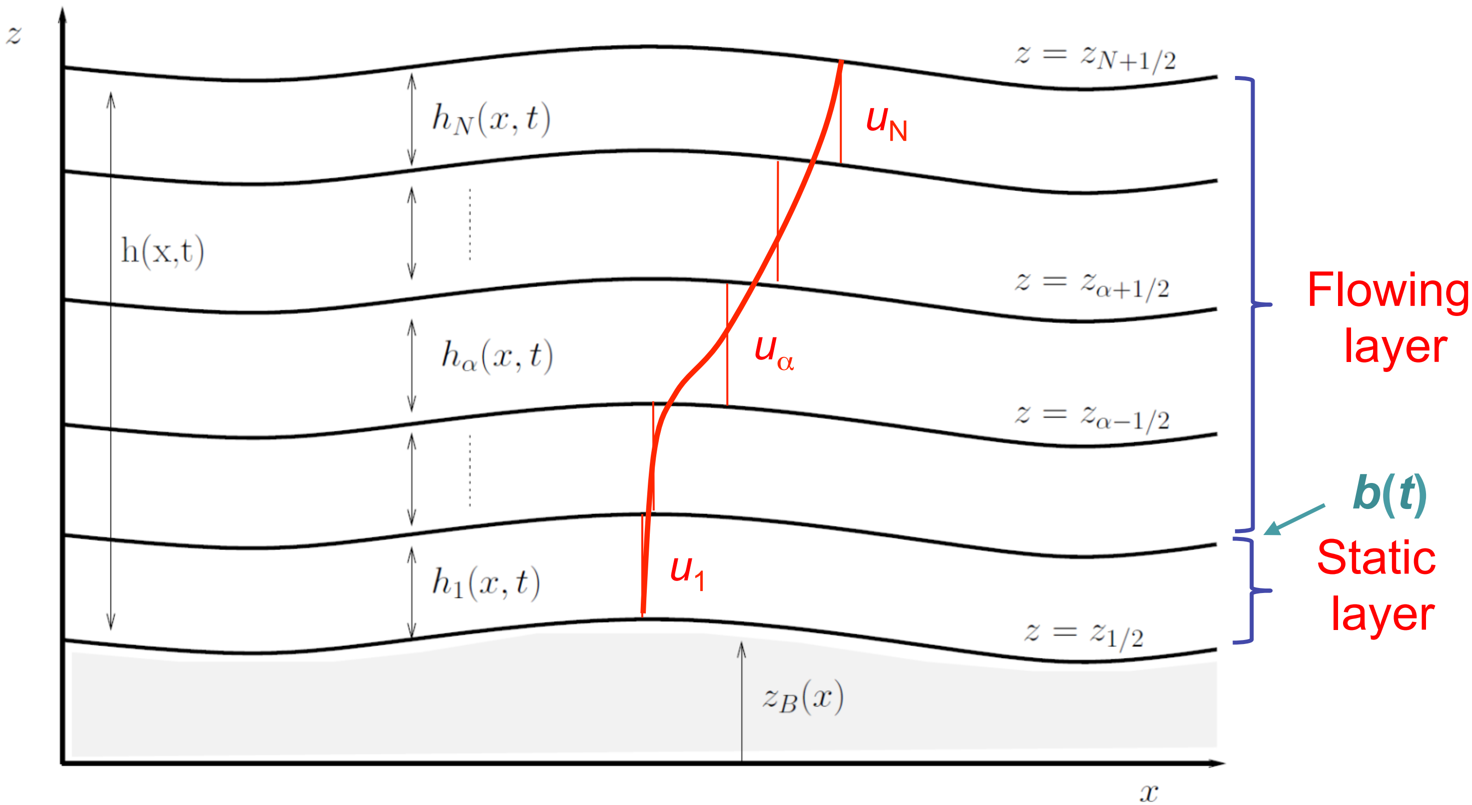

Fernandez-Nieto, Garres, Mangeney, Narbona-Reina, 2015

Multilayer Shallow Model

$$\partial_x \overline{u} + \partial_z \overline{w} = 0,$$
$$\rho\left(\partial_t \overline{u} + \overline{u}\partial_x \overline{u} + \overline{w}\partial_z \overline{u}\right) + \partial_x \overline{p} = -\rho\, g\, \sin\theta + \partial_z \left(\overline{\eta}\frac{\partial_z \overline{u}}{2}\right) - \frac{2}{W}\,\mu_w\,\overline{p}\,\frac{u}{|u|},$$
$$\partial_z \overline{p} = -\rho\, g \cos\theta.$$

Steady uniform flows on inclined planes

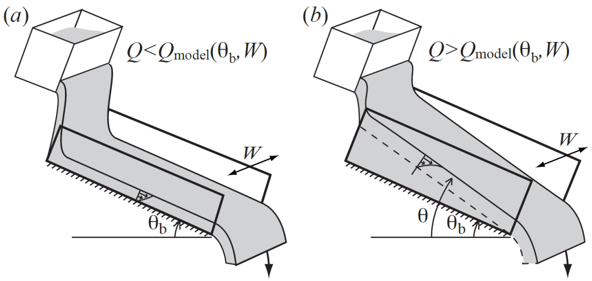

Jop et al., 2005

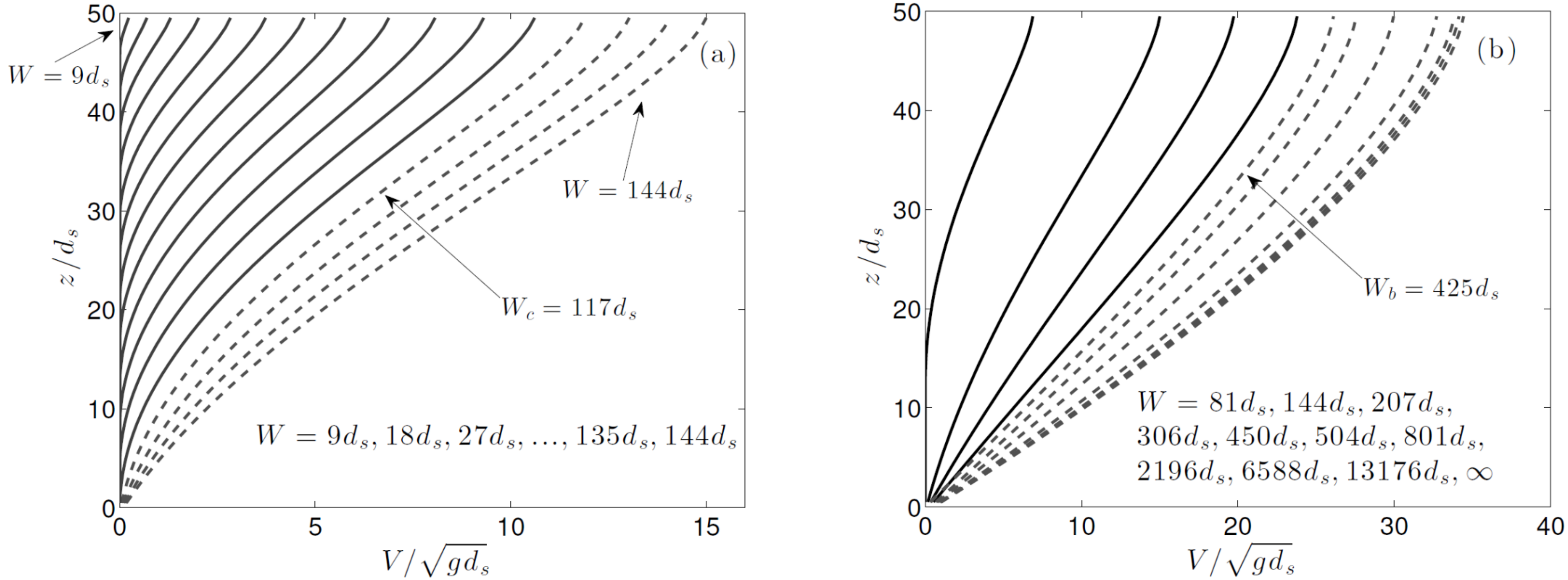

Unsteady flows on inclined planes

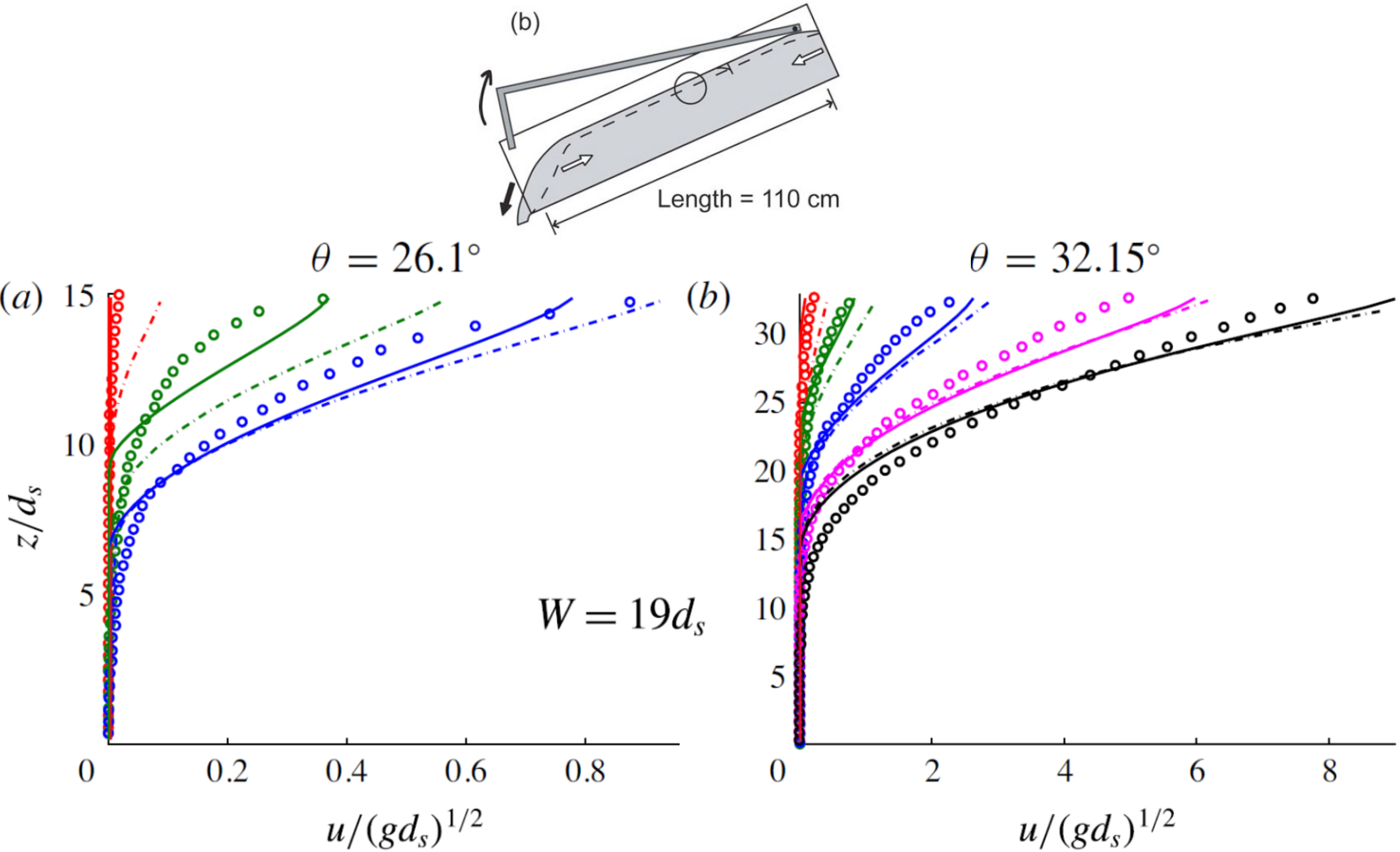

Fernandez-Nieto, Garres, Mangeney, Narbona-Reina, 2017

Monolayer (Saint-Venant) versus Multilayer models

$$\mu_s = \tan(25.5^\circ) \approx 0.48$$

$\theta = 22^\circ$

$\mu(I)$

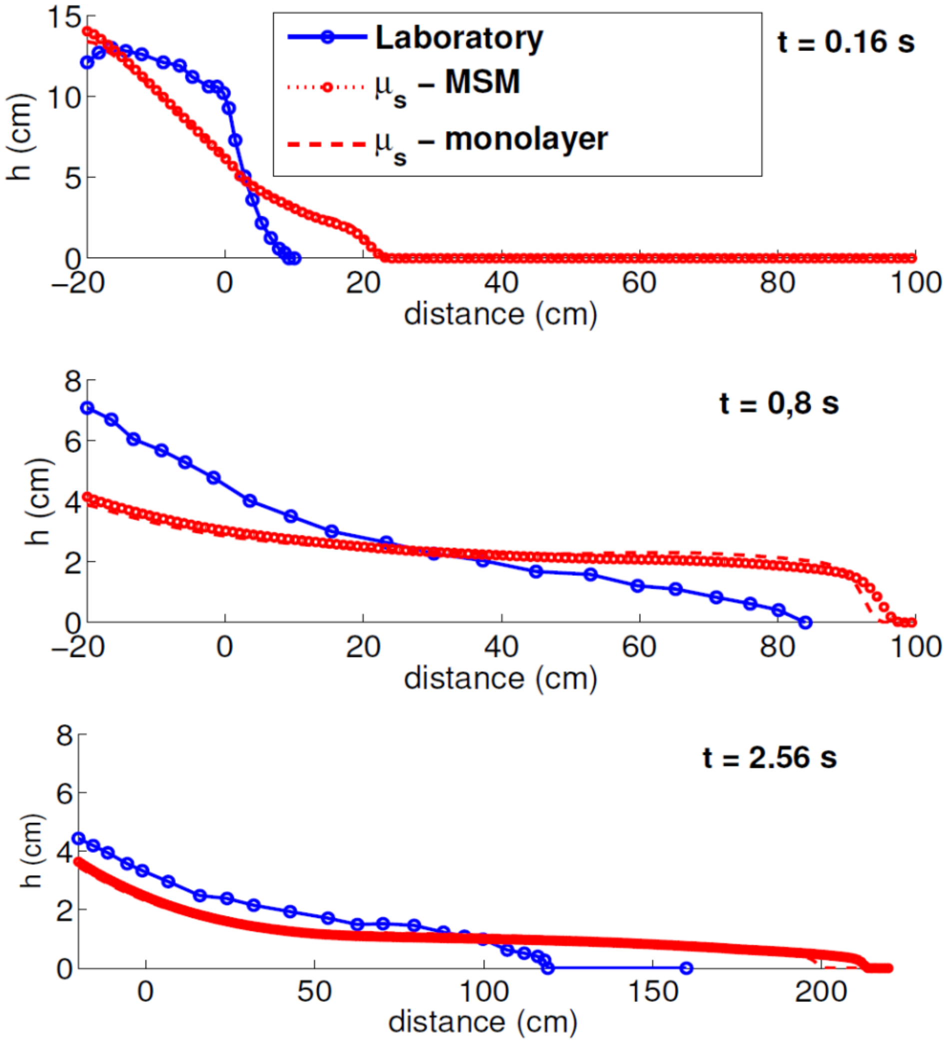

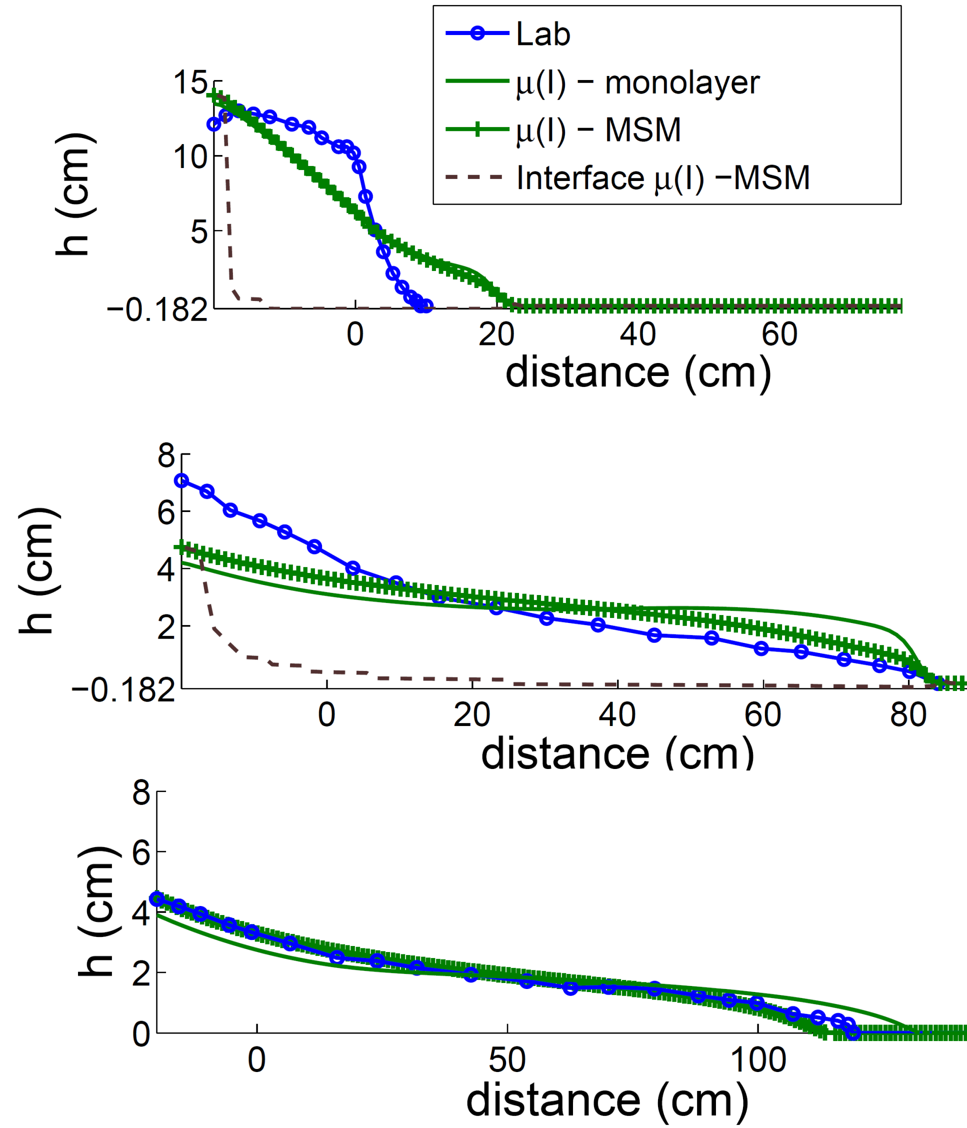

Fernandez-Nieto, Garres, Mangeney, Narbona-Reina, 2016

Multilayer models and wall friction

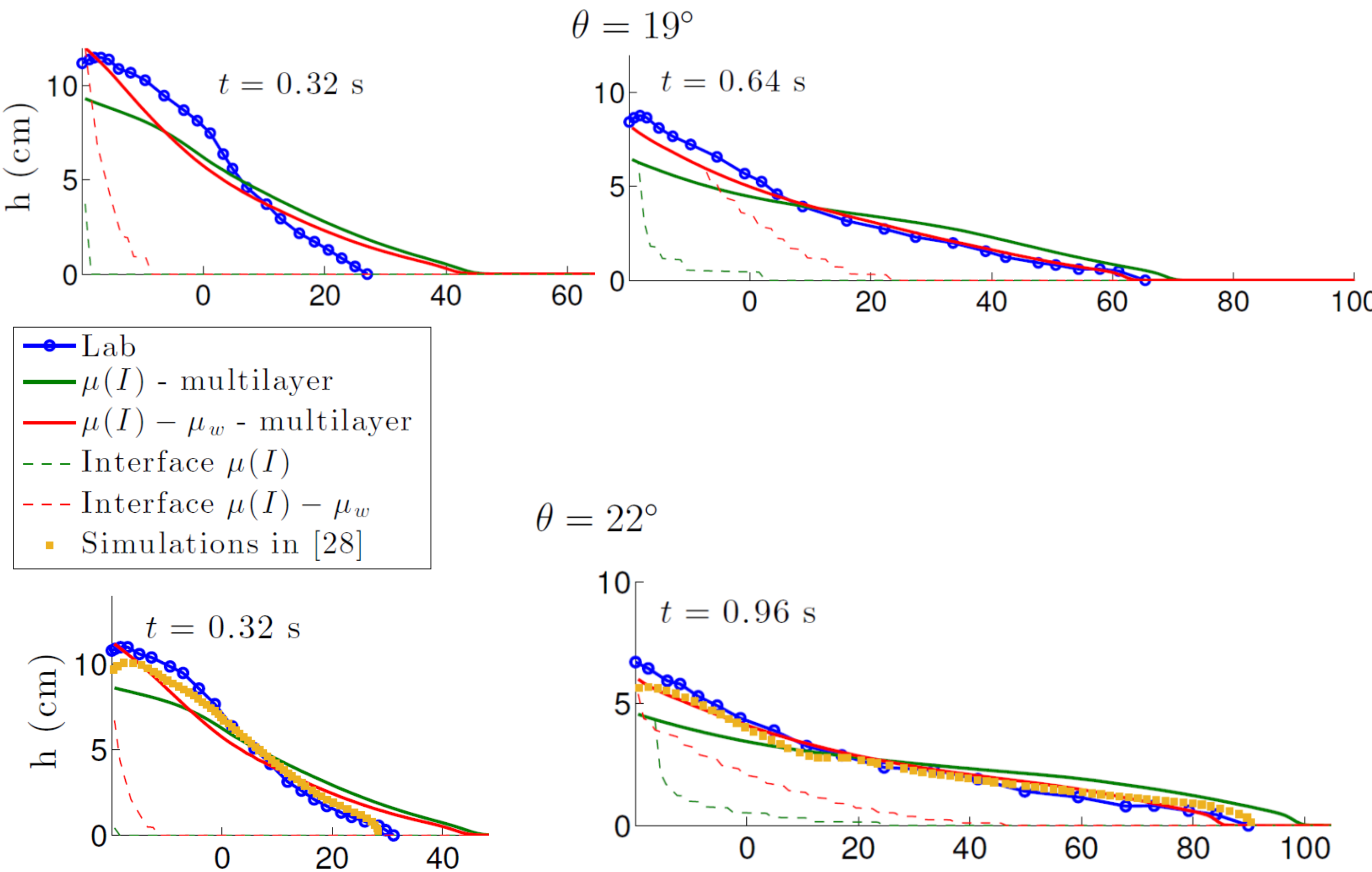

Static-/flowing interface within erodible bed

$$\theta = 22^\circ \qquad W = 10\ cm$$

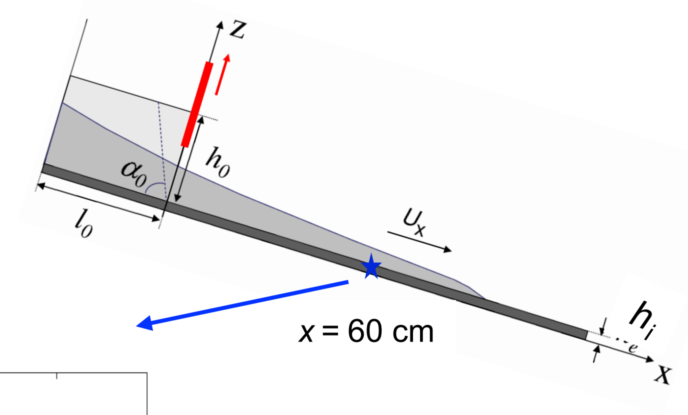

h_i = 0 mm $\qquad$ h_i = 4.6 mm

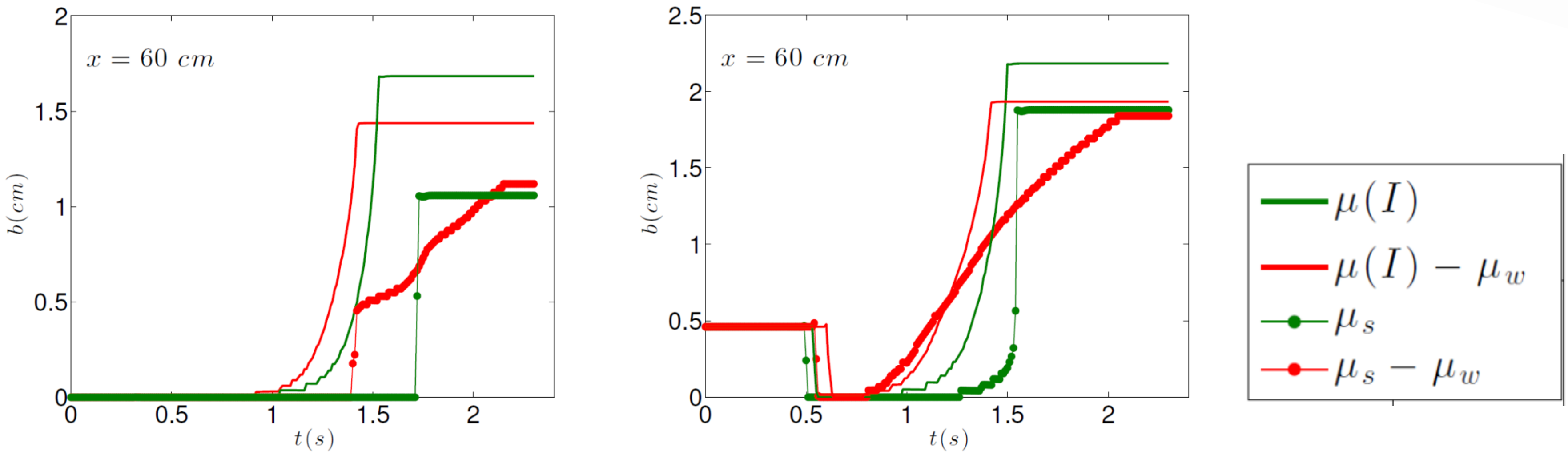

Strong effect of wall friction on the static/flowing interface dynamics

Comparison with shallow visco-plastic model

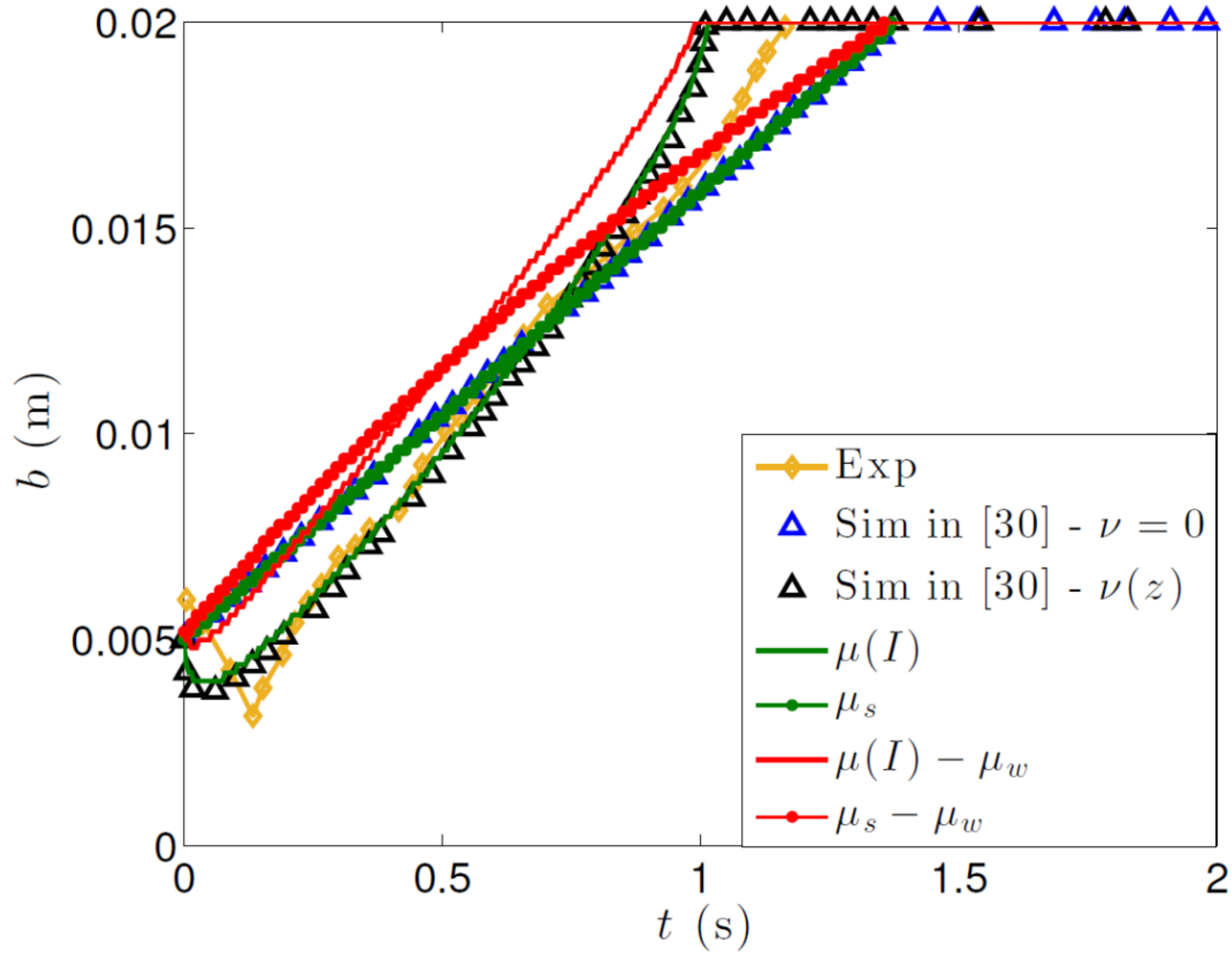

Strong effect of wall friction on the static/flowing interface dynamics

Erosion effects on avalanche runout

$\mu_s = \tan(25.5°) \approx 0.48$

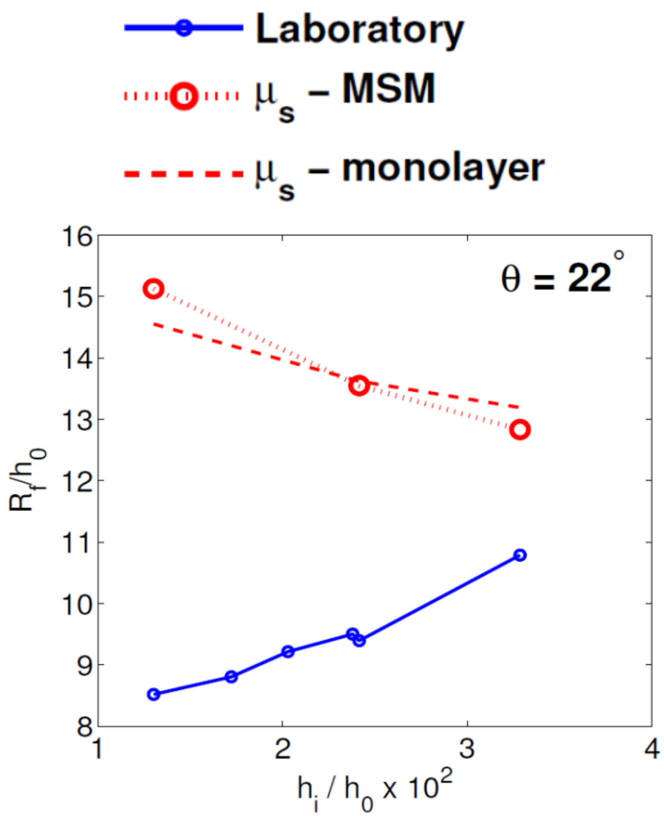

$\mu(I)$

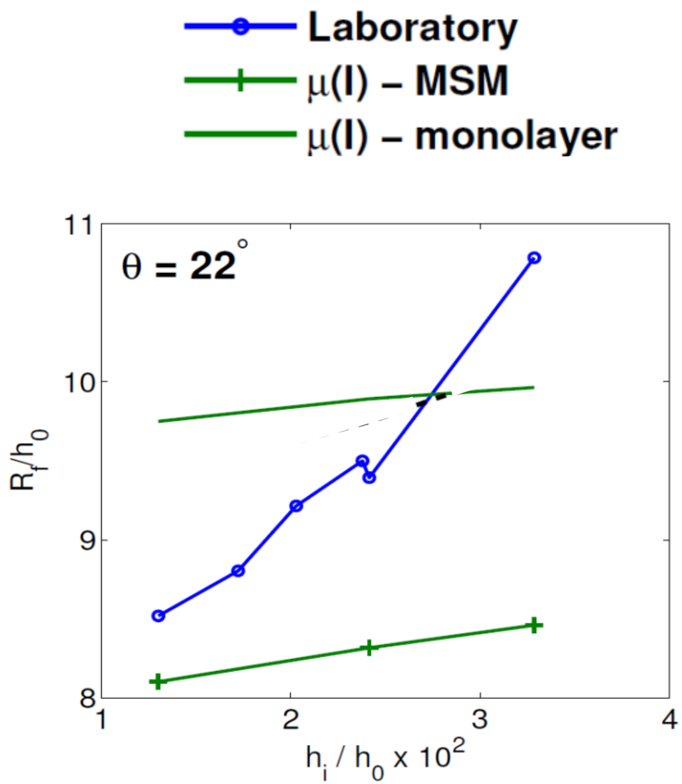

$\mu(I)$ in the Multilayer Shallow Model reproduces qualitatively the increase of runout due to entrainment on sloping erodible beds.

How to get quantitative agreement ? Non-hydrostatic effects, dilatancy ??

Erosion waves ?

$\theta = 25.2^\circ \quad h_i = 3.9\ \mathrm{mm}$

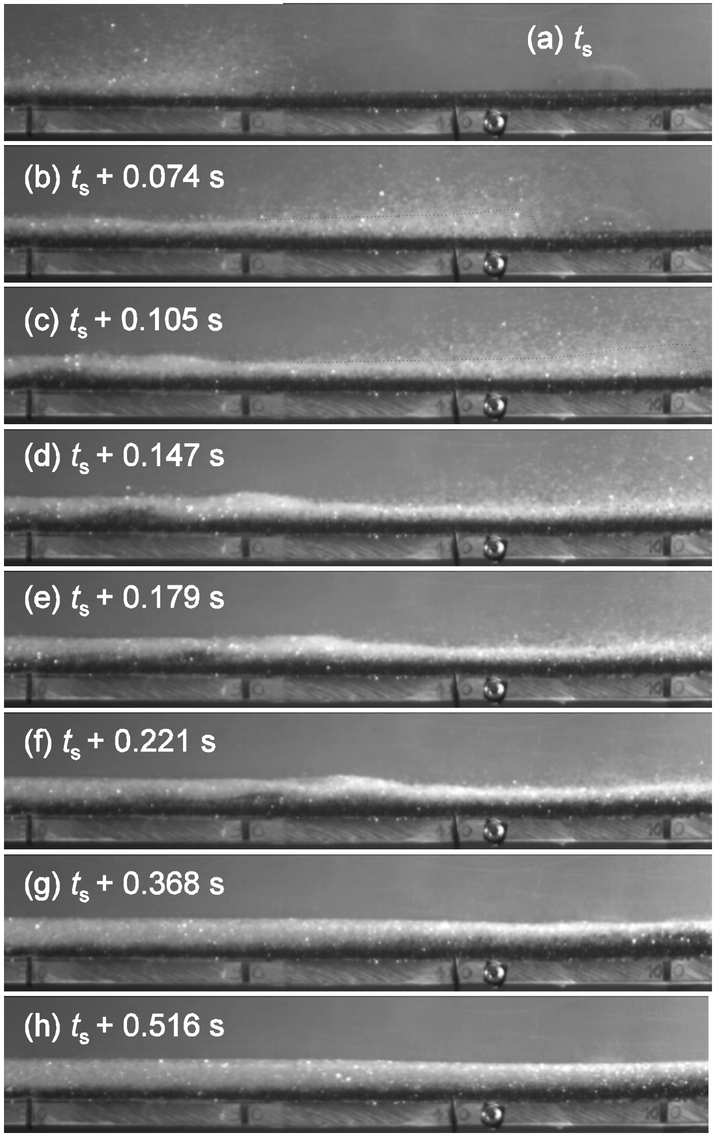

Erodible bed

$\theta = 25.2^\circ$ Rigid bed ($h_i = 0\ \mathrm{mm}$)

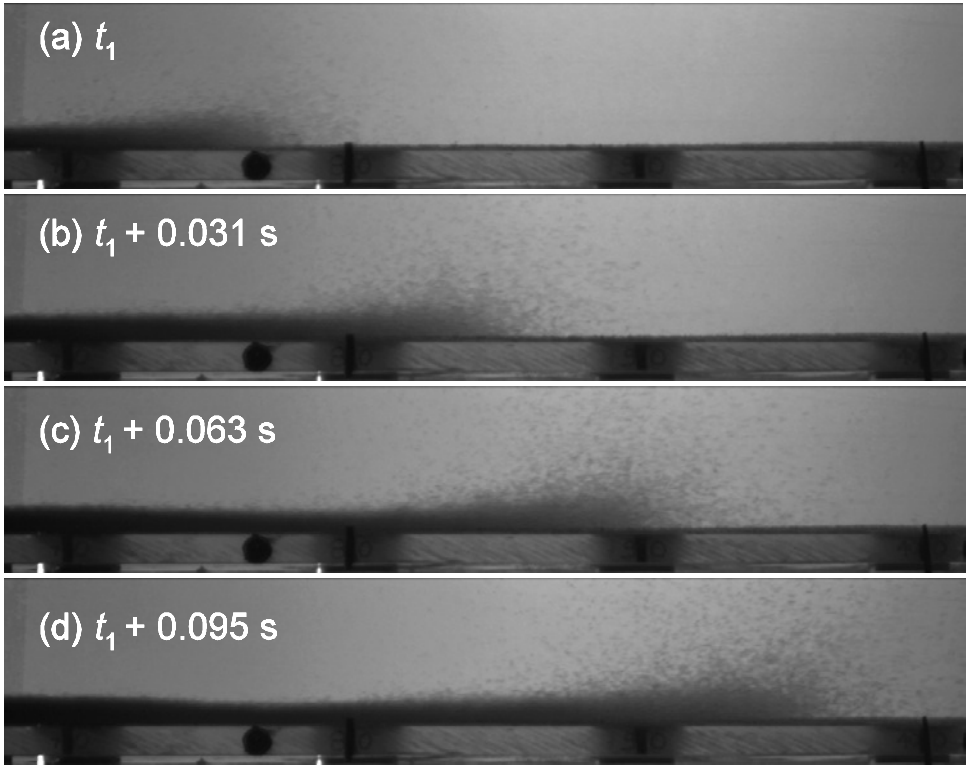

- **Steep front over rigid and erodible bed**
- **Waves located behind the front**

vertical motion that removes grains from the erodible bed

Force chains ahead of the front

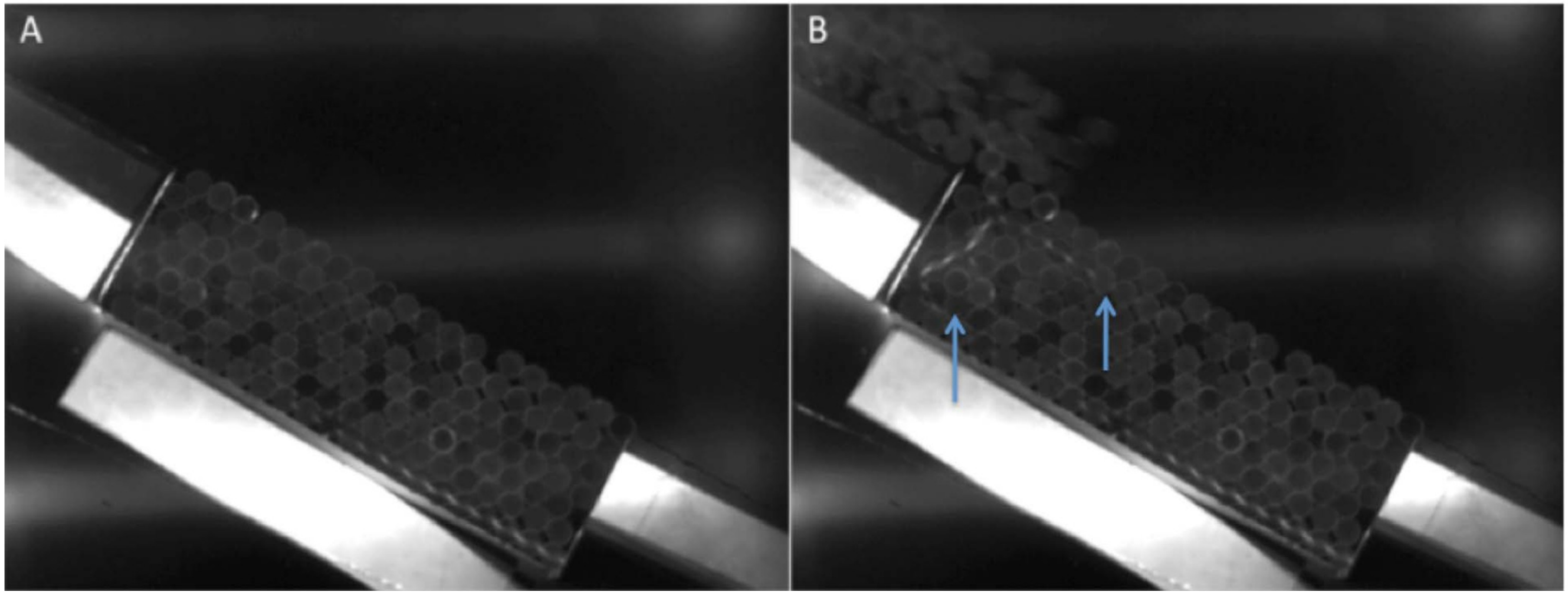

Estep and Dufek, 2012

Force chains in granular media

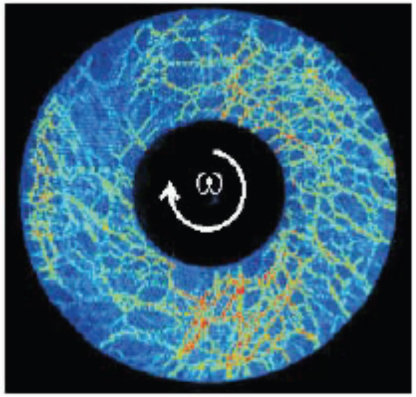

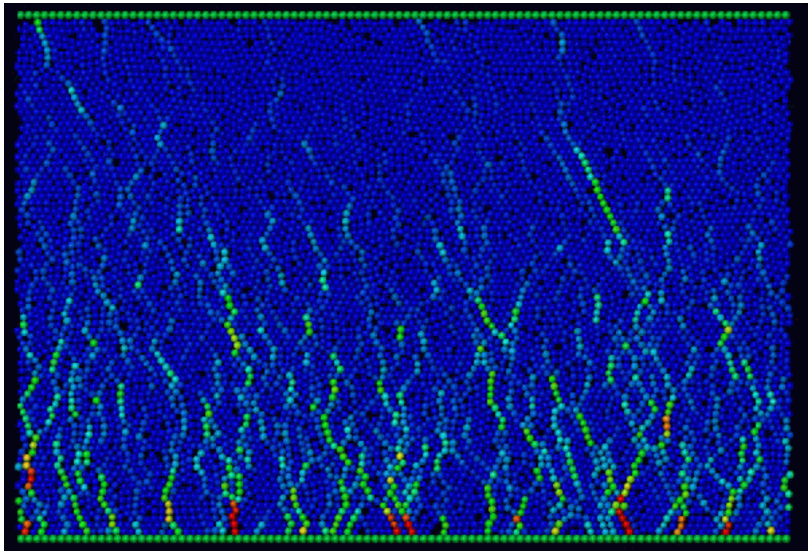

Role of force chains in granular media

Dilatancy effects

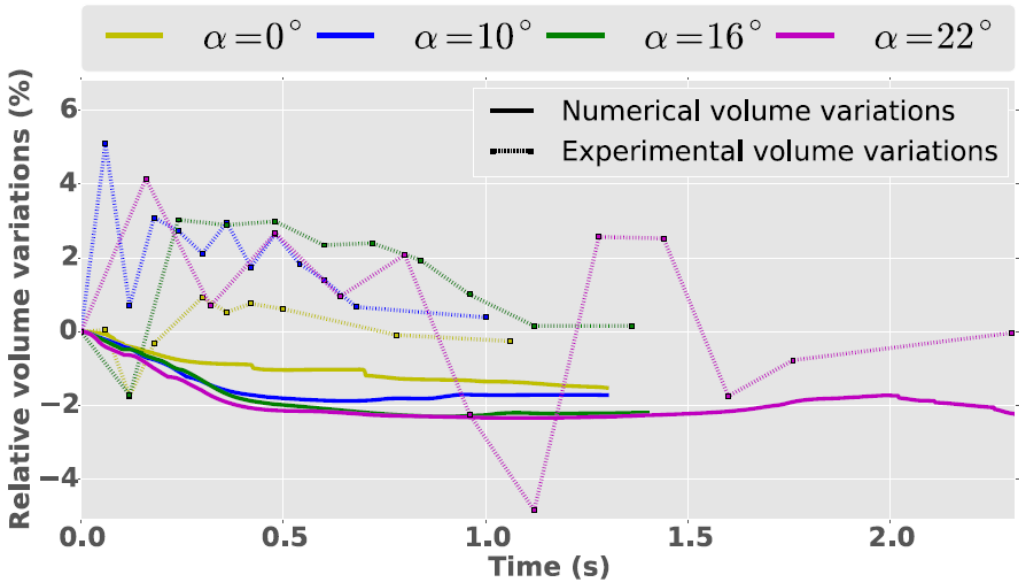

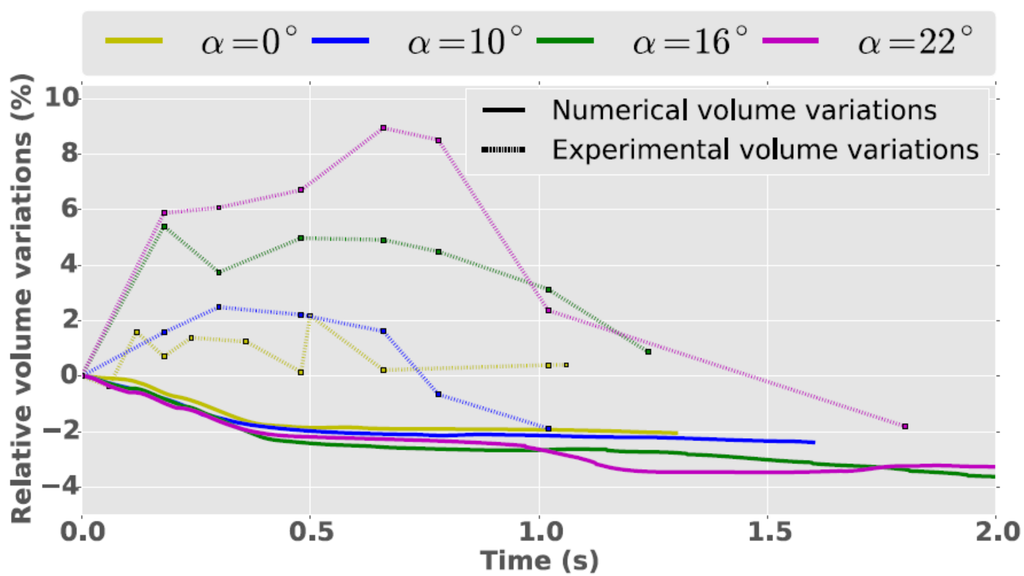

Up to 10% of dilatation in granular collapse !

Influence of the compaction of the erodible bed

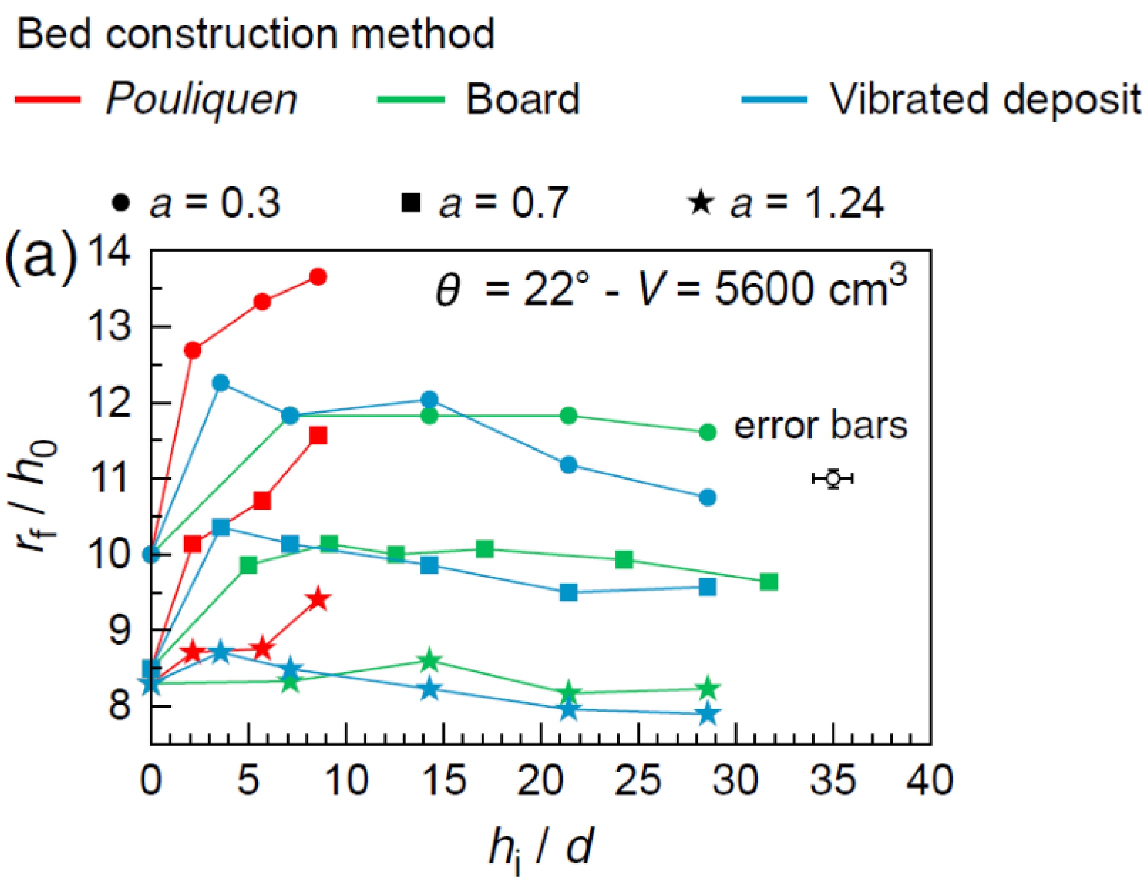

$\mu(I)$

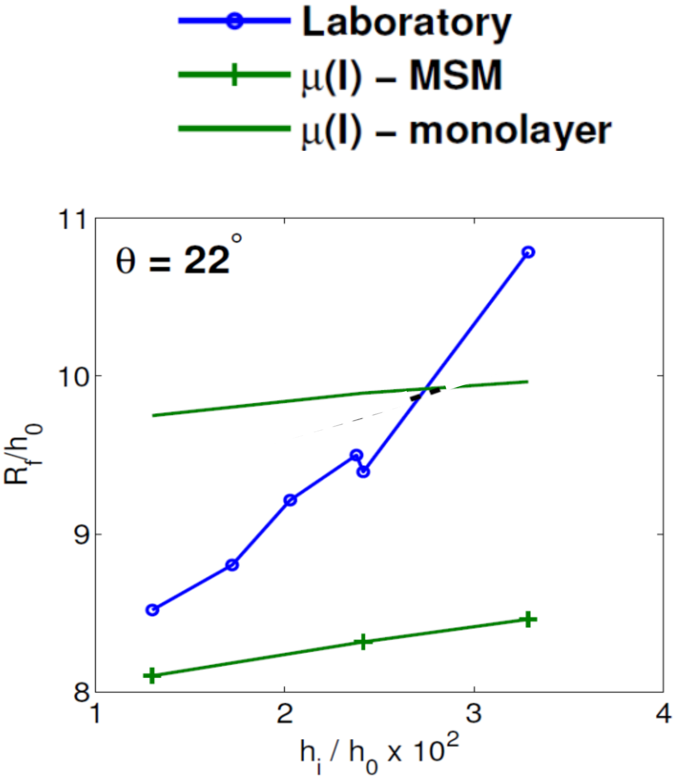

I – Fluis/solid model with dilatancy

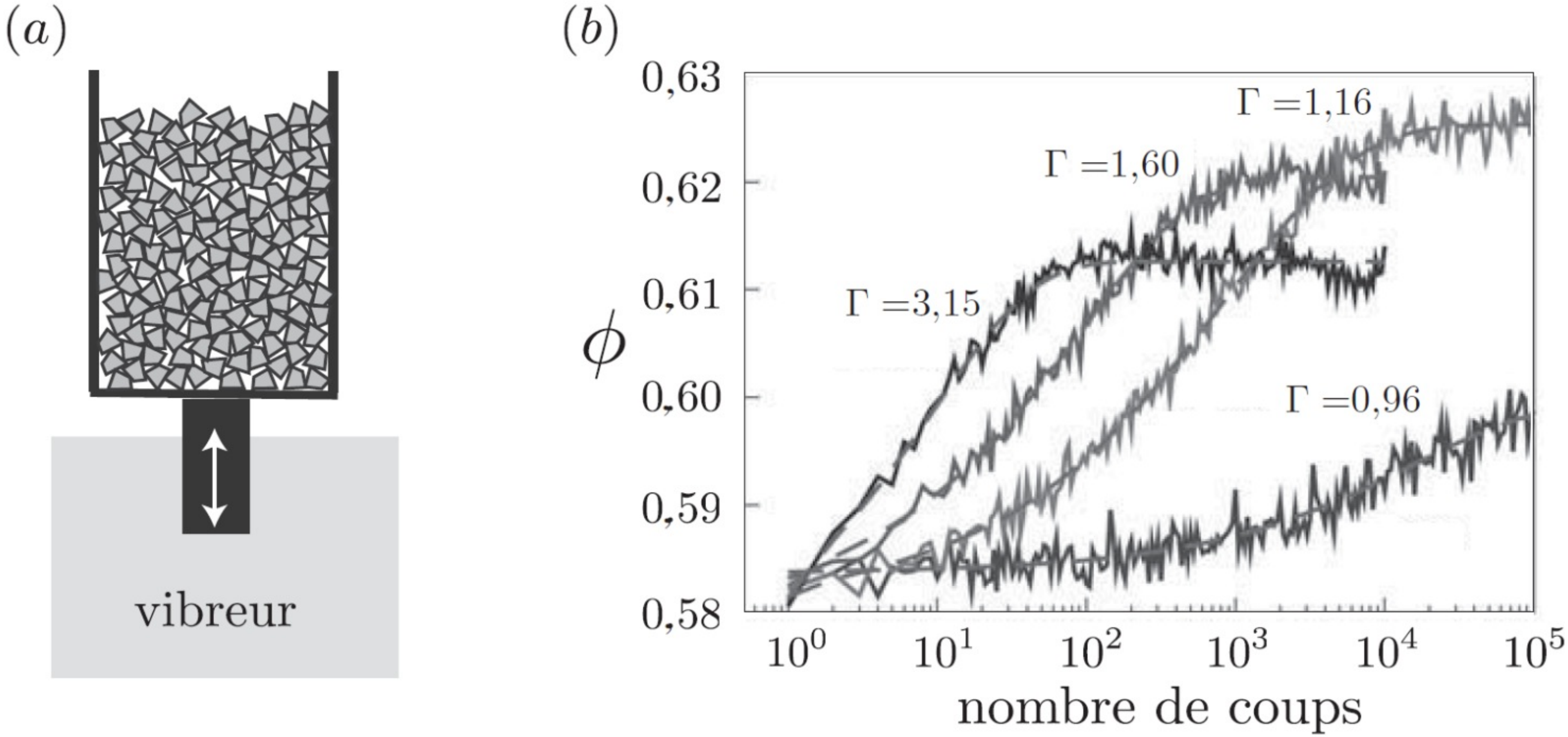

(a) Compaction sous vibration. (b) Évolution de la fraction volumique en fonction du nombre de coups imposés, pour différentes accélerations relatives Γ (d'après Richard *et al.*, 2005).

Essai en cisaillement à déformation imposée

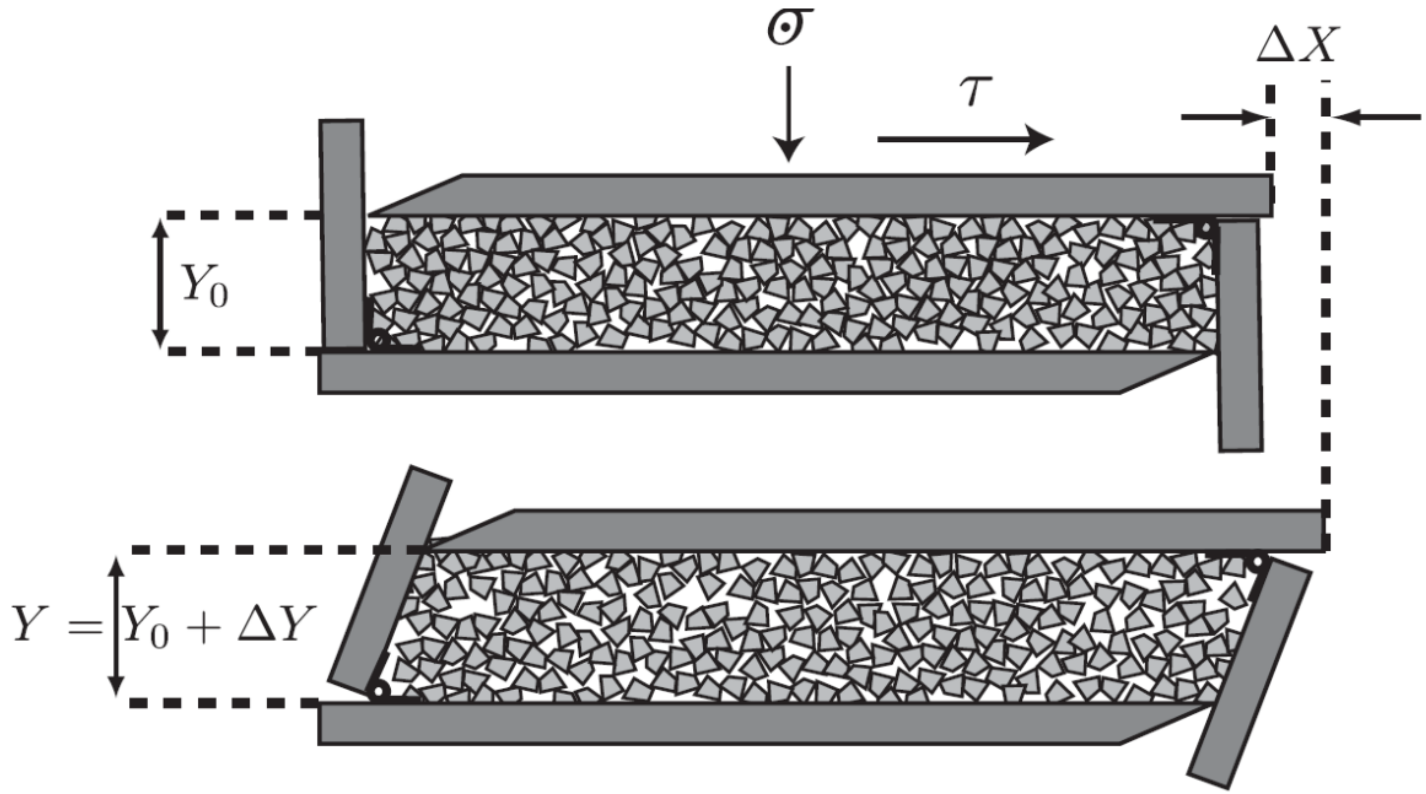

Principe de la cellule de cisaillement simple : une contrainte normale σ est appliquée sur la demi-boite supérieure et une déformation $\gamma = \Delta X/Y_0$ est imposée. On mesure la contrainte tangentielle τ et la variation de volume donnée par ΔY.

Le comportement du matériau dépend de sa préparation initiale

Pour des déformations > 60 %, l'état initial semble oublié et on atteint une contrainte tangentielle τ_c et une fraction volumique ϕ_c ne dépendant plus de la déformation ni de la préparation. Cet état est appelé *état critique*. Il dépend de la contrainte normale de confinement

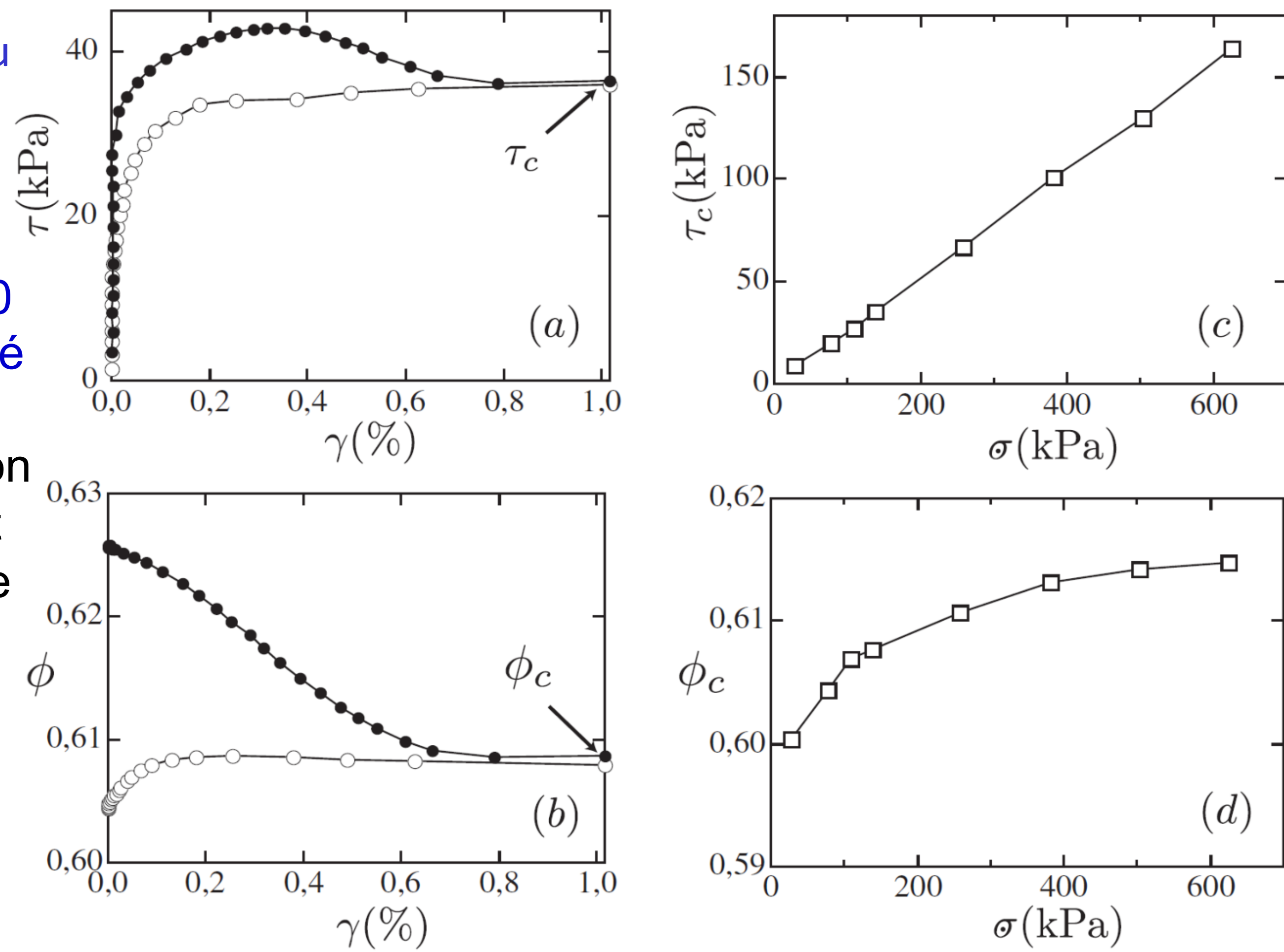

Mesures obtenues en cellule de cisaillement avec des billes d'acier de 1 mm (données issues de Wroth, 1958). (a) Variation de la contrainte tangentielle τ en fonction de la déformation imposée $\gamma = \Delta X/Y_0$ pour une contrainte de confinement σ de 140 kPa pour un empilement initialement dense (●) et initialement lâche (○). (b) Fraction volumique ϕ fonction de γ. (c) et (d) Variation de la contrainte tangentielle critique τ_c et de la fraction volumique critique ϕ_c en fonction de la contrainte normale appliquée.

(a)

(b)

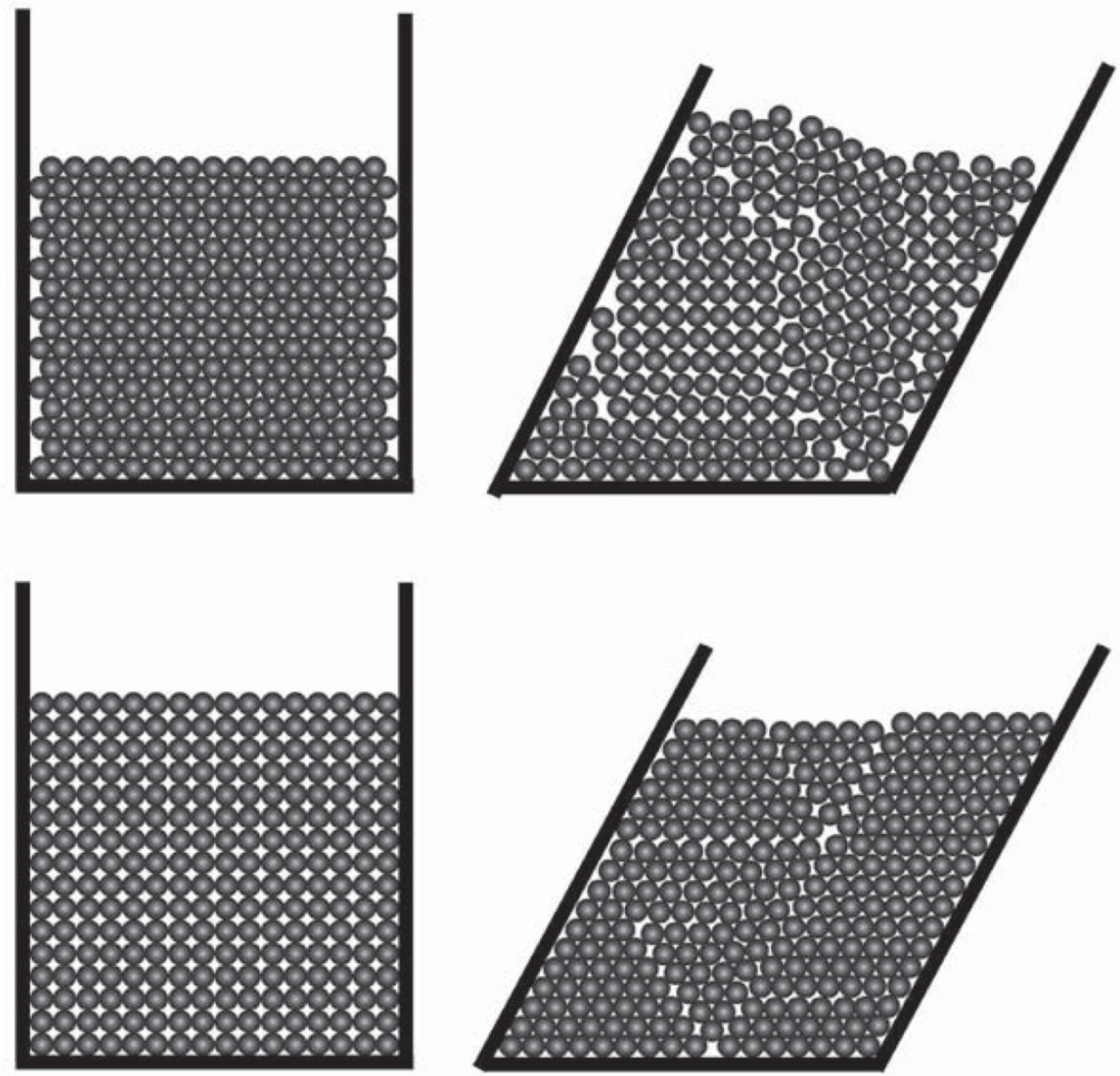

(a) Dilatance observée lorsqu'on cisaille un empilement bidimensionel triangulaire. (b) Contractance observée lorsqu'on cisaille un empilement carré (dessins inspirés d'expériences de Brown & Richards, 1970).

Modeling of debris flows (grain/fluid)

Solid volume fraction: $0.4 < \varphi < 0.8$

At the field scale

- Thin layer approximation $hm/Lm = \varepsilon \ll 1$

$$h_m = \mathcal{O}(\epsilon), u^{\mathrm{x}} = \mathcal{O}(1), u^z = O(\epsilon), \ldots$$

- Depth-averaged model

Mixture model

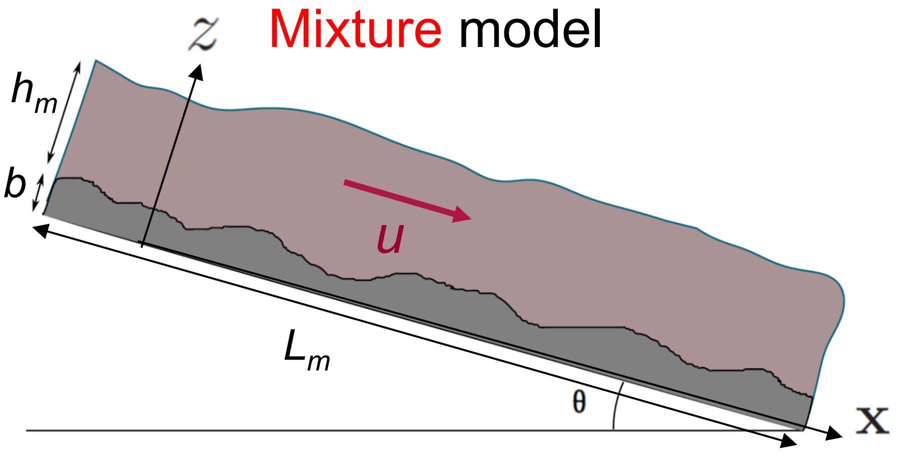

Iverson, Denlinger; Denlinger, Iverson 2001, Iverson, George; George, Iverson 2014

Two-phase model

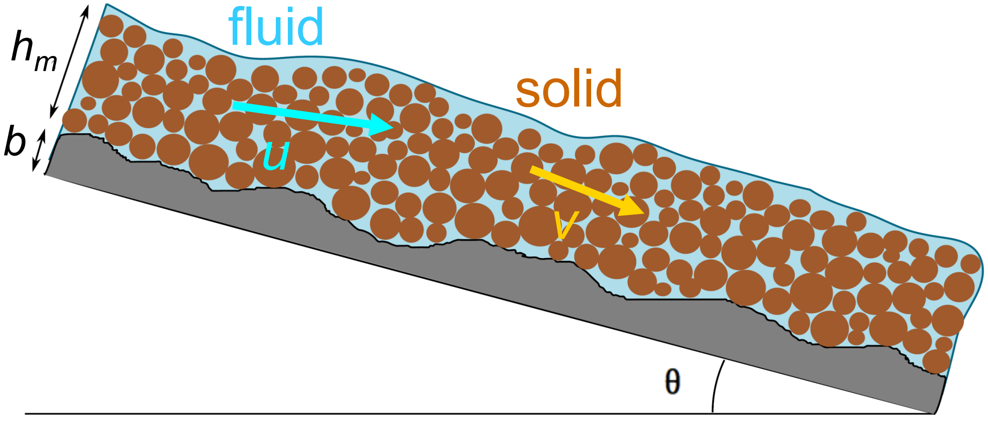

Pitman and Le 2005, Pelanti et al. 2008, 2011

Modeling of debris flows (grain/fluid)

Solid volume fraction: $0.4 < \varphi < 0.8$

At the field scale

- Thin layer approximation $hm/Lm = \varepsilon \ll 1$

$$h_m = \mathcal{O}(\epsilon), u^{\mathrm{x}} = \mathcal{O}(1), u^z = O(\epsilon), \ldots$$

- Depth-averaged model

Mixture model

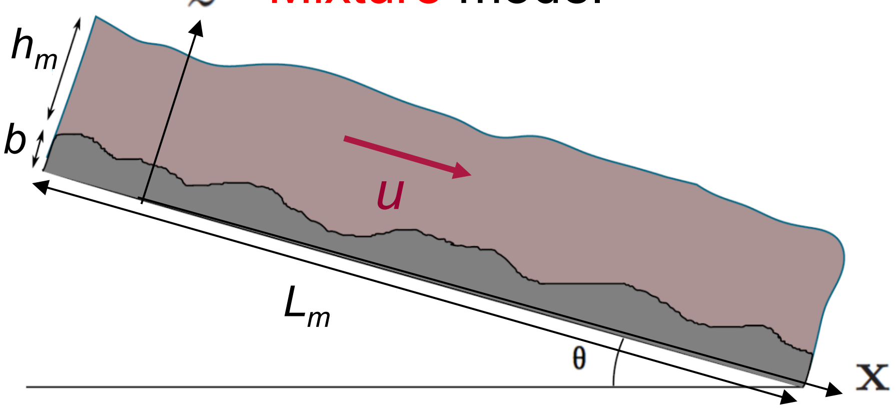

Iverson, Denlinger; Denlinger, Iverson 2001,
Iverson, George; George, Iverson 2014

Two-phase model

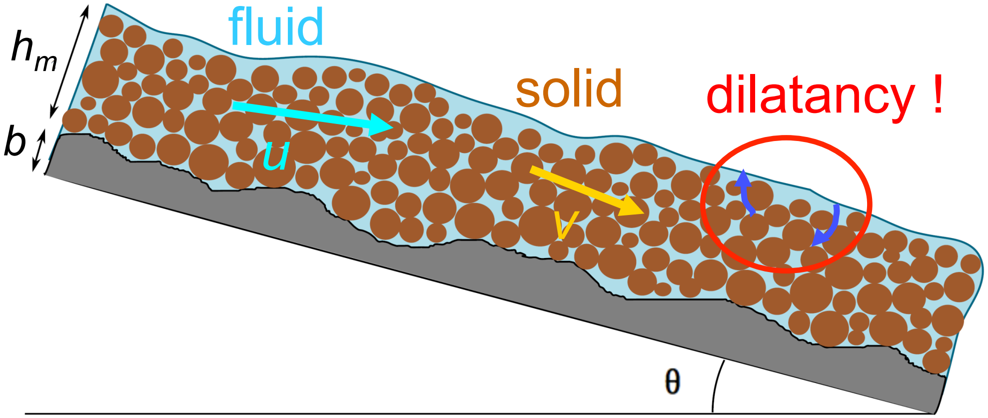

Pitman and Le 2005, Pelanti et al. 2008, 2011

Jackson's model

Jackson, 2000

φ : solid volume fraction, $1-\varphi$: fluid volume fraction

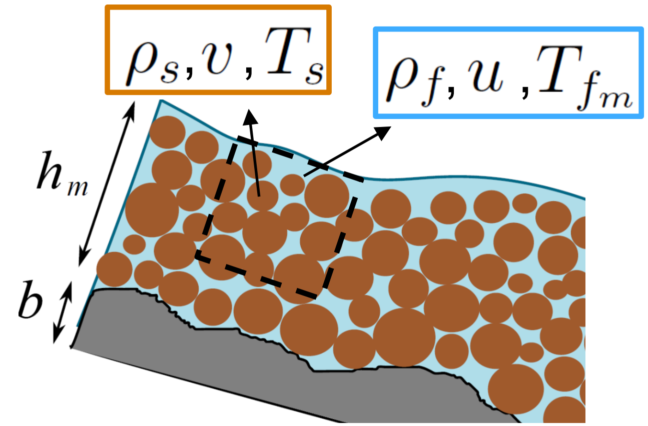

- Mass conservation :

$$
\begin{aligned}
* \quad \partial_t(\rho_s\varphi) + \nabla\cdot(\rho_s\varphi v) &= 0 \\
* \quad \partial_t(\rho_f(1-\varphi)) + \nabla\cdot(\rho_f(1-\varphi)u) &= 0
\end{aligned}
$$

- Momentum conservation :

$$* \quad \rho_s\varphi(\partial_t v + (v\cdot\nabla)v) = -\nabla\cdot T_s - \varphi\nabla p_{f_m} + f + \rho_s\varphi\mathbf{g}$$

$$* \quad \rho_f(1-\varphi)(\partial_t u + (u\cdot\nabla)u) = -\nabla\cdot T_{f_m} + \varphi\nabla p_{f_m} - f + \rho_f(1-\varphi)\mathbf{g}$$

$$T_s = p_s\,\mathrm{Id} + \widetilde{T}_s \qquad T_{f_m} = p_{f_m}\,\mathrm{Id} + \widetilde{T}_{f_m}$$

Friction between the solid and fluid phases : $f = \beta(u-v)$

5 unknowns : φ, v, u, p_s, p_{f_m}, 4 equations

A constitutive equation is required to close the system

Bouchut, Fernandez-Nieto, Mangeney, Narbona-Reina, 2015, 2016

Qualitative explanation of dilatancy effects

Critical state : φ_c^{eq} *when deformed*

$\varphi < \varphi_c^{eq}$ (loose)	$\varphi > \varphi_c^{eq}$ (dense)
Granular medium contracts	Granular medium dilates
⬇	⬇
Fluid is expelled ($\mathcal{V}_f$)	Fluid is sucked ($-\mathcal{V}_f$)
⬇	⬇
Fluid pore pressure $p_{fm}=p_{hydro}+p^e_{fm}$ increases	Fluid pore pressure decreases
⬇	⬇
Liquefaction	Stiffening of the granular matrix

$\mathcal{V}_f$

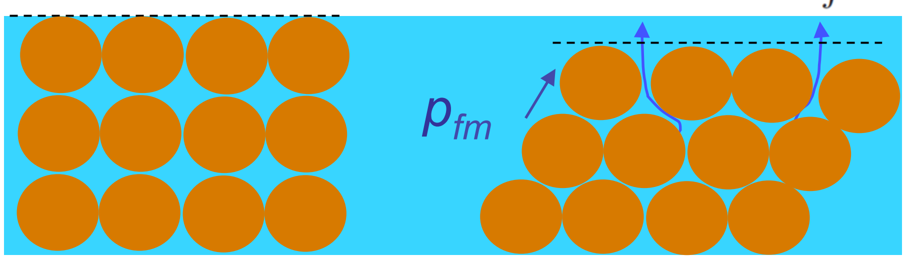

$-\mathcal{V}_f$

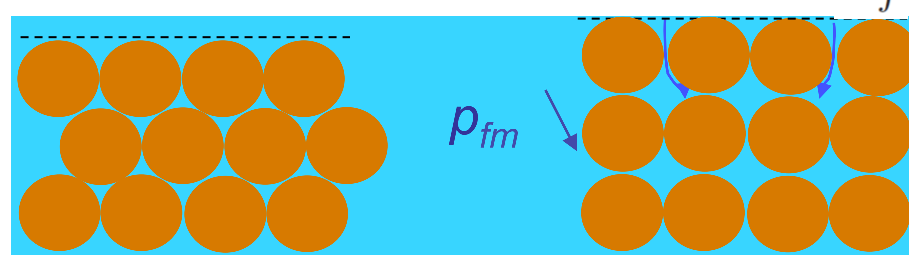

Excess pore pressure $p^e_{fm} \geq 0$ $\qquad$ $p^e_{fm} \leq 0$

Coulomb friction: $T^{\mathbf{x}z}_{s\,|b} = \tan\overline{\delta_{\text{eff}}}\left(\bar{\varphi}(\rho_s - \rho_f)g\cos\theta h_m - (p^e_{f_m})_{|b}\right)$

e. g. Schofield and Wroth, 1968, Wood, 1990, Pailha and Pouliquen, 2009

Differential motion of the fluid and solid phases

A crucial element :

Make it possible for the fluid to enter/escape the granular phase

Solid free surface ≠ fluid free surface !

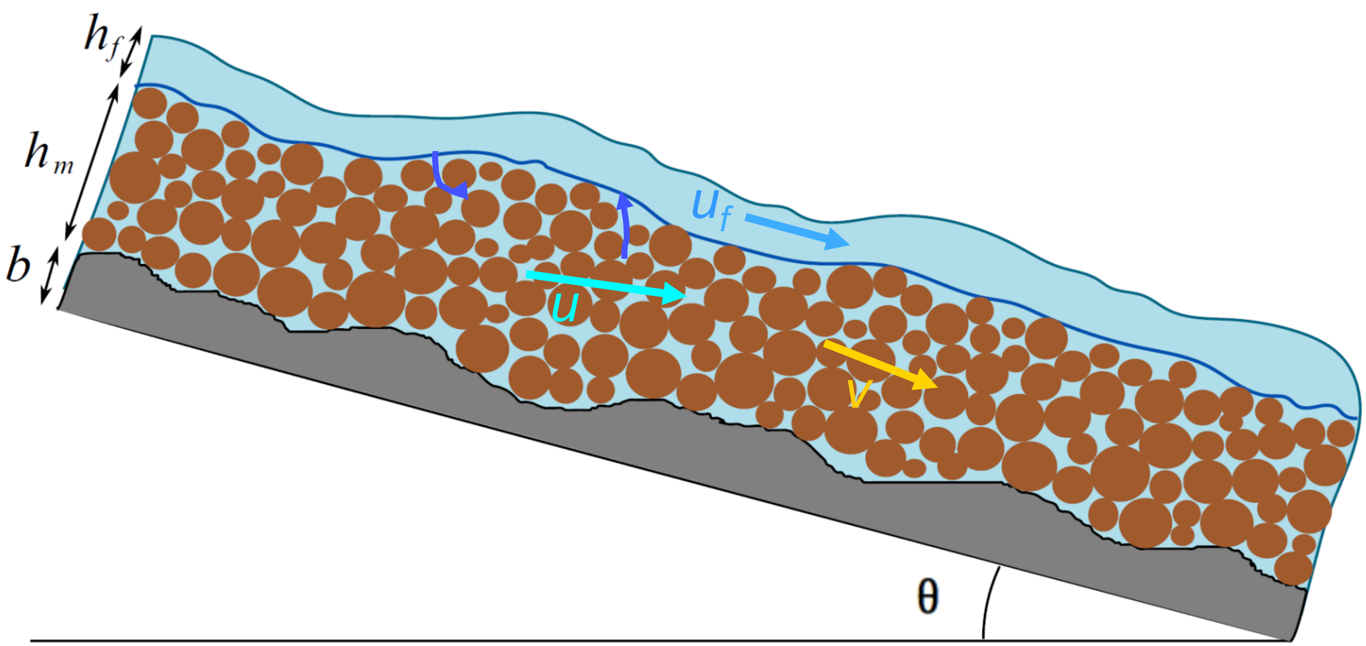

Bouchut, Fernandez-Nieto, Mangeney, Narbona-Reina, JFM, 2016

Modeling of dilatancy effects

- Compression/dilatation of the solid phase :

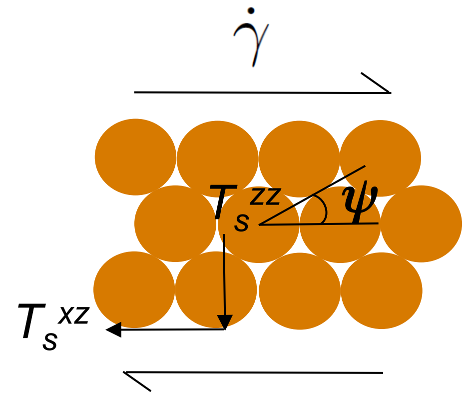

$$\nabla \cdot v = \dot{\gamma} \tan \psi$$ *Roux and Radjai, 1998*

ψ : dilatancy angle, $\dot{\gamma}$: shear strain rate

$$\tan \psi = K(\varphi - \varphi_c^{eq})$$ *Pailha and Pouliquen, 2009*

➡ $\boxed{\text{Closure equation : } \nabla \cdot v = K\dot{\gamma}(\varphi - \varphi_c^{eq})}$

$\varphi < \varphi_c^{eq}$: compression $\qquad$ $\varphi > \varphi_c^{eq}$: dilatation

- Impact of the dilatancy angle on the Coulomb friction force :

$$\boxed{T_s^{\mathbf{x}z} = -\tan\underbrace{(\delta + \psi)}_{\delta_{\text{eff}}} \,\text{sign}(v)\, T_s^{zz}}$$

Dilatation increases friction in addition to decrease of fluid pore pressure

Submarine granular column collapse

Simulation of laboratory experiments of *Rondon et al., 2011*

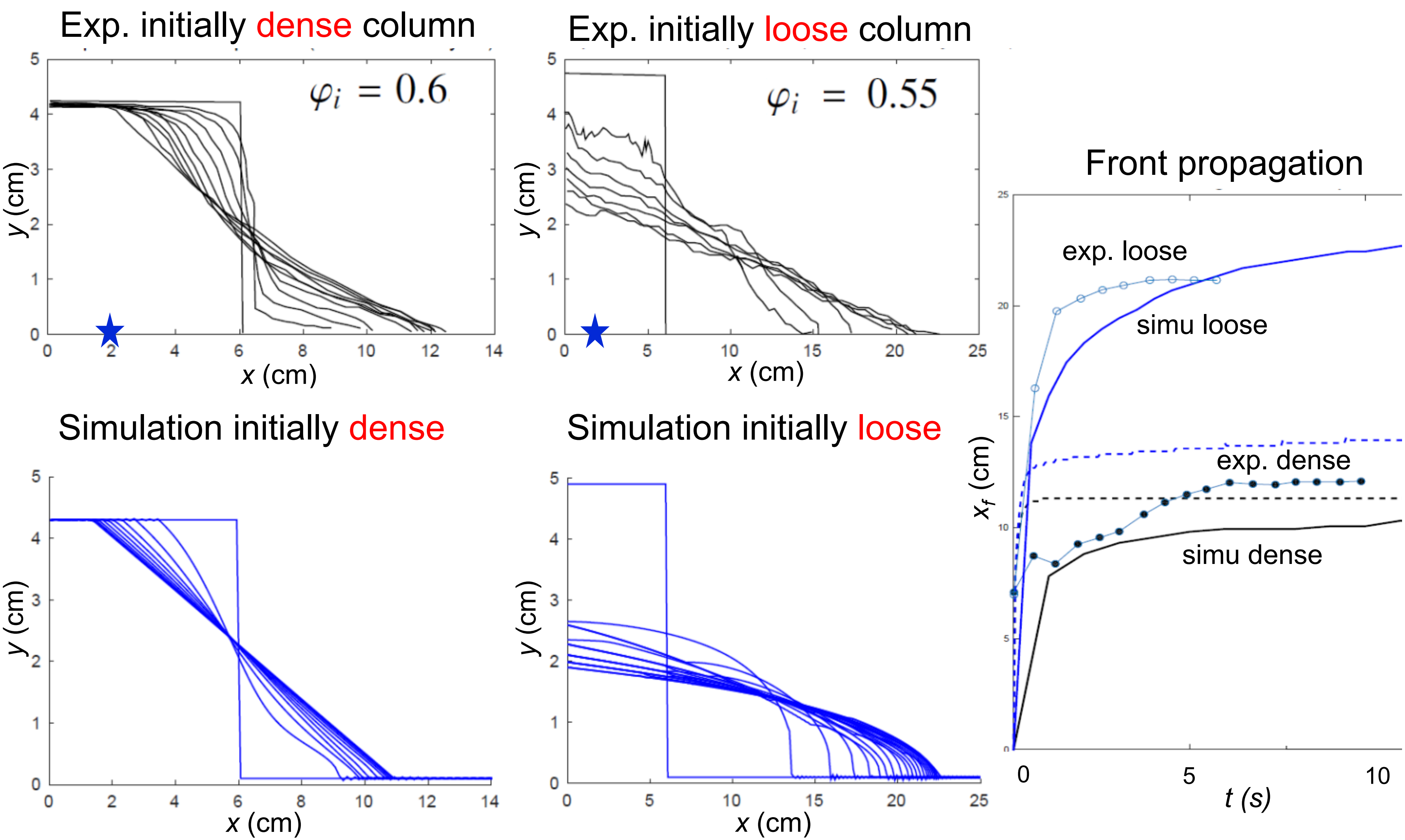

Submarine granular column collapse

Simulation and measurement of excess pore fluid pressure

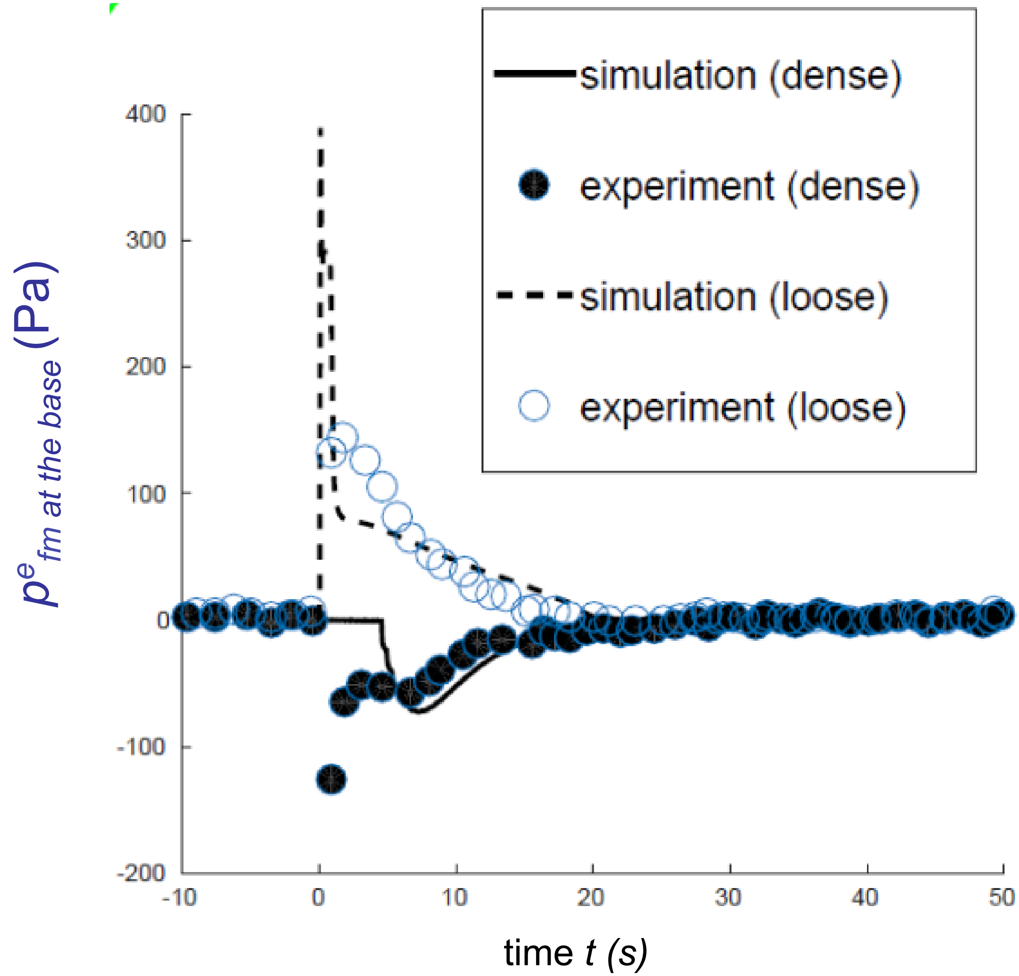

Modeling of debris flows (grain/fluid)

Solid volume fraction: $0.4 < \varphi < 0.8$

At the field scale

- Thin layer approximation $hm/Lm = \varepsilon \ll 1$

$$h_m = \mathcal{O}(\epsilon), u^{\mathrm{x}} = \mathcal{O}(1), u^z = O(\epsilon), \ldots$$

- Depth-averaged model

Mixture model

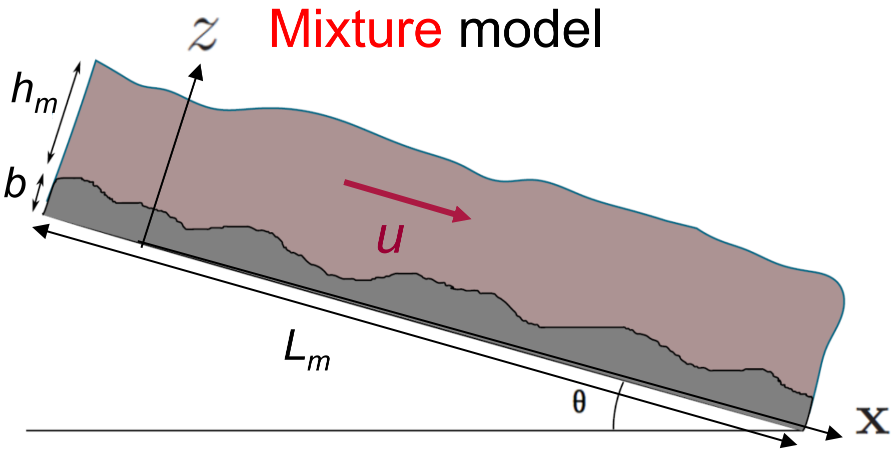

Iverson, Denlinger; Denlinger, Iverson 2001, Iverson, George; George, Iverson 2014

Two-phase model

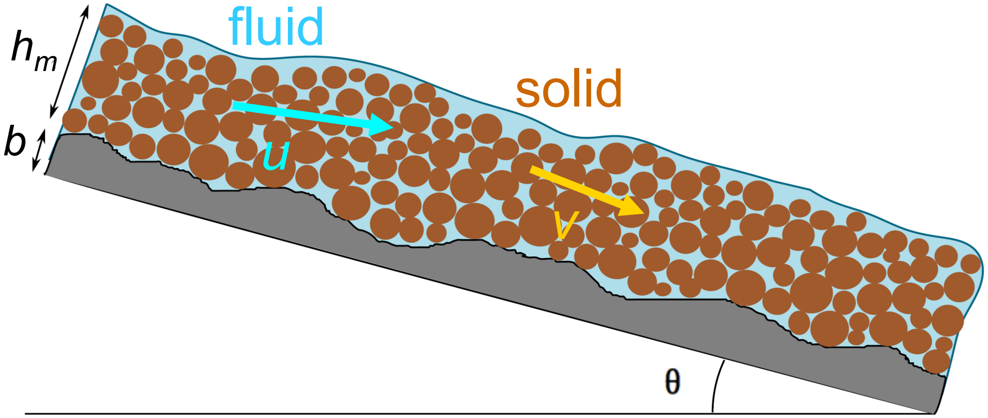

Pitman and Le 2005, Pelanti et al. 2008, 2011

Modeling of debris flows (grain/fluid)

Solid volume fraction: $0.4 < \varphi < 0.8$

At the field scale

- Thin layer approximation $hm/Lm = \varepsilon \ll 1$

$$h_m = \mathcal{O}(\epsilon), u^{\mathrm{x}} = \mathcal{O}(1), u^z = O(\epsilon), \ldots$$

- Depth-averaged model

Mixture model

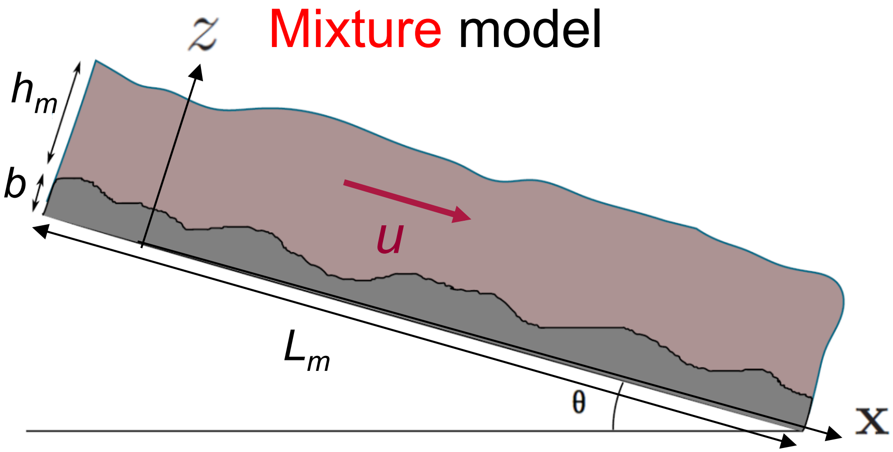

Iverson, Denlinger; Denlinger, Iverson 2001, Iverson, George; George, Iverson 2014

Two-phase model

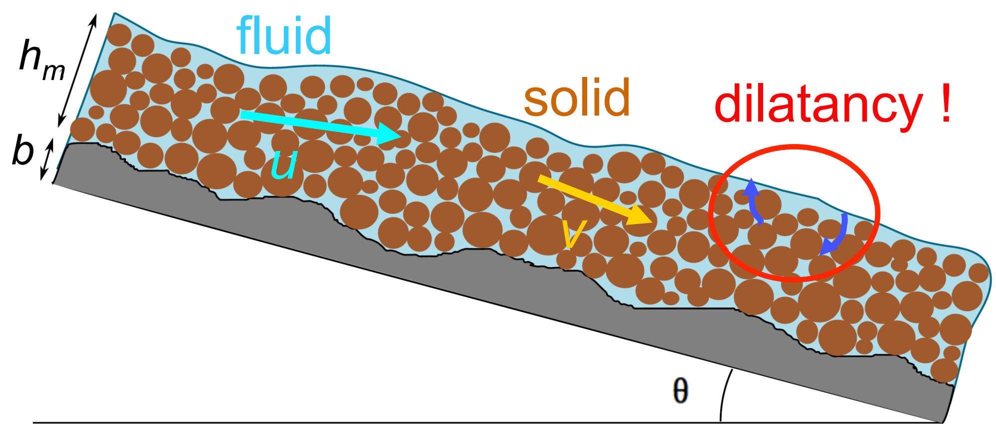

Pitman and Le 2005, Pelanti et al. 2008, 2011

Jackson's model

Jackson, 2000

φ : solid volume fraction, $1-\varphi$: fluid volume fraction

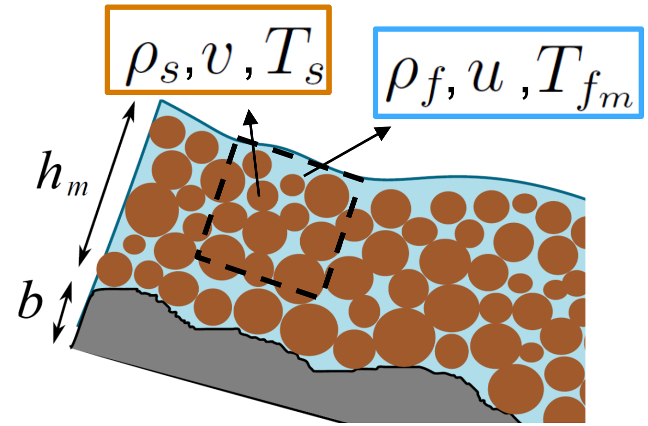

- Mass conservation :

$$\ast \quad \partial_t(\rho_s\varphi) + \nabla\cdot(\rho_s\varphi v) = 0$$

$$\ast \quad \partial_t(\rho_f(1-\varphi)) + \nabla\cdot(\rho_f(1-\varphi)u) = 0$$

- Momentum conservation :

$$\ast \quad \rho_s\varphi(\partial_t v + (v\cdot\nabla)v) = -\nabla\cdot T_s - \varphi\nabla p_{f_m} + f + \rho_s\varphi\mathbf{g}$$

$$\ast \quad \rho_f(1-\varphi)(\partial_t u + (u\cdot\nabla)u) = -\nabla\cdot T_{f_m} + \varphi\nabla p_{f_m} - f + \rho_f(1-\varphi)\mathbf{g}$$

$$T_s = p_s\,\mathrm{Id} + \widetilde{T}_s \qquad T_{f_m} = p_{f_m}\,\mathrm{Id} + \widetilde{T}_{f_m}$$

Friction between the solid and fluid phases : $f = \beta(u-v)$

5 unknowns : φ, v, u, p_s, p_{f_m}, 4 equations

A constitutive equation is required to close the system

Bouchut, Fernandez-Nieto, Mangeney, Narbona-Reina, 2015, 2016

Qualitative explanation of dilatancy effects

Critical state : φ_c^{eq} *when deformed*

$\varphi < \varphi_c^{eq}$ (loose)	$\varphi > \varphi_c^{eq}$ (dense)
Granular medium contracts	Granular medium dilates
⬇	⬇
Fluid is expelled ($\mathcal{V}_f$)	Fluid is sucked ($-\mathcal{V}_f$)
⬇	⬇
Fluid pore pressure $p_{fm}=p_{hydro}+p^e_{fm}$ increases	Fluid pore pressure decreases
⬇	⬇
Liquefaction	Stiffening of the granular matrix

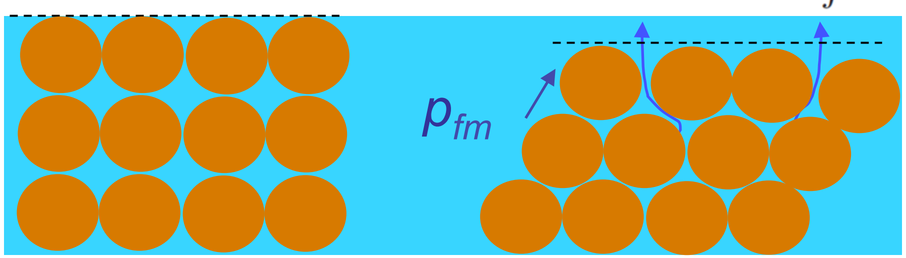

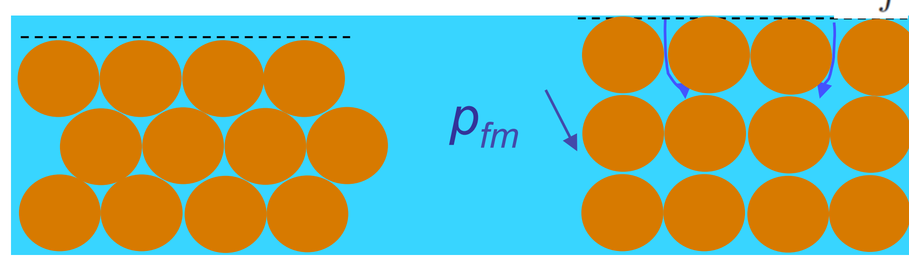

Excess pore pressure $p^e_{fm} \geq 0$

$p^e_{fm} \leq 0$

Coulomb friction: $T_{s\,|b}^{\mathbf{x}z} = \tan\overline{\delta_{\text{eff}}}\left(\bar{\varphi}(\rho_s - \rho_f) g \cos\theta h_m - (p^e_{f_m})_{|b}\right)$

e. g. Schofield and Wroth, 1968, Wood, 1990, Pailha and Pouliquen, 2009

Differential motion of the fluid and solid phases

A crucial element :

Make it possible for the fluid to enter/escape the granular phase

Solid free surface ≠ fluid free surface !

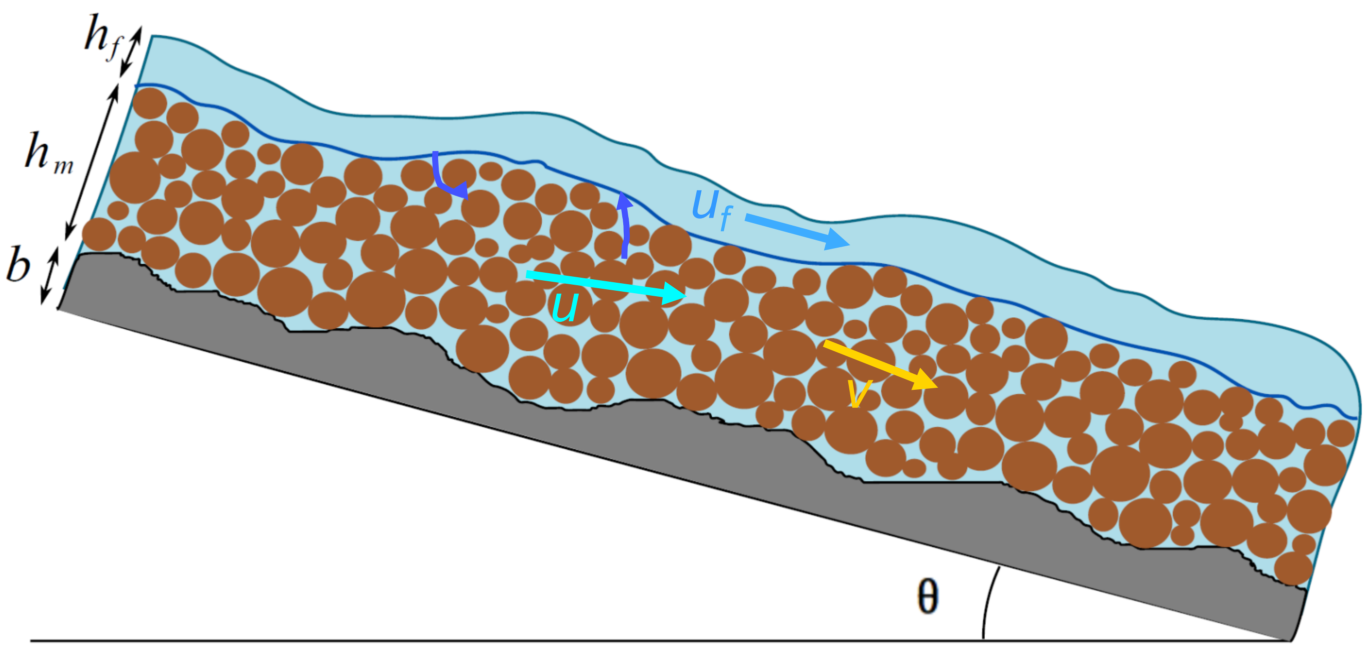

Bouchut, Fernandez-Nieto, Mangeney, Narbona-Reina, JFM, 2016

Modeling of dilatancy effects

- Compression/dilatation of the solid phase :

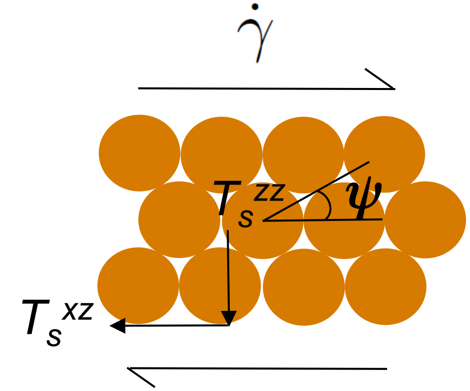

$$\nabla \cdot v = \dot{\gamma}\, \tan \psi$$ *Roux and Radjai, 1998*

ψ : dilatancy angle, $\dot{\gamma}$: shear strain rate

$$\tan \psi = K(\varphi - \varphi_c^{eq})$$ *Pailha and Pouliquen, 2009*

➡ $\boxed{\text{Closure equation : } \nabla \cdot v = K\dot{\gamma}(\varphi - \varphi_c^{eq})}$

$\varphi < \varphi_c^{eq}$: compression $\qquad$ $\varphi > \varphi_c^{eq}$: dilatation

- Impact of the dilatancy angle on the Coulomb friction force :

$$\boxed{T_s^{\mathbf{x}z} = -\tan\underbrace{(\delta + \psi)}_{\delta_{\mathrm{eff}}}\, \mathrm{sign}(v)\, T_s^{zz}}$$

Dilatation increases friction in addition to decrease of fluid pore pressure

Fluid pore pressure

in thin layer depth-averaged models

- From the fluid momentum conservation in the direction normal to the slope

$$\cancel{\varepsilon\rho_f(1-\varphi)(\partial_t u^z + u^{\mathbf{x}}\cdot\nabla_{\mathbf{x}} u^z + u^z\partial_z u^z)} =$$
$$-(1-\varphi)\partial_z p_{f_m} - g\cos\theta\rho_f(1-\varphi) - \beta(u^z - v^z) - \cancel{\varepsilon\nabla_{\mathbf{x}}\cdot T_{f_m}^{\mathbf{x}z}}$$

$$p_{f_m} = \rho_f g\cos\theta(b + h_m + h_f - z) + p_{f_m}^e + O(\epsilon^2)$$

with $$p_{f_m}^e \equiv \frac{\bar\beta}{1-\bar\varphi}\int_z^{b+h_m}(u^z - v^z)(z')dz'$$

using the dilatancy closure equation $\nabla\cdot v = K\dot\gamma(\varphi - \varphi_c^{eq})$

$\Downarrow$

- Non-hydrostatic (excess) fluid pressure

$$(p_{f_m}^e)_{|b} = \frac{\bar\beta}{1-\bar\varphi}h_m(\overline{u^{\mathbf{x}}} - \overline{v^{\mathbf{x}}})\cdot\nabla_{\mathbf{x}} b - \frac{\bar\beta}{1-\bar\varphi}\frac{h_m^2}{2}\left(\nabla_{\mathbf{x}}\cdot(\overline{u^{\mathbf{x}}} - \overline{v^{\mathbf{x}}}) + \frac{K\bar{\dot\gamma}(\bar\varphi - \varphi_c^{eq})}{1-\bar\varphi}\right)$$

Bouchut, Fernandez-Nieto, Mangeney, Narbona-Reina, JFM, 2016

Equilibrium state and parameters

- Critical state :

$$\bar{\varphi}^{\infty} = \bar{\varphi}_c^{stat} - \frac{K_2}{K_1}\left(|\tan\theta| - \tan\delta\right),$$
$$\frac{\eta_f \bar{\dot{\gamma}}^{\infty}}{p_{s|b}^{\infty}} = \frac{1}{K_1}\left(|\tan\theta| - \tan\delta\right).$$

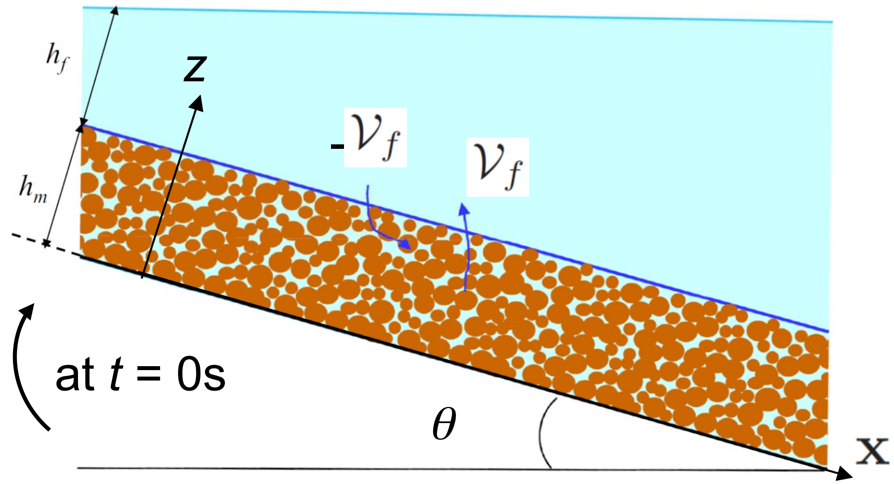

Our model :

$$h_m^{\infty} = \frac{\bar{\varphi}^0}{\bar{\varphi}^{\infty}} h_m^0,$$
$$p_{s|b}^{\infty} = \bar{\varphi}^{\infty} h_m^{\infty} (\rho_s - \rho_f) g \cos\theta,$$
$$\overline{v^{\mathbf{x}}}^{\infty} = \frac{1}{3} h_m^{\infty} \bar{\dot{\gamma}}^{\infty}.$$

Pailha-Pouliquen model :

$$h_m^{\infty} = h_m^0,$$
$$p_{s|b}^{\infty} = \bar{\varphi}_c^{stat} h_m^{\infty} (\rho_s - \rho_f) g \cos\theta,$$
$$\overline{v^{\mathbf{x}}}^{\infty} = \frac{1}{3} h_m^{\infty} \bar{\dot{\gamma}}^{\infty}.$$

- Parameters for the laboratory experiments of *Pailha et al., 2008* :

$$\rho_s = 2500\,\mathrm{kg/m^3}, \quad \bar{\varphi}_c^{stat} = 0.582, \ \delta = 22.5°, \ K_1 = 90.5, \quad K_2 = 25$$

- $\eta_f = 96 \times 10^{-3}\,\mathrm{Pa\cdot s}, \ \rho_f = 1041\,\mathrm{kg/m^3}, \ |\theta| = 25^{\mathrm{o}}, \ h_m^0 = 4.9\,\mathrm{mm}$
- $\eta_f = 9.8 \times 10^{-3}\,\mathrm{Pa\cdot s}, \ \rho_f = 1026\,\mathrm{kg/m^3}, \ |\theta| = 28^{\mathrm{o}}, \ h_m^0 = 6.1\,\mathrm{mm}$

Boundary conditions

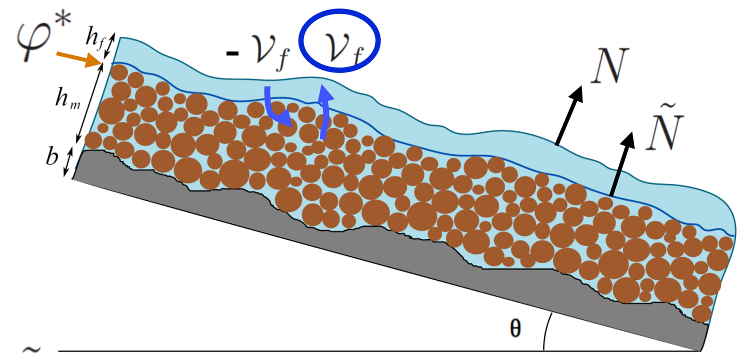

- **At the free surface,** for the fluid:
  - * no tension: $T_f N_X = 0$
  - * kinematic condition: $N_t + u_f \cdot N_X = 0$
- **At the interface mixture/fluid**:
  - * kinematic condition for the solid: $\tilde{N}_t + v \cdot \tilde{N}_X = 0$
  - * Rankine-Hugoniot (mass conservation) condition:

$$\tilde{N}_t + u_f \cdot \tilde{N}_X = (1-\varphi^*)(\tilde{N}_t + u \cdot \tilde{N}_X) \equiv \mathcal{V}_f$$

  - ** Rankine-Hugoniot (momentum conservation) condition:

$$\rho_f \mathcal{V}_f (u - u_f) + (T_s + T_{f_m})\tilde{N}_X = T_f \tilde{N}_X$$

  - ** stress transfer condition from the energy balance:

$$T_s \tilde{N}_X = \left(\frac{\rho_f}{2} \left((u - u_f) \cdot \frac{\tilde{N}_X}{|\tilde{N}_X|} \right)^2 + \left((T_{f_m} \tilde{N}_X) \cdot \frac{\tilde{N}_X}{|\tilde{N}_X|^2} - p_{f_m} \right) \frac{\varphi^*}{1-\varphi^*} \right) \tilde{N}_X$$

  - * Navier friction condition for the fluid:

$$\left(\frac{T_{f_m} + T_f}{2} \tilde{N}_X \right)_\tau = -k_i (u_f - u)_\tau$$

Boundary conditions

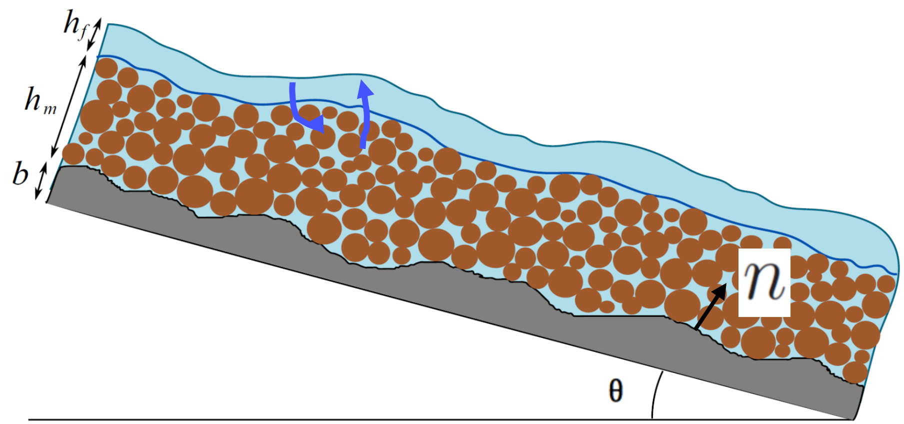

- Bottom boundary conditions:

  ** No penetration condition:

$$u \cdot n = 0, \qquad v \cdot n = 0$$

  * Coulomb friction for the solid:

$$(T_s n)_\tau = -\tan \delta_{\text{eff}} \; \text{sgn}(v)(T_s n) \cdot n$$

  * Navier friction for the fluid:

$$(T_{f_m} n)_\tau = -k_b u$$

Bouchut, Fernandez-Nieto, Mangeney, Narbona-Reina, 2016

Our model in the uniform immersed configuration

$$\overline{u_f} = 0,\ h_m(t) + h_f(t,x) + x\tan\theta = cst$$

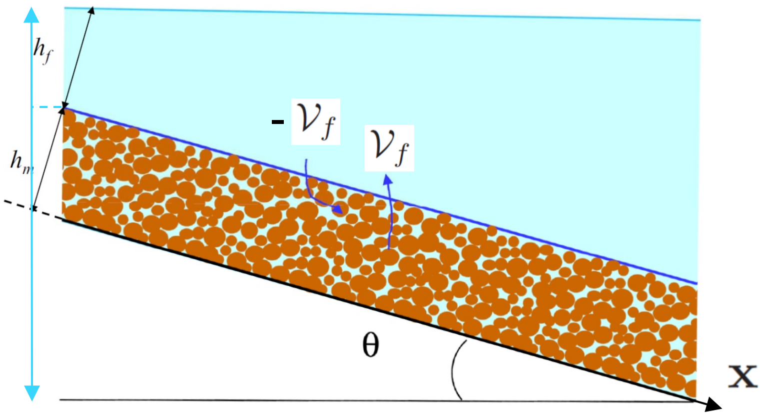

- Mass conservation :
  - $\partial_t(\bar{\varphi} h_m) = 0$
  - $\partial_t \bar{\varphi} = -\bar{\varphi}\bar{\Phi}$
- Momentum conservation :
  - $\rho_s \bar{\varphi} \partial_t \overline{v^{\mathbf{x}}} = -\operatorname{sgn}(\overline{v^{\mathbf{x}}})\dfrac{\tau_b}{h_m} + \bar{\beta}(\overline{u^{\mathbf{x}}} - \overline{v^{\mathbf{x}}}) - \bar{\varphi}(\rho_s - \rho_f) g \sin\theta$
  - $\rho_f(1-\bar{\varphi})\partial_t \overline{u^{\mathbf{x}}} = \left(\dfrac{1}{2}\rho_f \mathcal{V}_f - k_b\right)\dfrac{\overline{u^{\mathbf{x}}}}{h_m} - \bar{\beta}(\overline{u^{\mathbf{x}}} - \overline{v^{\mathbf{x}}})$

with $\mathcal{V}_f = -h_m \bar{\Phi}$, $\tau_b = \tan\overline{\delta_{\text{eff}}}\ p_{s|b} + K_1 \eta_f \bar{\dot{\gamma}}$

$$p_{s|b} = \bar{\varphi}(\rho_s - \rho_f) g \cos\theta h_m - (p^e_{fm})_{|b}\ ,\quad (p^e_{fm})_{|b} = -\frac{\bar{\beta}}{(1-\bar{\varphi})^2}\frac{h_m^2}{2}\bar{\Phi}$$

- Closure related to dilatancy :

$$\bar{\Phi} = \bar{\dot{\gamma}}\tan\psi\ ,\quad \tan\psi = K(\bar{\varphi} - \bar{\varphi}_c^{eq}),\qquad \bar{\varphi}_c^{eq} = \bar{\varphi}_c^{stat} - K_2 \frac{\eta_f \bar{\dot{\gamma}}}{p_{s|b}},$$

$$\bar{\dot{\gamma}} = 3\frac{|\overline{v^{\mathbf{x}}}|}{h_m}\ ,\qquad \tan\overline{\delta_{\text{eff}}} = \tan\delta + \tan\psi$$

Simple tests on submarine granular flows

Laboratory experiments: *Pailha et al., 2008*

viscosity : $\eta_f = 96 \times 10^{-3}\,\mathrm{Pa\cdot s}$

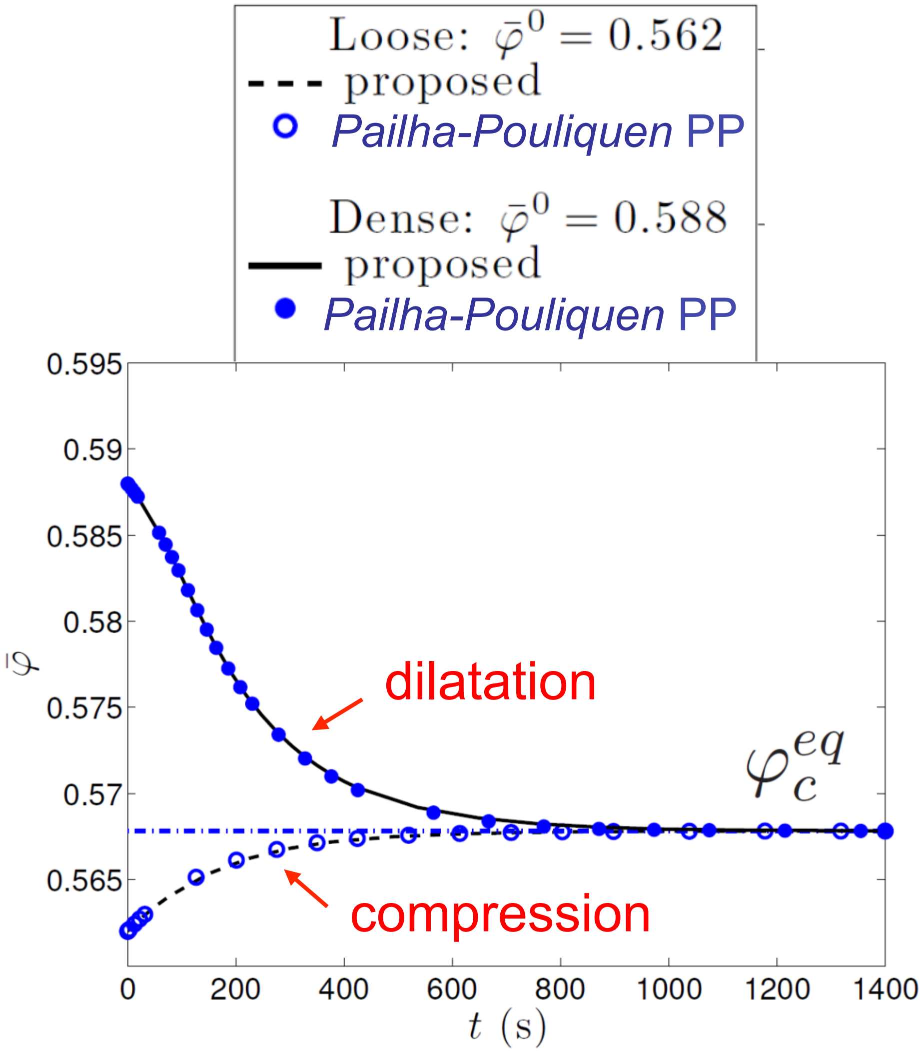

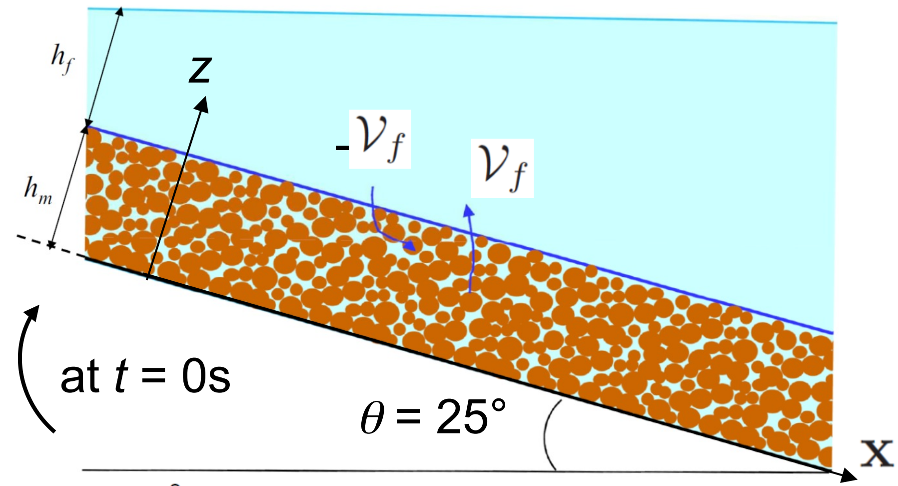

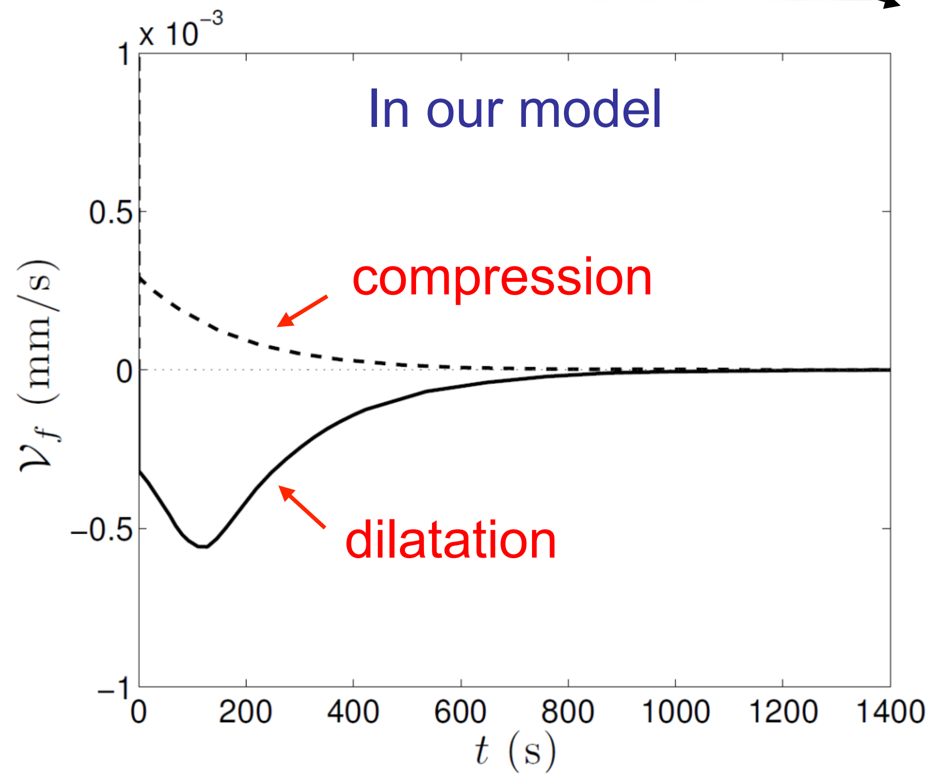

Simple tests on submarine granular flows

Good qualitative agreement with the experiments

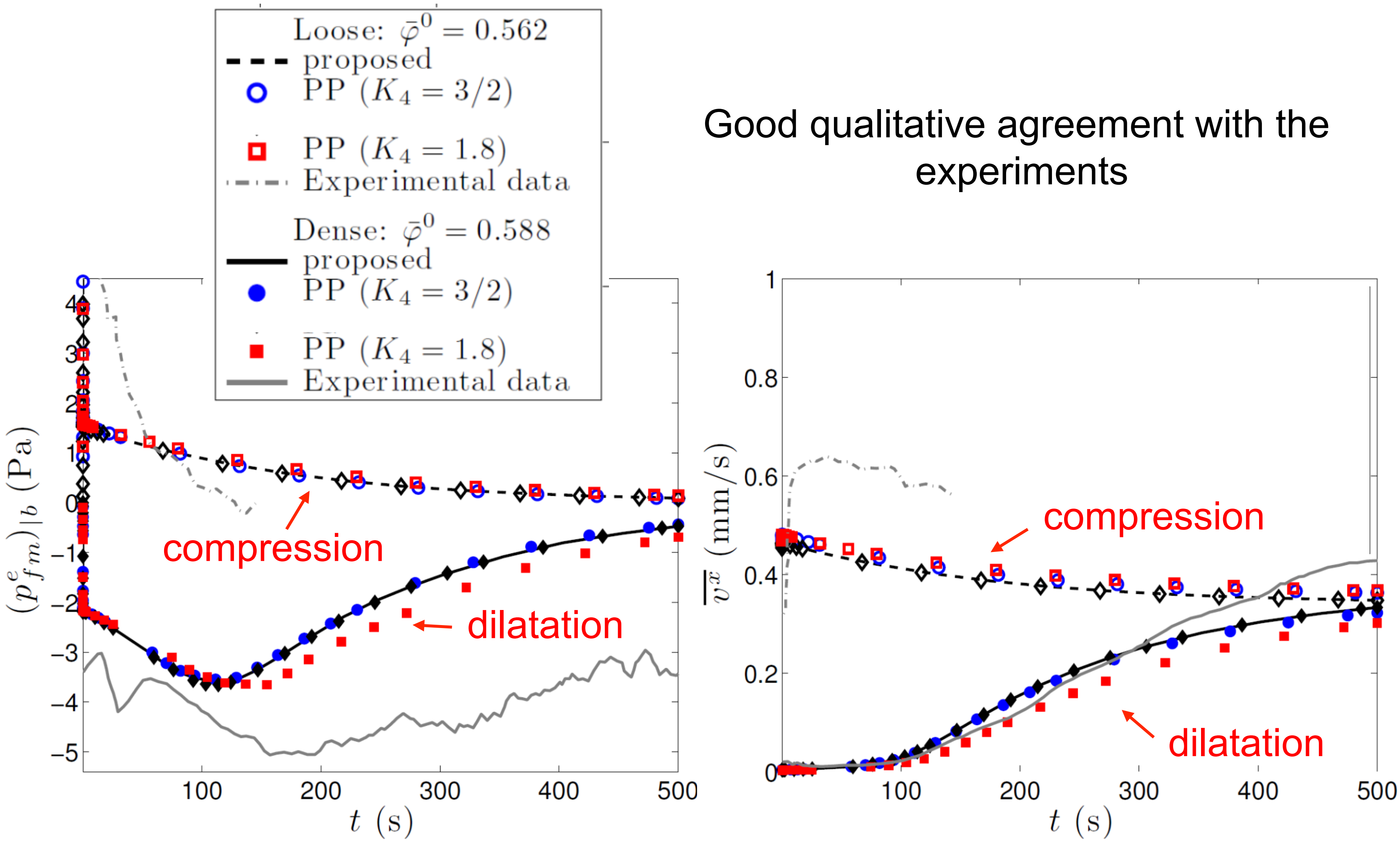

Bouchut, Fernandez-Nieto, Mangeney, Narbona-Reina, JFM, 2016

Simple tests on submarine granular flows

Low viscosity : $\eta_f = 9.8 \times 10^{-3}\,\mathrm{Pa \cdot s}$

	t_{crit}	t_{visc}	t_{rel}
low viscosity	$0.18\,\mathrm{s}$ to ∞	$3.7 \times 10^{-2}\,\mathrm{s}$	$5.4 \times 10^{-5}\,\mathrm{s}$
high viscosity	$4.7\,\mathrm{s}$ to ∞	$2.3 \times 10^{-3}\,\mathrm{s}$	$5.5 \times 10^{-6}\,\mathrm{s}$

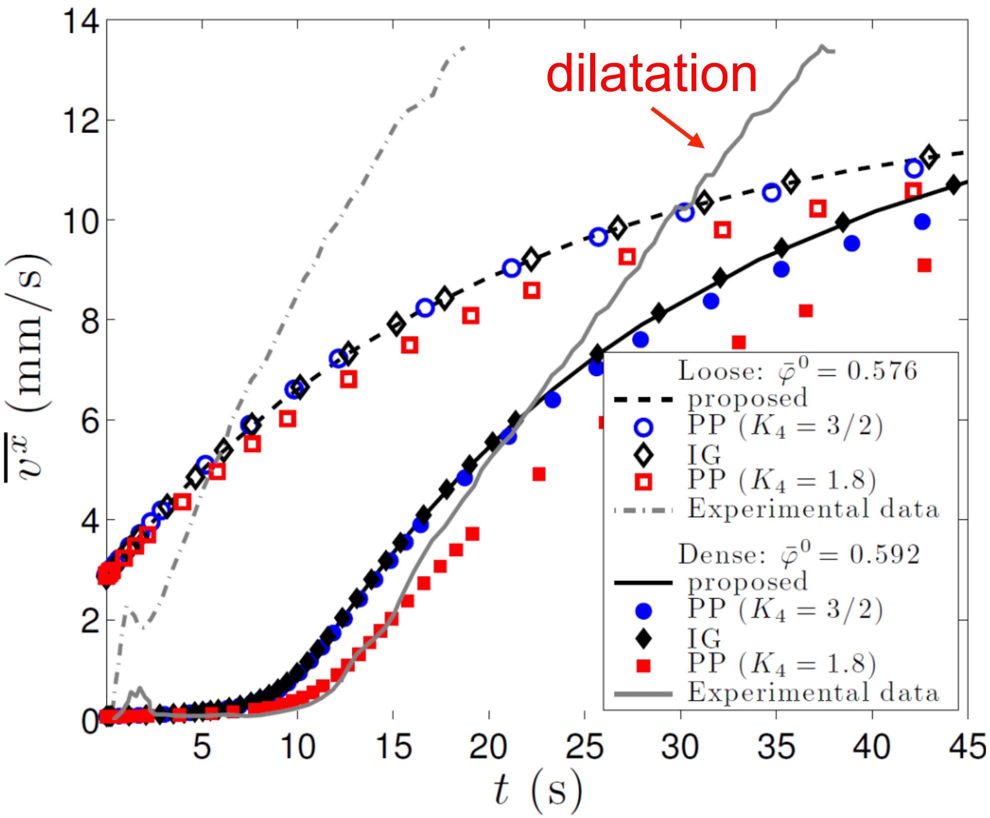

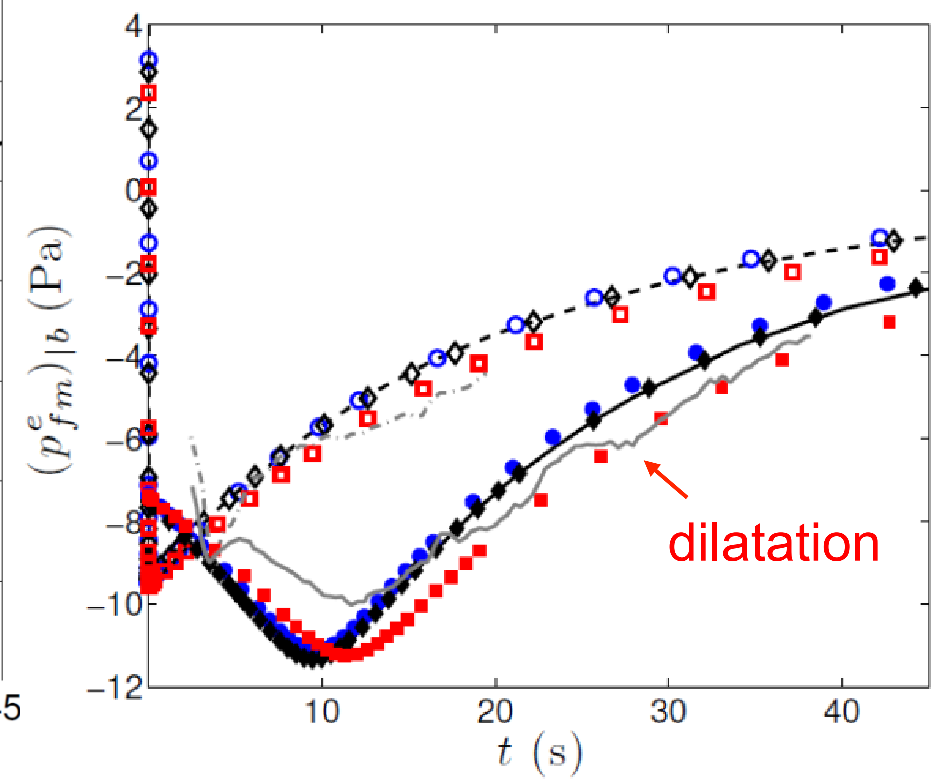

Submarine granular column collapse

Simulation of laboratory experiments of *Rondon et al., 2011*

Exp. initially dense column

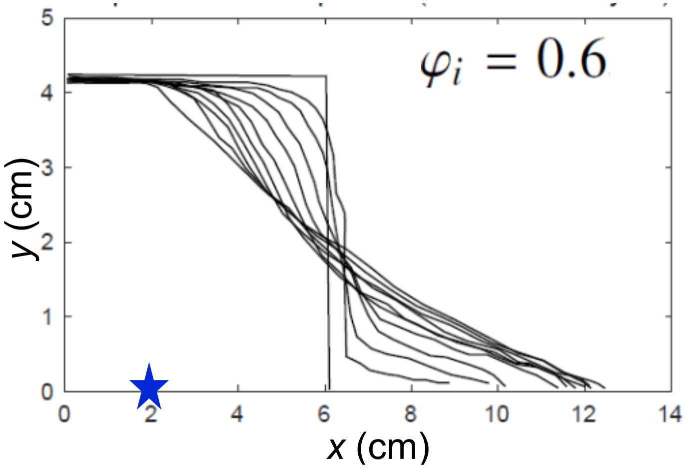

Exp. initially loose column

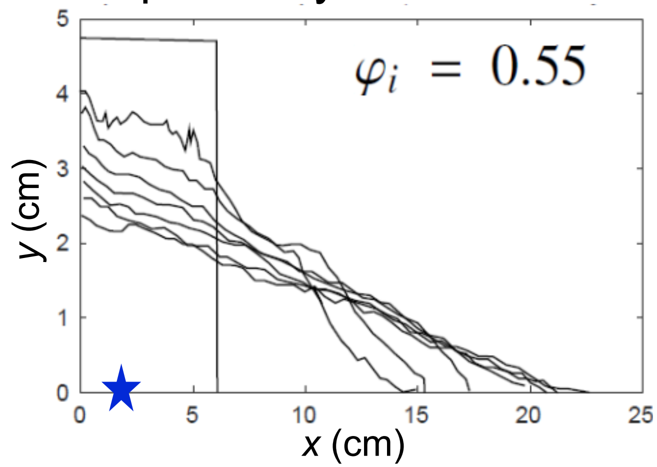

Simulation initially dense

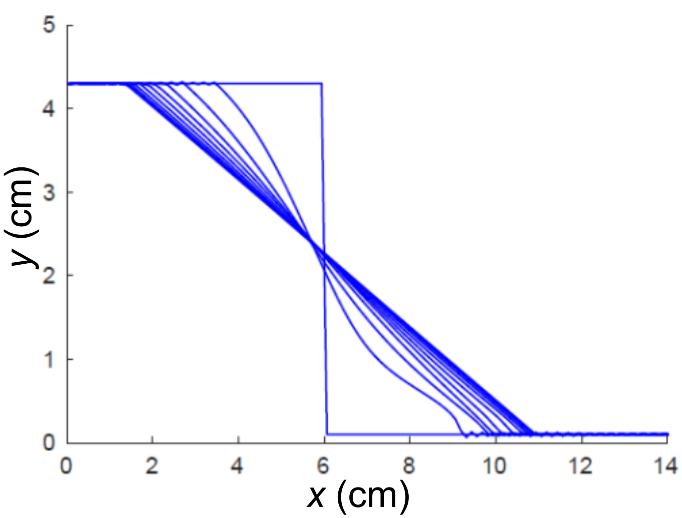

Simulation initially loose

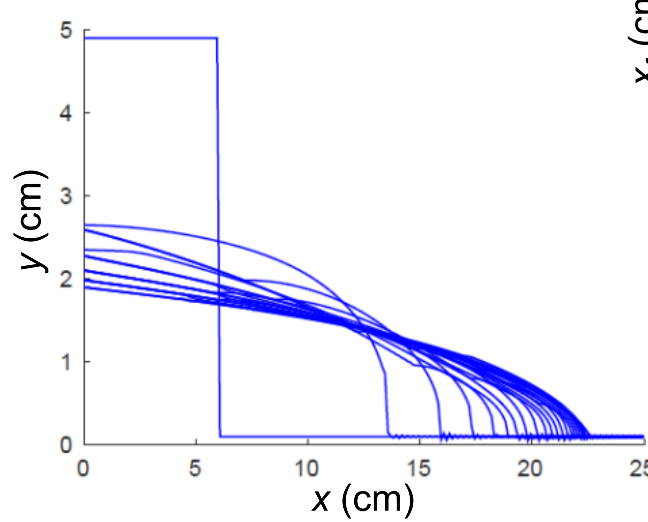

Front propagation

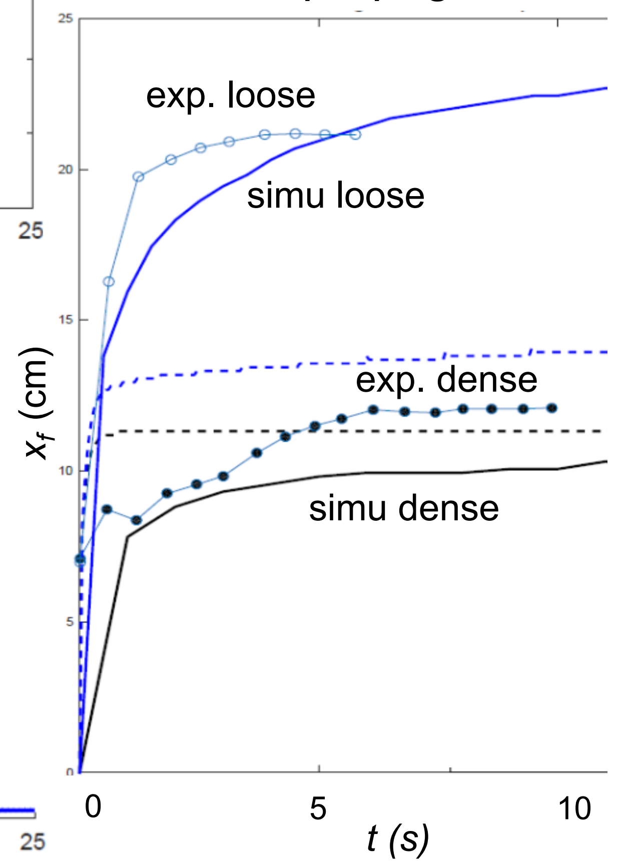

Submarine granular column collapse

Simulation and measurement of excess pore fluid pressure

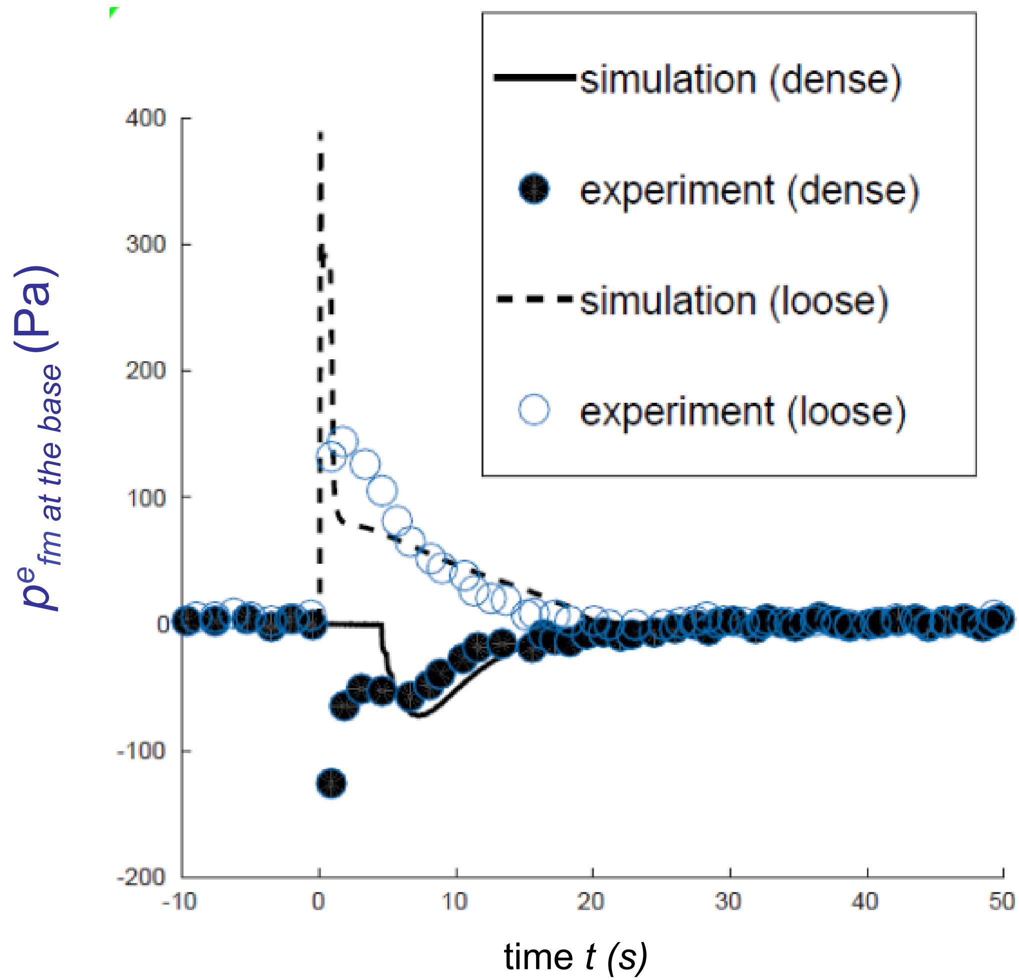

ou

$$N_{\mathrm{Sav}} = \frac{\rho_{\mathrm{p}}\dot{\gamma}^2 d^2}{(\rho_{\mathrm{p}} - \rho_{\mathrm{f}})gH}$$

$$N_{\mathrm{Bag}} = \frac{\phi\rho_{\mathrm{p}}\dot{\gamma}^2 d^2}{(1-\phi)\eta_{\mathrm{f}}\dot{\gamma}}$$

$$N_{\mathrm{Bag}} \sim I_{\mathrm{pi}}^2 / I_{\mathrm{v}}$$

Vertical velocity field and profiles

$\theta = 0°$

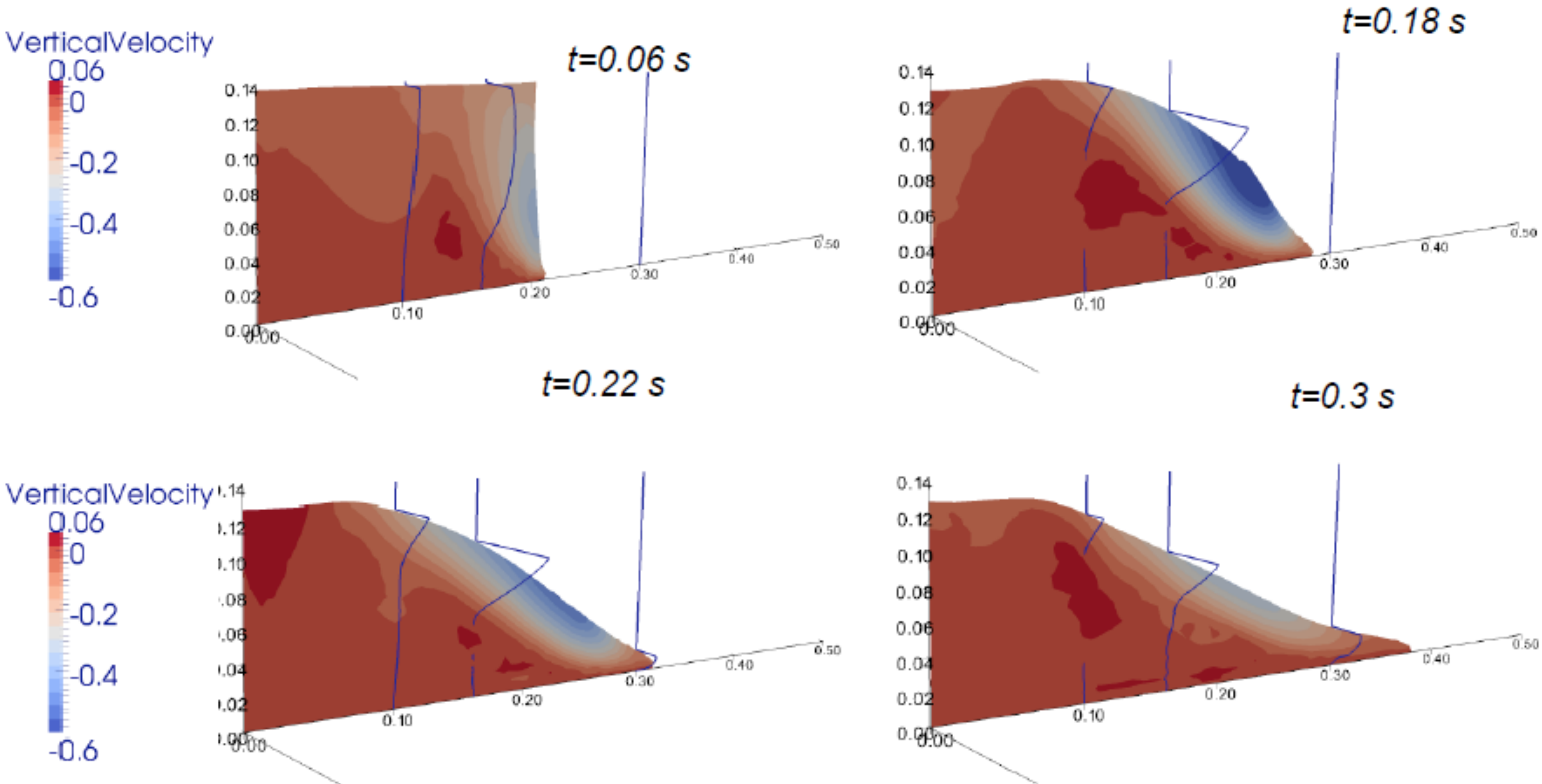

Significant vertical velocities (up to 50% of u)

Within the granular layer …

Velocity profiles at $x = 90$ cm

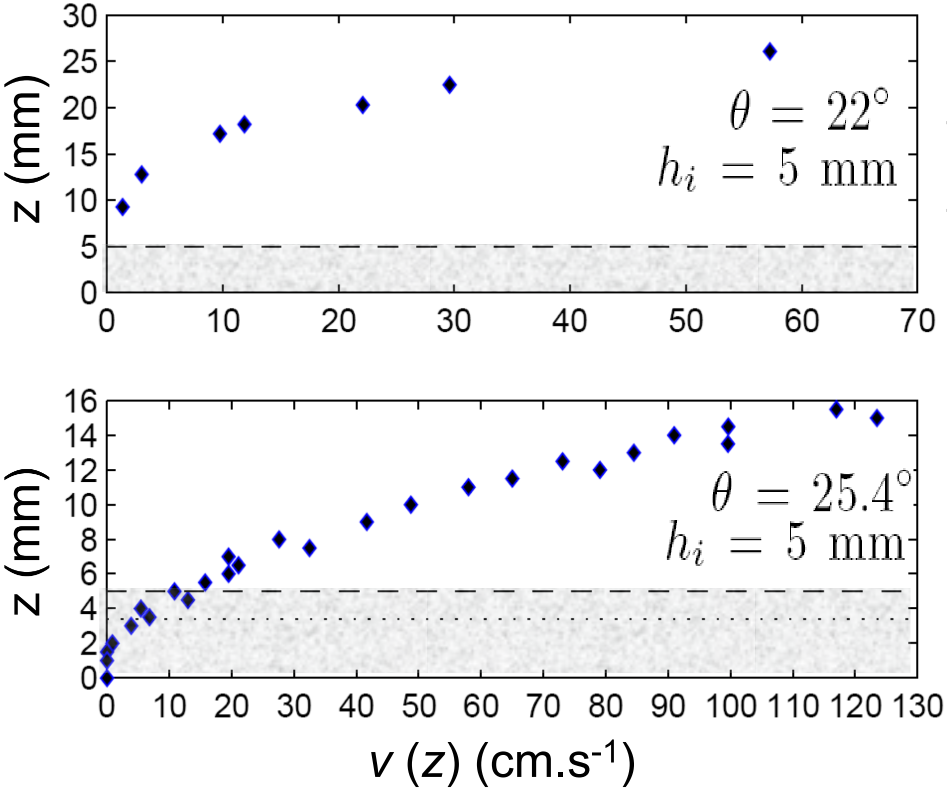

Depth of the static/mobile interface at $x = 90$ cm

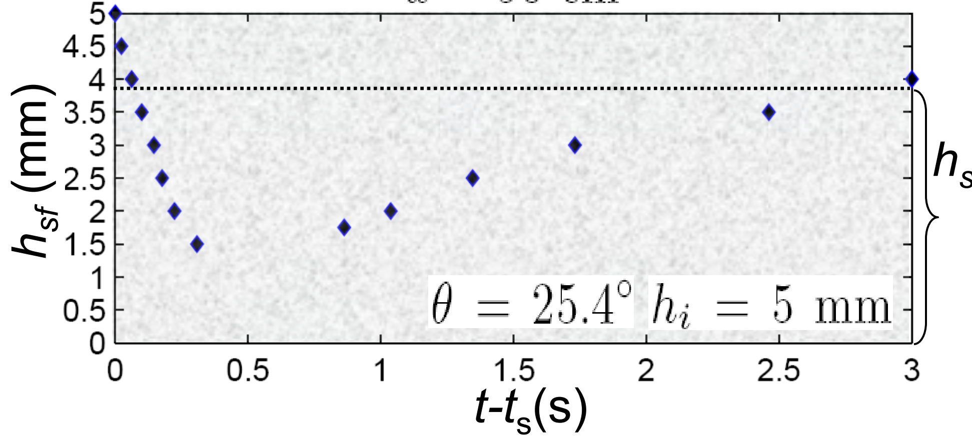

- **The front digs within the erodible bed** with a constant penetration velocity v_{sf} = 1.3 cm.s^{-1}
- **The static/flowing interface moves upward** (exponential relaxation) up to $z \approx h_s$
- **Very good agreement with** simulations using the **partial fluidization model** *Mangeney et al.*, 2007

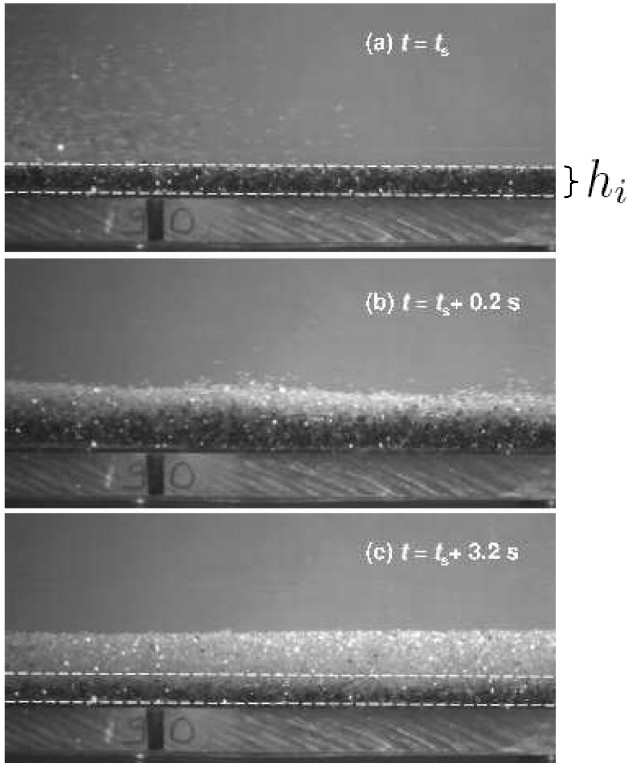

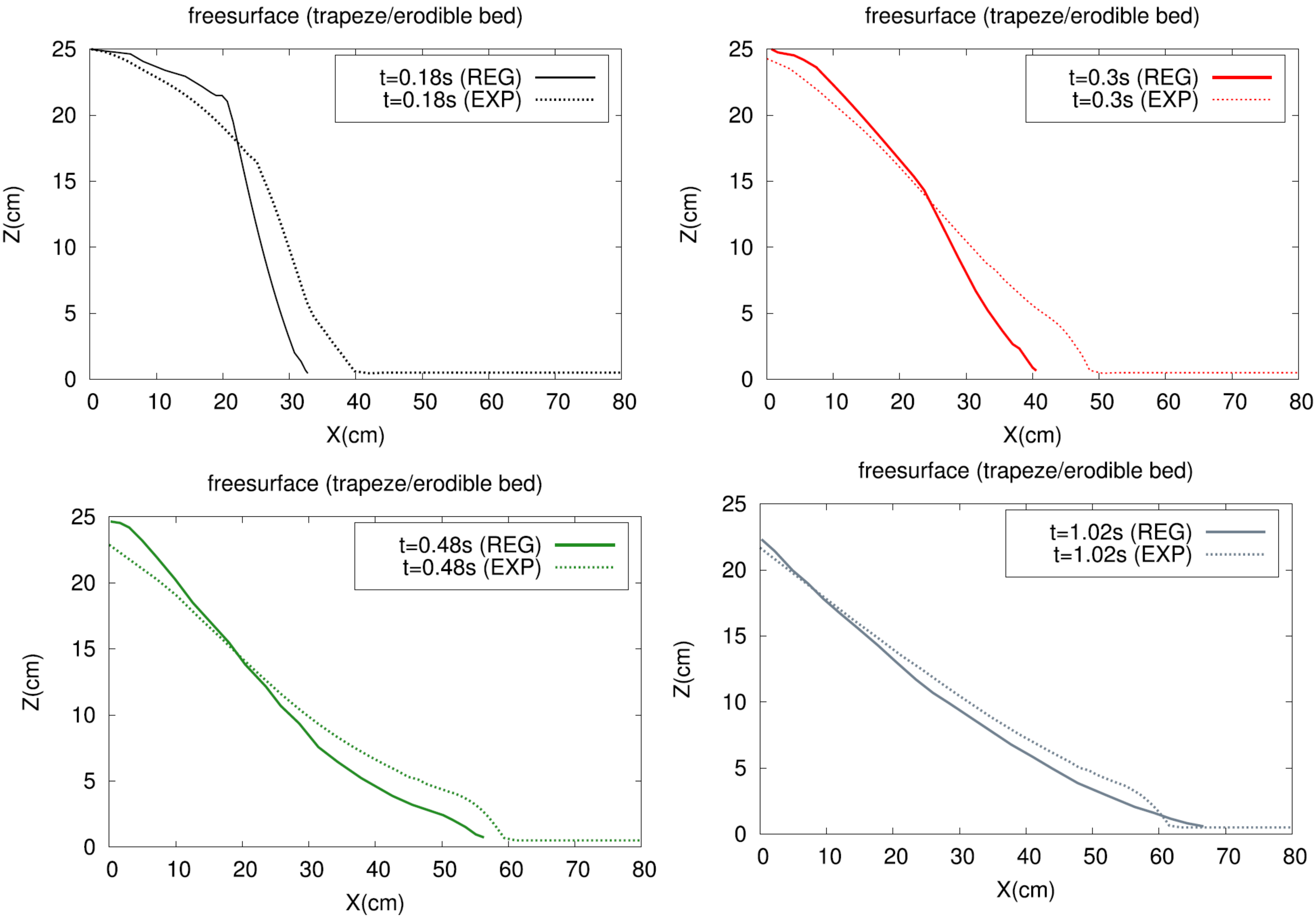
freesurface (trapeze/erodible bed)
t=0.18s (REG)
t=0.18s (EXP)
Z(cm)
X(cm)
freesurface (trapeze/erodible bed)
t=0.3s (REG)
t=0.3s (EXP)
Z(cm)
X(cm)
freesurface (trapeze/erodible bed)
t=0.48s (REG)
t=0.48s (EXP)
Z(cm)
X(cm)
freesurface (trapeze/erodible bed)
t=1.02s (REG)
t=1.02s (EXP)
Z(cm)
X(cm)

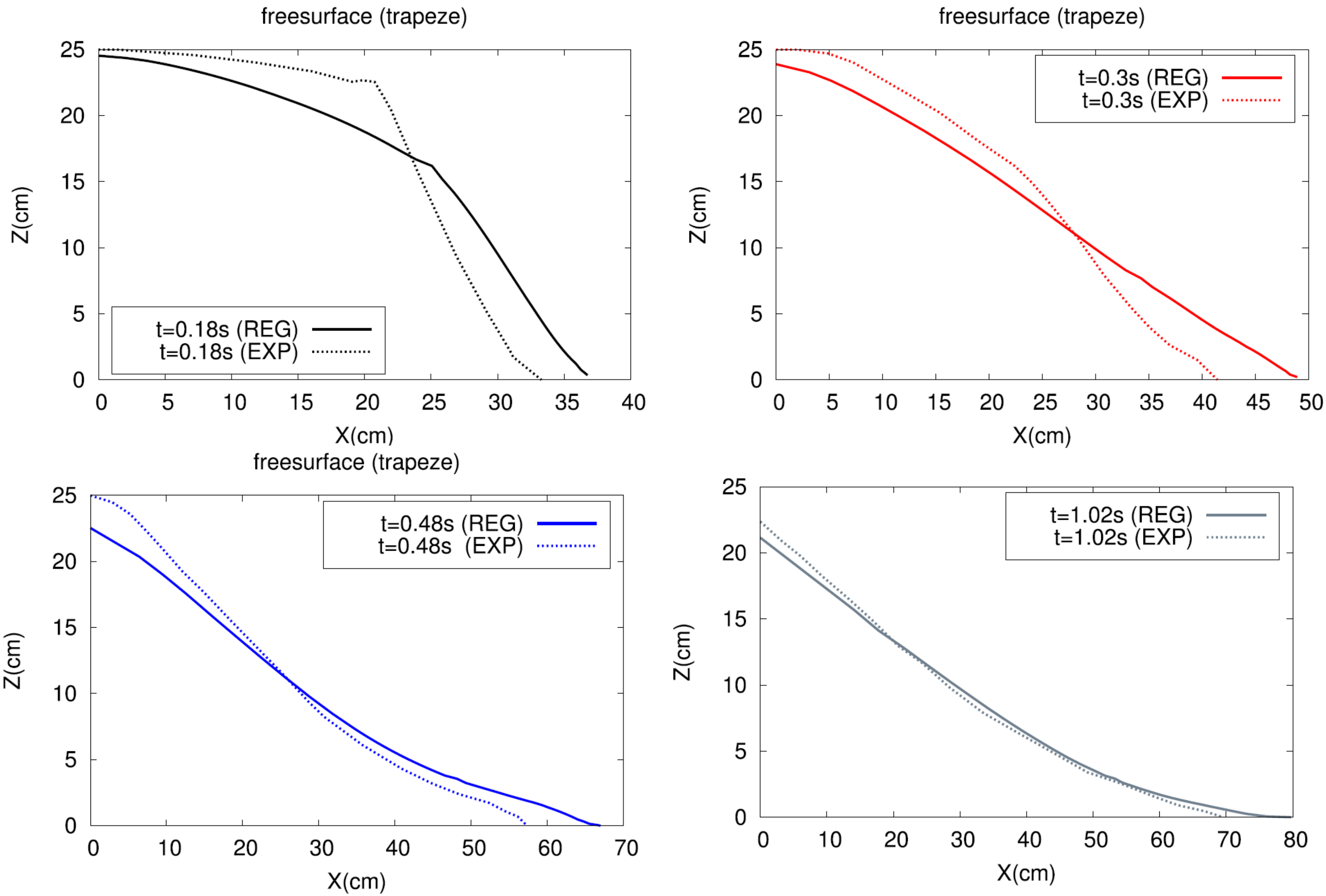
freesurface (trapeze)
t=0.18s (REG)
t=0.18s (EXP)
Z(cm)
X(cm)
freesurface (trapeze)
t=0.3s (REG)
t=0.3s (EXP)
Z(cm)
X(cm)
freesurface (trapeze)
t=0.48s (REG)
t=0.48s (EXP)
Z(cm)
X(cm)
t=1.02s (REG)
t=1.02s (EXP)
Z(cm)
X(cm)

Critère de rupture – seuil de plasticité

Le modèle de Mohr-Coulomb repose sur le critère de rupture suivant. Le milieu cède au point P, s'il existe en ce point un plan repère par sa normale **n** selon lequel on a

$$|\tau| = \tan\delta\,\sigma.$$

où τ et $\cdot\sigma$ sont les contraintes normale et tangentielle au plan **n**, et tan δ est le coefficient de friction effectif du materiau. Si l'on connait *a priori* la direction du plan de rupture, le critère de Mohr-Coulomb se ramène au problème du patin frottant sur un plan. En revanche, les choses peuvent se compliquer dans des géométries différentes pour lesquelles on ne connait pas *a priori* les directions de glissement.

Fonction de charge:
$$\begin{aligned} F_{\text{Coulomb}}(\sigma_1, \sigma_2, \sigma_3) \equiv \max \big\{ &(\sigma_1 - \sigma_2)^2 - \sin\delta^2(\sigma_1+\sigma_2)^2, \\ &(\sigma_2 - \sigma_3)^2 - \sin\delta^2(\sigma_2+\sigma_3)^2, \\ &(\sigma_3 - \sigma_1)^2 - \sin\delta^2(\sigma_3+\sigma_1)^2 \big\}\,. \end{aligned}$$

$$F_{\text{Drucker}}(\boldsymbol{\sigma}) = q^2 - (\sin\delta)^2 P^2$$ avec $$P = \frac{1}{3}\text{tr}(\boldsymbol{\sigma})\,, \quad \text{et} \quad q = ||\boldsymbol{\tau}|| = ||\boldsymbol{\sigma} - P\mathbf{I}||$$

ou
$$\begin{aligned} F_{\text{Drucker}}(\sigma_1, \sigma_2, \sigma_3) \equiv &\frac{1}{6}\left((\sigma_1-\sigma_2)^2 + (\sigma_2-\sigma_3)^2 + (\sigma_3-\sigma_1)^2\right) \\ &-(\sin\delta)^2\left(\frac{\sigma_1+\sigma_2+\sigma_3}{3}\right)^2 . \end{aligned}$$

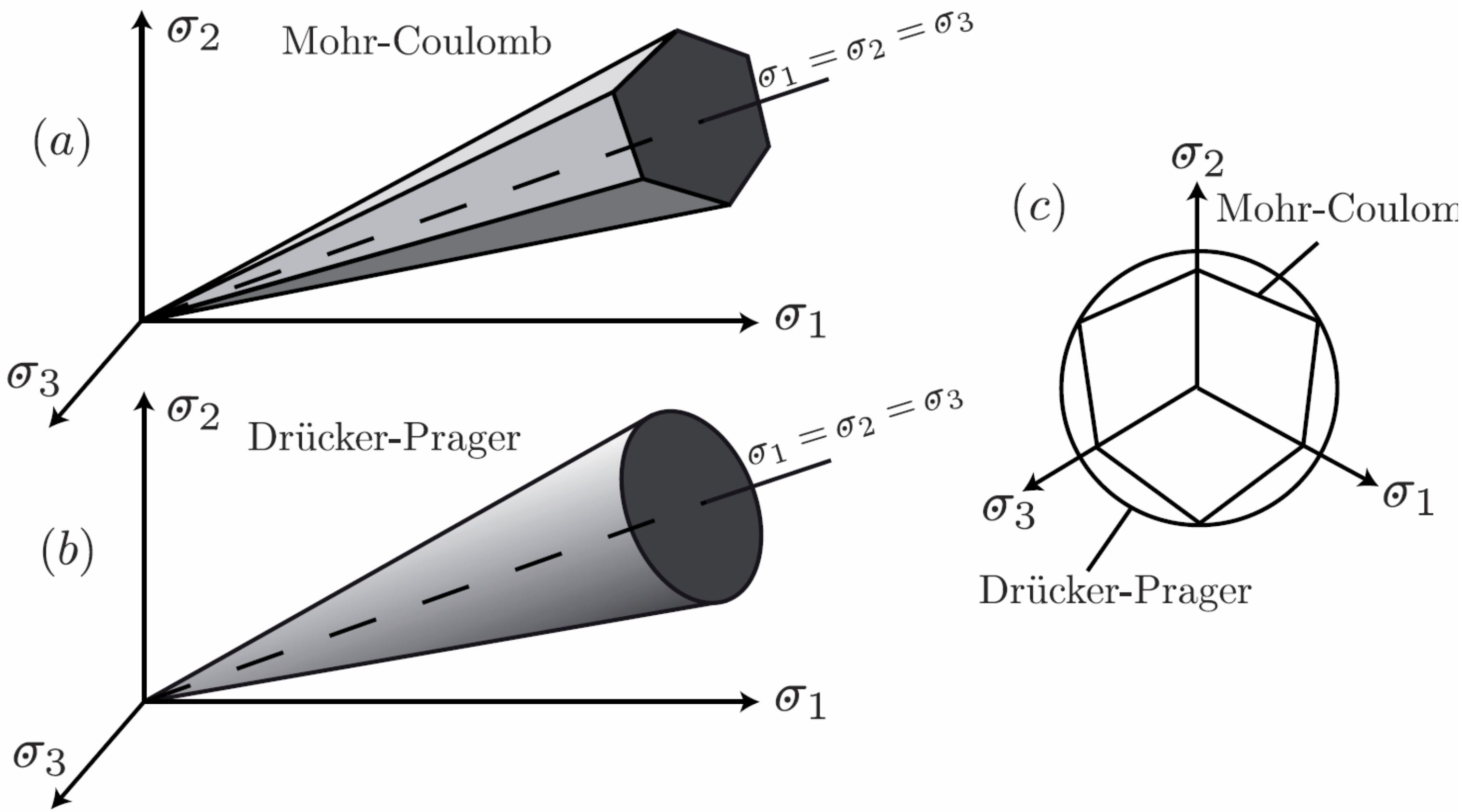

Surface de plasticité dans l'espace des contraintes principales. (a) Critère de Mohr-Coulomb. (b) Critère de Drücker-Prager. (c) Section perpendiculaire à l'axe des cylindres.

Les observations montrent que la surface de plasticité dans la section des contraintes principales présente une forme arrondie plus proche de Drucker-Prager que de Mohr-Coulomb. La forme n'est pas exactement circulaire, et d'autres critères ont été proposés, notamment le critère de Lade (1977)

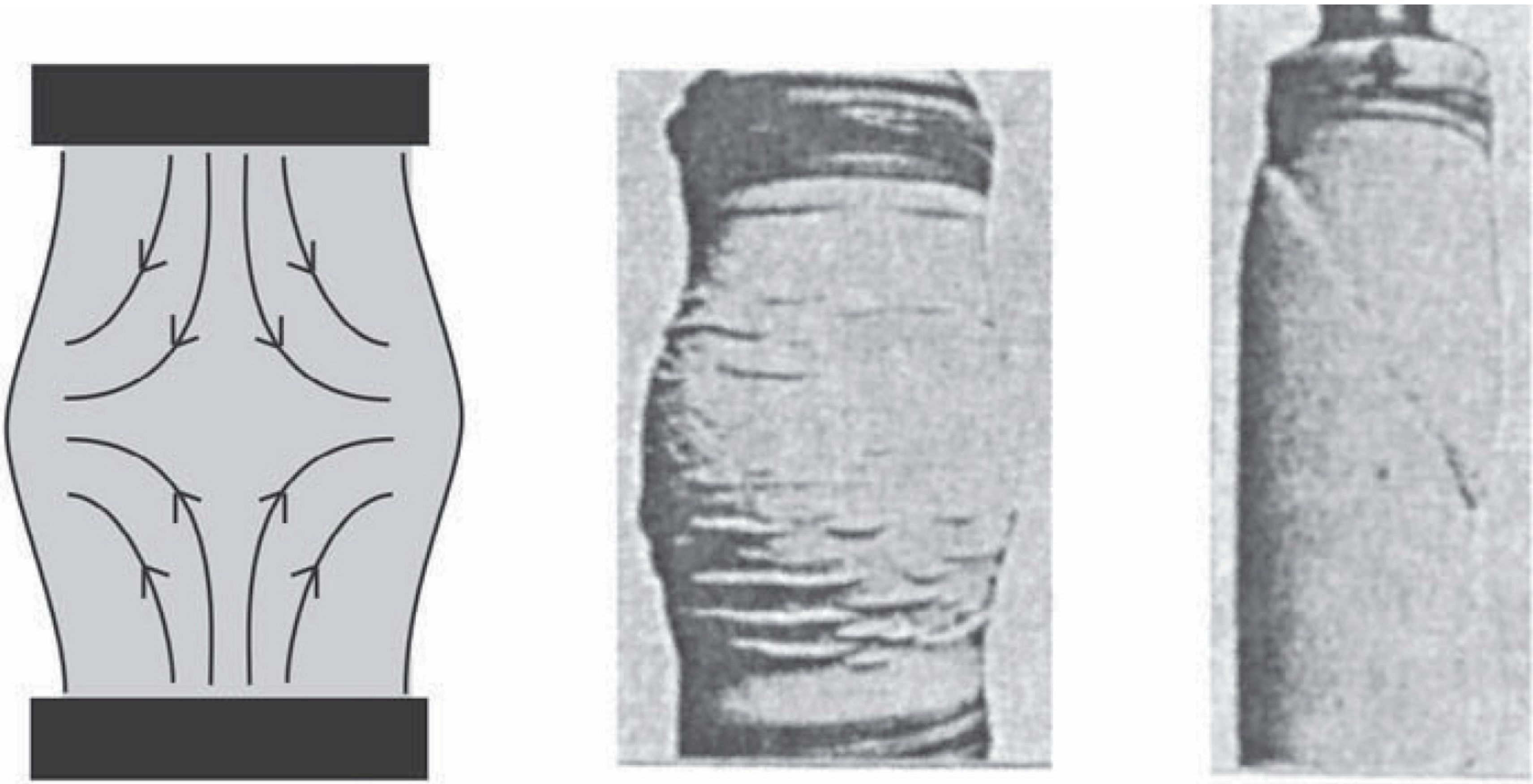

(a) (b) (c)

(a) Déformation prédite par le modèle de Mohr-Coulomb dans un triaxial. Déformation observée pour un milieu initialement lache (b) et initialement dense (c) (d'après Taylor, 1948).

2D granular flows over erodible bed : Experiments

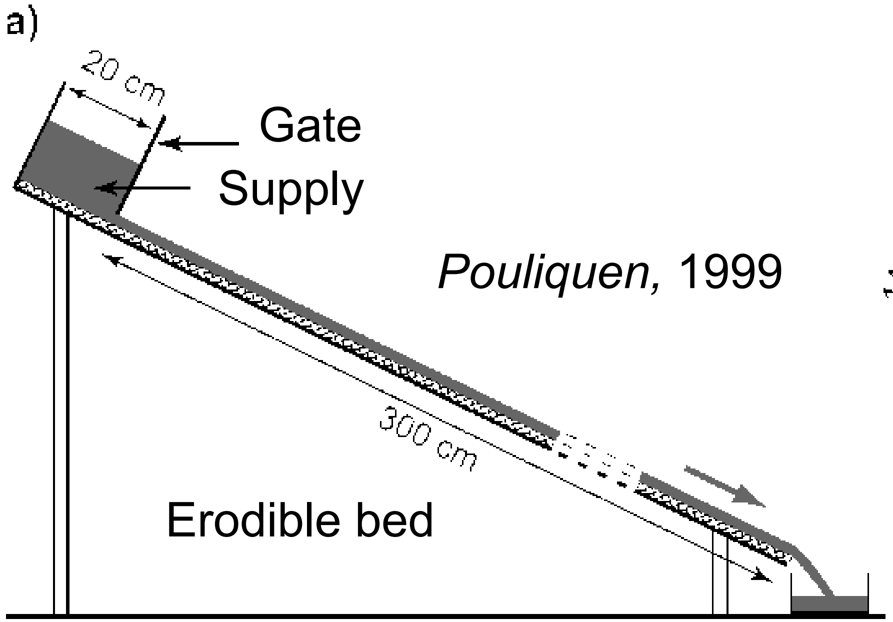

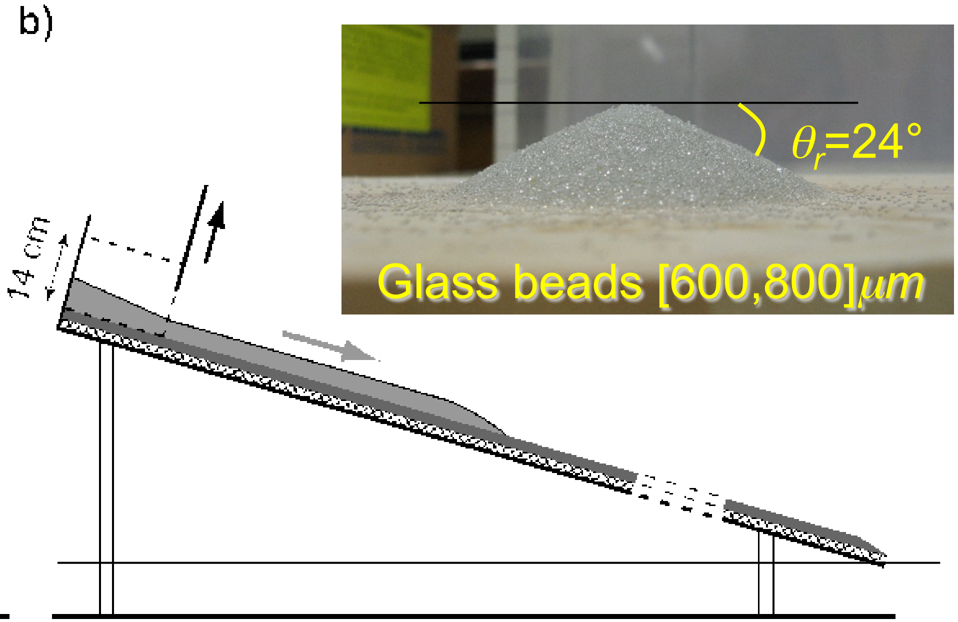

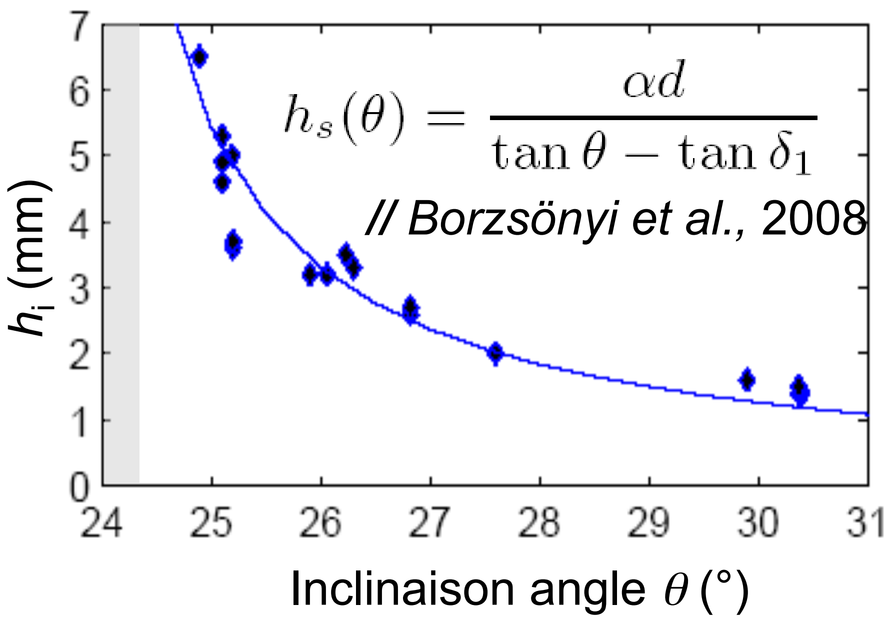

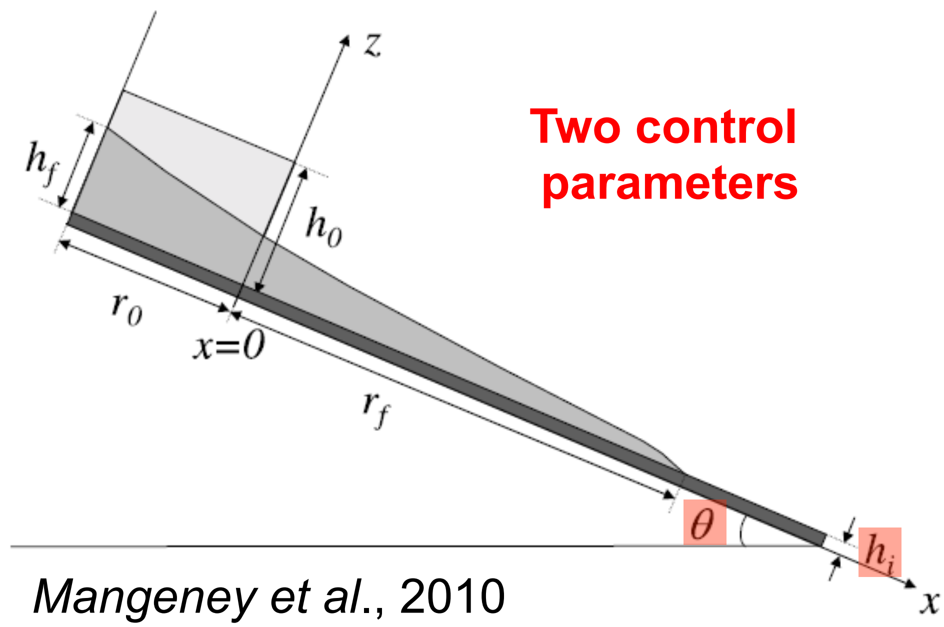

Granular collapse over an erodible bed

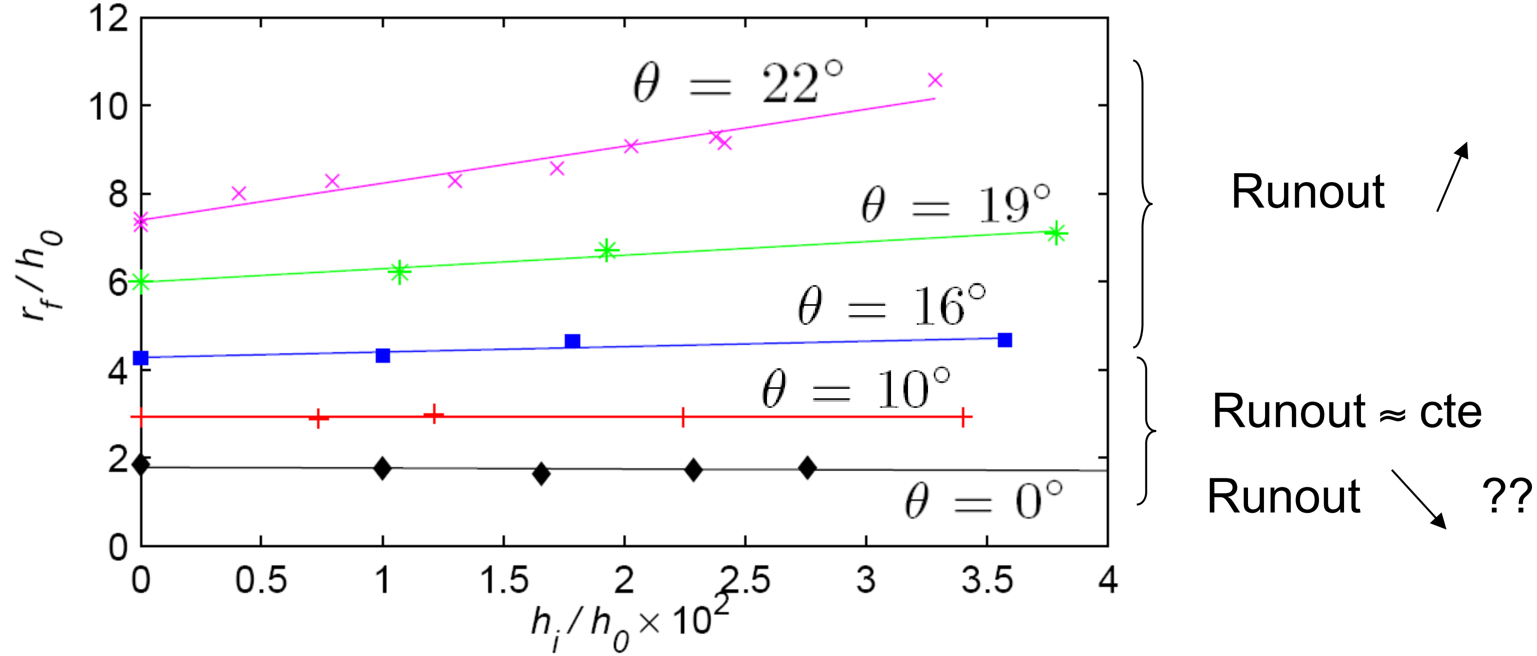

$\Rightarrow$ **Entrainment depends on mass availability**, for a given angle θ

Critical angle : $\theta_c \simeq 12^\circ \simeq \theta_r/2$: above which erosion increases flow mobility

$$\frac{r_f}{h_0} = \frac{1}{\tan\delta - \tan\theta} + \gamma(\theta)\frac{h_i}{h_0}$$

$$\gamma(\theta) = \frac{0.02}{\tan 23^\circ - \tan\theta}$$

Strong tests for erosion models !!

Strong implication for risk assessme

Mangeney et al., 2010

Within the granular layer …

Velocity profiles at $x = 90$ cm

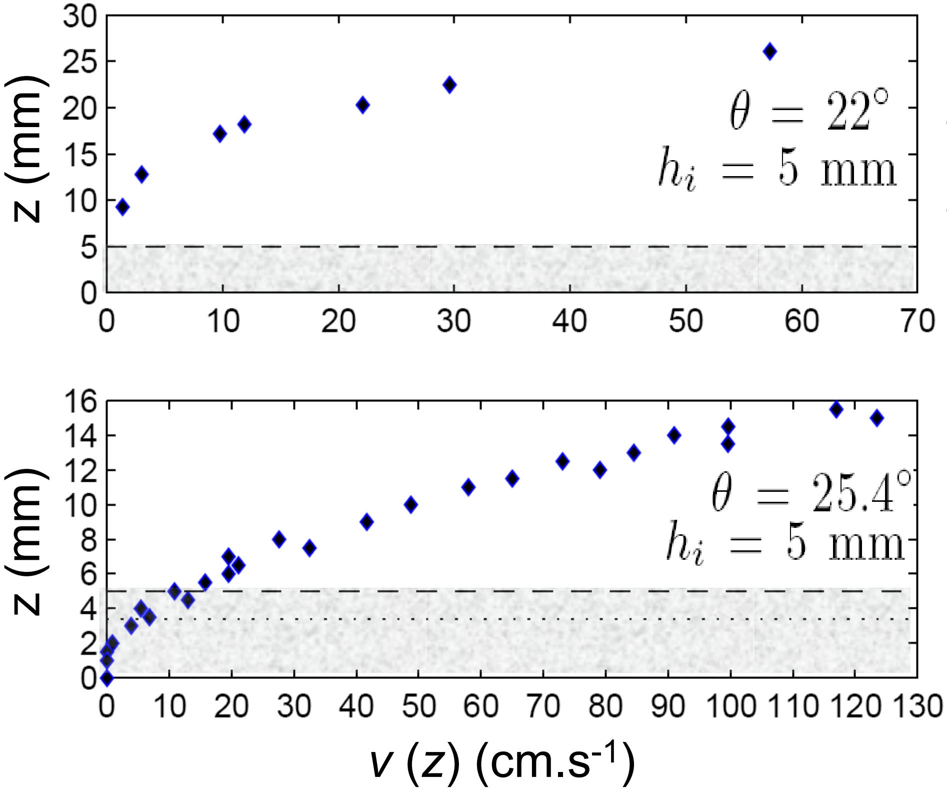

Depth of the static/mobile interface at $x = 90$ cm

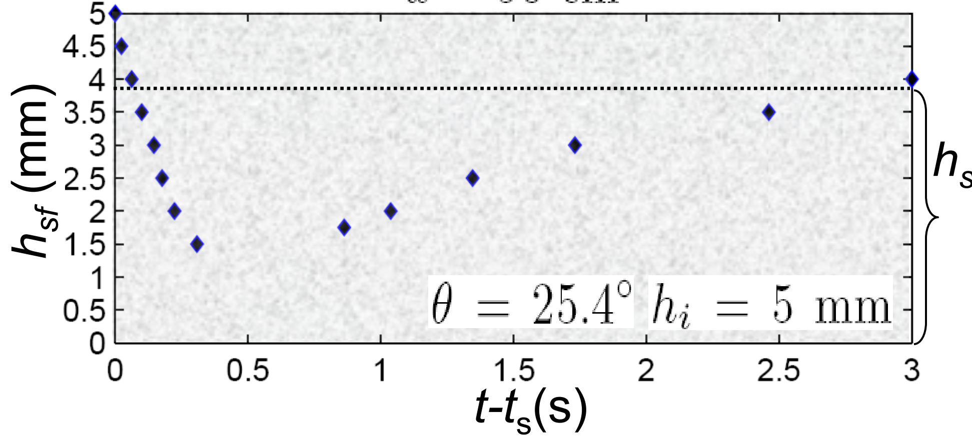

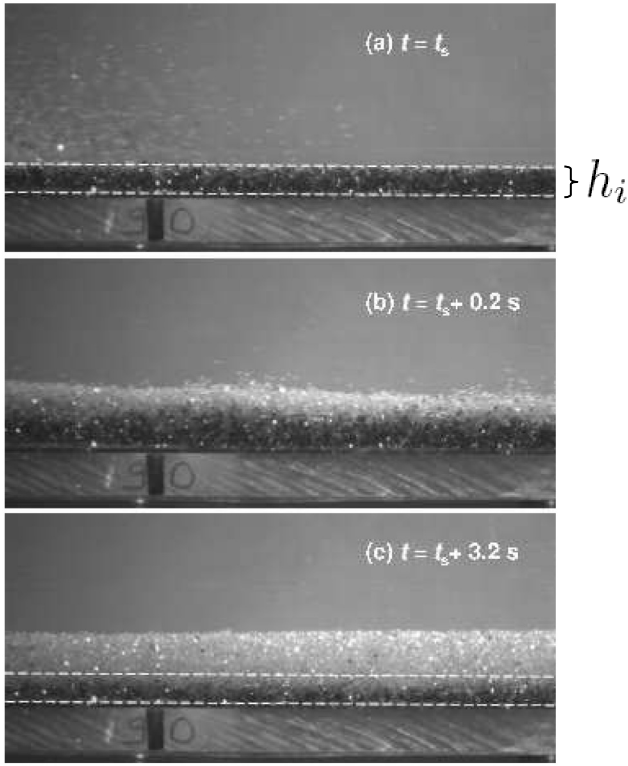

- **The front digs within the erodible bed** with a constant penetration velocity v_{sf} = 1.3 cm.s^{-1}
- **The static/flowing interface moves upward** (exponential relaxation) up to $z \approx h_s$
- **Very good agreement with** simulations using the **partial fluidization model** *Mangeney et al.*, 2007

Wave-like motion

$\theta = 25.2^\circ \quad h_i = 3.9\ \mathrm{mm}$

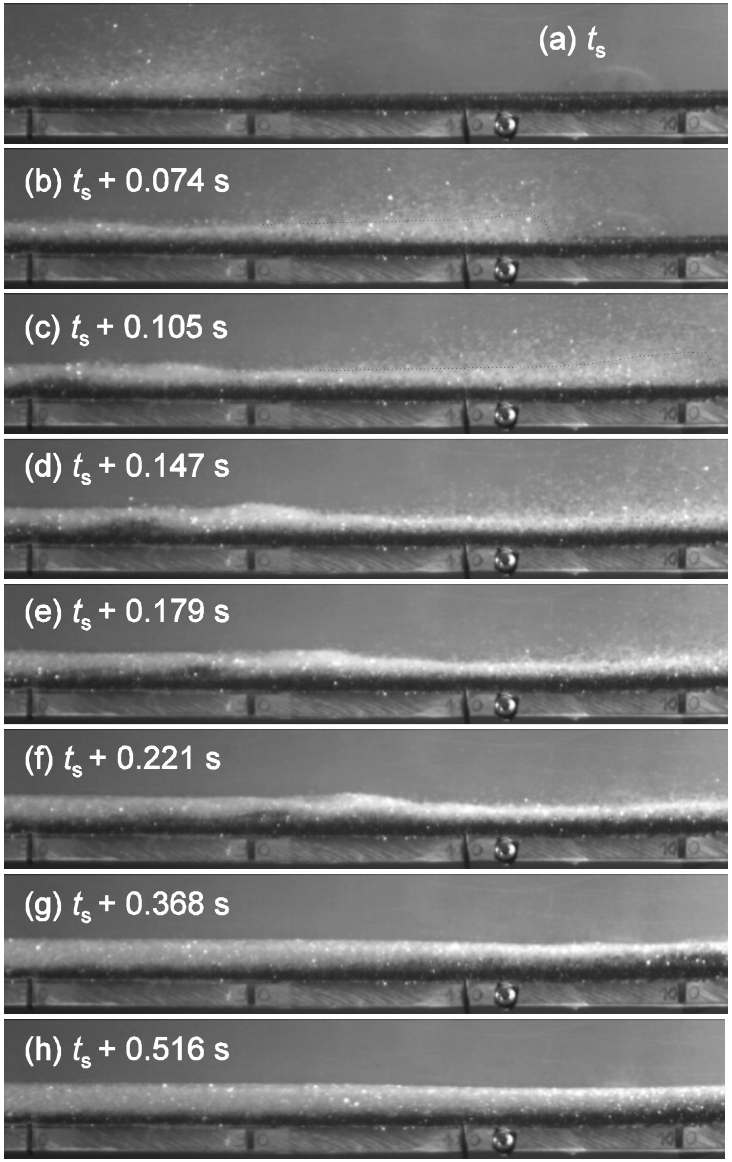

Erodible bed

$\theta = 25.2^\circ$ Rigid bed ($h_i = 0\ \mathrm{mm}$)

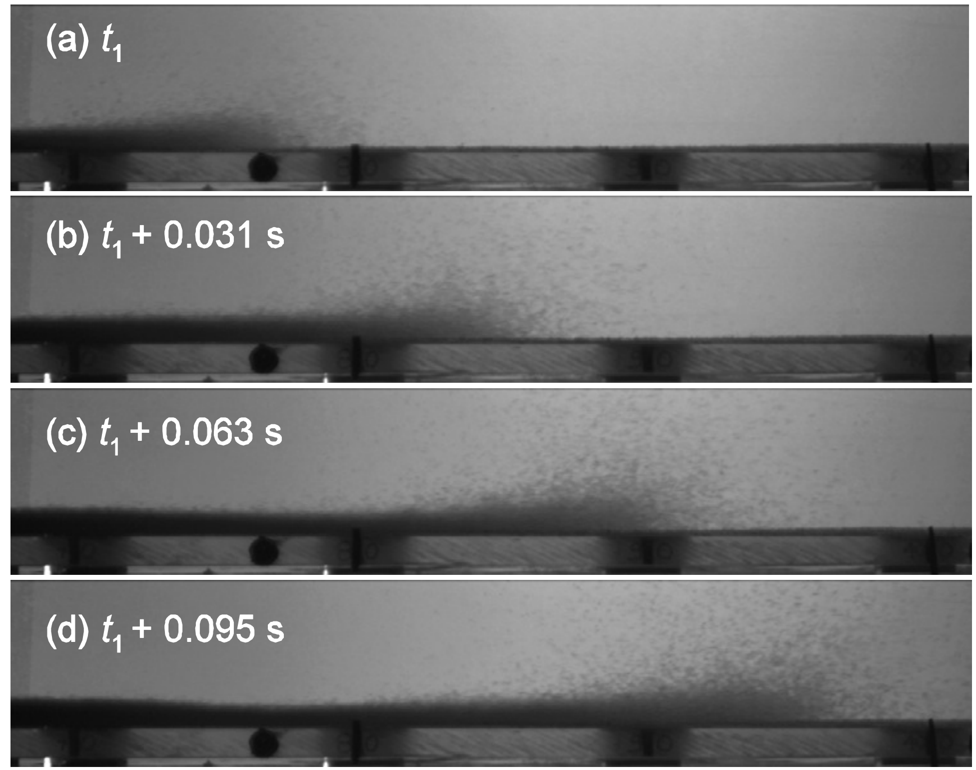

- **Steep front over rigid and erodible bed**
- **Waves located behind the front**

vertical motion that removes grains from the erodible bed comparaison quantitative avec experiences de laboratoire :

- Effet de la guillotine
- Effet des bords
- Manque un effet : dilatance ??

Drucker- Praguer η = 1 Pa.s versus μ (I)

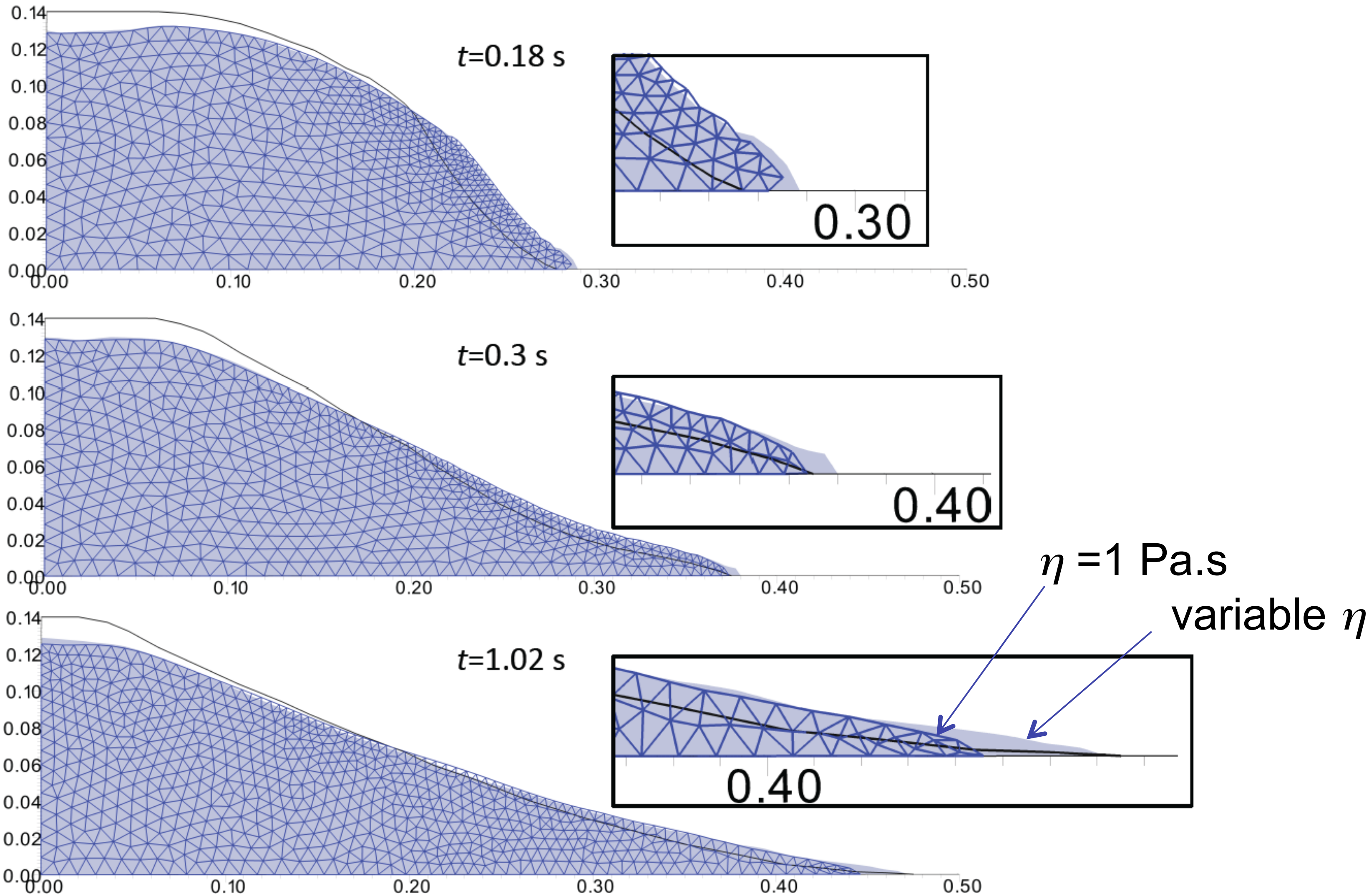

Very similar results with the variable and constant viscosity η =1 Pa.s

μ (I) parameters

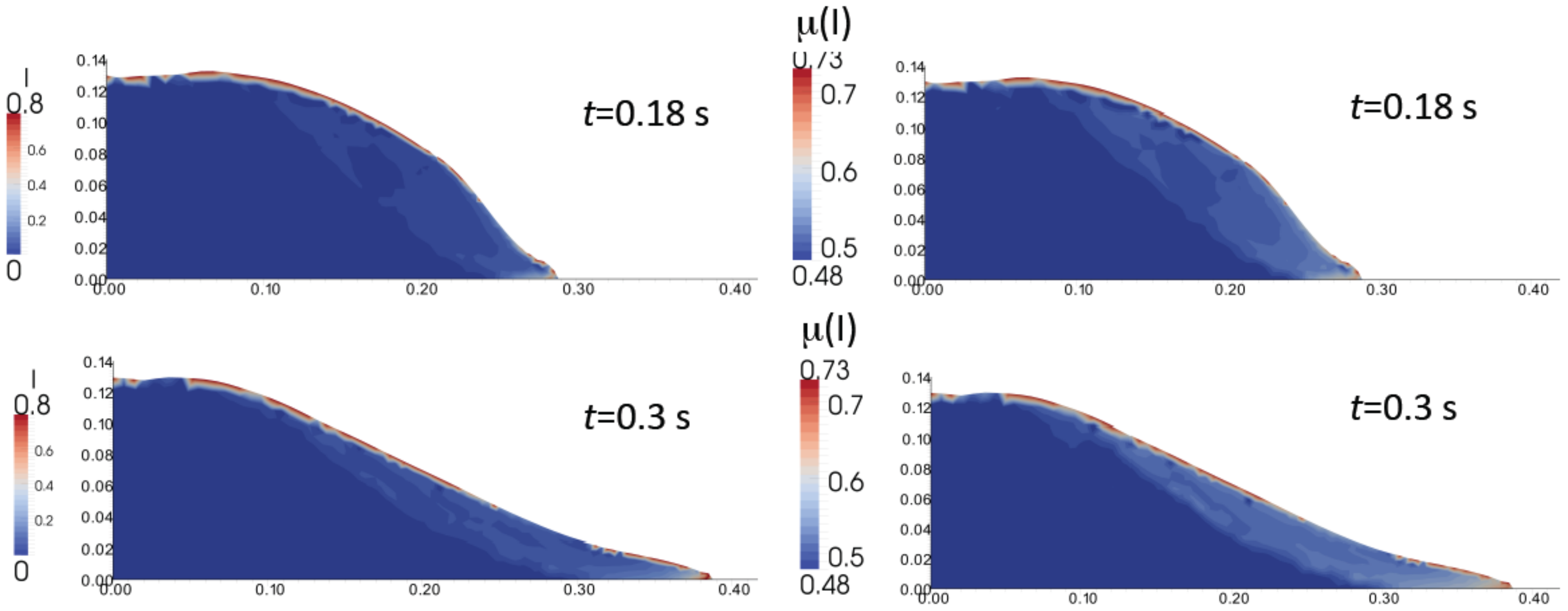

$$I = \frac{2\|\boldsymbol{D}\|d}{\sqrt{p/\rho_s}}$$

$$\mu(I) = \mu_s + \frac{\mu_2 - \mu_s}{1 + I_0/I}$$

Conclusion

- Drucker-Prager with a constant viscosity and $\mu(I)$ rheology reproduce **quantitatively** granular collapse experiments

↓

Insight into flow dynamics

- Only the $\mu(I)$ rheology reproduces **qualitatively** the increase in runout when the thickness of the erodible bed increases

- Still to repoduce quantitatively erosion effects

A big challenge for application to natural landslides

- Derive from Drucker-Prager equations

two layers Saint-Venant equations : a flowing layer over a static layer

Bayesian inversion of landslide characteristics

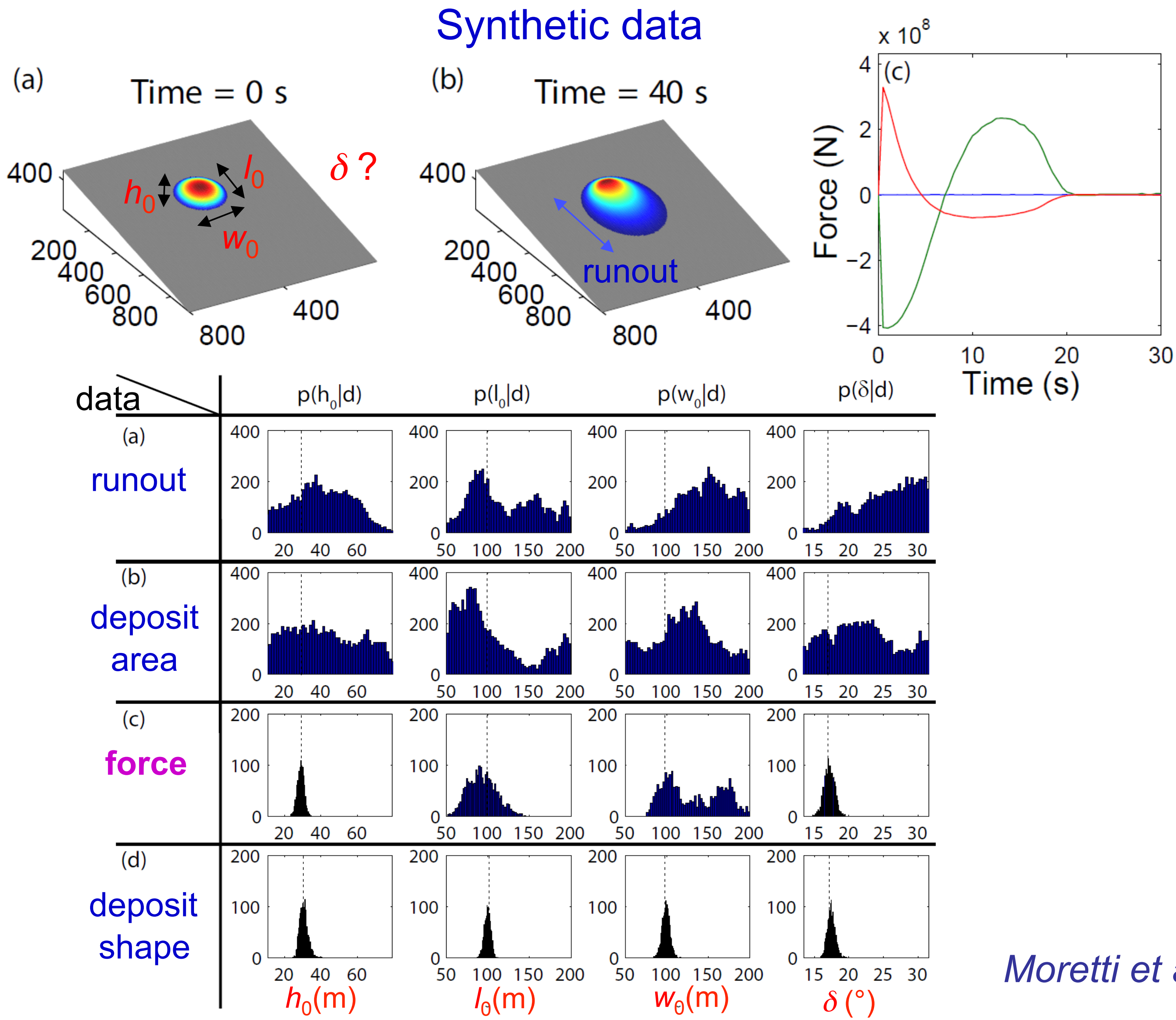

Moretti et al. 2017

Bayesian inversion of landslide characteristics

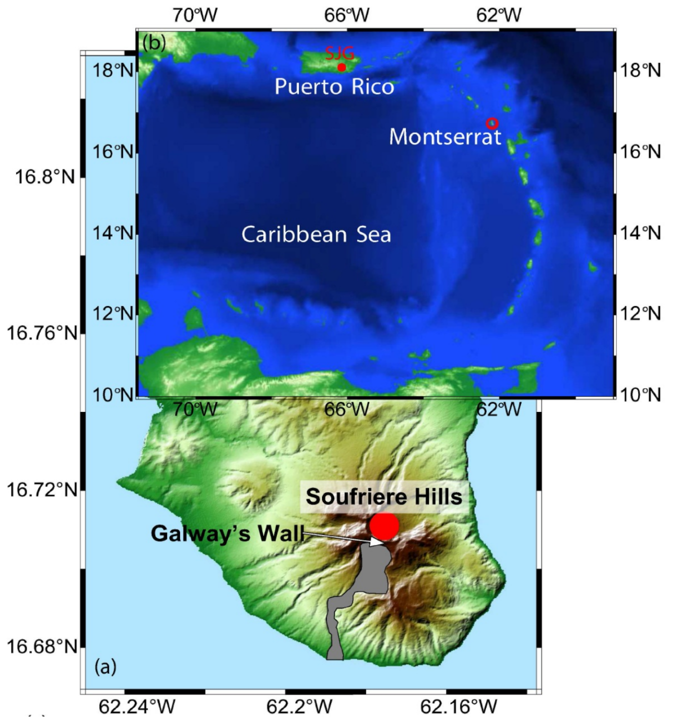

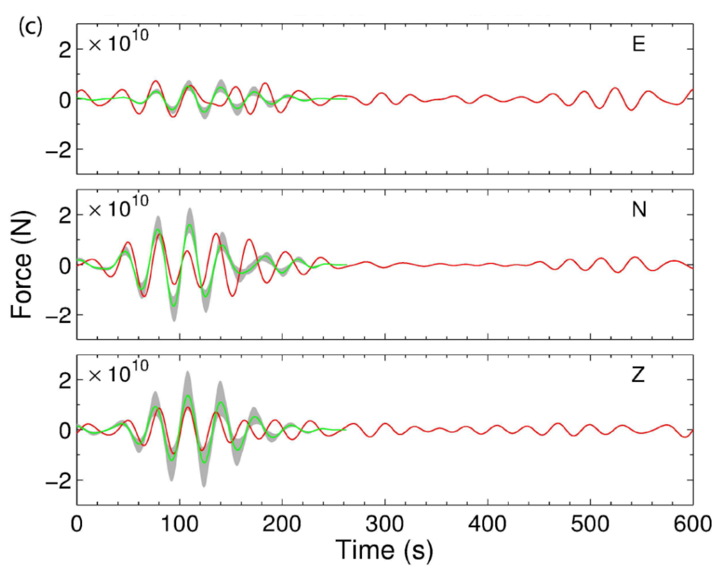

Boxing Day debris avalanche, Montserrat

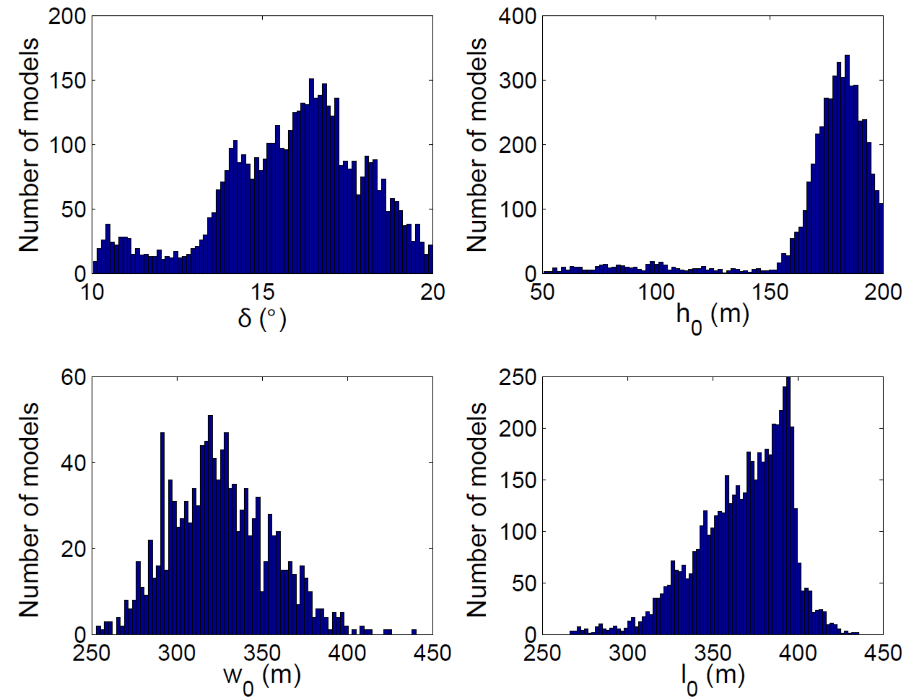

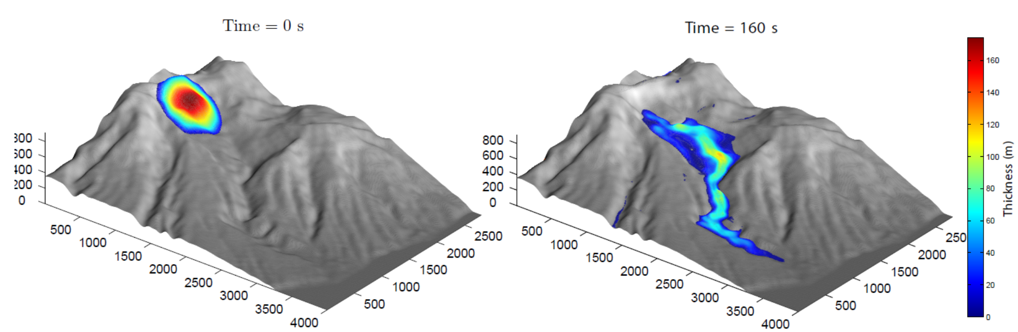

$V \in [32\ 59]$ Mm^3 with a central value of V =45.8 Mm^3

Moretti et al. 2017

Series of rockfalls and pyroclastic flows

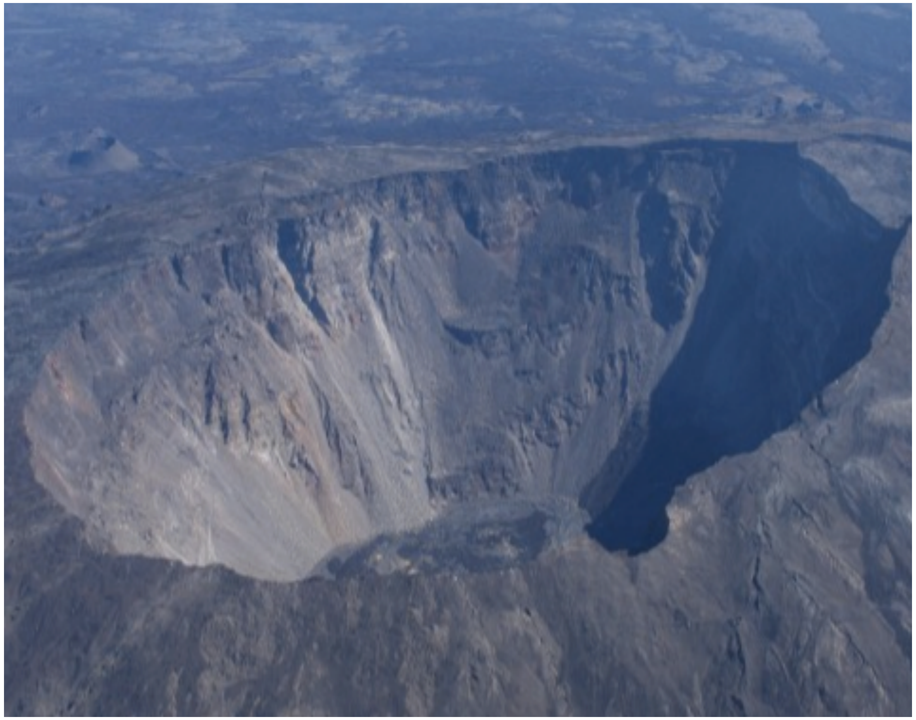

Piton de la Fournaise, La Réunion

V = 1 - 10^3 m^3

Montserrat, Lesser Antilles

V = 10^2 - 10^6 m^3

Observation : seismology, photogrammetry

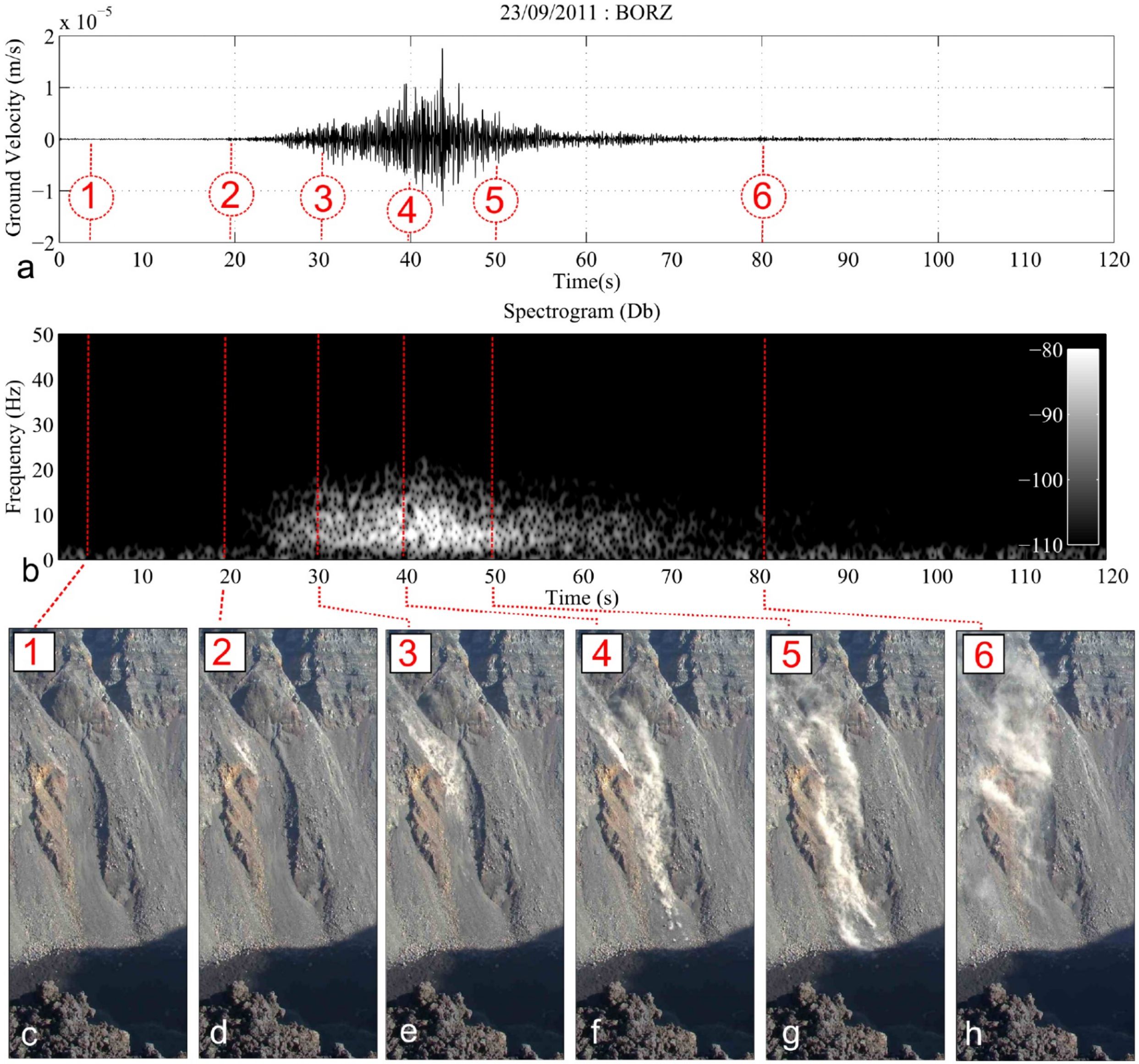

$t_s \approx t_f$

Hibert et al., 2011, 2014, 2016

High frequency Detection, localization, monitoring

Time (s)   Kurtosis based method

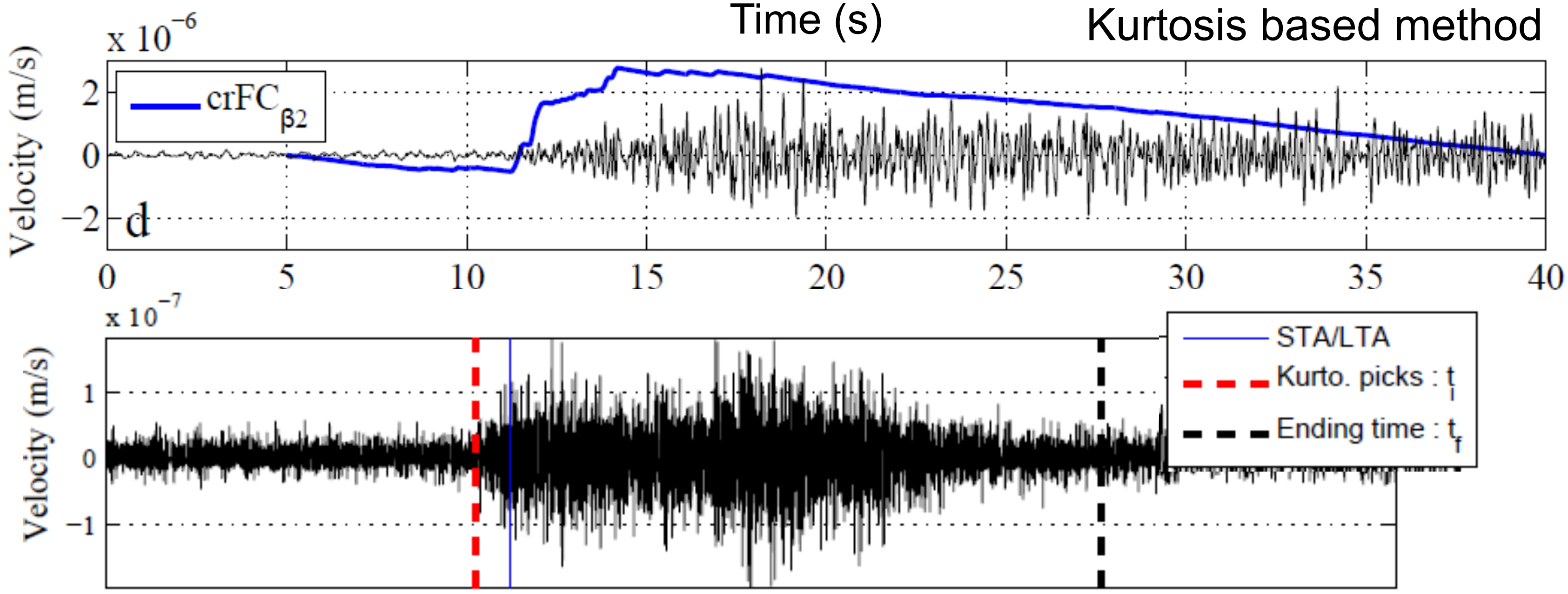

Hibert et al., 2014

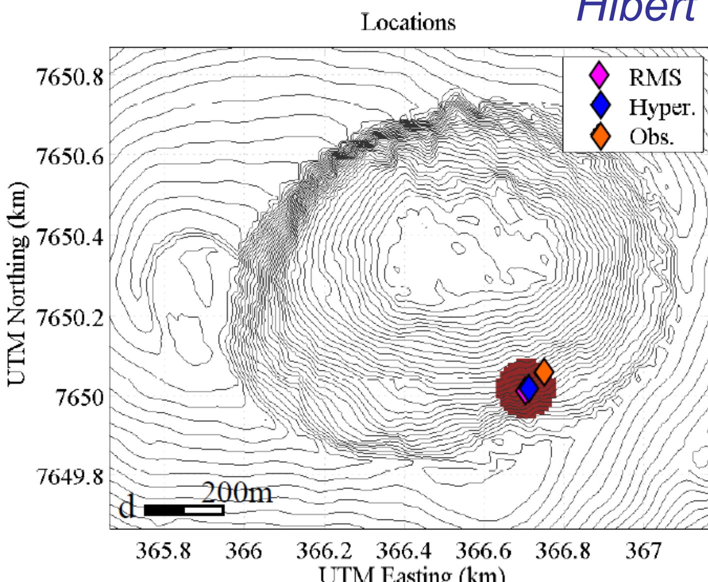

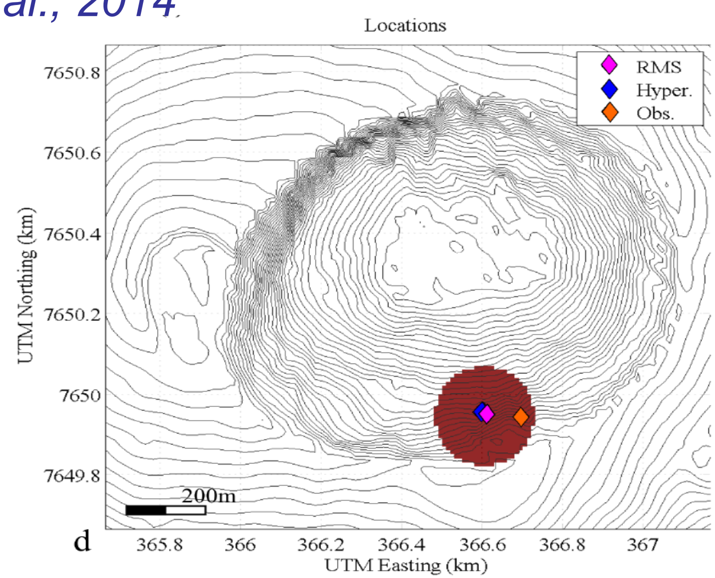

Power law: seismic energy versus duration

Seismic energy : $$Es = \int_{t_1}^{t_2} 2\pi r \rho h c\, u_{env}(t)^2 e^{\alpha r}\, dt$$ *Vilajosana et al., 2008*

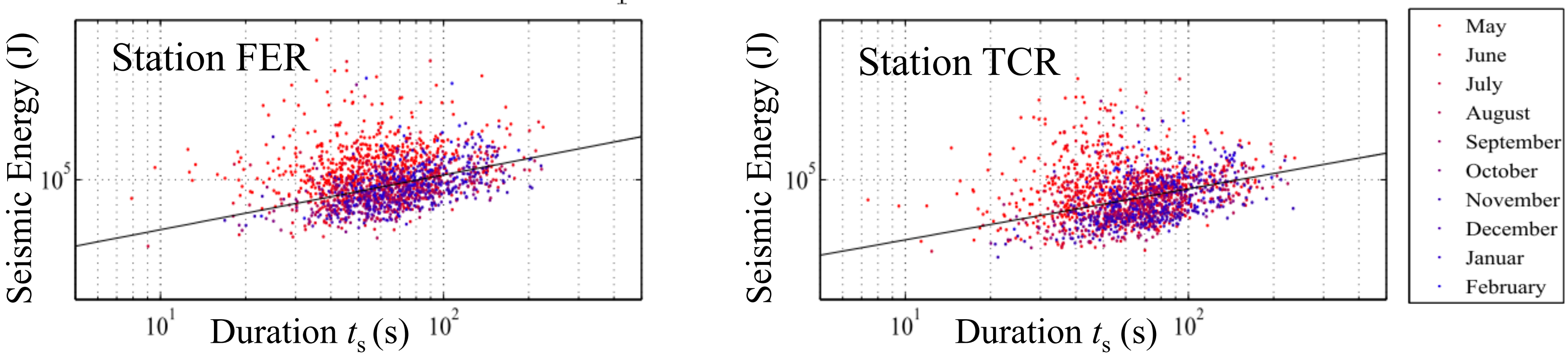

Regression lines and corresponding coefficients computed for each month

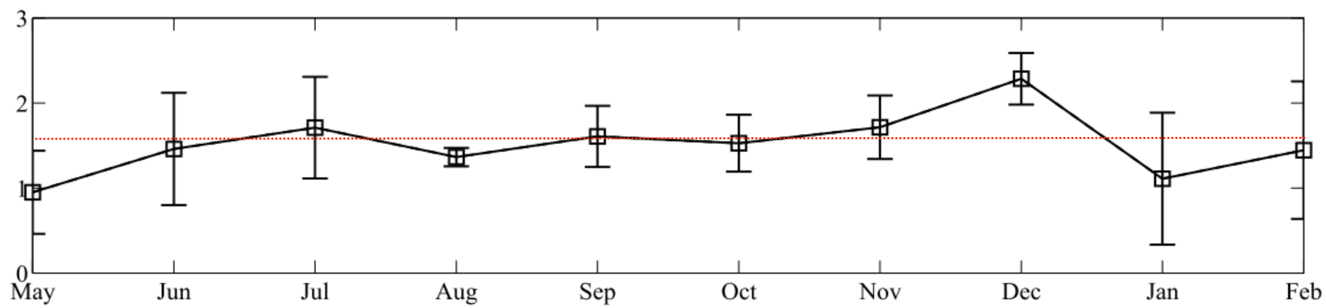

Scaling law between **seismic energy** and **duration** :

$E_s \, \alpha \, t_s^{\beta_s}$

with

$\beta_s \approx 1.56$

Power law: potential energy versus flow duration

- Analytical development for a rectangular mass on a flat slope

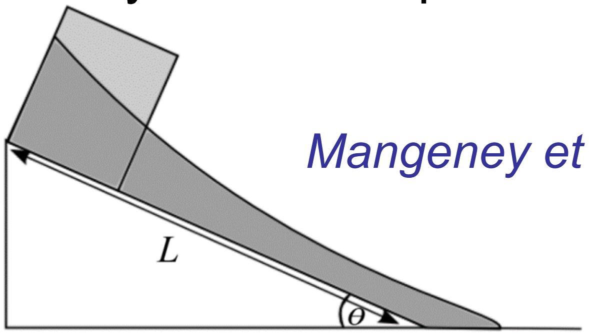

Mangeney et al., 2010

$$\Delta E_p \; \alpha \; t_f^{\beta a}$$ with $$\beta_a = 2$$

- Numerical simulation of granular flows over real topography using the code SHALTOP *Mangeney et al.*. 2007

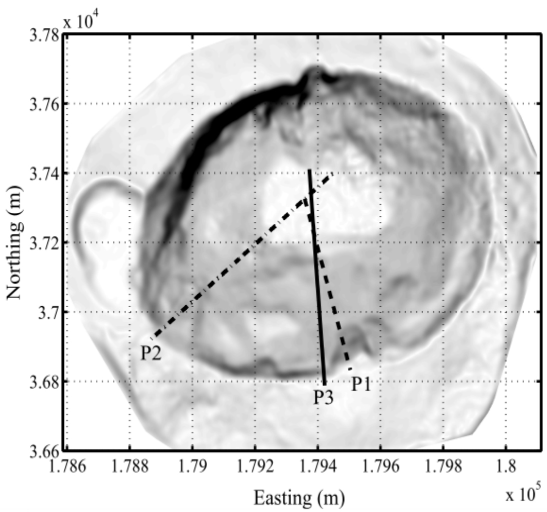

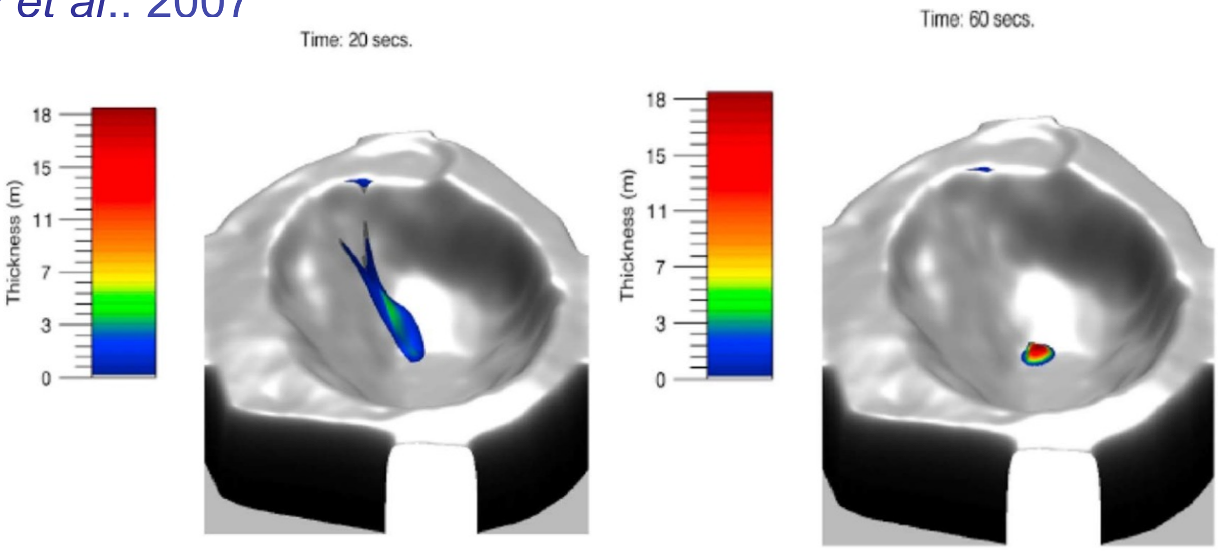

Topography Effects

Rugosity $\nearrow \Rightarrow \beta_p \searrow$

$$\Delta E_p \; \alpha \; t_f^{\beta p}$$ with $$\beta_p = 1.65$$

From seismic energy to rockfall volume

- Scaling laws Energy/Duration : $E_{\text{seismic}}\ \alpha\ t_s{}^{\beta}$ and $\Delta E_{\text{potential}}\ \alpha\ t_f{}^{\beta}$

$R_{s/p}=E_s/\Delta E_p\sim 10^{-4}$

Volume $$V=\frac{3E_s}{R_{s/p}.\rho g L(\tan\alpha\cos\theta-\sin\theta)}$$

simulations

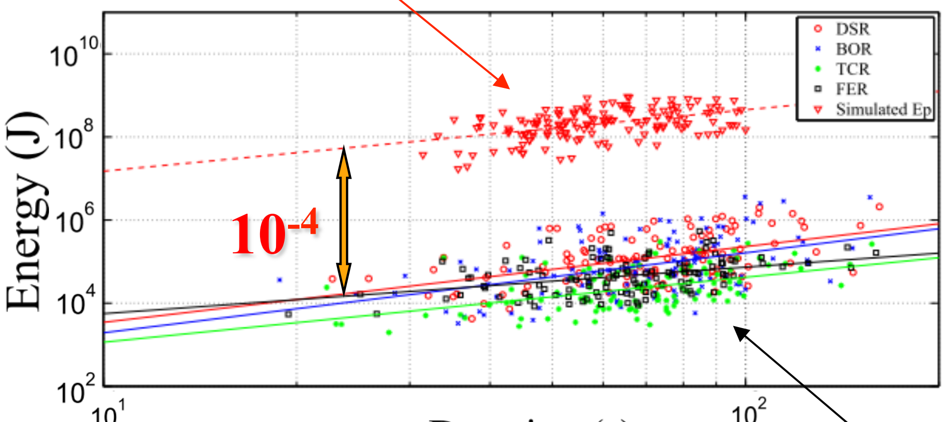

t_f or t_s

Seismic data

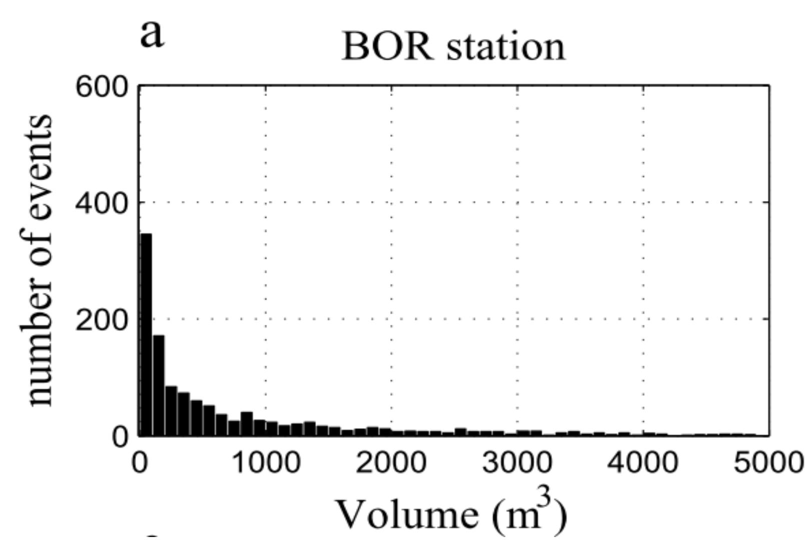

- Cumulative volume from May 2007 to February 2008 : V=1.85 10^6 m^3

Hibert et al., 2011, 2014, 2017

Detection, localization, monitoring

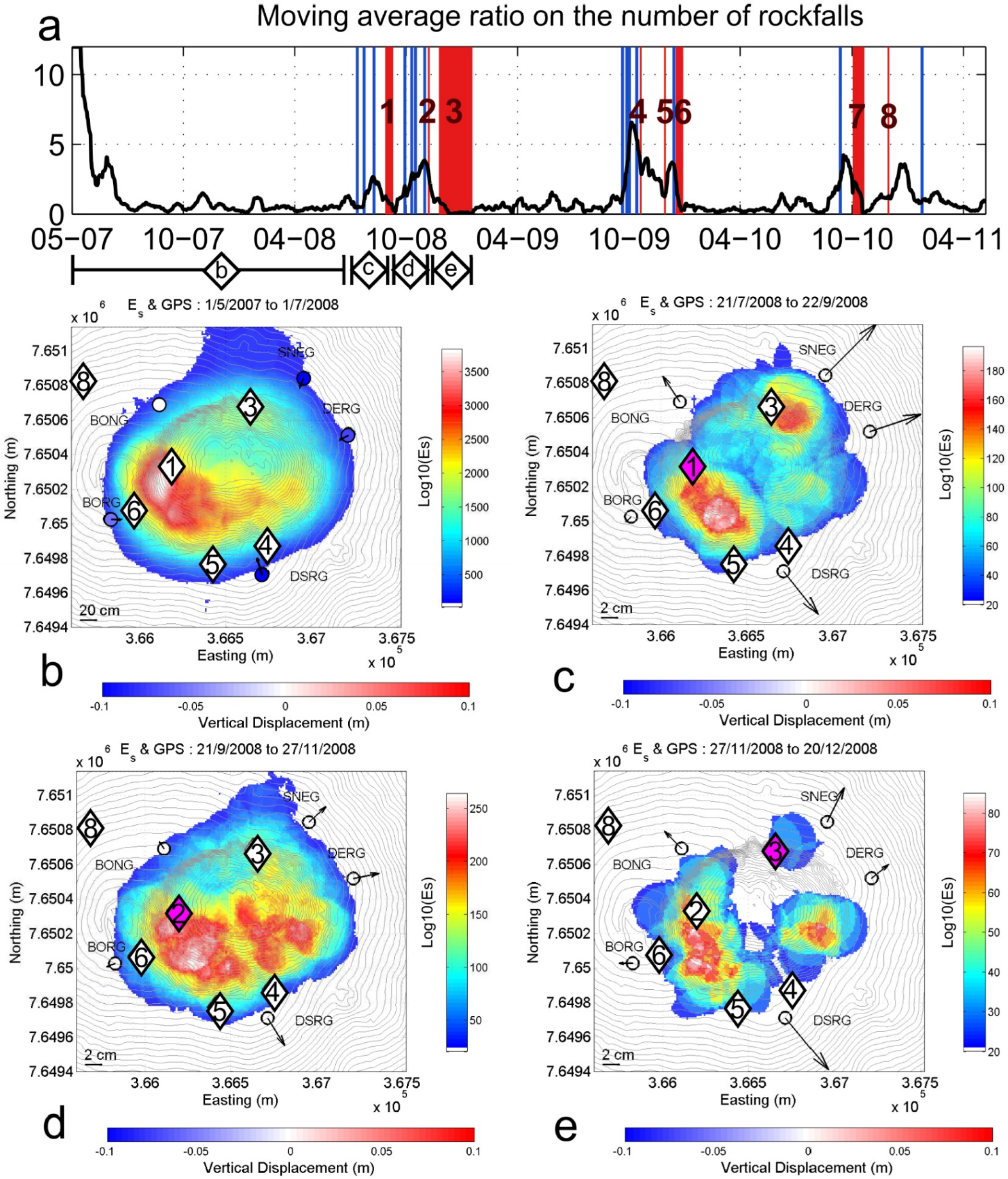

- Spatio-temporal distribution of rockfall characteristics

- Link with volcanic activity

Hibert et al., 2017

Friction weakening signature on seismic data

$$E_s \propto t_s^{\beta} \quad \text{and} \quad \Delta E_p \propto t_f^{\beta} \quad \Rightarrow \quad \text{As} \quad t_f \simeq t_s \quad E_s/\Delta E_p \simeq 10^{-5}$$

Hibert et al. 2011

Rockfalls and pyroclastic flows in Montserrat

$\mu=1/V^{0.0774}$

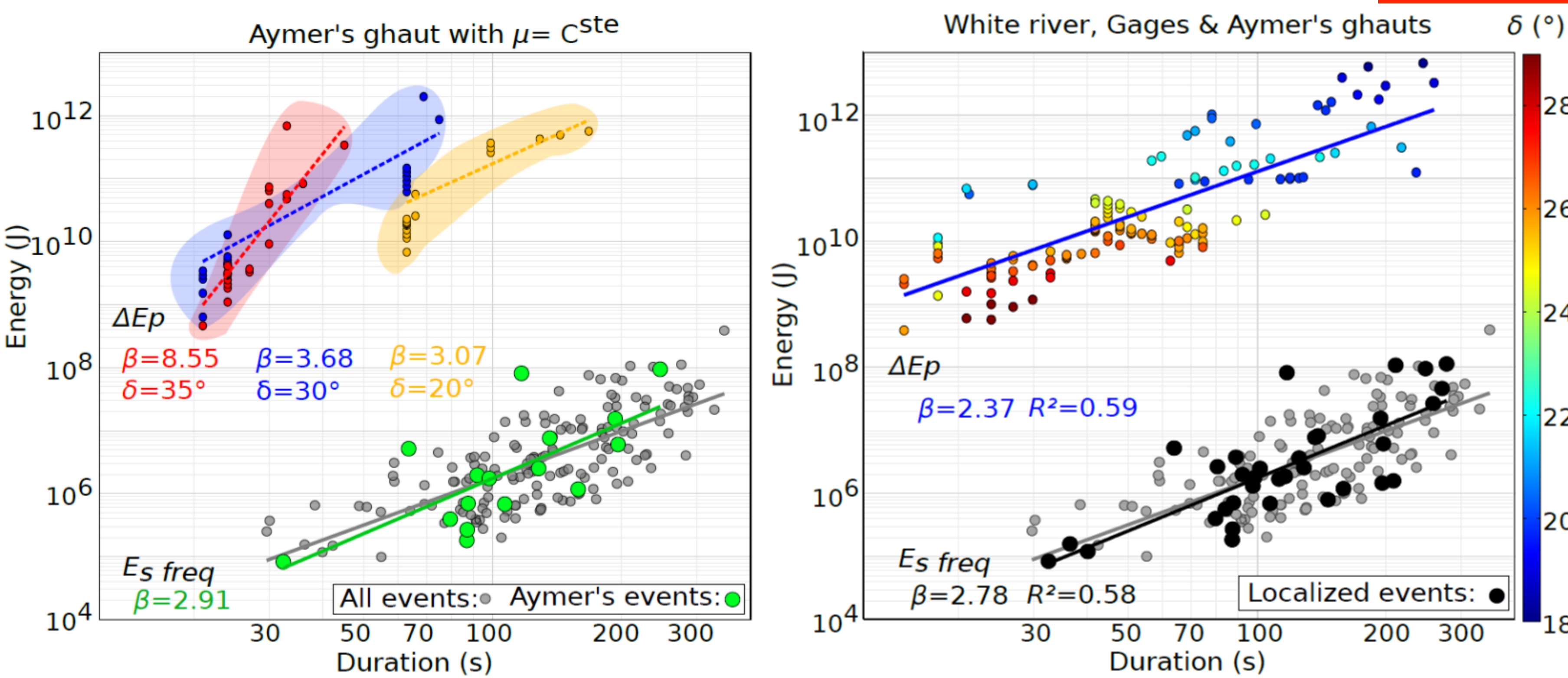

Friction weakening makes it possible to reproduce seismic data

Levy et al. 2015

Friction weakening signature on seismic data

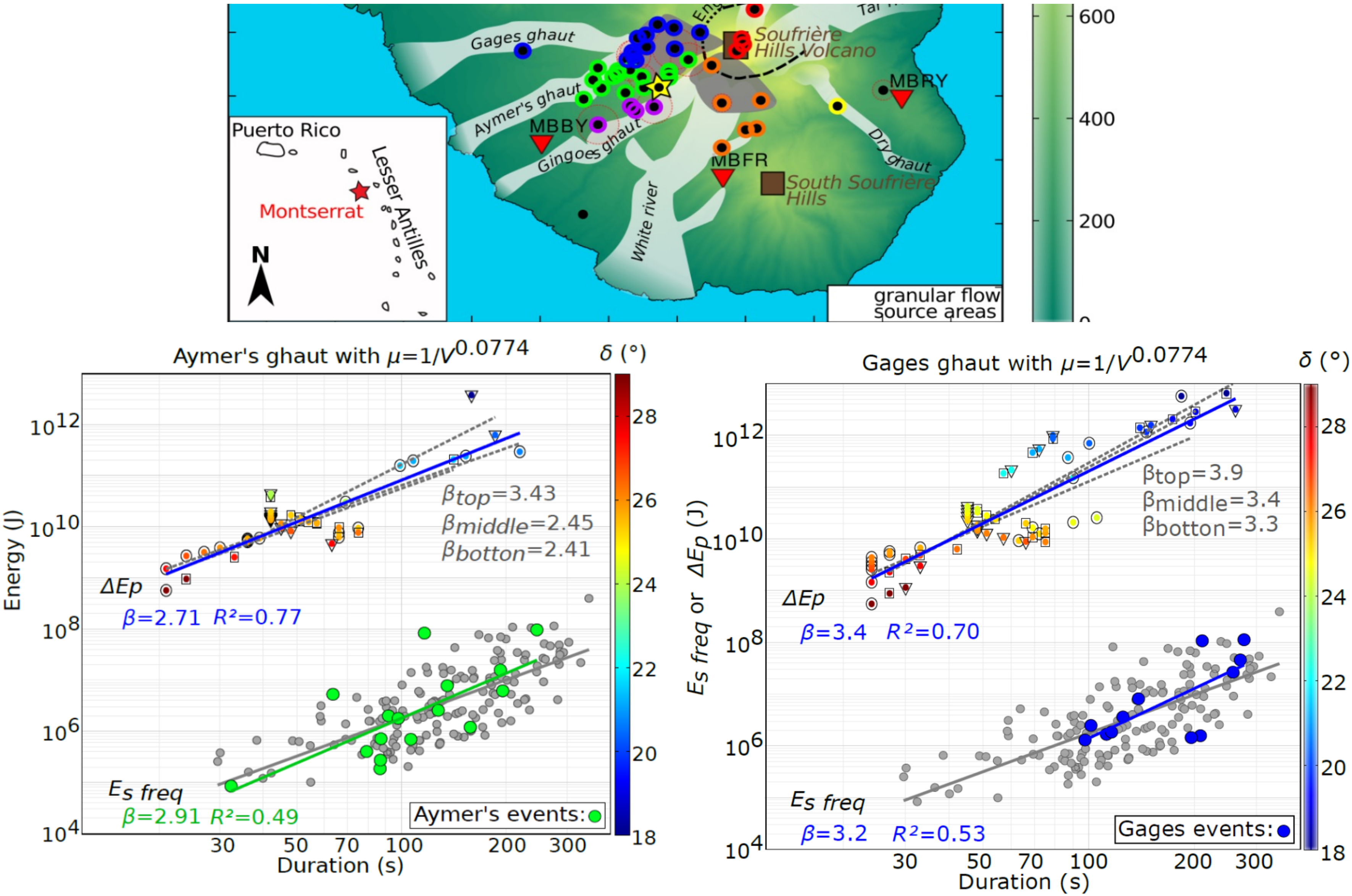

The parameters of the power law depend on the valley !

High frequency seismic data and flow dynamics

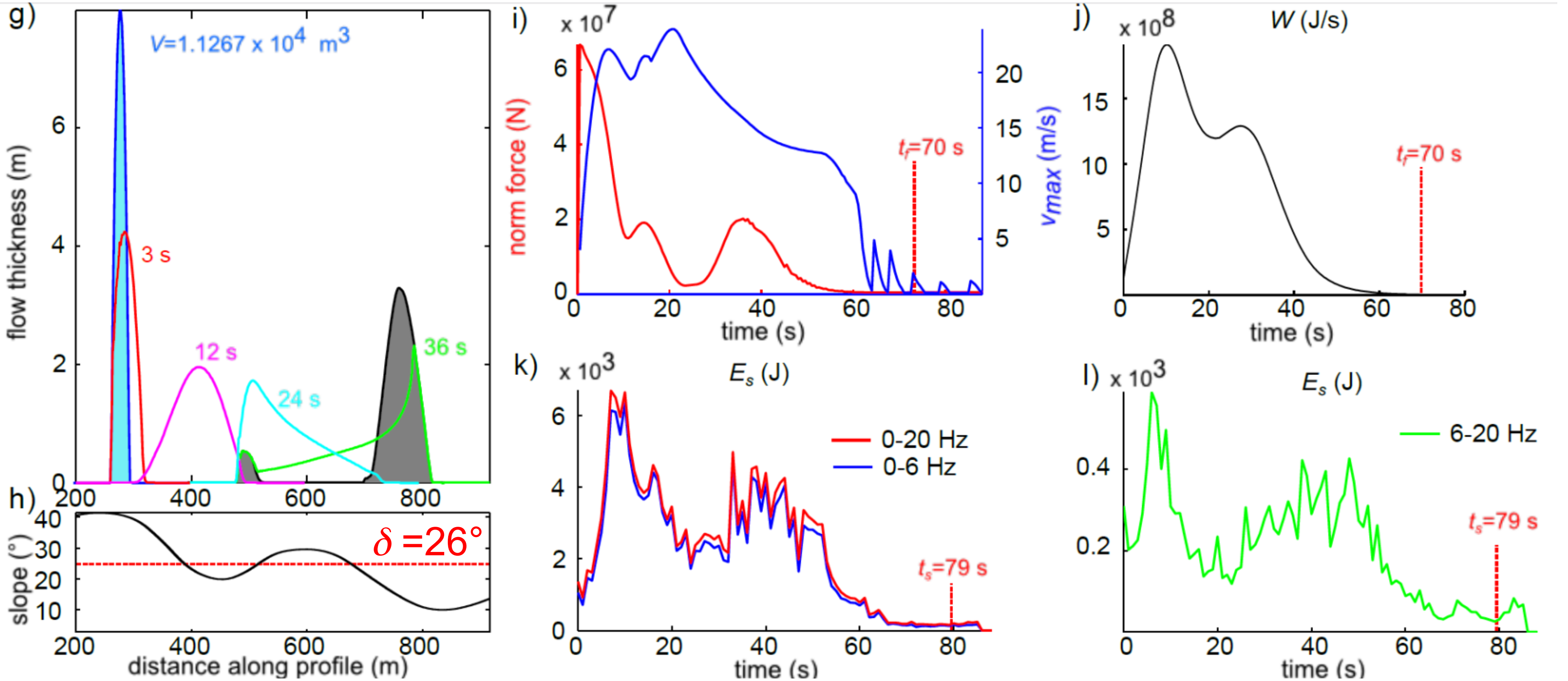

Seismic power fluctuations are related to the force variation that reflects the interaction of the flow with the topography

Experiments of acoustic emission

Impact and rolling of individual grains and granular flows

Energy partition (potential, acoustic, etc.)
From acoustic emissions to grain/substrate properties

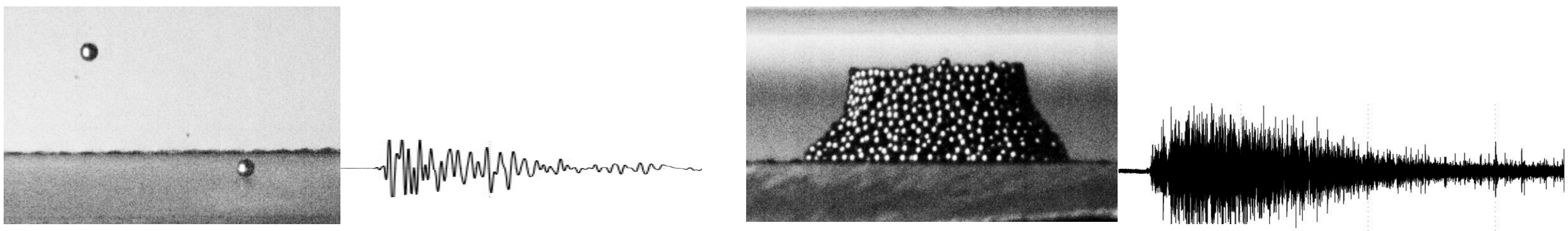

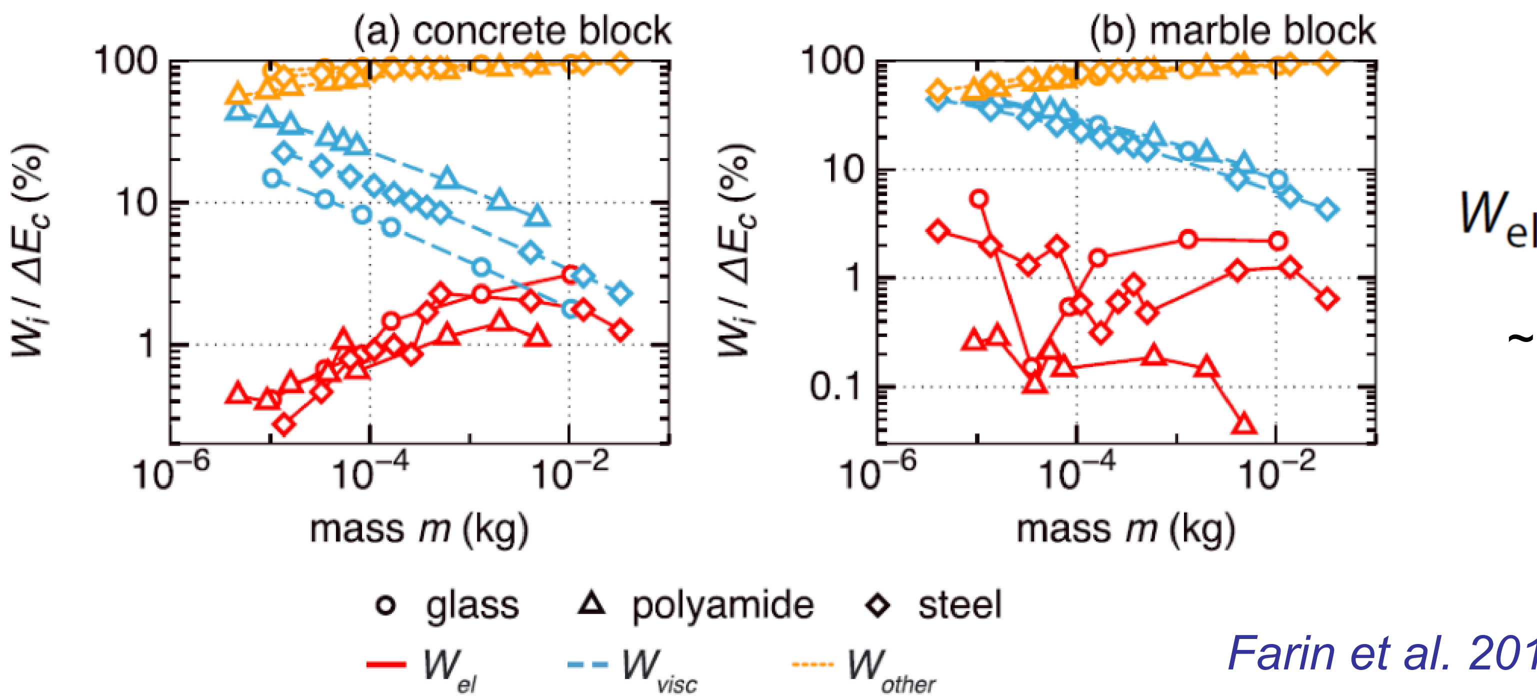

$W_{\mathrm{el}} / \Delta E_c$

~10^{-4}-10^{-3}

Farin et al. 2015a, b

Conclusion

• Seismic signal ➔ temporal change of the force applied by the landslide to the ground

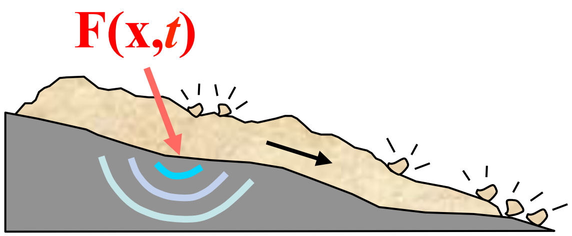

• Low frequency force history + landslide simulation well constrain the geometry and volume of the mass and gives an estimate of the friction coefficient

Moretti et al., 2015a, 2015b

• High frequency seismic power correlates with the simulated force

• Signature of friction weakening on seismic data

Levy et al. 2015, Yamada et al. 2015

erc

Long period observed and simulated seismograms

Filtered between 20 and 80s

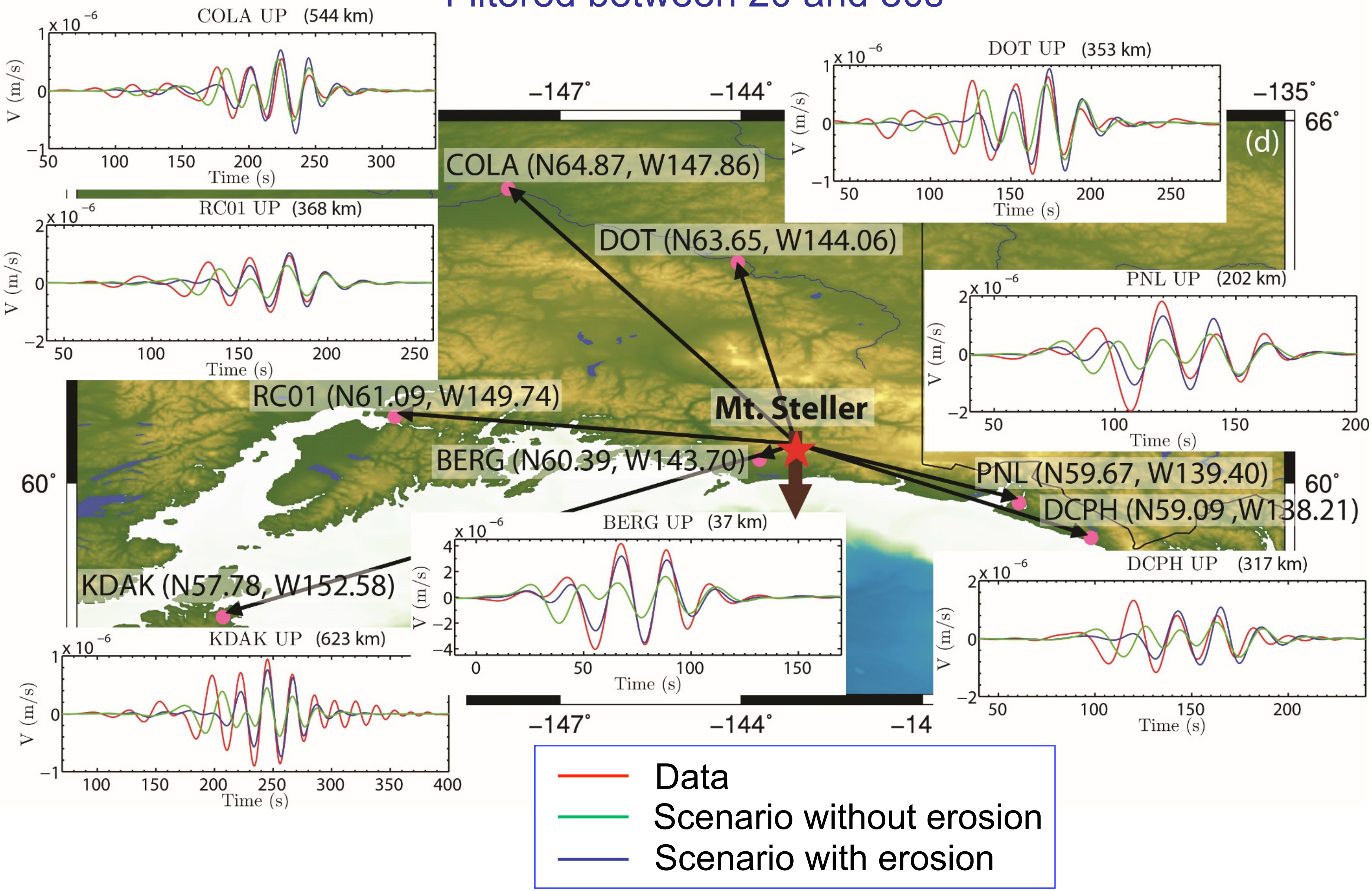

Spatio-temporal change of rockfall activity

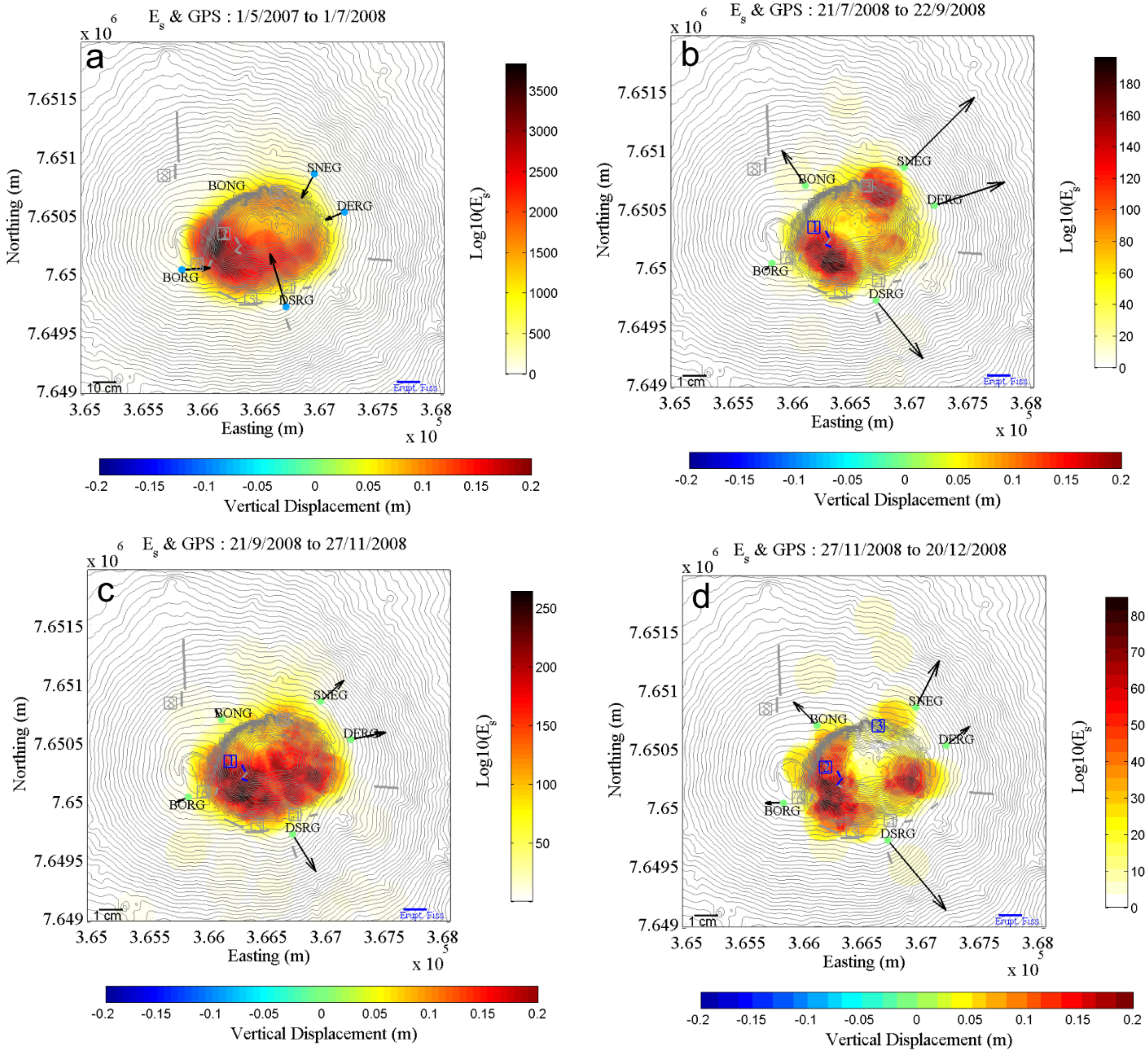

Monitoring rockfall activity

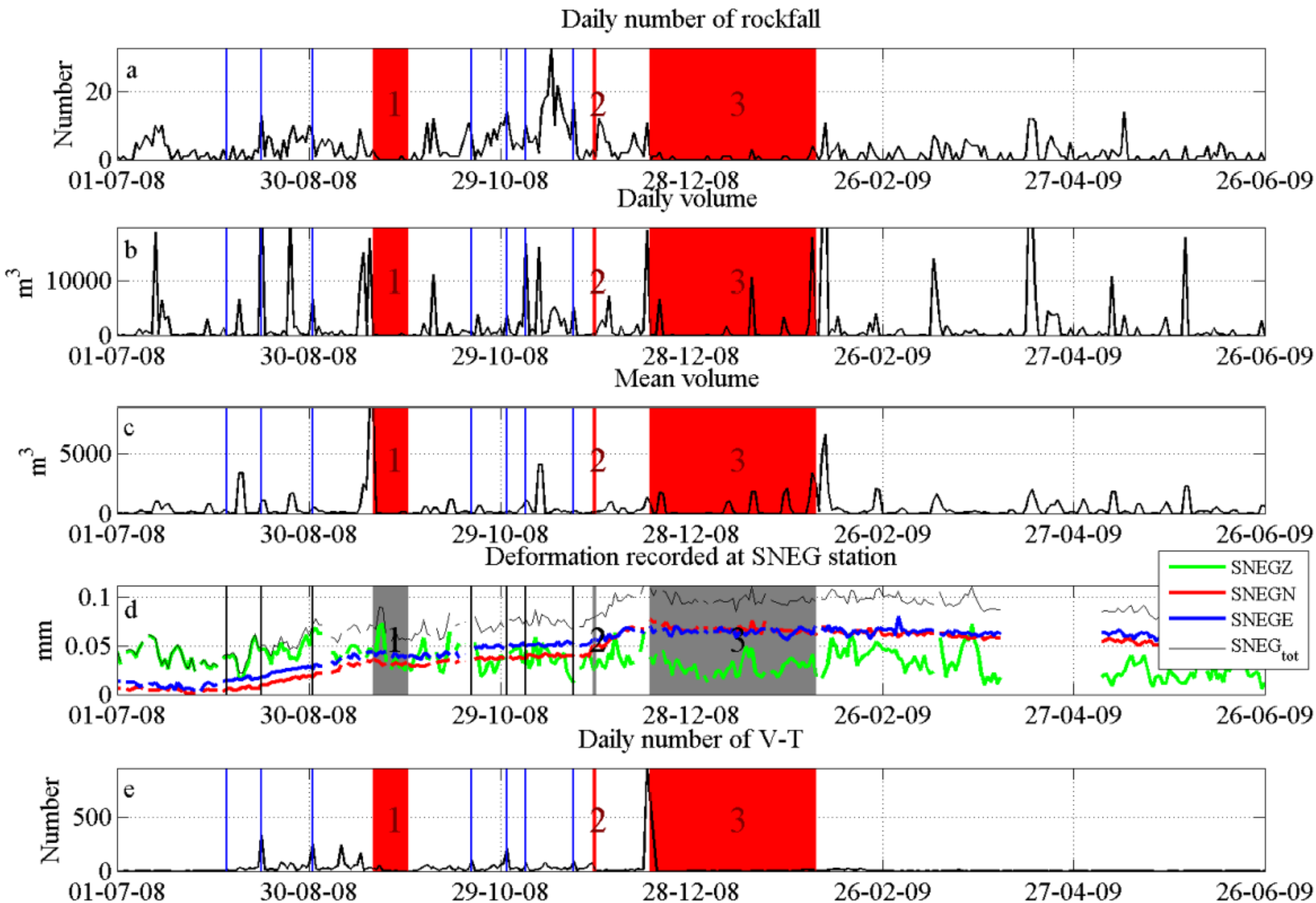

Comportement mécanique des écoulements gravitaires

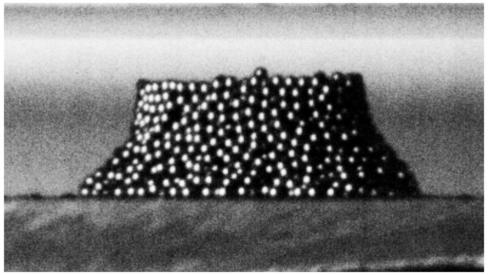

Comportement physique et mécanique? Effet d'échelle?

Conclusion

- Seismic signal ➔ information on the temporal evolution of the volcano stability
- Scaling laws between seismic energy and signal duration
- Transfer ratio of potential energy to seismic energy ➔ **volume = *f* (seismic energy)**
- Near-field, long-period observations can **discriminate between alternative scenarios for flow dynamics**
- Estimation of the **basal friction** and **physical processes during the flow** can be inferred from simulation of the seismic signal

To do …

- Validation on well characterized events
- Systematic study of the **influence of the volume, topography, friction coefficient** on the simulated seismic signal
- **Coupling** landslide and wave propagation **models**

Numerical simulation and inversion of landquakes

Low frequency direct or inverse approach

Landslide simulation **Earth Green functions** **Seismic data**

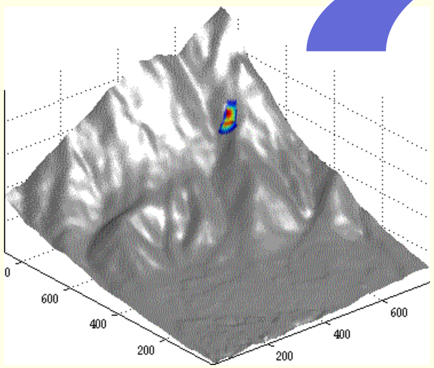

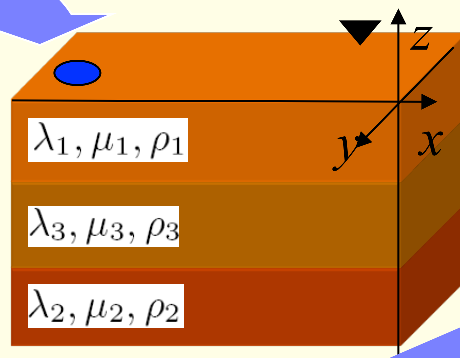

synthetic signal

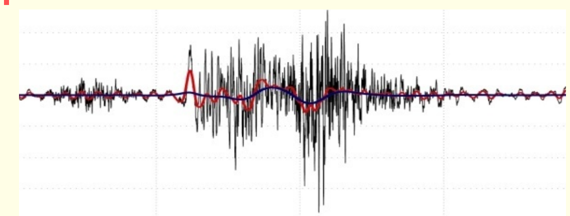

inverted force

Mangeney et al., 2005, 2007

Favreau et al., 2010
Moretti et al., 2012, 2015

Time-dependent basal stress field applied on top of the terrain

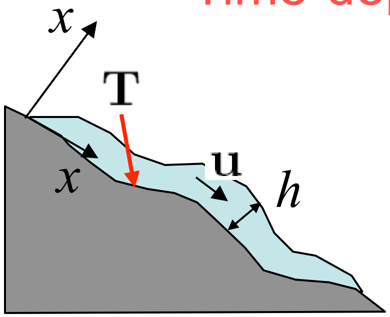

$$\mathbf{T} = \rho g h \left(\cos\theta + \boxed{\frac{\mathbf{u}_h^t \mathcal{H} \mathbf{u}_h}{g \cos^2\theta}} \right) \left(\mu \frac{u_X}{\|\mathbf{u}\|}, \mu \frac{u_Y}{\|\mathbf{u}\|}, -1 \right)$$

Curvature effects

Simulation of the Thurweiser landslide

Thurweiser rock avalanche, Italie
September 2004

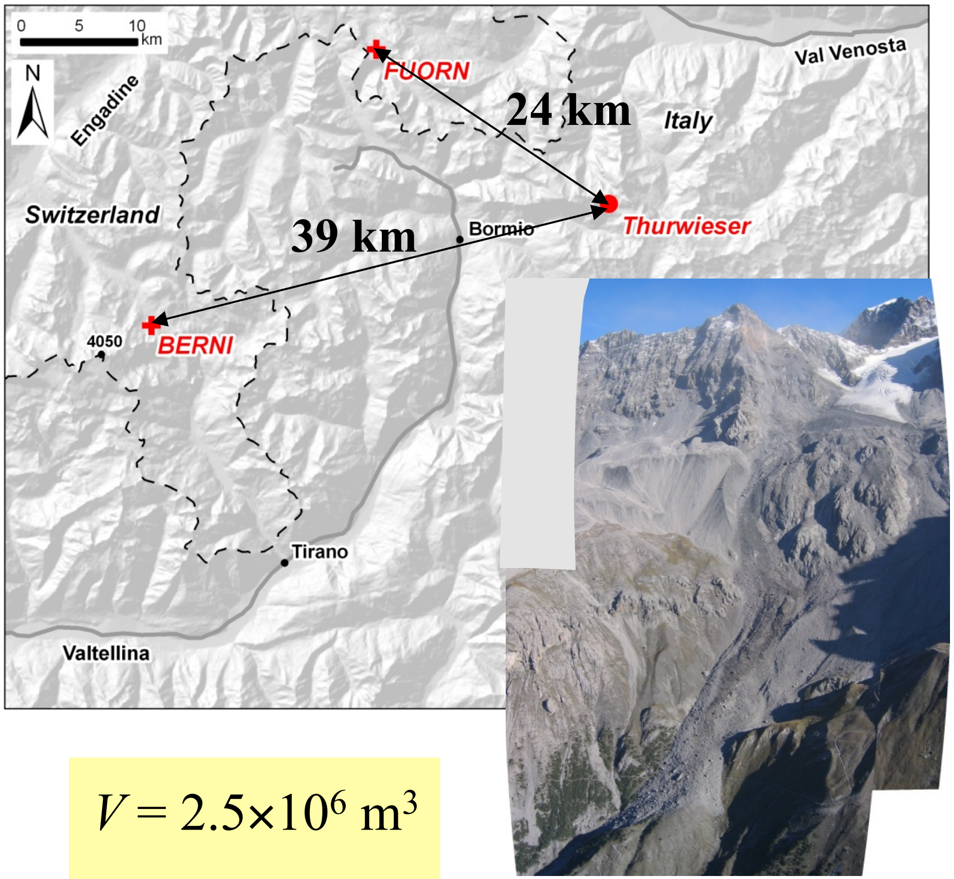

$V = 2.5 \times 10^6$ m^3

$R_f = 2.9$ km

$T_f \approx 90$ s

Sosio et al., 2008, Favreau et al., 2010

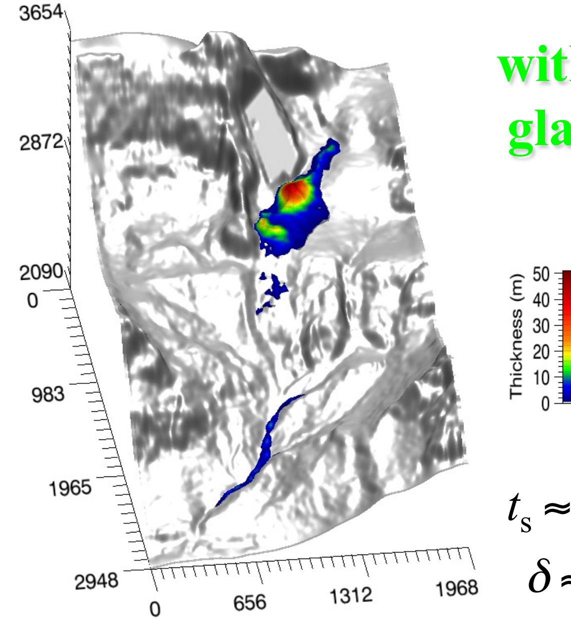

without glacier

$t_s \approx 100$ s

$\delta \approx 23°$

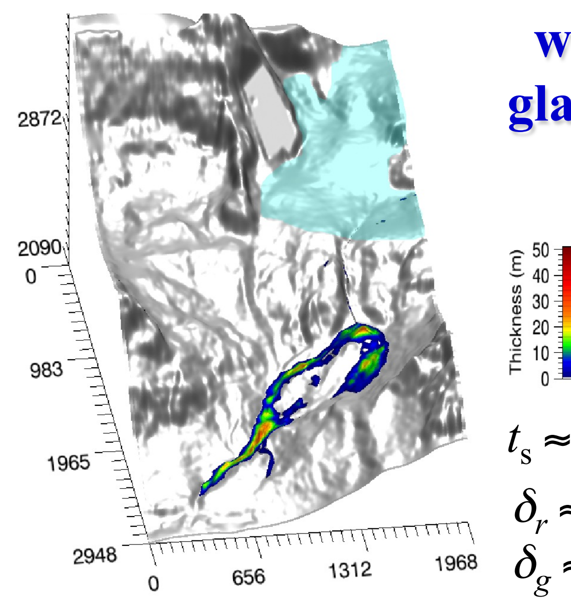

with glacier

$t_s \approx 100$ s

$\delta_r \approx 26°$

$\delta_g \approx 6°$

STS2 Data

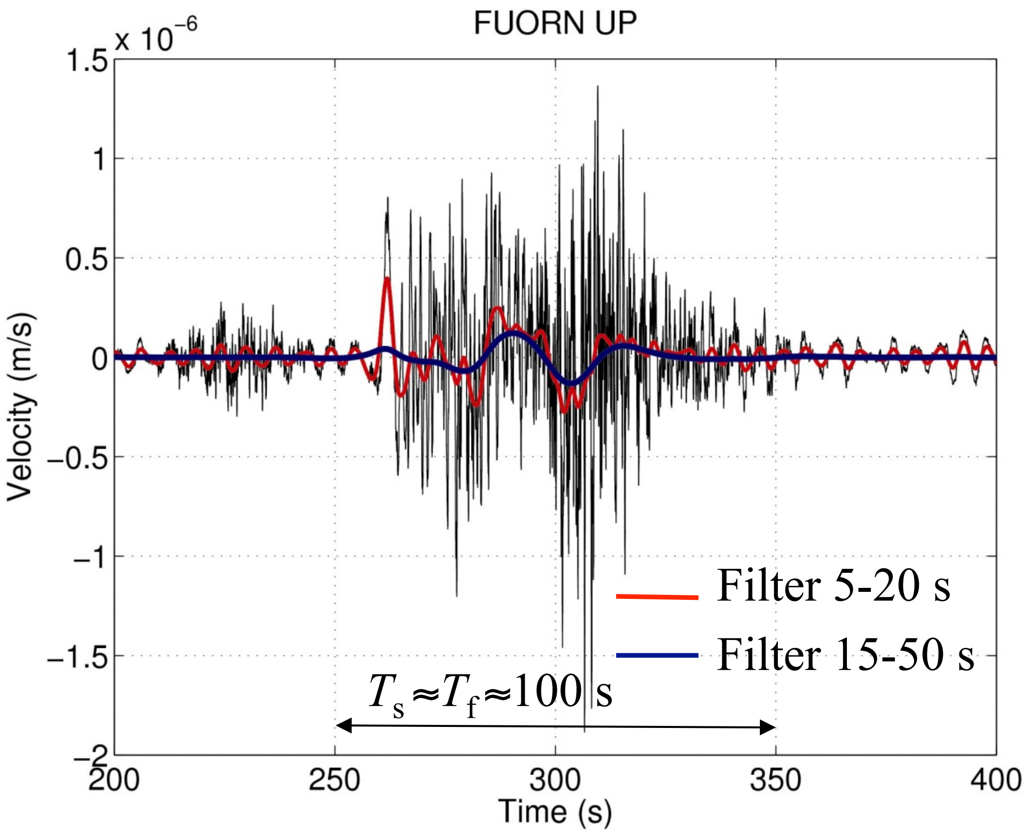

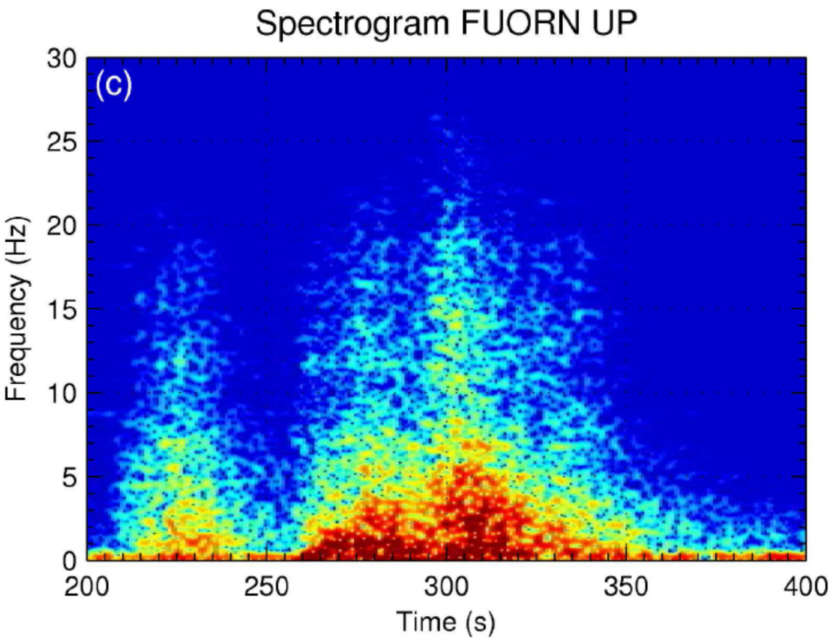

$0.01 \text{ Hz} < f < 15 \text{ Hz}$

$(L_{\text{source-station}} = 24 \text{ km})$

For $T > 15$ s, $\lambda = cT \approx 45$ km

Topographic and complex media effects on wave propagation are expected to be **small**

Simulation of the generated seismic waves

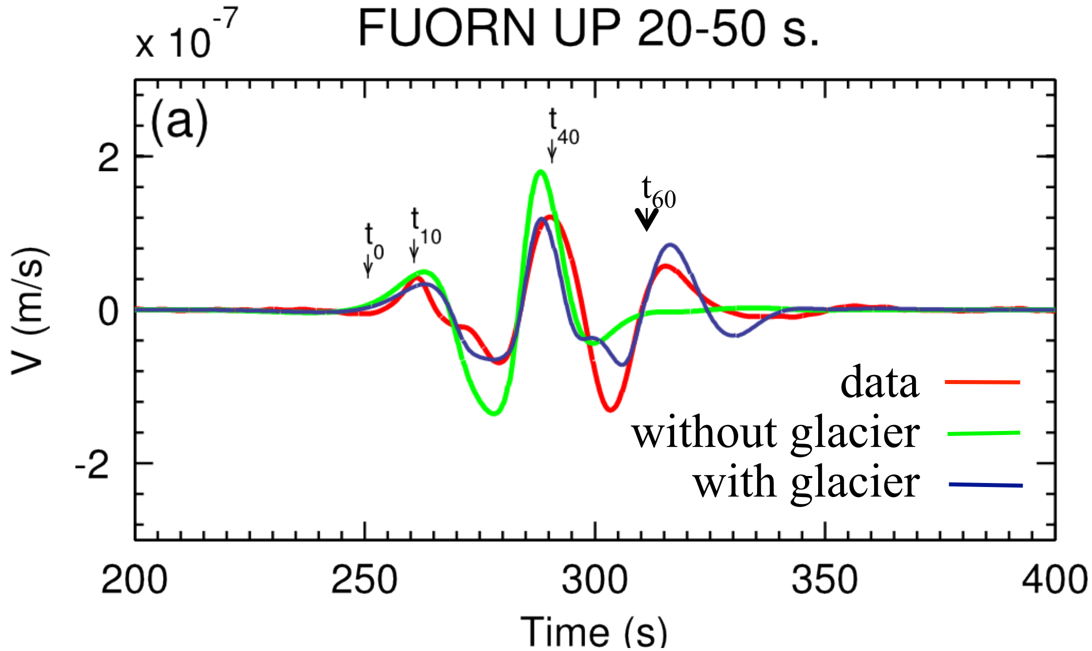

The scenario **with glacier** better reproduces the vertical waveform

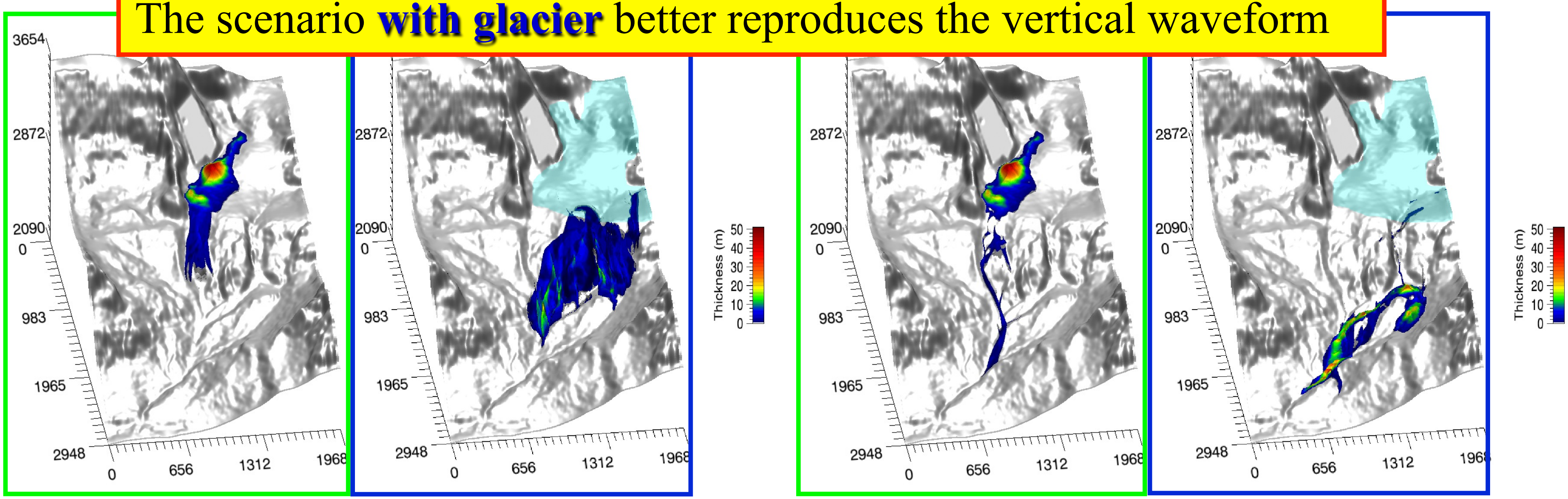

Reproduce small to large landslides

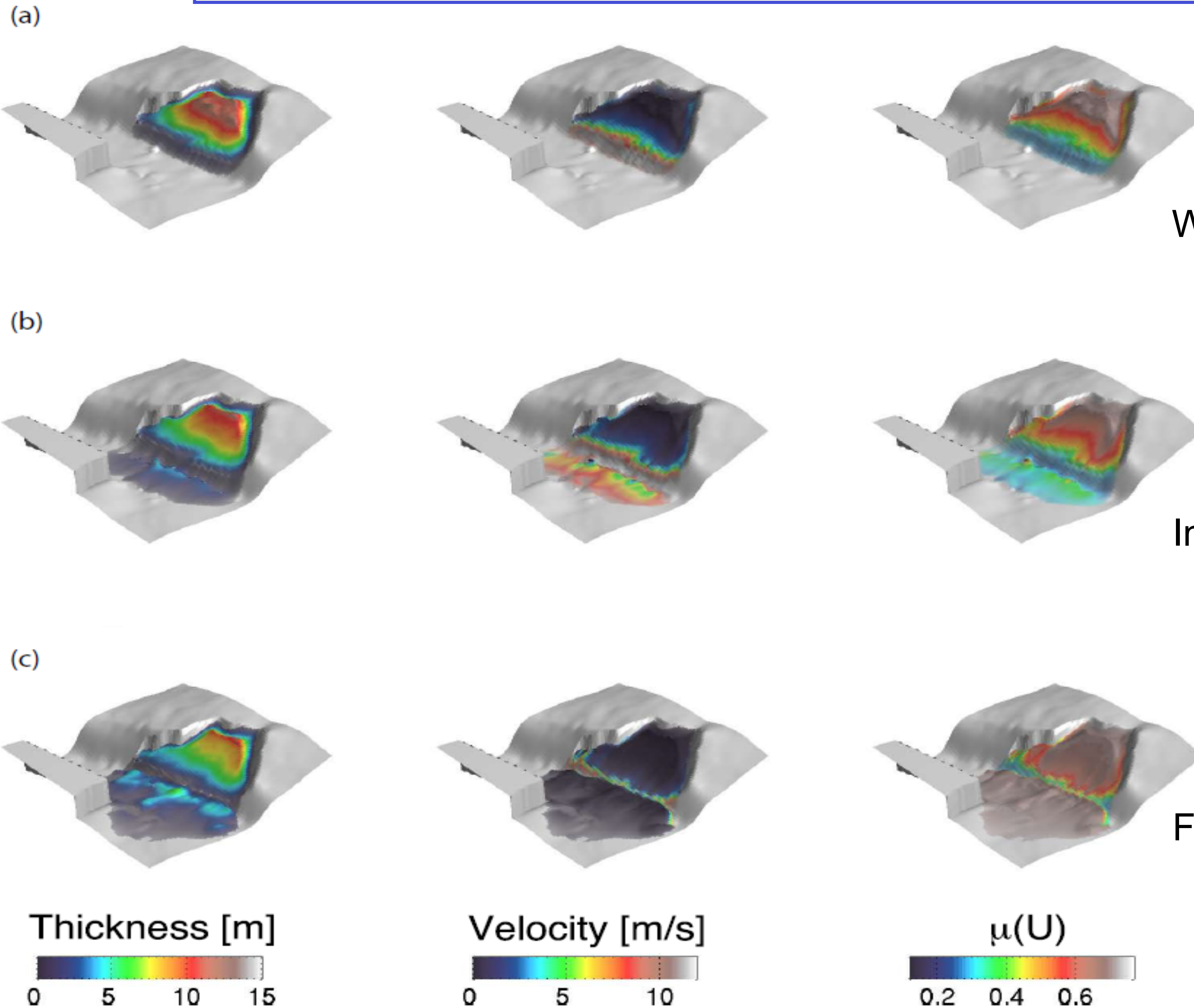

With the same parameters

Improve deposit structure

Friction coefficient
$0.1 < \mu < 0.8$

Curvature effects on the generated seismic waves

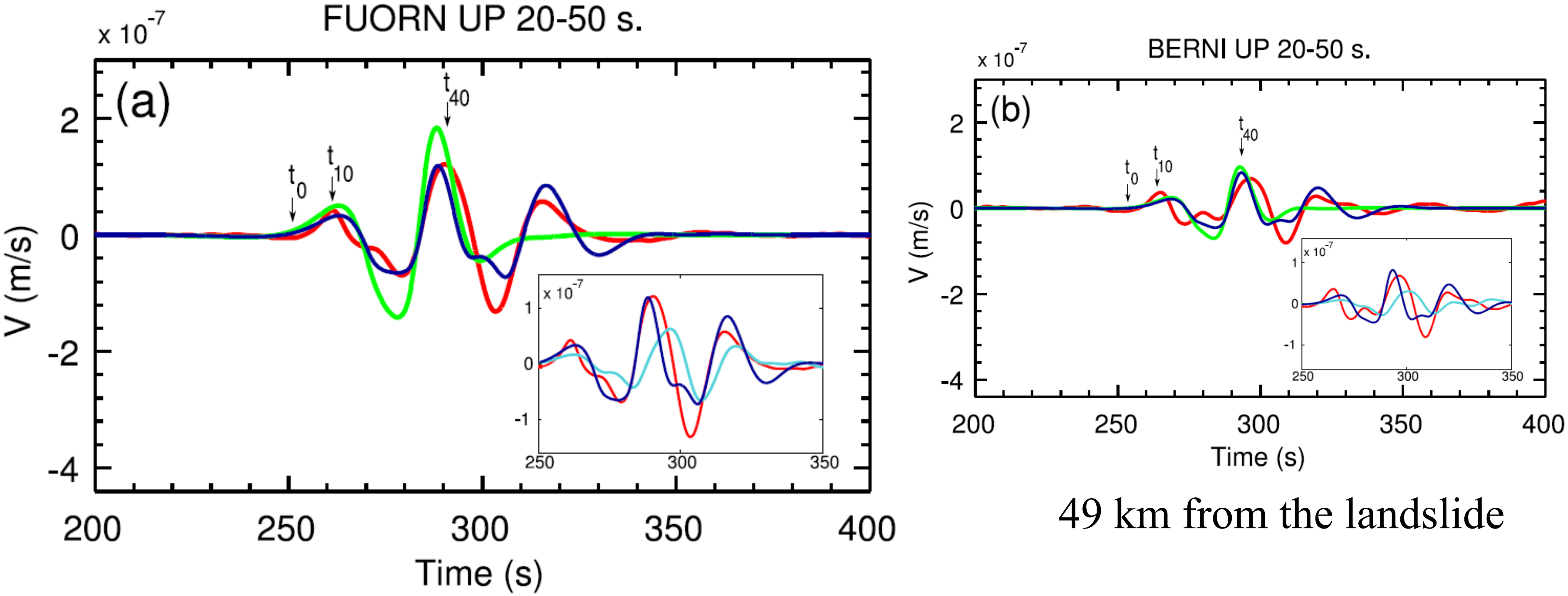

49 km from the landslide

$$\mathbf{T} = \rho g h \left(\cos\theta + \boxed{\frac{\mathbf{u}_h^t \mathcal{H} \mathbf{u}_h}{g \cos^2\theta}} \right) \left(\mu \frac{u_X}{\|\mathbf{u}\|}, \mu \frac{u_Y}{\|\mathbf{u}\|}, -1 \right)$$

Curvature effects

Curvature effects on flow dynamics has a major impact
on the generated seismic signal

Friction coefficient and simulated seismic waves

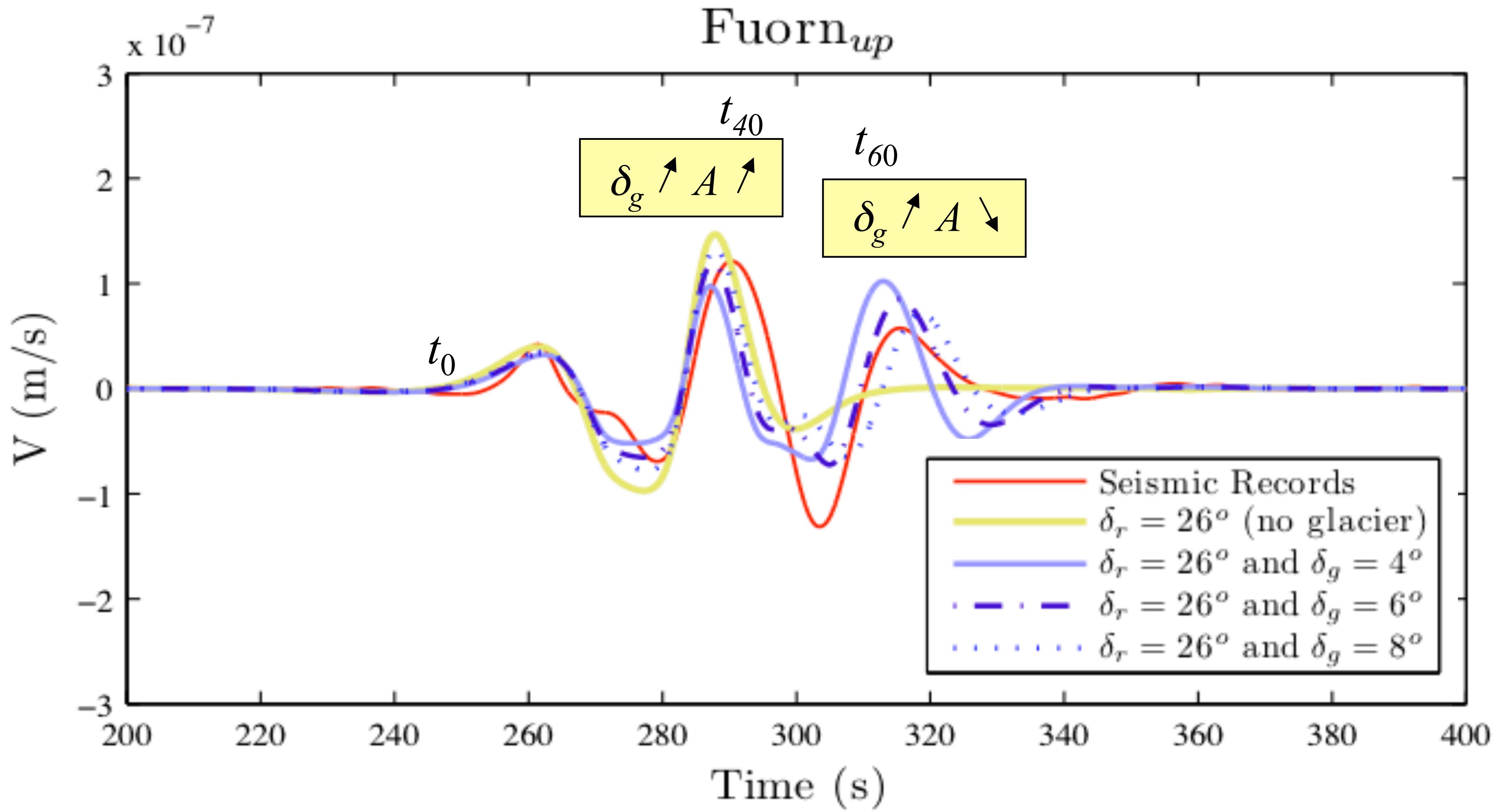

Comparison between simulated and recorded seismic signal

⬇

Calibration of the friction coefficients

Comparaison with discrete element simulations

Limits of the thin layer approximation

- **Non-hydrostatic effets** are important when $a \nearrow$

$$\frac{\partial p}{\partial z} = g + \frac{dw}{dt} \longrightarrow \frac{dw}{dt} \sim 20\%\, g \quad \text{for} \quad a = 0.9$$

Mangeney et al., 2006

$\Downarrow$

- **New asymptotic developments** including **vertical accélération**

- **Description of the static/mobile transition** in granular flows

Models proposed in the literature : no physically relevant energy equation !

Bouchut, Fernandez-Nieto, Mangeney, Lagrée, 2008; Lusso, Mangeney, Bouchut, Ern, 2014

Mt Steller rock-ice avalanche and associated landquake

Alaska, September 2005

Recorded by 7 seismic stations from 37 km to 623 km

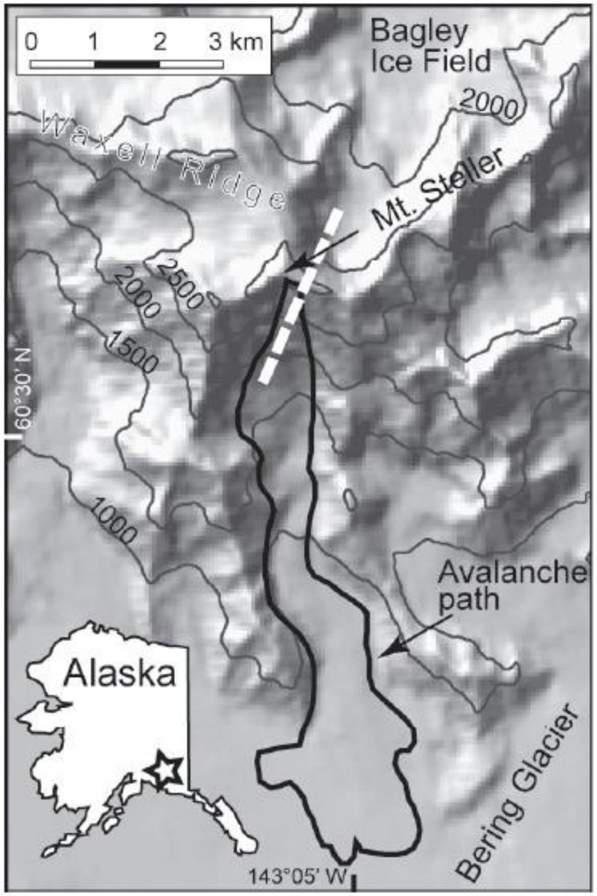

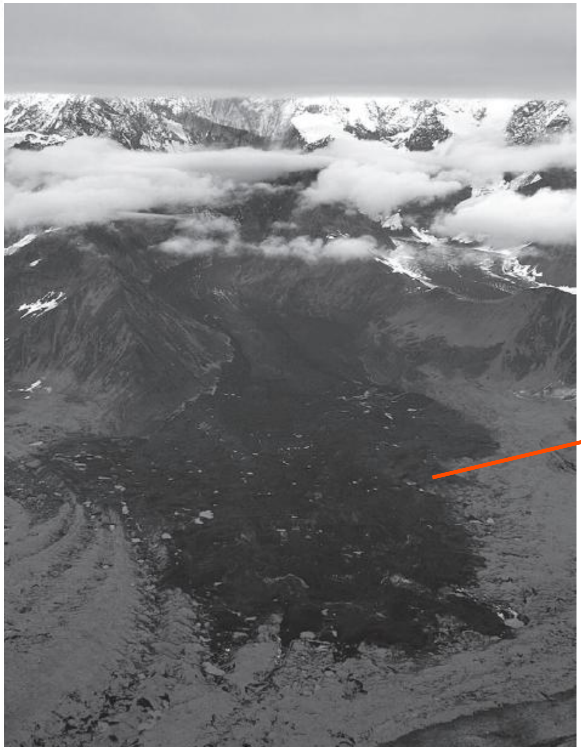

37 km from the source :

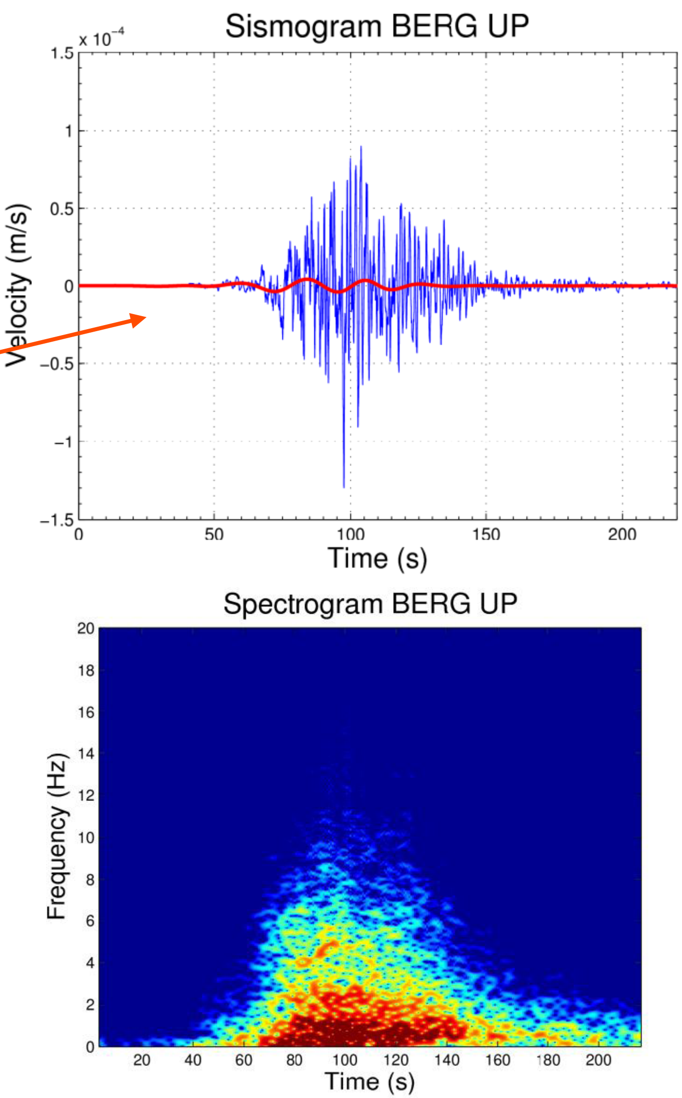

Ice **eroded** from the glacier:

$V \sim 20$ Mm^3

$V \sim 50$ Mm^3

$R_f = 10$ km

$T_f \approx 130$ s

Huggel et al., 2008

Simulation of the Mt Steller rock-ice avalanche

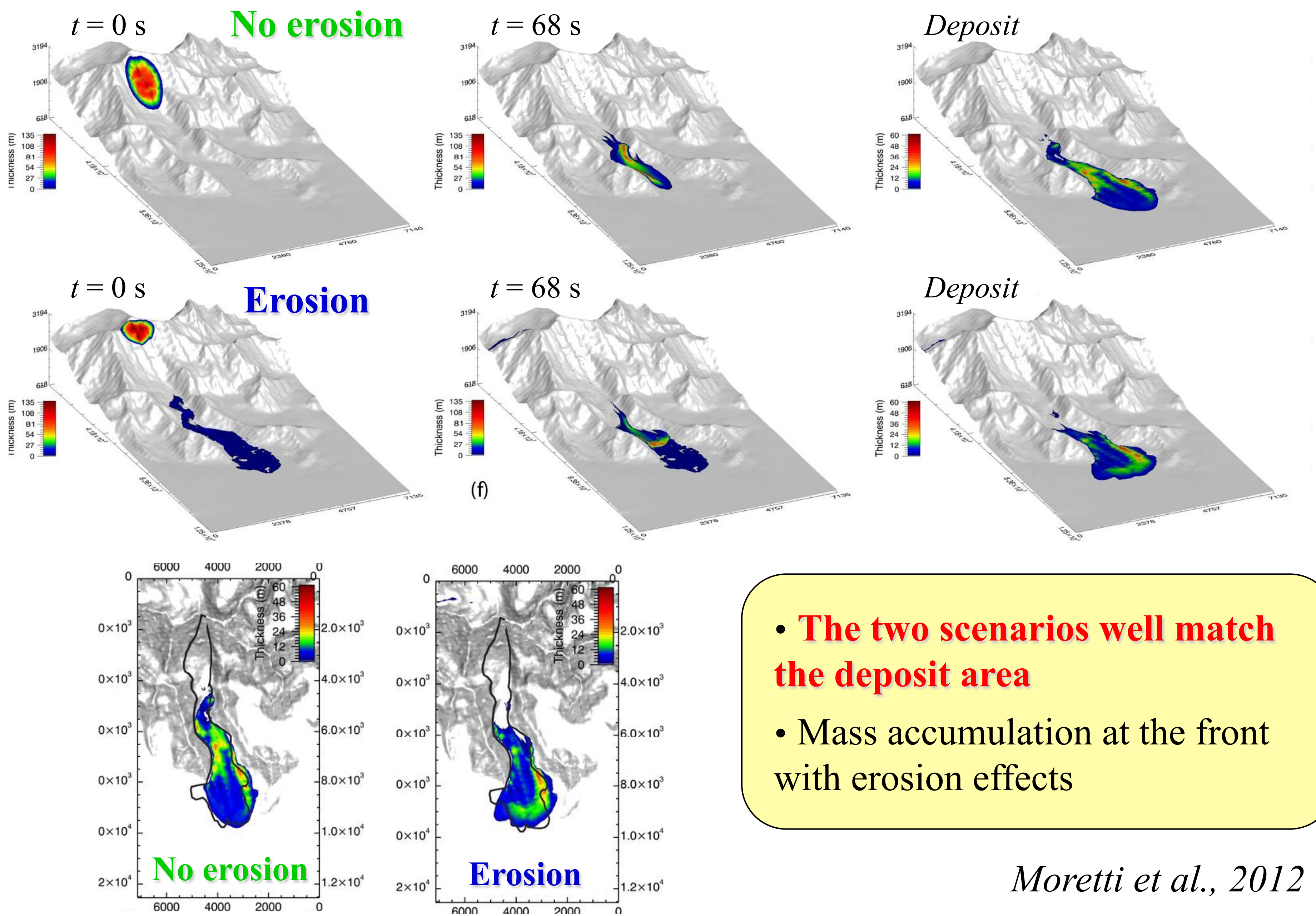

- **The two scenarios well match the deposit area**
- Mass accumulation at the front with erosion effects

Moretti et al., 2012

Simulation of the Mt Steller landquake

Vertical ground velocity *filtered between 20 s and 50 s* at 7 seismic stations

Data — **No erosion** — **Erosion**

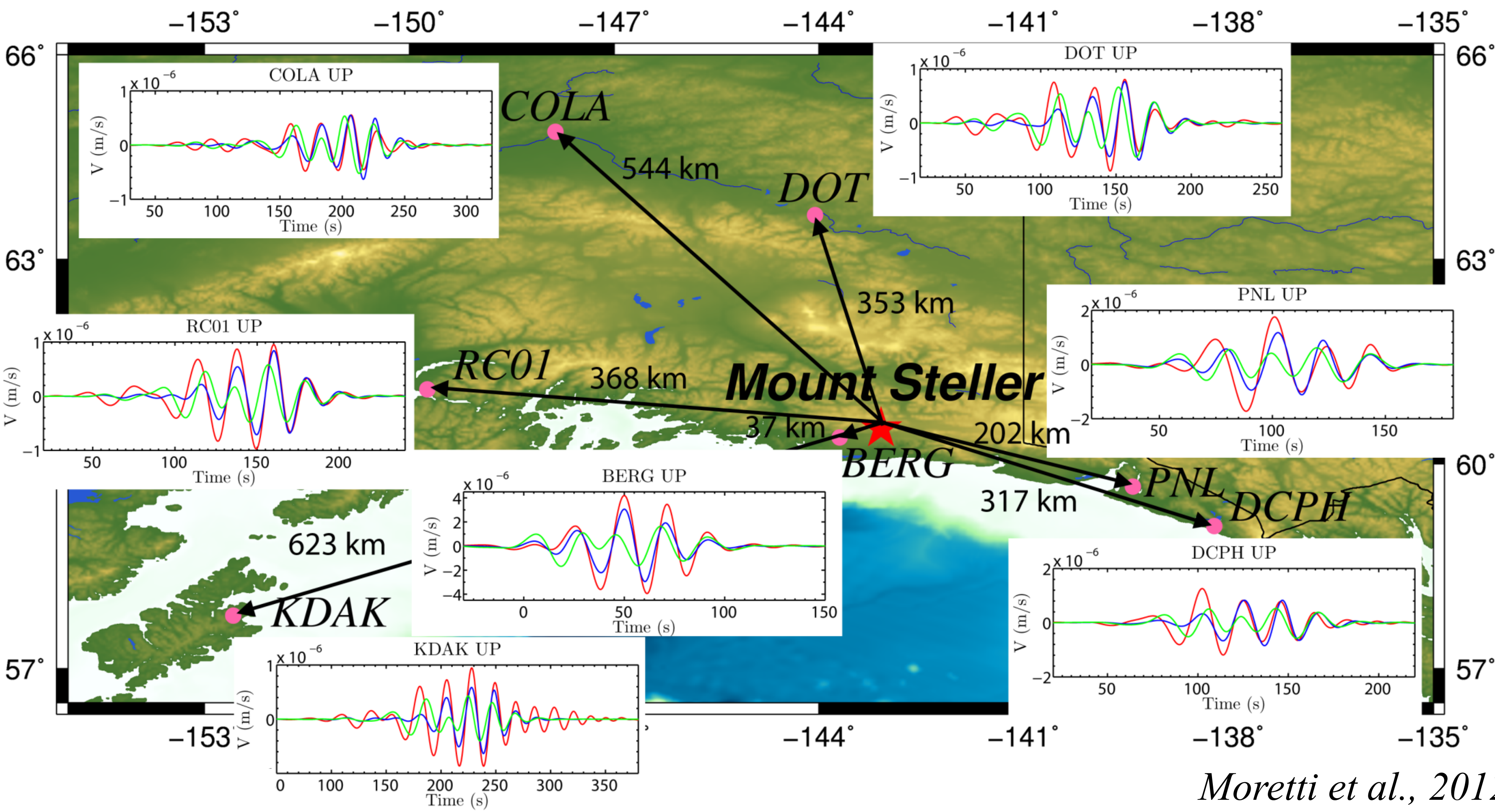

Moretti et al., 2012

The scenario with erosion better reproduces the observed waveform

Conclusion

Numerical models: **empirical tool** to study natural flows

Calibrated on past events

prediction of the dynamics and deposit in the same geological context

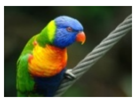

First operational tools for hazard assessment

- Data on the dynamics : **seismology**

- More **physics** in the models : solid/fluid mixture, erosion/deposition …

New equations to solve…..


Thank you !

Numerical modeling of erosion in granular flows

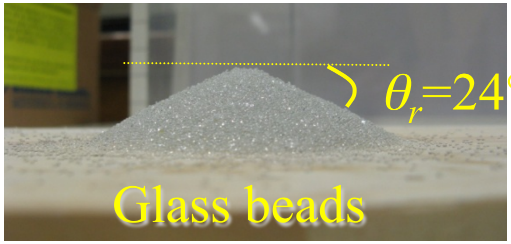

a = 0,7

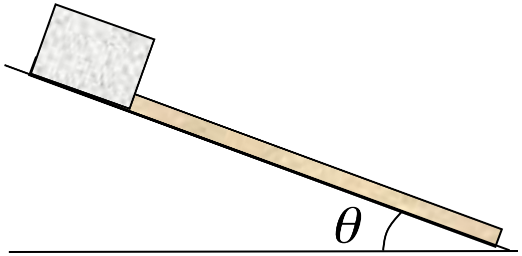

Mangeney et al., 2010

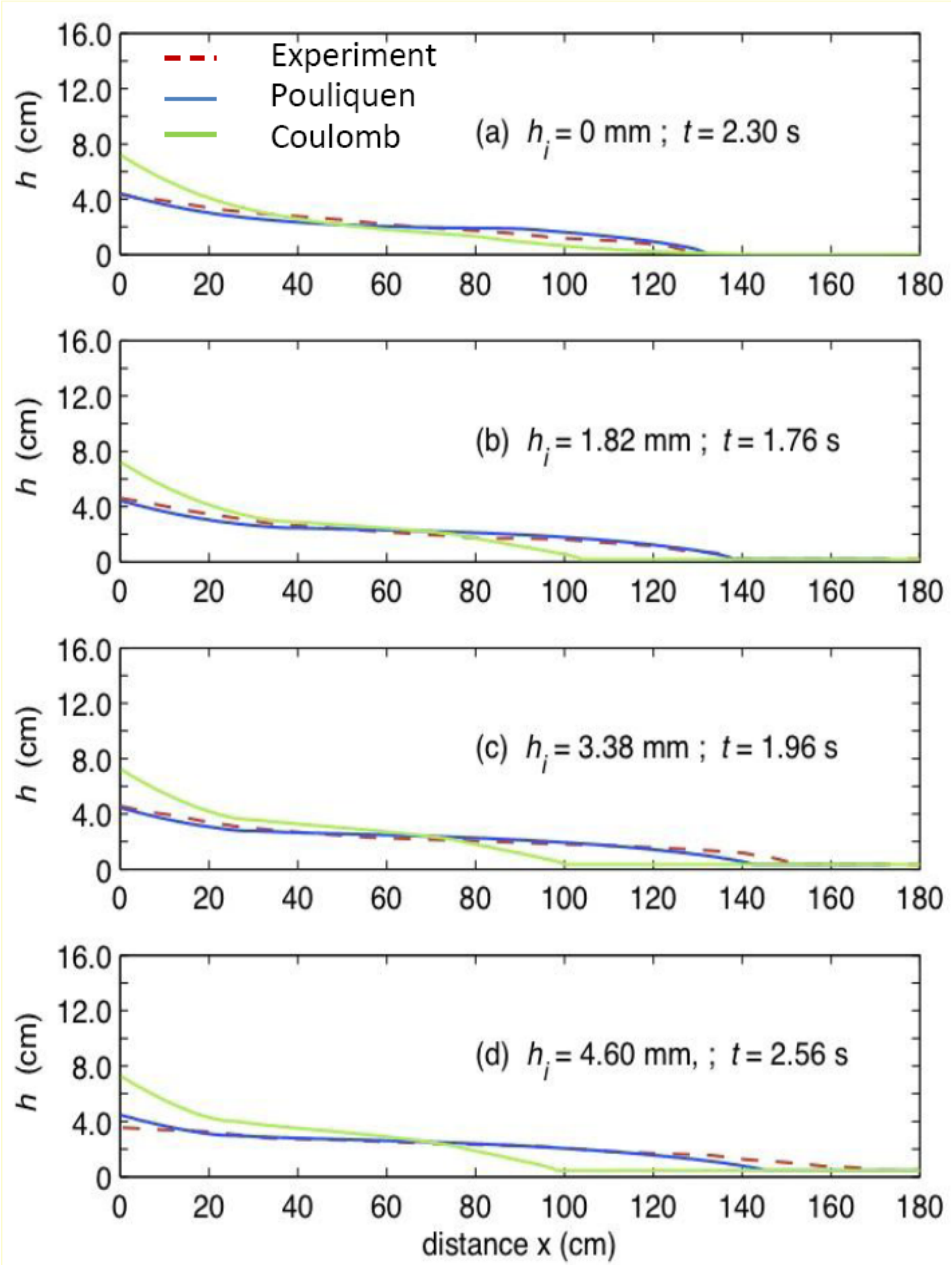

Morphological signature of flow processes

Gullies, Iceland

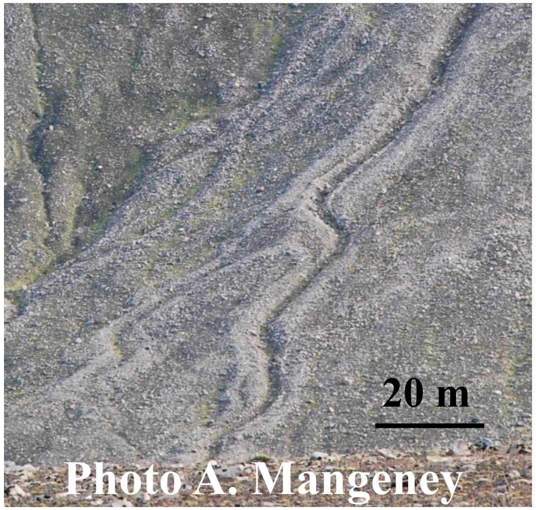

Pyroclastic flows,
Lascar volcano, Chili

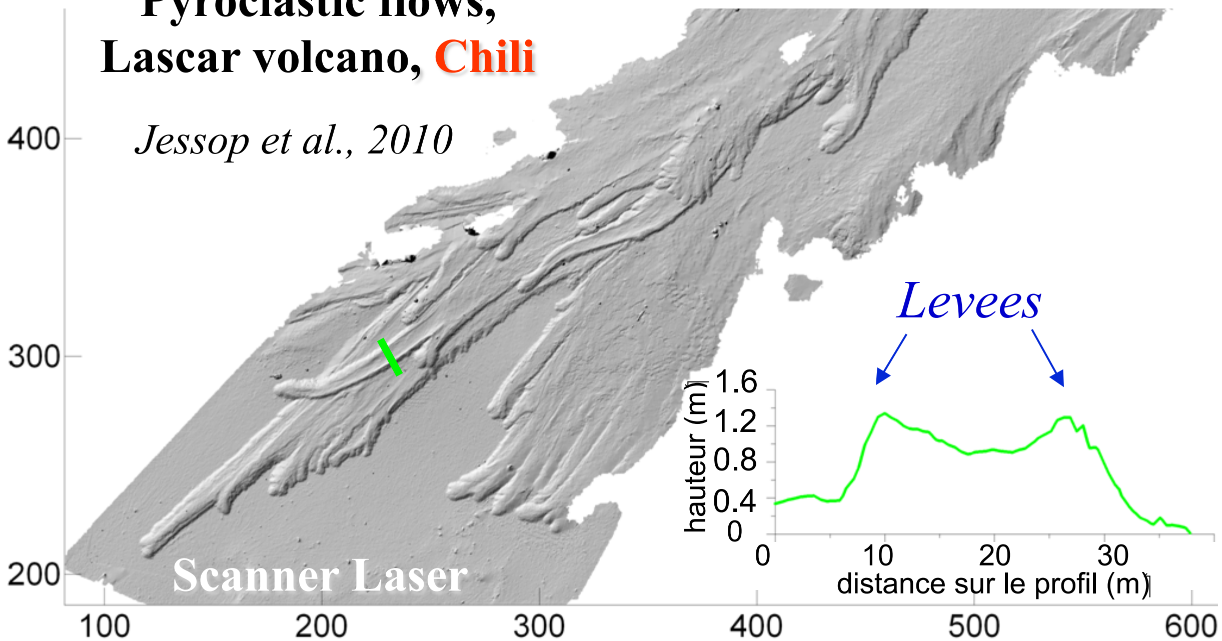

Gullies, Mars

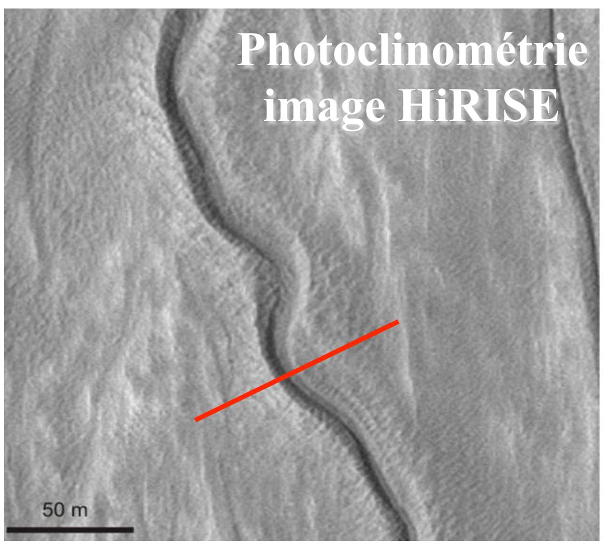

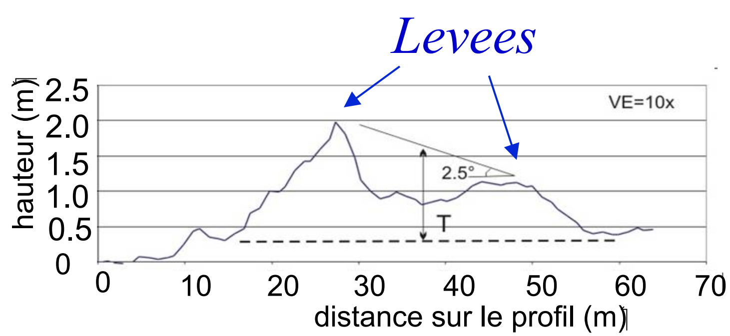

Mangold et al. 2010

2D granular flows over erodible bed : Experiments

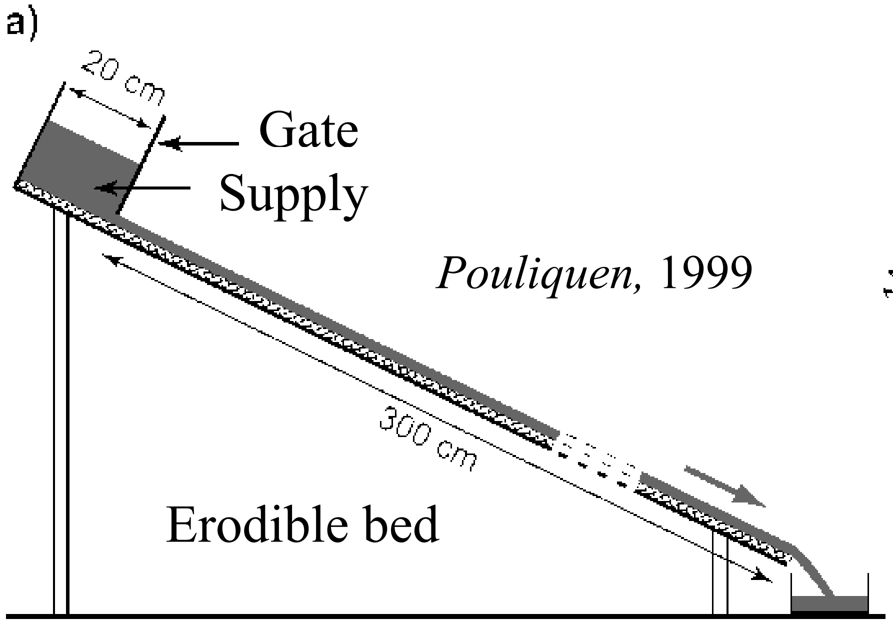

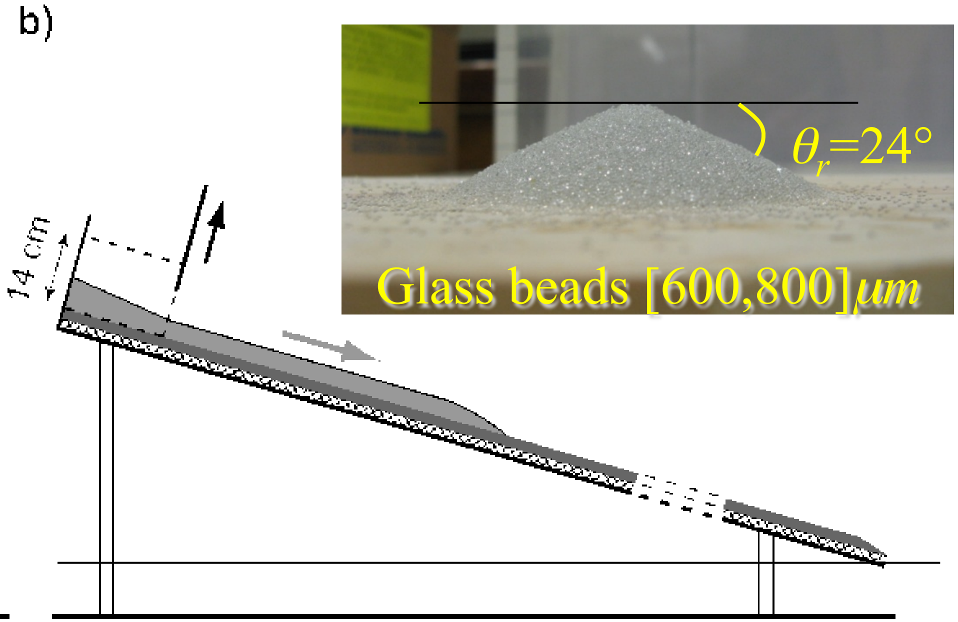

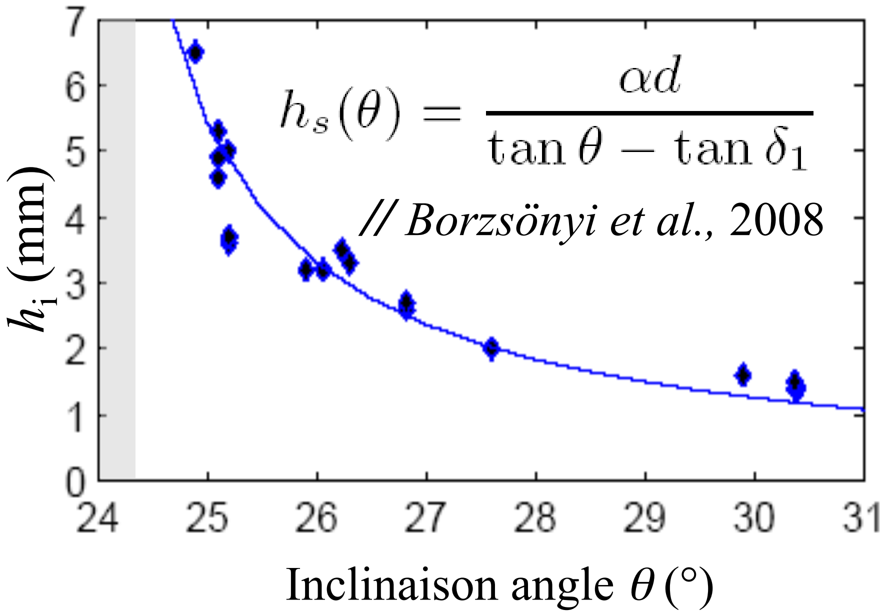

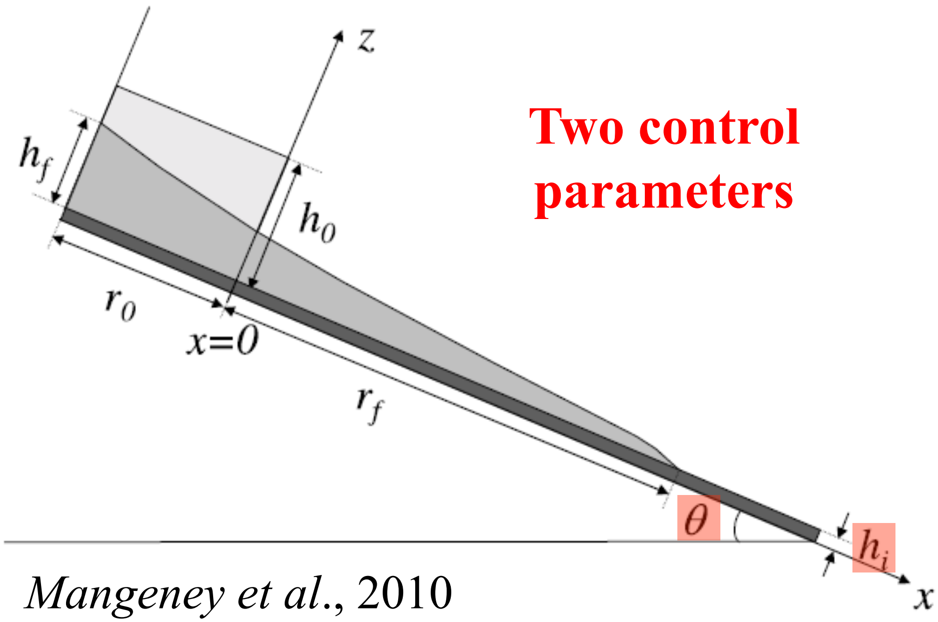

Two control parameters

Mangeney et al., 2010

Granular collapse over a rigid bed

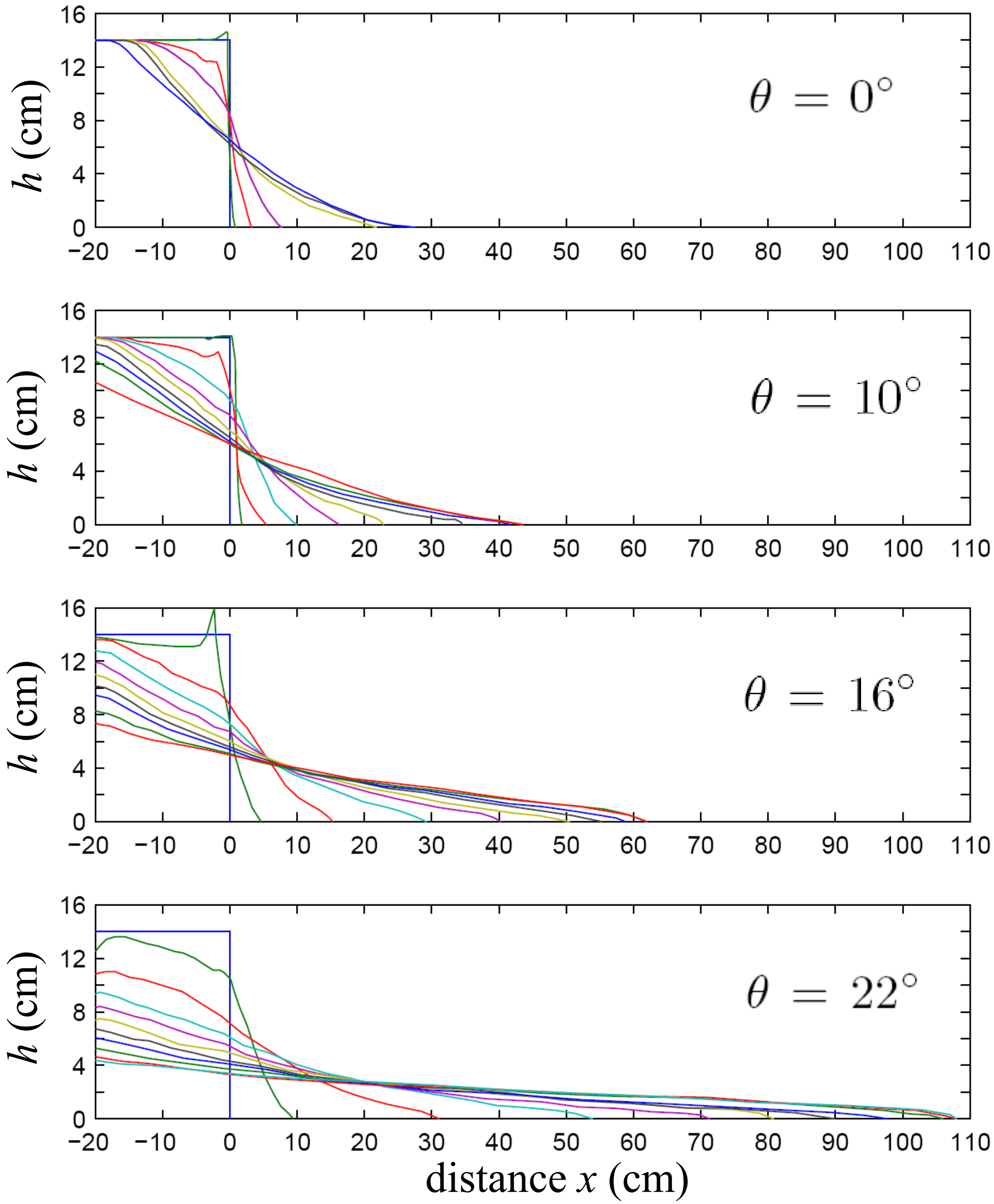

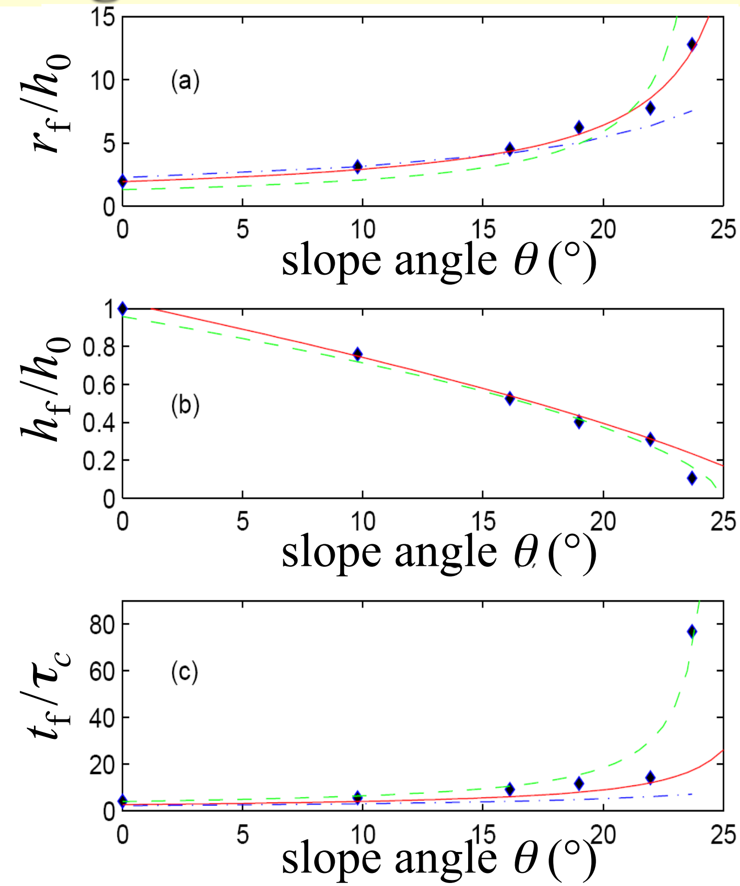

$$\frac{r_f}{h_0} = \frac{2k}{\tan\delta - \tan\theta}$$

$$\frac{h_f}{h_0} = \left(\frac{\tan\delta - \tan\theta}{ak}\right)^{\beta}$$

$$\frac{t_f}{\tau_c} = \frac{2\sqrt{k}}{\tan\delta - \tan\theta}$$

Granular collapse over an erodible bed

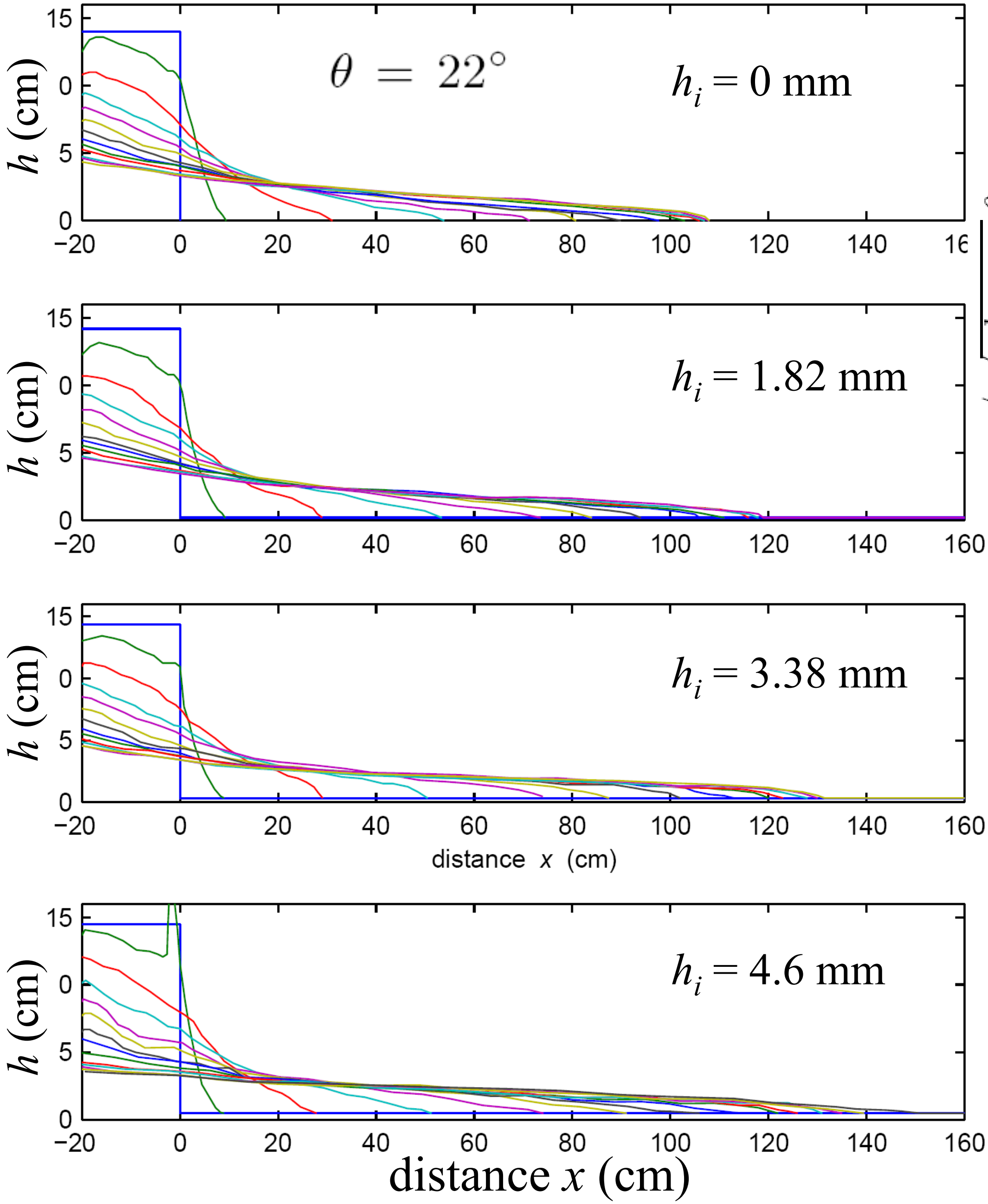

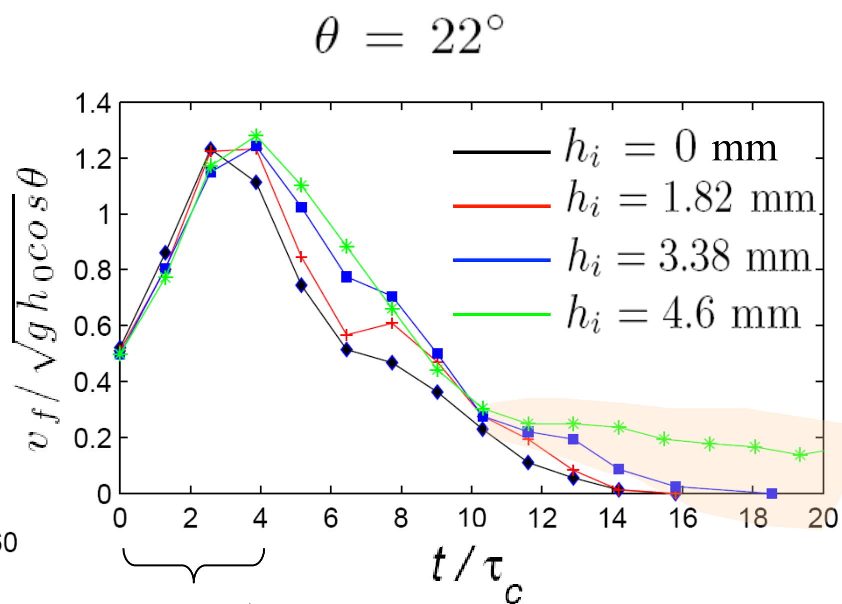

$v_f \approx$ cte

$t \geq 4 - 5\tau_c\,,\ v_f \nearrow$ if $h_i \nearrow$

For $t \geq 10\tau_c$ and $h_i = 4.6$ mm

Slow flow

2D granular flows over erodible bed : Simulations

The partial fluidization model :

static grains flowing grains

Pyroclastic flows, Lascar volcano, Chili

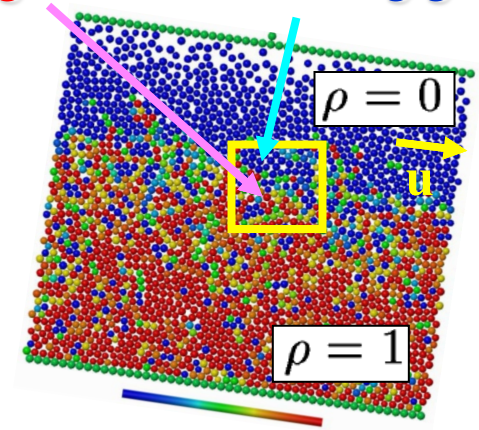

Discrete elements simulation

Flow law valid for both static and flowing grains??

$$\boxed{\sigma_{ij} = \sigma^f_{ij} + \sigma^s_{ij}} \qquad \begin{cases} \sigma^f_{ij} & \text{- flowing grains} \\ \sigma^s_{ij} & \text{- static grains} \end{cases}$$

$$\sigma^f_{xy} = q(\rho)\,\sigma_{xy}$$

ρ characterizes the **« state » of the granular matter** $\rho = \dfrac{\Sigma \text{ static contacts}}{\Sigma \text{ contacts}}$

Aranson and Tsimring, 2002; *Aranson et al.*, 2008

INLS, ***UC San Diego***

Modeling of erosion processes

- 2D numerical modeling

Mangeney et al., 2007

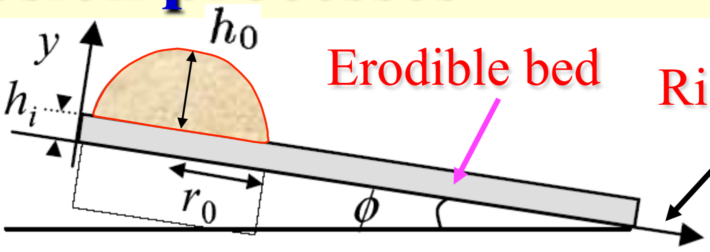

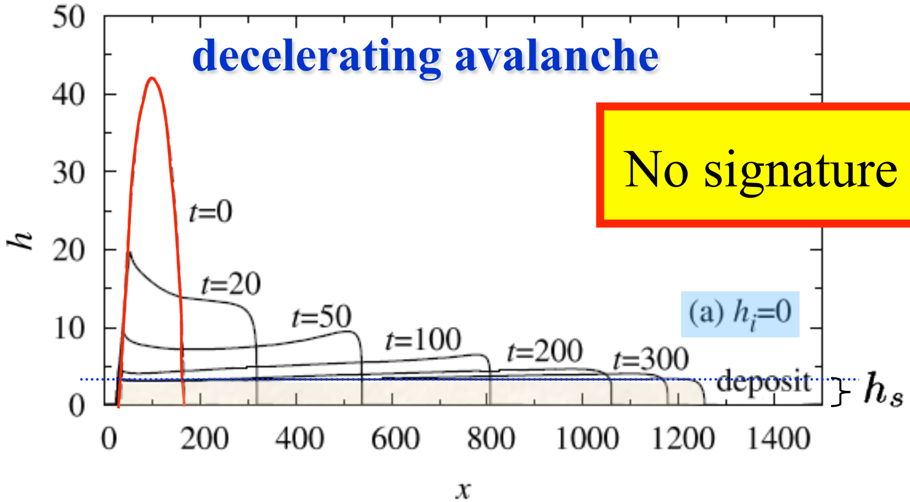

No signature on the deposit !

Data on the dynamics ?!?

In agreement with experiments *Pouliquen and Forterre*, 2002, *Mangeney et al., 2010*, …